# Modeling, Discretization, Optimization, and Simulation of Fluid-Structure Interaction

## Thomas Wick

AG Wissenschaftliches Rechnen (GWR)

Institut für Angewandte Mathematik (IfAM)

Gottfried Wilhelm Leibniz Universität Hannover (LUH)

Welfengarten 1

30167 Hannover

https://www.ifam.uni-hannover.de/wick.html

thomas.wick@ifam.uni-hannover.de

Last update:
Thursday, November 28, 2019



colored by Céline Wick

# Foreword

These lecture notes on **fluid-structure interaction** are in the truest sense **interdisciplinary** and **international** since they have undergone (so far!) materials and research experiences in three different countries: Germany (Heidelberg, München, Hannover), Austria (Linz), and France (Ecole Polytechnique).

## 5th version

The fifth version is prepared for a winter school at IIT Indore (India) in Feb 2020 and the upcoming summer semester 2020 at the Leibniz University Hannover.

Thomas Wick

(Hannover, November 2019)

## 4th version

The fourth version has been prepared without underlying lecture. The main purpose was to correct several errors: thanks to Pratik Rai.

Thomas Wick

(Palaiseau, June 2017)

## 3rd version

The third Linz-version of lecture notes is based on the Munich version and differs only in the correction of spelling mistakes and minor modifications.

Thomas Wick

(Linz, September 2015)

## 2nd version

This second Munich-version of lecture notes is based on a compact class that I prepared for Heidelberg University in November 2014. Then, they have been significantly extended (Chapters 1-7) during a fluid-structure interaction class at Technische Universität München in summer 2015. I am specifically grateful to my students in München since they asked many questions that helped to improve the manuscript.

Thomas Wick

(München, July 2015)

## 1st version

I am very grateful to the organizers of the winter school at Heidelberg University; namely Thomas Richter, Boris Vexler, Dominik Meidner, and Rolf Rannacher, for the opportunity to hold this lecture on fluid-structure interaction (FSI) problems at IWR Heidelberg. Still, fluid-structure interaction is one of the most challenging problems that extend into all parts of applied mathematics: modeling and theory, numerical techniques, large-scale high performance computations, sensitivity analysis and optimization. These notes represent a mixture

of state-of-the-art research; as well as teaching material of basic techniques that have been well known for a long time now.

In order to access, understand, and work with the content of these notes, I suggest as academical requirements classes for numerical methods for ordinary and partial differential equations (ODEs and PDEs). Furthermore, PDE analysis, Sobolev spaces, functional analysis, and concepts in continuum mechanics would be very helpful.

I wish to express my special gratitude to Thomas Richter with whom I have had many discussions on fluid-structure interaction in the last years.

Thomas Wick

(Heidelberg, November 2014)

# Contents

## 8 Temporal and Spatial Discretization      111

## 9 Numerical Solution Algorithms      139

## 10 Error Estimation and Mesh Adaptivity      159

# 1 Main literature

1. T. Richter: Fluid-structure interactions: models, analysis, and finite elements (2017) [199]

2. Y. Bazilevs and K. Takizawa and T.E. Tezduyar: Computational Fluid-Structure Interaction: Methods and Applications (2013) [21]

3. Y. Bazilevs and K. Takizawa: Advances in Computational Fluid-Structure Interaction and Flow Simulation (2016) [20]

4. Tomas Bodnar, Giovanni P. Galdi, Sarka Necasova: Fluid-Structure Interaction and Biomedical Applications (2014) [40]

5. H.-J. Bungartz and M. Schäfer: Fluid-Structure Interaction: Modelling, Simulation, Optimization (2006) [56]

6. H.-J. Bungartz and Miriam Mehl and M. Schäfer: Fluid-Structure Interaction II: Modelling, Simulation, Optimization (2010) [55]

7. Luca Formaggia and Alfio Quarteroni and Alessandro Veneziani: Cardiovascular Mathematics: Modeling and simulation of the circulatory system (2009) [94]

8. G. Galdi and R. Rannacher: Fundamental Trends in Fluid-Structure Interaction (2010) [103]

9. R. Rannacher: Probleme der Kontinuumsmechanik und ihre numerische Behandlung (2017) [193]

10. S. Frei and B. Holm and T. Richter and T. Wick and H. Yang: Fluid-structure interactions: Fluid-Structure Interaction: Modeling, Adaptive Discretisations and Solvers (2017) [98]

## 1.1 Own materials

To accomodate with preliminaries and notations, we recommend to look into

1. T. Wick; Numerical Methods for Partial Differential Equations; Lecture notes at the Leibniz Universität Hannover, 2017 - 2020 [247]. The current version Nov 28, 2019 is available via [http://www.thomaswick.org/links/lecture_notes_Numerics_PDEs_Nov_28_2019.pdf](http://www.thomaswick.org/links/lecture_notes_Numerics_PDEs_Nov_28_2019.pdf)

2. Specifically Chapter 13 (Nonlinear problems) and Chapter 14 (Coupled problems) are recommended.

# 2 A Brief Motivation for FSI-Research and Challenges

## 2.1 First definitions

In fluid-structure interaction (FSI)[1] we study the interaction of movable or deformable solids with fluid flow.

**Definition 2.1** (FSI meaning in this lecture). *In these notes, we define FSI as the interaction of elastic bodies with the isothermal, incompressible Navier-Stokes equations.*
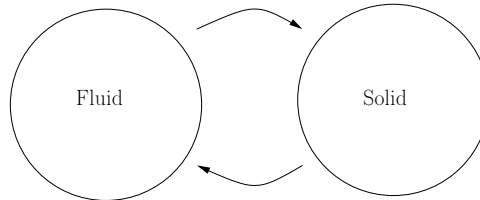


Traditionally, elasticity and solid mechanics on the one hand and the Navier-Stokes equations on the other hand are two different subjects. Consequently their coupling, leading to fluid-structure interaction, remains one of the most challenging topics to date, although many publications have appeared with specific emphasize on applications, coupling algorithms, and theory. Classical examples are found in industrial processes, mechanical engineering, aero-elasticity, and biomechanics. Specifically, fluid-structure interactions (FSI) are important to describe flows around elastic structures as for instance in the flutter analysis of airplanes, parachute FSI, bridges, wind turbines, or blood flow in the cardiovascular system, possibly with hyperelastic structure models, and heart valve dynamics, see, for example [22, 54–56, 94, 162, 173, 177, 185, 186, 197, 212, 218] (of course, these references are by far not sufficient - if I would list all, we would arrive at $\gg 1000$). However, fluid-structure interaction is implicitly contained in many other fields as for example in porous media flow (here fluid-structure interaction is needed on the microscopic level where solid pores interact with the flow; through homogenization, the so-called Biot equations are obtained [37–39, 171]).

Let us start with two examples I have been involved in [2]. The first topic is health (specifically the heart) [3]:
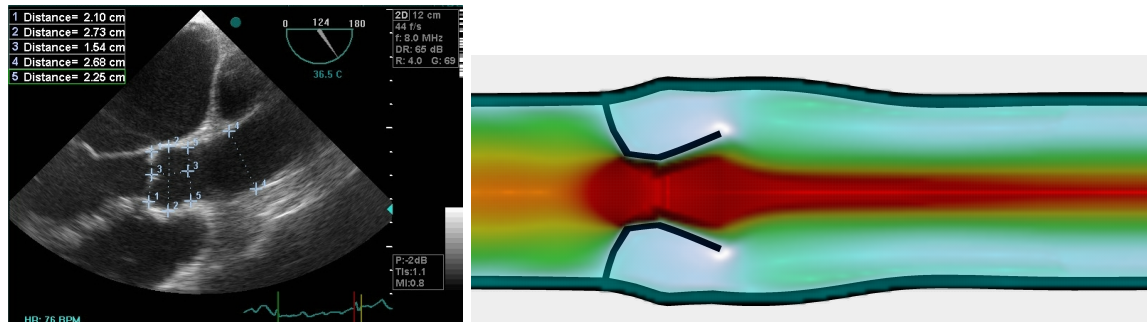


Figure 1: Long axis heart valve. Provided by Jeremi Mizerski [172] (and in collaboration with Rolf Rannacher; my PhD thesis [239]) .

---

[1]In these notes, I use both notations: 'structure' and 'solid'.

[2]There are so many interesting topics in FSI research, please forgive me at this point that I only mention two topics I have been working on.

[3]Simulation of the heart is a very difficult topic and I am not claiming that I completely solved this. I rather restricted my focus on the development of adaptive finite element methods.

## 2.2 Three questions

Ideally, the three basic questions we have to ask are:

- Why are we doing this? (Is there a link to our real-world? What is the impact?)

- How are we doing this? (Modeling, solution theory, numerical discretization, simulation, optimization, uncertainty analysis, comparison with experimental data, verification and validation)

- What are we doing? (What is the example or application?)

The circle of research that we are entering is highlighted in Figure 3.
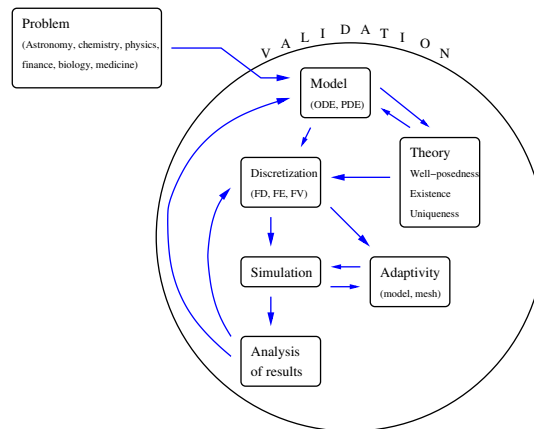


Figure 2: 'The third pillar of science: scientific computing/computational engineering and sciences'. Forward modeling and validation.
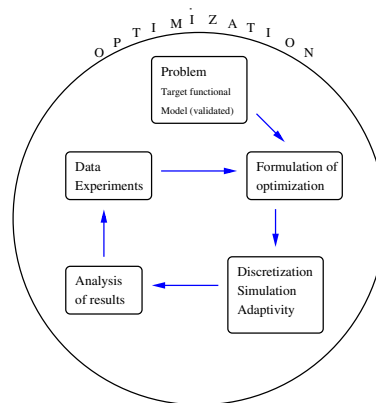


Figure 3: 'The third pillar of science: scientific computing/computational engineering and sciences'. Optimization.

Having sufficient trust into our forward model, we can go one step further and think about optimization (i.e., inverse modeling): parameter estimation, optimal control, inverse problems, optimal experimental design.

- Why should we do this?

Well, having the forward model (the state equation) is one part, but often (except in academic examples and simplified situations), material parameters or the geometry are not known, for instance. Or, we are given some output but do not know the state that caused this output (inverse problems). Or, we want to control the PDE into a certain solution/state (optimal control). As sketch of the abstract optimization process is provided in Figure 4.

## 2.3 Guiding questions in differential equations

1. What type of equations are we dealing with?

2. Are we dealing with a single PDE, coupled problems, nonlinear PDEs?

3. What are the physical conservation properties?

4. Are theoretical results known? Can the equations be related to (simplified) known PDEs?

5. What kind of discretization scheme(s) shall we use?

6. How do we design algorithms to compute the discrete solution $u_h$?

7. Can we proof that these algorithms really work?

8. Are they robust (stable with respect to parameter variations), accurate, and efficient?

9. Can we construct physics-based algorithms that maintain as best as possible conservation laws; in particular when several equations interact (couple)?

10. How far is $u_h$ away from $u$ in a certain (error) norm? Hint: comparing color figures gives a first impression, but is not science!

11. The discretized systems (to obtain $u_h$) are often large with a huge number of unknowns: how do we solve these linear equation systems?

12. What is the computational cost?

13. How can we achieve more efficient algorithms? Hint: adaptivity, parallel computing, model order reduction.

14. Are analytical solutions or experimental results available to compare with?

15. How can we check that the solution is correct?

16. How do we present numerical results: figures, graphs, tables?

17. What parts of the solution are of interest? The entire solution? Only certain goal functionals?

18. What is my personal task or goal: theory, numerical analysis or implementation? For the latter, what software is available on the market?

## 2.4 Errors

In order to realize these algorithmic questions, we go ahead and implement them in a software (for instance Matlab/octave, python, fortran, C++) using a computer or cluster. Here, we face **five** major error sources that need to be taken into account:

- The set of numbers is finite and a calculation is limited by machine precision (floating point arithmetics), which results in **round-off errors**. Typical issues are overflow and underflow of numbers.

- The memory of a computer (or cluster) is finite and thus functions and equations can only be represented through approximations. Thus, continuous information has to be represented through discrete information, which results into the investigation of so-called **discretization errors**.

- All further simplifications of a numerical algorithm (in order to solve the discrete problem), with the final goal to reduce the computational time, are so-called **systematic errors**. Mostly, these are so-called **iteration errors**, for instance the stopping criterion after how many steps an iterative method terminates.

- So called **(numerical) model/regularization errors** play a role when the governing PDE(s) need to be extended in an artificial way in order to guarentee numerical robustness. Examples are pure (first-order) hyperbolic problems in which artificial diffusion is added in order to solve them in a more or less robust way. A second application are coupled and interface problems in which the interface needs to be tracked (level-set, phase-field, fully Eulerian techniques).

- Finally, **programming errors (code bugs)** are an important error source. Often these can be identified since the output is strange. But there are many, which are hidden and very tedious to detect.

Numerical simulations are also subject to **physical model errors** that additionally the influence the interpretation of numerical results:

- In order to make a 'quick guess' of a possible solution and to start the development of an algorithm to address at a later stage a difficult problem, often complicated (nonlinear) differential equations are reduced to simple (in most cases linear) versions, which results in the so-called **model error**.

- **Data errors**: the data (e.g., input data, boundary conditions, parameters) are finally obtained from experimental data and may be inaccurate themselves.

It it very important to understand and to accept that we **never can avoid** all these errors. The important aspect is to **control** these errors and to provide answers if these errors are too big to influence the interpretation of numerical simulations or if they can be assumed to be negliable. A big branch of numerical mathematics is to derive error estimates that allow to predict quantitative information about the arising errors.

## 2.5 Concepts in numerical mathematics

In introductory classes to numerical methods, we deal with concepts that are very characteristic for numerical modeling. In [205], we summarized them into seven points, which will frequently encounter us in the forthcoming chapters:

1. **Approximation**: since analytical solutions are not possible to achieve as we just learned in the previous section, solutions are obtained by **numerical approximations**.

2. **Convergence**: is a qualitative expression that tells us when members $a_n$ of a sequence $(a_n)_{n \in \mathbb{N}}$ are sufficiently close to a limit $a$. In numerical mathematics this limit is often the solution that we are looking for.

3. **Order of convergence**: While in analysis, we are often interested in the convergence itself, in numerical mathematics we must pay attention how long it takes until a numerical solution has sufficient accuracy. The longer a simulation takes, the more time and more energy (electricity to run the computer, air conditioning of servers, etc.) are consumed. Therefore, we are heavily interested in developing fast algorithms. In order to judge whether a algorithm is fast or not we have to determine the order of convergence.

4. **Errors**: Numerical mathematics can be considered as the branch 'mathematics of errors'. What does this mean? Numerical modeling is not wrong, inexact or non-precise! Since we cut sequences after a final number of steps or accept sufficiently accurate solutions obtained from our software, we need to say *how well the (unknown) exact solution by this numerical solution is approximated.* In other words, we need to determine the error, which can arise in various forms as we discussed in the previous section.

5. **Error estimation**: This is one of the biggest branches in numerical mathematics. We need to derive error formulae to judge the outcome of our numerical simulations and to measure the difference of the numerical solution and the (unknown) exact solution in a certain norm.

6. **Efficiency**: In general we can say, the higher the convergence order of an algorithm is, the more efficient our algorithm is. Therefore, we obtain faster the numerical solution to a given problem. But numerical efficiency is not automatically related to resource-effective computing. For instance, developing a parallel code using MPI (message passing interface) will definitely yield in less CPU (central processing unit) time a numerical solution. However, whether a parallel machine does need less electricity (and thus less money) than a sequential desktop machine/code is a priori unclear.

7. **Stability**: Despite being the last concept, in most developments, this is the very first step to check. How robust is our algorithm against different model and physical parameters? Is the algorithm stable with respect to different input data? This condition relates to the third condition of Hadamard. In practice non-robust or non-stable algorithms exhibit very often non-physical oscillations. For this reason, it is important to have a feeling about the physics whether oscillations in the solution are to be expected or if they are introduced by the numerical algorithm.

## 2.6 Illustration of physical oscillations versus numerical instabilities

To illustrate the numerical concept No. 7, we study an example (taken from [239]) of periodic flow interacting with an elastic beam (fluid-structure interaction).
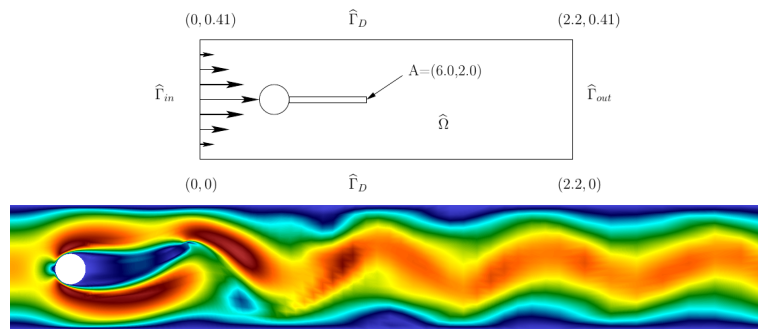


Figure 4: Fluid flow (Navier-Stokes) interacts with an elastic beam. Due to a non-symmetry of the cylinder, the beam starts oscillating. These oscillations are physical!

- Observe the tip of the elastic beam!

$\rightarrow$ Physical oscillations! Shown in red color for a 'good' numerical scheme.
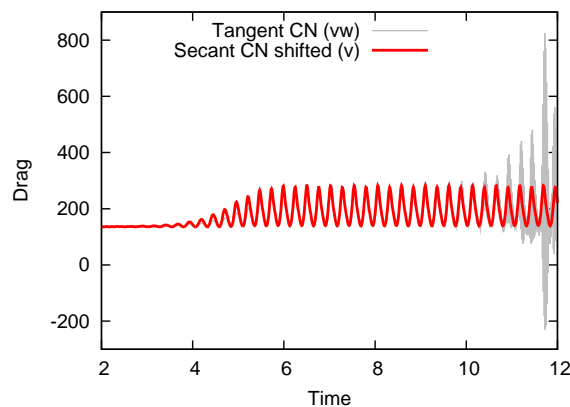


- The grey numerical scheme exhibits at some time around $t \approx 10$ micro-oscillations which are due to numerical instabilites. Finally the grey numerical scheme has a blow-up and yields garbage solutions.

## 2.7 The challenges of FSI from a mathematical perspective

After identification of possible topics that FSI-research is associated with, it remains the question:

**Why is FSI difficult?**

**Challenge 2.2.** *The answers are:*

1. *Dealing and coupling of different classes of PDEs: elliptic, parabolic, hyperbolic that require different mathematical analysis and numerical tools;*

2. *Multidomain character and interface coupling conditions;*

3. *Combining different coordinate systems (basics in continuum mechanics required);*

4. *Moving boundary, i.e., moving interface;*

5. *Well-posedness of these type of coupled systems is hard and proofs just recently have appeared;*

6. *Designing robust and efficient numerical methods that ideally provide optimal convergence order;*

7. *Since theory and numerics/simulations are each demanding themselves, it is hard (from the pure individual effort) to study both simultaneously. This is additionally hindered since practical applications violate immediately regularity assumptions on the domain or functions.*

*Let me emphasize that 1. and 2. do also pose challenges in many other multiphysics problems. It is the combination of 3. and 4. that distuinghises FSI from many other problems. Often, the physics of a problem allow us to assume small (that is to say, infinitesimal) displacements such that Lagrangian and Eulerian type coordinate systems allow for a first order approximation and thus coincide; see Section 5.1.5 for a mathematical quantification. In the classical view of fluid-structure interaction this assumption cannot be made anymore. Together with the moving interface/boundary this leads to a challenge that characterizes classical FSI. The remaining points 5., 6. and 7. are again challenging for all types of nonlinear multiphysics problems but due to 1., 2., 3. and 4. in particular demanding in FSI.*

**Warning 2.3.** *On the first view, it seems natural to consider large problems as I advertised at the beginning. And of course we should go for it. And it seems straightforward to add more and more equations to capture all physics and perform correct modeling. However, this is neither accessible from the theoretical point of view nor due to computational cost. Consider the simple example of an aircraft with Reynolds number $10^8$. A direct numerical simulation (DNS) that captures the smallest scales of order $O(Re^{9/4})$, would lead to a mesh with $10^{18}$ mesh points. This is simply infeasible with todays supercomputers [211] [4]. Consequently, we have to find approximations with less computational cost.*

**Benefit 2.4** (of studying and learning FSI techniques)**.** *Learning FSI particularly helps a lot in understanding and applying similar techniques to other coupled problems in multiphysics. Since coupled problems become more and more important, it is more and more worthy being well prepared in solid mechanics and fluid dynamics, i.e., consequently in fluid-structure interaction, since they already cover a lot of important topics.*

## 2.8 First conclusions and outline of these notes

I try to provide a mixture of basic techniques and sophisticated algorithms and examples. The main parts concentrate on continuum mechanics and forward modeling of fluid-structure interaction. Later, we also extend to sensitivity analysis including dual-weighted residual a posteriori error estimation and PDE-based optimization with flow and fluid-structure interaction and provide corresponding algorithmic details. Hopefully, everybody will identify himself with some parts of these notes and learn something new.

---

[4]This note is inspired by a talk given by Johan Jansson at IWH Heidelberg, Nov 2014.

# 3 Notation, Spaces, and Mathematical Tools

## 3.1 Domains

We consider open, bounded domains $\Omega \subset \mathbb{R}^d$ where $d = 1, 2, 3$ is the dimension. The boundary is denoted by $\partial\Omega$. The outer normal vector with respect to (w.r.t.) to $\partial\Omega$ is $n$. We assume that $\Omega$ is sufficiently smooth (i.e., a Lipschitz domain or domain with Lipschitz boundary) such that $n$ can be defined. What also works for most of our theory are convex, polyhedral domains with finite corners. For specific definitions of nonsmooth domains, we refer to the literature, e.g., [120].

## 3.2 Independent variables

A point in $\mathbb{R}^d$ is denoted by

$$x = (x_1, \ldots, x_d).$$

The variable for 'time' is denoted by $t$. The Euclidian scalar product is denoted by $(a, b)$ or via $a \cdot b$.

## 3.3 Function, vector and tensor notation

We start with

**Definition 3.1.** *Let $x$ and $y$ be variable. If $x$ is given and there is a unique associated $y$, then $y$ is a function and we write*

$$y = f(x)$$

*The variable $x$ is the 'independent' variable or also called the argument. All $x$ values form the set of definition of $f(x)$. The variable $y$ is called 'dependent'. All $y$ values form the image space of $f(x)$.*

In these notes, functions are often denoted by

$$u := u(x)$$

if they only depend on the spatial variable $x = (x_1, \ldots, x_d)$. If they depend on time and space, they are denoted by

$$u = u(t, x).$$

Usually in physics or engineering vector-valued and tensor-valued quantities are denoted in bold font size or with the help of arrows. Unfortunately in mathematics, this notation is only sometimes adopted. We continue this crime and do not distinguish scaler, vector, and tensor-valued functions. Thus for points in $\mathbb{R}^3$ we write:

$$x := (x, y, z) = \mathbf{x} = \vec{x}.$$

Similar for functions from a space $u : \mathbb{R}^3 \supseteq U \to \mathbb{R}^3$:

$$u := (u_x, u_y, u_z) = \mathbf{u} = \vec{u}.$$

And also similar for tensor-valued functions (which often have a bar or two bars under the tensor quantity) as for example the Cauchy stress tensor $\sigma_f \in \mathbb{R}^{3 \times 3}$ of a fluid:

$$\sigma_f := \underline{\sigma}_f = \begin{pmatrix} \sigma_{xx} & \sigma_{xy} & \sigma_{xz} \\ \sigma_{yx} & \sigma_{yy} & \sigma_{yz} \\ \sigma_{zx} & \sigma_{zy} & \sigma_{zz} \end{pmatrix}.$$

## 3.4 Partial derivatives

We frequently use:

$$\frac{\partial u}{\partial x} = \partial_x u$$

and

$$\frac{\partial u}{\partial t} = \partial_t u$$

and

$$\frac{\partial^2 u}{\partial t \partial t} = \partial_t^2 u$$

and

$$\frac{\partial^2 u}{\partial x \partial y} = \partial_{xy} u$$

## 3.5 Chain rule

Let the functions $g : (a, b) \to \mathbb{R}^m$ and $f : \mathbb{R}^m \to \mathbb{R}$ and its composition $h = f(g) \in \mathbb{R}$ be given and specifically $g := (t, x) := (t, x_2, x_3, \ldots, x_m)$:

$$
\begin{aligned}
D_t h(x) = D_t f(g(x)) &= D_t f(t, x) = D_t f(t, x_2, \ldots, x_k) \\
&= \sum_{k=1}^m \partial_k f(g(x)) \cdot \partial_t g_k \\
&= \sum_{k=1}^m \partial_k f(t, x_2, \ldots, x_m) \cdot \partial_t x_k, \quad \text{where } x_1 := t \\
&= \partial_t f \cdot \partial_t t + \sum_{k=2}^m \partial_k f(t, x_2, \ldots, x_k) \cdot \partial_t x_k \\
&= \partial_t f + \nabla f \cdot (\partial_t x_2, \cdots, \partial_t x_m)^T.
\end{aligned}
$$

For instance $m = 4$ means that we deal with a four-dimensional continuum $(t, x, y, z)$.

**Remark 3.2.** *See also [153][page 54 and page 93] for definitions of the chain rule.*

## 3.6 Multiindex notation

For a general description of ODEs and PDEs the multiindex notation is commonly used.

- A multiindex is a vector $\alpha = (\alpha_1, \ldots, \alpha_n)$, where each component $\alpha_i \in \mathbb{N}_0$. The order is

$$|\alpha| = \alpha_1 + \ldots + \alpha_n.$$

- For a given multiindex we define the partial derivative:

$$D^\alpha u(x) := \partial_{x_1}^{\alpha_1} \cdots \partial_{x_n}^{\alpha_n} u$$

- If $k \in \mathbb{N}_0$, we define the set of all partial derivatives of order $k$:

$$D^k u(x) := \{ D^\alpha u(x) : |\alpha| = k \}.$$

**Example 3.3.** *Let $\alpha = (2, 0, 1)$. Then $|\alpha| = 3$ and $D^\alpha u(x) = \partial_x^2 \partial_z^1 u(x)$.*

## 3.7 Gradient, divergence, trace, Laplace, rotation/curl

Well-known in physics, it is convenient to work with the **nabla-operator** to define derivative expressions. The gradient of a single-valued function $v : \mathbb{R}^n \to \mathbb{R}$ reads:

$$\nabla v = \begin{pmatrix} \partial_1 v \\ \vdots \\ \partial_n v \end{pmatrix}.$$

The gradient of a vector-valued function $v : \mathbb{R}^n \to \mathbb{R}^m$ is called **Jacobian matrix** and reads:

$$\nabla v = \begin{pmatrix} \partial_1 v_1 & \ldots & \partial_n v_1 \\ \vdots & & \vdots \\ \partial_1 v_m & \ldots & \partial_n v_m \end{pmatrix}.$$

The divergence is defined for vector-valued functions $v : \mathbb{R}^n \to \mathbb{R}^n$:

$$\text{div } v := \nabla \cdot v := \nabla \cdot \begin{pmatrix} v_1 \\ \vdots \\ v_n \end{pmatrix} = \sum_{k=1}^{n} \partial_k v_k.$$

The divergence for a tensor $\sigma \in \mathbb{R}^{n \times n}$ is defined as:

$$\nabla \cdot \sigma = \Big( \sum_{j=1}^{n} \frac{\partial \sigma_{ij}}{\partial x_j} \Big)_{1 \leq i \leq n}.$$

The trace of a matrix $A \in \mathbb{R}^{n \times n}$ is defined as

$$tr(A) = \sum_{i=1}^{n} a_{ii}.$$

**Definition 3.4** (Laplace operator)**.** *The Laplace operator of a two-times continuously differentiable scalar-valued function $u : \mathbb{R}^n \to \mathbb{R}$ is defined as*

$$\Delta u = \sum_{k=1}^{n} \partial_{kk} u.$$

**Definition 3.5.** *For a vector-valued function $u : \mathbb{R}^n \to \mathbb{R}^m$, we define the Laplace operator component-wise as*

$$\Delta u = \Delta \begin{pmatrix} u_1 \\ \vdots \\ u_m \end{pmatrix} = \begin{pmatrix} \sum_{k=1}^{n} \partial_{kk} u_1 \\ \vdots \\ \sum_{k=1}^{n} \partial_{kk} u_m \end{pmatrix}.$$

Let us also introduce the **cross product** of two vectors $u, v \in \mathbb{R}^3$:

$$\begin{pmatrix} u_1 \\ u_2 \\ u_3 \end{pmatrix} \times \begin{pmatrix} v_1 \\ v_2 \\ v_3 \end{pmatrix} = \begin{pmatrix} u_2 v_3 - u_3 v_2 \\ u_3 v_1 - u_1 v_3 \\ u_1 v_2 - u_2 v_1 \end{pmatrix}.$$

With the help of the cross product, we can define the **rotation** or **curl** :

$$\text{rot} v = \nabla \times v = \begin{pmatrix} \partial_x \\ \partial_y \\ \partial_z \end{pmatrix} \times \begin{pmatrix} v_1 \\ v_2 \\ v_3 \end{pmatrix} = \begin{pmatrix} \partial_y v_3 - \partial_z v_2 \\ \partial_z v_1 - \partial_x v_3 \\ \partial_x v_2 - \partial_y v_1 \end{pmatrix}.$$

## 3.8 Some properties of matrices

### 3.8.1 Positive definite, eigenvalues and more

Let $Q : \mathbb{R}^n \to \mathbb{R}$ be a quadratic form with $Q(x) = x^T A x$. The quadratic form (and also its representing matrix $A$) have certain names according to their properties:

- $Q$ is positive definite, when $Q(x) > 0$ for all $x \neq 0$

- $Q$ is positive semi-definite, when $Q(x) \geq 0$ for all $x$

- $Q$ is negative definite, when $Q(x) < 0$ for all $x \neq 0$

- $Q$ is negative semi-definite, when $Q(x) \leq 0$ for all $x$

- $Q$ is indefinite, when $Q$ has positive and negative values.

The relation to the eigenvalues is:

- $Q > 0$ if and only if all eigenvalues $\lambda_i > 0$

- $Q \geq 0$ if and only if all eigenvalues $\lambda_i \geq 0$

- $Q < 0$ if and only if all eigenvalues $\lambda_i < 0$

- $Q \geq 0$ if and only if all eigenvalues $\lambda_i \leq 0$

- $Q$ indefinite if and only if eigenvalues $\lambda_i < 0$ and $\lambda_i > 0$ arise.

### 3.8.2 Invariants of a matrix

The principal invariants of a matrix $A$ are the coefficients of the characteristic polynomial $\det(A - \lambda I)$. A matrix $A \in \mathbb{R}^{3 \times 3}$ has three principal invariants; namely $i_A = (i_1(A), i_2(A), i_3(A))$ with

$$\det(\lambda I - A) = \lambda^3 - i_1(A)\lambda^2 + i_2(A)\lambda - i_3(A).$$

Let $\lambda_1, \lambda_2, \lambda_3$ be the eigenvalues of $A$, we have

$$i_1(A) = \operatorname{tr}(A) = \lambda_1 + \lambda_2 + \lambda_3,$$
$$i_2(A) = \frac{1}{2}(\operatorname{tr} A)^2 - \operatorname{tr}(A)^2 = \lambda_1\lambda_1 + \lambda_1\lambda_3 + \lambda_2\lambda_3,$$
$$i_3(A) = \det(A) = \lambda_1\lambda_2\lambda_3.$$

**Remark 3.6.** *If two different matrices have the same principal invariants, they also have the same eigenvalues.*

**Remark 3.7** (Cayley-Hamilton)**.** *Every second-order tensor (i.e., a matrix) satisfies its own characteristic equation:*
$$A^3 - i_1 A^2 + i_2 A - i_3 I = 0.$$

## 3.9 Vector spaces

Let $\mathbb{K} = \mathbb{R}$. In fact, $\mathbb{K} = \mathbb{C}$ would work as well and any general field. But we restrict our attention in the entire lecture notes to real numbers $\mathbb{R}$.

**Definition 3.8** (Vector space)**.** *A **vector space** or **linear space** over a field $\mathbb{K}$ is a nonempty set $X$ (later often denotes by $V, U$ or also $W$). The space $X$ contains elements $x_1, x_2, \ldots$ which are the so-called **vectors**. We define two algebraic operations:*

- *Vector addition: $x + y$ for $x, y \in X$.*

- *Multiplication of vectors with scalars: $\alpha x$ for $x \in X$ and $\alpha \in \mathbb{K}$.*

*These operations satisfy the usual laws that they are commutative, associative, and satisfy distributive laws.*

## 3.10 Scalar product

Let $V$ be a vector space over $\mathbb{R}$ (note $\mathbb{C}$ would work as well). A mapping $(\cdot, \cdot) : V \times V \to \mathbb{R}$ is a scalar product (or inner product) if

1. $(u + v, w) = (u, w) + (v, w)$ for all $u, v, w \in V$

2. $(\alpha u, v) = \alpha(u, v)$ for all $u, v \in V$ and $\alpha \in \mathbb{R}$

3. $(u, v) = \overline{(v, u)}$ for all $u, v \in V$

4. $(u, u) \geq 0$ for all $u \in V$

5. $(u, u) = 0$ if and only if when $u = 0$.

Moreover:

1. $(u, v + w) = (u, v) + (u, w)$ for all $u, v, w \in V$

2. $(u, \alpha v) = \bar{\alpha}(u, v)$ for all $u, v \in V$ and $\alpha \in \mathbb{R}$

For real-valued functions, the scalar product is **bilinear** and in the complex-valued case the scalar product is called **sesquilinear**.

It holds:

**Proposition 3.9** (Cauchy-Schwarz). *Let $V$ be a vector space with $(\cdot, \cdot)$. Then, it holds*

$$|(u, v)| \leq \|u\|\|v\| \quad \text{for all } u, v \in V.$$

## 3.11 Normed spaces

Let $X$ be a linear space. The mapping $|| \cdot || : X \to \mathbb{R}$ is a norm if

| | | |
|---|---|---|
| i) | $\|x\| \geq 0 \quad \forall x \in X$ | (Positivity) |
| ii) | $\|x\| = 0 \Leftrightarrow x = 0$ | (Definiteness) |
| iii) | $\|\alpha x\| = |\alpha| \, \|x\|, \quad \alpha \in \mathbb{K}$ | (Homogeneity) |
| iv) | $\|x + y\| \leq \|x\| + \|y\|$ | (Triangle inequality) |

A space $X$ is a normed space when the norm properties are satisfied. If condition ii) is not satisfied, the mapping is called a semi-norm.

## 3.12 Linear mappings

Let $\{U, \| \cdot \|_U\}$ and $\{V, \| \cdot \|_V\}$ be normed spaces over $\mathbb{R}$.

**Definition 3.10** (Linear mappings). *A mapping $T : U \to V$ is called **linear** or **linear operator** when*

$$T(u) = T(au_1 + bu_2) = aT(u_1) + bT(u_2),$$

*for $u = au_1 + bu_2$ and for $a, b \in \mathbb{R}$.*

**Example 3.11.** *We discuss two examples:*

1. *Let $T(u) = \Delta u$. Then:*

$$T(au_1 + bu_2) = \Delta(au_1 + bu_2) = a\Delta u_1 + b\Delta u_2 = aT(u_1) + bT(u_2).$$

*Thus, $T$ is linear.*

*2. Let $T(u) = (u \cdot \nabla)u$. Then:*

$$T(au_1 + bu_2) = ((au_1 + bu_2) \cdot \nabla)(au_1 + bu_2) \neq a(u_1 \cdot \nabla)u_1 + b(u_2 \cdot \nabla)u_2 = aT(u_1) + bT(u_2).$$

*Here, $T$ is nonlinear.*

**Exercise 1.** *Classify $T(u) = |u|$.*

**Definition 3.12** (Linear functional)**.** *A mapping $T : U \to V$ with $V = \mathbb{R}$ is called **linear functional**.*

**Definition 3.13.** *A mapping $T : U \to V$ is called **continuous** when*

$$\lim_{n \to \infty} u_n = u \quad \Rightarrow \quad \lim_{n \to \infty} Tu_n = Tu.$$

**Definition 3.14.** *A linear operator $T : U \to V$ is called **bounded**, when the following estimate holds true:*

$$\|Tu\|_V \leq c\|u\|_U.$$

**Theorem 3.15.** *A linear operator is bounded if and only if it is continuous.*

*Proof.* See [238], Satz II.1.2. □

**Definition 3.16.** *Let $T : U \to V$ be a linear and continuous operator. The norm of $T$ is defined as*

$$\|T\| = \sup_{\|u\|_U = 1} \|Tu\|_V.$$

*Since a linear $T$ is bounded (when continuous) there exists $\|Tu\|_V \leq c\|u\|_U$ for all $u \in U$. The smallest number for $c$ is $c = \|T\|$.*

**Definition 3.17.** *The linear space of all linear and bounded operators from $U$ to $V$ is denoted by*

$$L(U, V).$$

*The norm of $L(U, V)$ is the operator norm $\|T\|$.*

**Definition 3.18** (Dual space)**.** *The linear space of all linear, bounded functionals on $U$ (see Def. 3.12) is the dual space, denoted by $U^*$, i.e.,*

$$U^* = L(U, \mathbb{R}).$$

*For $f \in U^*$, the norm is given by:*

$$\|f\|_{U^*} = \sup_{\|u\|_U = 1} |f(u)|.$$

*The dual space is always a Banach space; see again [238].*

## 3.13 Domains and boundaries

Let $\Omega \subseteq \mathbb{R}^d, d \in \{2, 3\}$ be a bounded domain with boundary $\partial\Omega$. We generally assume the boundary to be Lipschitzian. A precise definition is given in [1, 120]. The outer unit normal vector to $\partial\Omega$ is denoted by $n$.
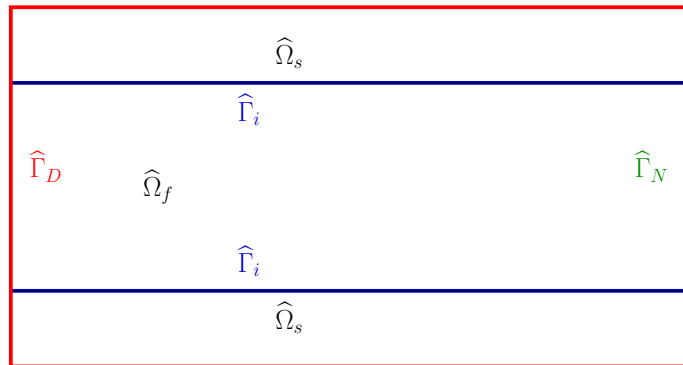


Figure 5: Definitions of domains and boundaries.

We denote by $\Omega := \Omega(t) \subset \mathbb{R}^d$, $d = 2, 3$, the domain of the fluid-structure interaction problem. This domain consists of two time-dependent subdomains $\Omega_f(t)$ and $\Omega_s(t)$. The interface between both domain is denoted by $\Gamma_i(t) = \partial\Omega_f(t) \cap \partial\Omega_s(t)$. The initial (or later reference) domains are denoted by $\widehat{\Omega}_f$ and $\widehat{\Omega}_s$, respectively, with the interface $\widehat{\Gamma}_i = \partial\widehat{\Omega}_f \cap \partial\widehat{\Omega}_s$. Furthermore, we denote the outer boundary by $\partial\widehat{\Omega} = \widehat{\Gamma} = \widehat{\Gamma}_D \cup \widehat{\Gamma}_N$ where $\widehat{\Gamma}_D$ and $\widehat{\Gamma}_N$ denote Dirichlet and Neumann boundaries, respectively. For the convenience of the reader and when we expect no confusion, we omit the explicit time-dependence and we use $\Omega := \Omega(t)$ to indicate time-dependent domains. Throughout these notes, we indicate with 'f' and 's' suffixes, fluid and structure related terms, respectively.

## 3.14 Weak derivatives

The motivation to define weak derivatives is based on the integration by parts formula. We have

**Definition 3.19** (Weak derivative). *Let $u, v \in L^1_{loc}$ and $\alpha$ a multi-index. Then $v$ is the $\alpha$-th weak paritial derivative of $u$ denoted by $\nabla^\alpha u = v$ if*

$$\int_\Omega u \nabla^\alpha \phi \, dx = (-1)^{|\alpha|} \int_\Omega v\phi \, dx,$$

*holds true for all test functions $\phi \in C^\infty_c(\Omega)$.*

**Proposition 3.20** (Uniqueness of weak derivatives). *A weak $\alpha$-th partial derivative of $u$ is unique if it exists.*

## 3.15 Function spaces on fixed domains

We adopt standard notation for the usual Lebesgue and Sobolev spaces [1, 77, 250]. Let $X \subset \mathbb{R}^d$, $d = 2, 3$ be a time-independent domain. For instance, we later use $X := \widehat{\Omega}_f$ or $X := \widehat{\Omega}_s$. We indicate by $L^p(X), 1 \leq p \leq \infty$ the standard Lebesgue space that consists of measurable functions $u$, which are Lebesgue-integrable to the $p$-th power. The set $L^p(X)$ forms a Banach space with the norm $\|u\|_{L^p(X)}$.

$$\|u\|_{L^p(X)} := \left( \int_X |u(x)|^p \, \mathrm{d}x \right)^{\frac{1}{p}}, \quad 1 \leq p < \infty,$$
$$\|u\|_{L^\infty(X)} := \operatorname{ess\,sup} |u(x)|.$$

We obtain the Hilbert space $L^2(X)$ for $p = 2$, equipped with the inner product

$$(u, v)_{L^2(X)} := \int_X u(x)v(x) \, \mathrm{d}x.$$

The Sobolev space $W^{m,p}(X), m \in \mathbb{N}, 1 \leq p \leq \infty$ is the space of functions in $L^p(X)$ that have distributional derivatives of order up to $m$, which belong to $L^p(X)$. This space is equipped with the norm

$$\|u\|_{W^{m,p}(X)} := \left( \sum_{|\alpha| \leq m} \|D^\alpha u\|^p_{L^p(X)} \right)^{\frac{1}{p}}, \quad 1 \leq p < \infty,$$
$$\|u\|_{W^{m,\infty}(X)} := \max_{|\alpha| \leq m} \|D^\alpha u\|_{L^\infty(X)}.$$

The symbol $\alpha = (\alpha_1, \ldots, \alpha_d) \in \mathbb{N}^d$ denotes a multi-index with the properties

$$|\alpha| := \sum_{j=1}^d \alpha_j, \quad D^\alpha := \frac{\partial^{|\alpha|}}{\partial x_1^{\alpha_1} \cdots \partial x_d^{\alpha_d}}.$$

For $p = 2, H^m(X) := W^{m,2}(X)$ is a Hilbert space equipped with the norm with the inner product

$$(u, v)_{H^m(X)} := \sum_{|\alpha| \leq m} (D^\alpha u, D^\alpha v)_{L^2(X)},$$

and the norm $|| \cdot ||_{H^m(X)}$ [250]. The semi-norms are defined by

$$|u|_{W^{m,p}(X)} := \left( \sum_{|\alpha|=m} \|D^\alpha u\|_{L^p(X)}^p \right)^{\frac{1}{p}}, \quad 1 \le p < \infty,$$
$$|u|_{W^{m,\infty}(X)} := \max_{|\alpha|=m} \|D^\alpha u\|_{L^\infty(X)}.$$

Finally, we indicate the subspace $W^{m,p}(X)$ of functions with zero trace on $\partial X$ by $W_0^{m,p}(X)$. Specifically, we define $H_0^1(X) = \{u \in H^1(X) : u = 0 \text{ on } \Gamma_D \subset \partial X\}$. We use frequently the short notation

$$\hat{V}_X := H^1(X), \quad \hat{V}_X^0 := H_0^1(X),$$

and

$$\hat{L}_X := L^2(X), \quad \hat{L}_X^0 := L^2(X)/\mathbb{R}.$$

In particular (see [220]):

$$\hat{L}_X^0 := L^2(X)/\mathbb{R} = \left\{ f \in L^2(\Omega) : \int_\Omega f \, dx = 0 \right\}.$$

**Definition 3.21** (Spaces for fluid-structure interaction)**.** *We set:*

$$\hat{L}_f := L^2(\widehat{\Omega}_f), \quad \text{Pressure space}$$
$$\hat{L}_s := [L^2(\widehat{\Omega}_s)]^d,$$
$$\hat{L}_f^0 := L^2(\widehat{\Omega}_f)/\mathbb{R},$$
$$\hat{L}_s^0 := L^2(\widehat{\Omega}_s)/\mathbb{R},$$
$$\hat{V}_f^0 := \hat{V}_{\widehat{\Omega}_f}^0,$$
$$\hat{V}_s^0 := \hat{V}_{\widehat{\Omega}_s}^0.$$

*Specifically, we introduce the trial and the test space of the velocity variables (recall that the velocity is d-dimensional) in the fluid domain,*

$$\hat{V}_{f,\hat{v}}^0 := \{\hat{v}_f \in [H_0^1(\widehat{\Omega}_f)]^d : \hat{v}_f = \hat{v}_s \text{ on } \widehat{\Gamma}_i\}.$$

*Moreover, we introduce the trial and the test spaces for the mesh movement using ALE[5] in the fluid domain,*

$$\hat{V}_{f,\hat{u}}^0 := \{\hat{u}_f \in [H_0^1(\widehat{\Omega}_f)]^d : \hat{u}_f = \hat{u}_s \text{ on } \widehat{\Gamma}_i\},$$
$$\hat{V}_{f,\hat{u},\widehat{\Gamma}_i}^0 := \{\hat{\psi}_f \in [H_0^1(\widehat{\Omega}_f)]^d : \hat{\psi}_f = \hat{\psi}_s \text{ on } \widehat{\Gamma}_i \subset \partial X\}.$$

**Remark 3.22.** *In formulating fluid-structure interaction using variational monolithic coupling (e.g., [73, 74, 139] and see also these lecture notes) it does make sense to combine the two velocity variables for the fluid and solid to one global variable. In this case we define one momentum equation. The velocity spaces are then extended from $\widehat{\Omega}_f$ and $\widehat{\Omega}_s$ to the entire domain $\widehat{\Omega}$ such that we can work with global $H^1$ functions. Thus, we define:*

$$\hat{V}^0 := \{\hat{v} \in H^1(\widehat{\Omega})^d : \hat{v} = 0 \text{ on } \widehat{\Gamma}_{in} \cup \widehat{\Gamma}_D\}. \tag{1}$$

*By this choice, the kinematic and dynamic coupling conditions are automatically satisfied in a variational sense. Alternative definitions with a similar aim can be found, for example, in [53, 84, 86]. Morover such a formulation does also allow for a very convenient programming code as shown in [244].*

The dual space of $H_0^m(X)$ is denoted by $H^{-m}(X)$. We indicate the duality pairing between $H^{-m}(X)$ and $H_0^m(X)$ by

$$\langle f, u \rangle, \quad f \in H^{-m}(X), \quad u \in H_0^m(X).$$

---

[5]Arbitrary Lagrangian-Eulerian. Precise definition later in Section 7.3.

The dual space is a Banach space with the norm

$$\|f\|_{H^{-m}(X)} := \sup_{\varphi \in H_0^m(X)} \frac{\langle f, \varphi \rangle}{|\varphi|_{H^m(X)}}.$$

For the definition of space-time functions, let $I := (0, T)$ with $0 < T < \infty$ a bounded time interval. Let,

$$v(x, t), \quad \text{with } (x, t) \in X \times I$$

be such a function. For any Banach space $X$ and $1 \leq p \leq \infty$, the set $L^p(I, X)$ denotes the space of $L^p$-integrable functions $v$ from $I$ into $X$. This is a Banach space with the norm

$$\|v\|_{L^p(I,X)} := \left( \int_I \|v(t)\|_X^p \, dt \right)^{\frac{1}{p}}, \quad 1 \leq p < \infty,$$

$$\|v\|_{L^\infty(I,X)} := \text{ess sup}_{t \in I} \|v(t)\|_X.$$

Moreover, we also need the space

$$H^1(I, X) = \left\{ v \in L^2(I, X) \mid \partial_t v \in L^2(I, X) \right\}.$$

The space

$$C(I; X)$$

contains all continuous functions $u : I \to X$ with

$$\|u\|_{C(I;X)} := \max_{0 \leq t \leq T} \|u(t)\| < \infty.$$

**Definition 3.23** (Weak derivative of space-time functions)**.** *Let $u \in L^1(I; X)$. A function $v \in L^1(I; X)$ is the weak derivative of $v$, denoted as*

$$\partial_t u = v$$

*if*

$$\int_0^T \partial_t \varphi(t) u(t) \, dt = - \int_0^T \varphi(t) v(t) \, dt$$

*for all test functions $\varphi \in C_c^\infty(I)$.*

In particular, the following result holds:

**Theorem 3.24** ([77])**.** *Assume $v \in L^2(I, H_0^1)$ and $\partial_t v \in L^2(I, H^{-1})$. Then, $v$ is continuous in time, i.e.,*

$$v \in C(I, L^2)$$

*(after possible redefined on a set of measure zero). Furthermore, the mapping*

$$t \mapsto \|v(t)\|_{L^2(X)}^2$$

*is absolutely continuous with*

$$\frac{d}{dt} \|v(t)\|_{L^2(X)}^2 = 2 \langle \frac{d}{dt} v(t), v(t) \rangle$$

*for a.e. $0 \leq t \leq T$.*

*Proof.* See Evans [77], Theorem 3 in Section 5.9.2. □

The importance of this theorem lies in the fact that now the point-wise prescription of initial conditions does make sense in weak formulations.

More details of these spaces by means of the Bochner integral can be found in [67, 250] and also [77].

Let $\gamma$ be an open regular, i.e., Lipschitz continuous, and measurable subset of $\partial X$. We denote with $H^{1/2}(\gamma)$ the space of functions defined on $\gamma$ that are traces of functions in $H^1(X)$ [112]. Furthermore, Poincaré's inequality [112] reads

$$\|u\|_{L^2(X)}^2 \leq C_P(X) \|\nabla u\|_{L^2(X)}^2 \quad \forall u \in H_0^1(X)^d,$$

with a positive constant $C_P(X)$ depending on the domain $X$. We also remind the trace inequality [61, 250]:

**Theorem 3.25.** *Let $\Omega$ be sufficiently regular with polygonal or $C^1$ boundary. For $1 \leq p < \infty$ we have*

$$tr \in L(W^{1,p}, L^{p^*}) \quad \Leftrightarrow \quad \|\cdot\|_{L^{p^*}} \leq C_T(X)\|\cdot\|_{W^{1,p}},$$

*with $\frac{1}{p^*} = \frac{1}{p} - \frac{1}{(d-1)}(\frac{p-1}{p})$ if $1 \leq p < d$. Specifically, for $p^* = 4$, it does hold for all functions with $1 \leq p \leq 4$:*

$$\|u\|_{L^2(\partial X)} \leq C_T(X)\|u\|_{H^1(X)} \quad \forall u \in H^1(X)^d,$$

*with a positive constant $C_T(X)$ depending on the domain $X$. This result gives sense to Dirichlet conditions whenever we seek for a solution in $W^{1,p}$. Specifically, the trace operator*

$$\gamma_0 : W^{1,p}(\Omega) \mapsto L^{p^*}(\partial\Omega)$$

*is not surjective and consquently, the functions of $L^2(\Gamma)$ which are traces of $H^1$-functions is a subspace of $L^2(\Gamma)$ that is denoted as $H^{1/2}(\Gamma)$.*

## 3.16 Conventions for vector-valued functions

For the corresponding spaces of the $d$-dimensional vector-valued functions, we bear the notation $L^p(X)^d$, $H^1(X)^d$, etc. in mind, equipped with the usual product norm. The scalar products and corresponding norms are defined in an analogous way as those for scalar functions. We expect that the reader is familiar with the Navier-Stokes equations and structural mechanics in $d$-dimensions. Consequently, we do not differentiate between one-dimensional and $d$-dimensional spaces and the corresponding solution variables. Finally, we remark that we will abuse notation for vector-valued function spaces:

$$\varphi \in V_f^0 \quad \text{means } \varphi \in (V_f^0)^d \quad \text{means } \begin{pmatrix} \varphi_1 \\ \varphi_2 \\ \vdots \\ \varphi_d \end{pmatrix} \in (V_f^0)^d \quad \text{means } \begin{pmatrix} \varphi_1 \\ \varphi_2 \\ \vdots \\ \varphi_d \end{pmatrix} \in \begin{pmatrix} V_f^0 \\ V_f^0 \\ \vdots \\ V_f^0 \end{pmatrix}.$$

## 3.17 Notational conventions

For the reader's convenience, we often use

$$(\cdot,\cdot)_X := (\cdot,\cdot)_{L^2(X)} \quad \text{and} \quad \|\cdot\|_X := \|\cdot\|_{L^2(X)},$$

where $X = \Omega_f, \Omega_s$ or the corresponding spaces in the fixed reference domains $\widehat{X} = \widehat{\Omega}_f, \widehat{\Omega}_s$. Furthermore, in time-dependent spaces in which we need explicitly the dependence on time, we use

$$(\cdot,\cdot)_{X^n} := (\cdot,\cdot)_{L^2(X^n)} \quad \text{and} \quad \|\cdot\|_{X^n} := \|\cdot\|_{L^2(X^n)}.$$

In other cases, we denote explicitly the used scalar product and the induced norm, for instance,

$$(\cdot,\cdot)_{H^1(X^n)} \quad \text{and} \quad \|\cdot\|_{H^1(X^n)}.$$

For matrix or tensor valued functions, we interpret the scalar product as follows:

**Definition 3.26** (Scalar product notation for tensor-valued functions). *Let $A, B \in \mathbb{R}^{n\times n}$. Then, the $L^2$ scalar product is denoted as:*

$$(A,B) := \int_X A : B\, dx,$$

*where the colon-operator has been defined above.*

## 3.18 Function spaces on moving domains

For the stability analysis of our equations, it is convenient to work in time-dependent domains. Thus, we introduce (on a moving domain $\Omega$):

$$V := \{v : \Omega \times I \to \mathbb{R}^d : v \circ \hat{\mathcal{A}} = \hat{v}, \ \hat{v} \in [H^1(\widehat{\Omega})]^d\},$$

$$L := \{p : \Omega \times I \to \mathbb{R} : p \circ \hat{\mathcal{A}} = \hat{p}, \ \hat{p} \in [L^2(\widehat{\Omega})]\},$$

where $\hat{\mathcal{A}} : \widehat{\Omega} \to \Omega$ denotes the ALE transformation that is explained below. The admissibility of the spaces is given by the relations

$$V \subseteq [H^1(\Omega)]^d, \quad \text{and} \quad L \subseteq [L^2(\Omega)].$$

This relation was proven by Formaggia and Nobile [91] and is recalled in Section 7.3.4. A deeper discussion of fluid-structure interaction in moving domains can be found in Formaggia et al. [94] (chapter 3) and the many references cited therein.

## 3.19 Inequalities

The Hölder inequality reads:

**Proposition 3.27** (Hölder's inequality)**.** *Let $1 \leq p \leq \infty$ and $\frac{1}{p} + \frac{1}{q} = 1$ (with the convention $\frac{1}{\infty} = 0$). Let $f \in L^p$ and $g \in L^q$. Then,*

$$fg \in L^1,$$

*and*

$$\|fg\|_{L^1} \leq \|f\|_{L^p} \|g\|_{L^q}.$$

*Proof.* See Werner [238]. □

**Corollary 3.28** (Cauchy-Schwarz inequality)**.** *Set $p = q = 2$. Then*

$$\|fg\|_{L^1} \leq \|f\|_{L^2} \|g\|_{L^2}.$$

**Proposition 3.29** (Minkowski's inequality)**.** *Let $1 \leq p \leq \infty$ and let $f \in L^p$ and $g \in L^p$. Then,*

$$\|f + g\|_{L^p} \leq \|f\|_{L^p} + \|g\|_{L^p}.$$

**Proposition 3.30** (Cauchy's inequality with $\varepsilon$)**.**

$$ab \leq \varepsilon a^2 + \frac{b^2}{4\varepsilon}$$

*for $a, b > 0$ and $\varepsilon > 0$. For $\epsilon = \frac{1}{2}$, the original Cauchy inequality.*

**Proposition 3.31** (Young's inequality)**.** *Let $1 < p, q < \infty$ and $\frac{1}{p} + \frac{1}{q} = 1$. Then,*

$$ab \leq \frac{a^p}{p} + \frac{b^q}{q}, \quad a, b > 0.$$

## 3.20 Gauss' divergence theorem, Green's theorem, integration by parts

**Proposition 3.32** (Gauss' divergence theorem / Gauss-Green theorem)**.** *Let $\Omega \subset \mathbb{R}^n$ be bounded and open, and let $\partial\Omega$ of class $C^1$. Let $f \in C^1(\bar{\Omega})$. Then,*

$$\int_\Omega divf \, dx = \int_{\partial\Omega} f \cdot n \, ds. \tag{2}$$

*The outer normal of $\partial\Omega$ is given by $n$.*

**Proposition 3.33** (Partial integration)**.** *Let $f, g \in C^1(\bar{\Omega})$. Then,*

$$\int_\Omega \partial_i f\, g\, dx = -\int_\Omega f \partial_i g\, dx + \int_{\partial\Omega} f g n_i\, ds \quad for\ i = 1, \dots, n.$$

*Proof.* Apply Gauss' divergence theorem component wise. □

**Proposition 3.34** (Green's theorem)**.** *Let $f, g \in C^2(\overline{\Omega})$. Then,*

$$\int_\Omega \nabla f \cdot \nabla g\, dx = -\int_\Omega f \Delta g\, dx + \int_{\partial\Omega} \partial_n g f\, ds. \tag{3}$$

*Proof.* Set $g := \partial_i g$ in the integration by parts formula. □

## 3.21 Gâteaux and Fréchet derivatives, the inverse function theorem

Given a function $f : X \to Y$ and $f'(a) \in L(X, Y)$ where $L$ is as usually the space of linear and continuous operators. Recall that $L(X, \mathbb{R}) =: X'$ is the dual space.

**Definition 3.35** (Gâteaux/directional derivative)**.** *The derivative $f'(a)$ of a function $f$ is computed as action on vectors of $X$, i.e.,*

$$f'(a)\delta a = \lim_{\varepsilon \to 0} \frac{f(a + \varepsilon \delta a) - f(a)}{\varepsilon} = \frac{d}{d\varepsilon} f(a + \varepsilon \delta a)|_{\varepsilon = 0} \in Y.$$

*The element $f'(a)\delta a \in Y$ is called the directional derivative or Gâteaux derivative of the function $f$ into the direction of the vector $\delta a \in X$ at $a \in X$. We notice that the choice of the direction $\delta a \in X$ is arbitrary.*

In a Hilbert space, we have the special case:

$$f'(a)(\delta a) = (\nabla f(a), \delta a) \quad \forall \delta a \in X$$

where we denote $\nabla f(a)$ as the gradient.

**Definition 3.36** (Fréchet derivative)**.** *A mapping $f : \Omega \subset X \to Y$ ($\Omega$ open) is called Fréchet differentiable at a point $a \in \Omega$ if there exists an element $f'(a)$ of the space $L(X, Y)$ such that*

$$f(a + h) = f(a) + f'(a)h + o(h),$$

*with $o(h) = \|h\|\varepsilon(h)$ with $\lim_{h \to 0} \varepsilon(h) = 0$ in $Y$. Then, the element $f'(a) \in L(X, Y)$ is called the Fréchet derivative at $a \in \Omega$. The Fréchet derivative is necessarily unique and does imply that $f$ is continuous at $a \in \Omega$.*

**Remark 3.37.** *If the directional derivative exists for all directions, we call the derivative Gateaux-derivative. Moreover, the Fréchet-derivative is a stronger concept of derivatives; consequently, each Fréchet derivative is also a Gateaux-derivative.* ⋄

**Definition 3.38** (Isomorphism and isometry)**.** *A continuous, linear operator $T : \Omega \to Y$ is an isomorphism if*

- *$T$ is bijective (i.e., injective and surjective; one-to-one and onto);*

- *$T^{-1}$ is continuous.*

*If furthermore $\|T(x)\| = \|x\|$, the operator $T$ is called an isometry. The latter propery immediately implies that $T$ is injective.*

Having established the Fréchet derivative, we can define the space of $m$-times continuously differentiable functions as $\mathcal{C}^m$.

**Definition 3.39** ($\mathcal{C}^m$-diffeomorphism)**.** *Let $m \geq 1$. A mapping $T : \Omega \to Y$ is a $\mathcal{C}^m$-diffeomorphism if*

- *$T \in \mathcal{C}^m$;*

- *$T$ is bijective;*

- *the inverse mapping $T^{-1} : T(\Omega) \to \Omega$ is also of class $\mathcal{C}^m$.*

We later require that mappings in continuum mechanics and fluid-structure interaction modeling are of class $C^1$; namely $T \in C^1$ and $\hat{\mathcal{A}} \in C^1$.

Implicitly defined functions or mappings $f(x,y) = 0$ are very important since often an explicit solution cannot be obtained. In order to show solvability of such a construct, the implicit function theorem and a subsequent results, the inverse function theorem are provide essential techniques. In particular, the existence of a solution of an implicit function can be shown to be a $\mathcal{C}^m$-diffeomorphism with the help of the inverse function theorem.

**Theorem 3.40** (Inverse function theorem). *Let us assume $f \in C^1(\Omega; \mathbb{R}^n)$ and the Jacobian determinant $J := det(Df) \neq 0$, where $Df$ denotes the Jacobian of $f$. Then, there exists an open set $V \subset U$ with $x_0 \in V$ and an open set $W \subset \mathbb{R}^n$ with $z_0 \in W$ such that*

- *the mapping $f : V \to W$ is bijective*

- *the inverse function $f^{-1} : W \to V$ is of class $C^1$*

- *If $f \in C^k$, then $f^{-1} \in C^k$ for all $k \geq 2$.*

A fundamental theorem in analysis and in particular in ALE fluid-structure interaction is the transformation theorem that tells us how to transform integrals and derivatives from one domain into another domain:

**Theorem 3.41** (Integration by substitution / Transformation theorem). *Let $\widehat{\Omega} \subset \mathbb{R}^N$ be open. Let $T$ be a diffeomorphism in $\mathbb{R}^N$. Let $1 \leq p \leq +\infty$. Then $f \in L^p(T(\widehat{\Omega}))$ if and only if $f \circ T \in L^p(\widehat{\Omega})$ and we have*

$$\int_{T(\widehat{\Omega})} f \, dx = \int_{\widehat{\Omega}} f \circ T |det(\nabla T)| \, dx.$$

*Moreover, if $f \in W^{1,p}(T(\widehat{\Omega}))$ if and only if $f \circ T \in W^{1,p}(\widehat{\Omega})$ and we have*

$$(\nabla f) \circ T = ((\nabla T)^{-1})^T \nabla (f \circ T).$$

## 3.22 Functional analysis

Let us now introduce the classical projection from Lax-Milgram from functional analysis, which can be used to establish existence and uniquenss of a weak solution to (linear) boundary value problems.

**Theorem 3.42** (Lax-Milgram (1954)). *Let $W$ be a real Hilbert space with norm $\| \cdot \|$ and let $\langle \cdot \rangle$ denote the pairing of $W$ with its dual space $W^*$. Furthermore, let $A(u, \phi)$ be a bilinear continuous form on $W \times W$, i.e.,*

$$|A(u, \phi)| \leq \alpha \|u\| \, \|\phi\| \quad for \, u, \phi \in W, \quad \alpha > 0,$$

*and which is coercive, i.e.,*

$$A(u, u) \geq \beta \|u\|^2, \quad for \, u \in W, \quad \beta > 0.$$

*Additionally, let $f \in W^*$ be a bounded linear functional on $W$, i.e,*

$$|\langle f, \phi \rangle| \leq \gamma \|f\| \, \|\phi\|, \quad \phi \in W, \quad \gamma > 0.$$

*Then, there exists a unique element $u \in W$ such that*

$$A(u, \phi) = \langle f, \phi \rangle \quad \forall \phi \in W.$$

*Proof.* For proofs we refer for example to [77, 220]. $\qquad\square$

The Lax-Milgram is in particular useful for nonsymmetric boundary value problems. For symmetric cases, i.e., $A(u, \phi) = A(\phi, u)$, the Lax-Milgram theorem still applies of course, but here we could have used a more simple and elegant theorem from functional analysis, i.e., the Riesz representation theorem in a Hilbert space.

The key observation is that in this case $u \mapsto \sqrt{a(u,u)}$ defines a scalar product; and consequently a norm because we work in a Hilbert space. Then, there exists a unique element $l \in V$ such that

$$L(\phi) = a(l, \phi) \quad \forall \phi \in V.$$

and therefore $l = u$ is a unique solution to the original problem. For a proof the Riesz representation theorem, we refer to [48].

**Theorem 3.43.** *Let $l : V \to \mathbb{R}$ be a continuous linear functional on a Hibert space $V$. Then there exists a unique element $w \in V$ such that*

$$(w, \phi) = l(\phi) \quad \forall \phi \in V.$$

*Moreover, this operation is an isometry, that is to say, $\|l\|_* = \|w\|$.*

Thus, we have justified the following:

**Theorem 3.44.** *Assume that $A(u, \phi)$ is symmetric. Then, Theorem 3.42 holds true. Additionally, and due to the symmetry, seeking $u \in V$ is equivalent to the energy problem:*

$$J(u) = \inf_{\phi \in V} J(\phi)$$

*where*

$$J : \phi \in V \mapsto J(\phi) := \frac{1}{2} A(\phi, \phi) - F(\phi)$$

*with $F(\phi) = \langle f, \phi \rangle$.*

## 3.23 Main notation

Notation of scalar products, linear forms and bilinear forms. Let $\Omega$ be a domain in $\mathbb{R}^n$ with the usual properties to ensure integrability and differentiability:

1. Let $x, y \in V \subset R^n$. Then the scalar product is denoted by:

$$(x, y) = \int_\Omega xy \, dz \quad x, y \in V.$$

2. Let $X, Y \in V \subset R^{n \times n}$. Then the scalar product for a matrix is denoted by:

$$(X, Y) = \int_\Omega X : Y \, dz \quad X, Y \in V.$$

   Here, : stands for the Frobenius scalar product.

3. Often, we use: Find $u \in V$ such that

$$a(u, \varphi) = l(\phi) \quad \forall \varphi \in V.$$

   Here $a(u, \varphi) : V \times V \to \mathbb{R}$ is a bilinear form and $l(\varphi) \in V^*$ is a linear form (linear functional).

4. For nonlinear problems, the solution variable $u \in V$ is nonlinear while the test function is still linear. Here we use the notation: Find $u \in V$ such that

$$a(u)(\varphi) = l(\varphi) \quad \forall \varphi \in V.$$

   Here, $a(u)(\varphi)$ is a so-called semi-linear form.

5. For (linear) PDE systems, my notation is: Find $U \in X$ such that

$$A(U, \Psi) = F(\Psi) \quad \forall \Psi \in X.$$

6. For nonlinear PDE systems, my notation is: Find $U \in X$ such that

$$A(U)(\Psi) = F(\Psi) \quad \forall \Psi \in X.$$

# 4 Partial Differential Equations

Fluid-structure interaction is intended to model coupled physical phenomena that can be modeled in terms of continuum mechanics. The latter concept leads to equations that are described in terms of partial differential equations (PDEs). Consequently, we first review the basics of PDE theory in the present section and continue in Section 5 with physics. We recommend to look into [247].

Let us start with some definitions:

**Definition 4.1** (PDE [77])**.** *A partial differential equation (PDE) is an equation involving an unknown function with at least two variables and certain of its partial derivatives.* ⋄

**Definition 4.2** (Coupled system of PDEs)**.** *A coupled system of PDEs is a collection of at least two PDEs that interact through parameters, right-hand side forces or interface terms.* ⋄

**Definition 4.3.** *FSI is a nonlinear, nonstationary, coupled PDE system.*

Unfortunately[6], there is no general theory for studying PDEs and consequently, there is no common framework to approximate and compute these PDEs on a computer.

Apart from important PDE-analysis questions (which are discussed in standard textbooks such as [77, 250]) regarding to well-posedness, strong and weak solutions and their regularity, the **principal difficulty in fluid-structure interaction** is that we intend to couple three (perhaps the most important) classes of PDEs together:

- Second-order and fourth-order elliptic equations: the mesh motion equation (using ALE-FSI);

- Second-order parabolic equations: Navier-Stokes fluid flow (if we assume moderate Reynolds numbers) with a transition to a first-order hyperbolic system for large Reynold's numbers.

- Second-order hyperbolic equations: elasto-dynamic solid equation.

Fourth-order problems in this respect seem a bit fancy; however they are indeed important in solid and fluid mechanics:

**Remark 4.4** (Fourth-order equations in solid mechanics)**.** *Fourth-order equations are well known in solid mechanics since they include bending moments, e.g., Kirchhoff plates [46].*

**Remark 4.5** (Fourth-order problems in fluid mechanics)**.** *To derive Galerkin FEM methods for fluid problems, sometimes the derivation is made via the so-called streamline formulation. Here the intermediate step includes an explicit respresentation of the vorticity [192].*

## 4.1 Second-order elliptic equations

Let us go into more detail in the following:

**Definition 4.6** (Scalar-valued Laplace and Poisson problems)**.** *Let $x \in \Omega$ and $u : \bar{\Omega} \to \mathbb{R}$ (where $\Omega$ is an open set). Moreover, $f : \Omega \to \mathbb{R}$ is given. Then the Laplace equation and Poisson's problem are given as:*

$$-\Delta u = 0,$$

*and*

$$-\Delta u = f,$$

*respectively. The Laplace operator is defined as $\Delta u = \sum_{i=1}^{n} \partial_{ii} u$.*

The scalar-valued Laplace/Poisson problem can be extended to vector-valued problems by interpreting them component-wise:

---

[6]Maybe *fortunately* because otherwise there would be nothing else remaining to do.

**Definition 4.7** (Vector-valued Laplace; see also Definition 3.5). *Let $x \in \Omega \subset \mathbb{R}^n$ and $u : \bar{\Omega} \to \mathbb{R}^n$ (where $\Omega$ is an open set). Moreover, $f : \Omega \to \mathbb{R}$ is given. Then the vector-valued Laplace equation and Poisson's problem are given as:*

$$-\Delta u = -\Delta \begin{pmatrix} u_1 \\ u_2 \\ \vdots \\ u_n \end{pmatrix} = \begin{pmatrix} -\Delta u_1 \\ -\Delta u_2 \\ \vdots \\ -\Delta u_n \end{pmatrix} = 0.$$

In physics, there is usually a *material* parameter associated with modeling. For example in solid mechanics the stiffness controlled by $\mu_s$:

$$-\nabla(\mu_s \nabla u) = -\mu_s \Delta u = 0.$$

The first expression holds always true for $\mu_s := \mu_s(x)$ whereas the second calculation only holds true if $\mu_s$ is constant in $\Omega$.

Often, the material parameter also depends on the solution variable (and there is an interesting model specifically for fluid-structure interaction that we discuss later), i.e., $\mu_s := \mu_s(u) := \mu_s(u(x))$:

**Definition 4.8** (A nonlinear elliptic equation).

$$-\nabla(\mu_s(u)\nabla u) = 0.$$

More generally, the class of elliptic operators also contains differential operators of the form:

$$-\nabla(\mu_s \nabla u) + b\nabla u + cu,$$

with given (sufficiently smooth) functions $\mu_s, b, c$.

We finally state once an example of the full problem that also includes boundary conditions:

$$\begin{aligned} -\mu_s \Delta u &= f \quad \text{in } \Omega, \\ u &= g \quad \text{on } \Gamma_D, \\ \partial_n u &= h \quad \text{on } \Gamma_N, \end{aligned}$$

where $g$ denotes a non-homogeneous Dirichlet boundary condition and $h$ a non-homogeneous Neumann boundary condition. Furthermore, $\partial_n u = \nabla u \cdot n$, where $n$ denotes the normal vector.

**Remark 4.9** (Homework). *Please recall and make yourself familiar about the characteristics of each of these classes (e.g., existence and uniqueness, maximum principle, regularity).* ◇

## 4.2 Second-order parabolic equations

**Definition 4.10.** *Let $\Omega \subset \mathbb{R}^n$ be open and $T > 0$ a fixed end time. An example of a parabolic initial/boundary-value problem is defined as*

$$\begin{aligned} \partial_t u - \nu_s \Delta u &= f \quad \text{in } \Omega \times (0, T], \\ u &= g \quad \text{on } \Gamma_D \times (0, T], \\ \partial_n u &= h \quad \text{on } \Gamma_N \times (0, T], \\ u &= \omega \quad \text{in } \Omega \times \{t = 0\}, \end{aligned}$$

*for given functions and parameters $\nu_s, f, g, h$.*

Specific examples of realizations of parabolic problems are the heat equation or the Navier-Stokes equations in the case of sufficient large viscosity (i.e., moderate Reynolds numbers)

## 4.3 Second-order hyperbolic equations

These types of equations are linked to the wave equation.

**Definition 4.11.** *Let $\Omega \subset \mathbb{R}^n$ be open and $T > 0$ a fixed end time. An example of a hyperbolic initial/boundary-value problem is defined as*

$$\begin{aligned}
\partial_{tt}^2 u - \mu_s \Delta u &= f && in\ \Omega \times (0, T], \\
u &= g && on\ \Gamma_D \times (0, T], \\
\partial_n u &= h && on\ \Gamma_N \times (0, T], \\
u &= \omega_1 && in\ \Omega \times \{t = 0\}, \\
\partial_t u &= \omega_2 && in\ \Omega \times \{t = 0\},
\end{aligned}$$

*for given functions and parameters $\mu_s, f, g, h, \omega_1, \omega_2$.*

If $u$ describes a displacement (which is nearly always the case), the corresponding velocity is defined as $\partial_t u = v$. With this, $\partial_{tt}^2 u = \partial_t v$ describes the acceleration.

## 4.4 Fourth-order biharmonic equation

The fourth-order biharmonic problem reads: Find $u : \Omega \to \mathbb{R}$ such that

$$\begin{aligned}
\Delta^2 u &= 0 && in\ \Omega, \\
u &= g && on\ \Gamma_D \\
\partial_n u &= h && on\ \Gamma_D
\end{aligned}$$

Here, two boundary conditions must be described on the boundary $\Gamma_D$. However, various other choices are possible as well. A nice overview is provided in [148].

# 5 Basic Principles of Continuum Mechanics

Continuum mechanics is a key tool to describe physical phenomena of a macroscopic system without taking into account knowledge on detailed compositions of internal structures. Many classical important fields are covered by these concepts such as hydrodynamics and fluid mechanics, solid mechanics, or heat phenomena. Of course there are limitations when we consider phenomena on micro- or nanoscales in which other models such a particle representations are more appropriate to be used.

Befor we begin, one important remark: continuum mechanics is obviously linked to physics and one might think that the mathematical impact is rather limited. This is **not** the case for fluid-structure modeling! We encounter most of the presented concepts again in Section 7. It is worth to carefully studying the present section.

## 5.1 Kinematics with Eulerian and Lagrangian coordinate systems

In kinematics, we study the motion and deformation of bodies. All phenomena that we consider are described in an open subset of the three-dimensional space.

To study kinematics we introduce two different coordinate systems: Lagrangian coordinates $\hat{x}$ (also called reference $\widehat{\Omega}$ or material coordinates) and Eulerian coordinates $x$ (the current domain or spatial domain $\Omega$).

**Definition 5.1** (Domains). *We denote:*

- $\widehat{\Omega}$*: the reference/undeformed configuration;*

- $\Omega(t)$*: the current/deformed configuration.*

*Furthermore, $\Omega(t = 0)$ is the so-called initial configuration. Often, $\widehat{\Omega} := \Omega(t = 0)$. Moreover, in these notes we abbreviate $\Omega := \Omega(t)$.*
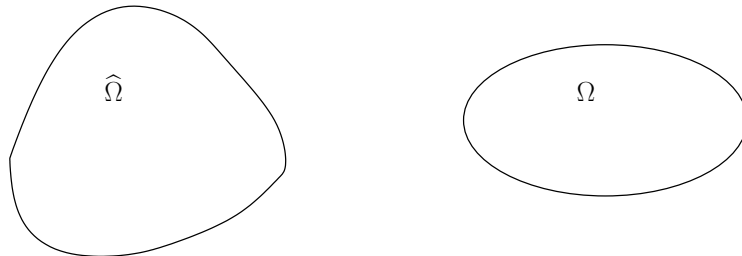


Figure 6: Domains: $\widehat{\Omega}$ and $\Omega$.

**Remark 5.2.** *The reasoning to work with two coordinate systems is that*

- *solids/elasticity are usually described in the Lagrangian system;*

- *fluids (i.e., Navier-Stokes) are usually described in Eulerian coordinates.*

In the Lagrangian coordinate system, a specific material point and its deformation (i.e., its evolution in time) are observed (see in Figure 7 the bold black line). In contrast, using Eulerian coordinates, we observe a fixed point in space and observe what is happening at this spatial point while time is evolving. It might be occupied by different materials while time advances (imagine a river; here you do not identify the single water particle but the general flow pattern). To make it more clear: please think of Linz' Hauptplatz[7] when there is Christmas market or any other day in the year. Imagine you observe people walking there: do you follow a specific person (that would be Lagrangian modeling) or do you look at the general flow of people (Eulerian point of view).

---

[7]Niki-de-Saint-Phalle-Promenade in Hannover; Linz' Hauptplatz or Munich's Marienplatz or Heidelberg's Hauptstraße.

- Goal of Lagrangian coordinates: deformation of a body, but not directly possibly since deformation is part of the transformation.

- Eulerian coordinates: the domain is fixed and not caused by a deformation. Goal: do not observe displacements of specific material points, but flow fields at given spatial points. Does not make sense to observe specific flow particle.

**Remark 5.3.** *In Figure 7 we already identify the principle difficulty in formulating a common coordinate system when the underlying physics are described in Lagrangian **and** Eulerian coordinates. Shall we 'move' the Eulerian system according to $h(x)$ or shall we find any other presentation of $h(x)$ that fits with an Eulerian description. One powerful possibility that we consider in detail in Section 7.3 is the arbitrary Lagrangian-Eulerian (ALE) framework in which the Eulerian system fits with $h(x)$ and is moved.* ◇
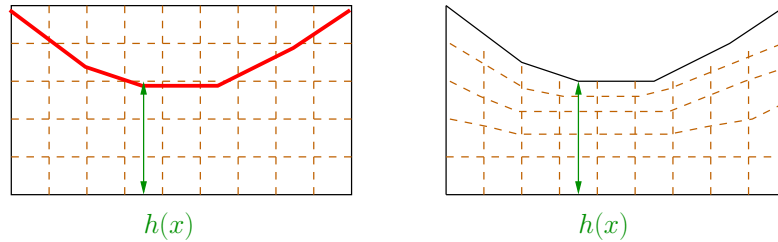


Figure 7: Fixed Eulerian domain and deformed Lagrangian domain: Shall we move the domain according to the (red) interface (right) or keep the fixed domain and describe $h(x)$ implicitly?

The *reference* configuration $\widehat{\Omega} \subset \mathbb{R}^d$ is assumed to be open and connected. Depending on the application, there are different possibilities of reference configurations; in particular when working with stress-free or pre-stressed configurations [137] (imagine a book that is just placed on a table or a hot sausage that you slice in order to peel off the skin).

The time-evolution of a material point $\hat{x} \in \widehat{\Omega}$ is described by the mapping:

$$t \mapsto x(t, \hat{x}).$$

For the following, let us introduce the following notation to describe (physical) variables:

- Lagrangian coordinates: $\hat{f}(t, \hat{x})$.

- Eulerian coordinates: $f(t, x)$.

Having two coordinate systems, brings us to the **principle question** whether one of these two systems might later serve as the *computational domain* or if combinations or intermediate domains are necessary to be introduced.

Let us work with the following:



Figure 8: Defining points $\hat{x}$ and $x$ in $\widehat{\Omega}$ and $\Omega$, respectively.

**Hypothesis 5.4.** *Let us assume:*

- *$(t, \hat{x}) \mapsto x(t, \hat{x})$ is continuously differentiable;*

- *For all $t \geq t_0$ the mapping $\hat{x} \mapsto x(t, \hat{x})$ is invertible;*

- *Orientation-preservation: the Jacobi determinant is always positive; namely $\hat{J} > 0$ (definition in 5.17).*

We now first define the deformation. Let $\widehat{T}$ be a motion of a body. In general, a motion will change body's shape, position and orientation. Specifically, a continuum body that changes its shape is called *deformable*. It is important to notice that a deformation is independent of time.

In more detail, we have:

**Definition 5.5** (Deformation field)*. A deformation of $\widehat{\Omega}$ is a smooth, one-to-one (i.e., injective), orientation-preserving mapping*

$$\widehat{T} : \widehat{\Omega} \to \Omega \quad with\ (t, \hat{x}) \mapsto (t, x) = (t, \widehat{T}(t, \hat{x})).$$

*This mapping associates each point $\hat{x} \in \widehat{\Omega}$ (of a reference domain) to a new position $x \in \Omega$ (of the physical domain).* ⋄
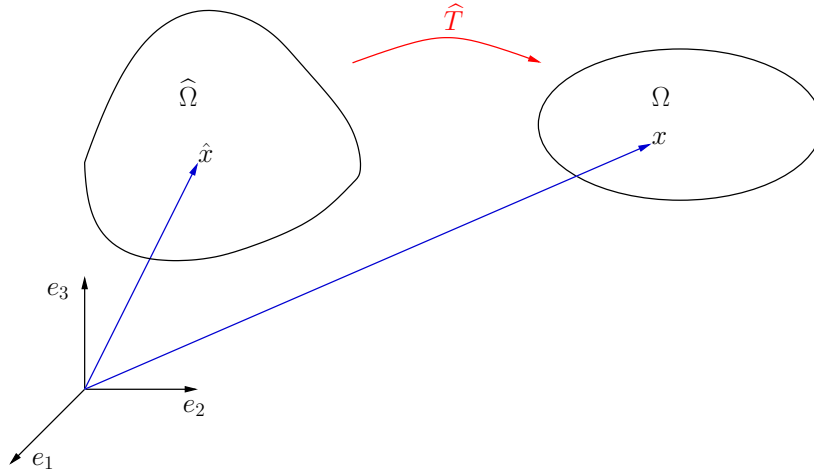


Figure 9: Definition of the deformation $\widehat{T}$.

The displacement field is defined as

**Definition 5.6** (Material/Lagrangian description of the displacement field)**.**

$$\hat{u} : (t, \hat{x}) \to \hat{u}(t, \hat{x}) = x(t, \hat{x}) - \hat{x}$$

*and it relates a particle's position in the reference configuration $\hat{x}$ to its corresponding position in the current configuration $x$ at time $t$.* ⋄

In the spatial description, we have

**Definition 5.7** (Spatial/Eulerian description of the displacement field)**.**

$$u(t, x) = x - \hat{x}(x, t).$$

*This is formulated in terms of the current displacement, which results from its original position $\hat{x}$ plus the displacement for that position.*



Figure 10: Descriptions of displacements: Going from the origin via $\widehat{\Omega}$ means $\hat{x} + \hat{u} = x$. Going from the origin via $\Omega$ leads to $x - u = \hat{x}$.

*We recapitulate that the two displacement descriptions can be transformed through the deformation; namely $x = T(t, \hat{x})$.* ⋄

It holds

**Definition 5.8** (Identification of function values)**.**

$$f(t, x(t, \hat{x})) = \hat{f}(t, \hat{x}).$$

◇

Next, we introduce several *time derivatives.* We start with the natural definitions for each domain and lastly formulate the time derivative between Lagrangian and Eulerian coordinates.

**Definition 5.9** (Total/Material time derivative of a Lagrangian field)**.**

$$D_t \hat{f}(t, \hat{x}) = \partial_t \hat{f}(t, \hat{x}).$$

*The material time derivative measures the rate at which $\hat{f}$ changes in time but following the path line of this article. This means we measure the rate-change in time of exactly the same particle at all times.*

**Definition 5.10** (Spatial time derivative of an Eulerian field)**.** *The local time derivative of an Eulerian field is defined as*

$$\partial_t f(t, x).$$

*The current position $x$ is held fixed while measuring the rate at which $f$ changes in time at this fixed point. This means, at each time, $f$ represents a new particle at $x$. The spatial time derivative is also known to be the local time derivative.*
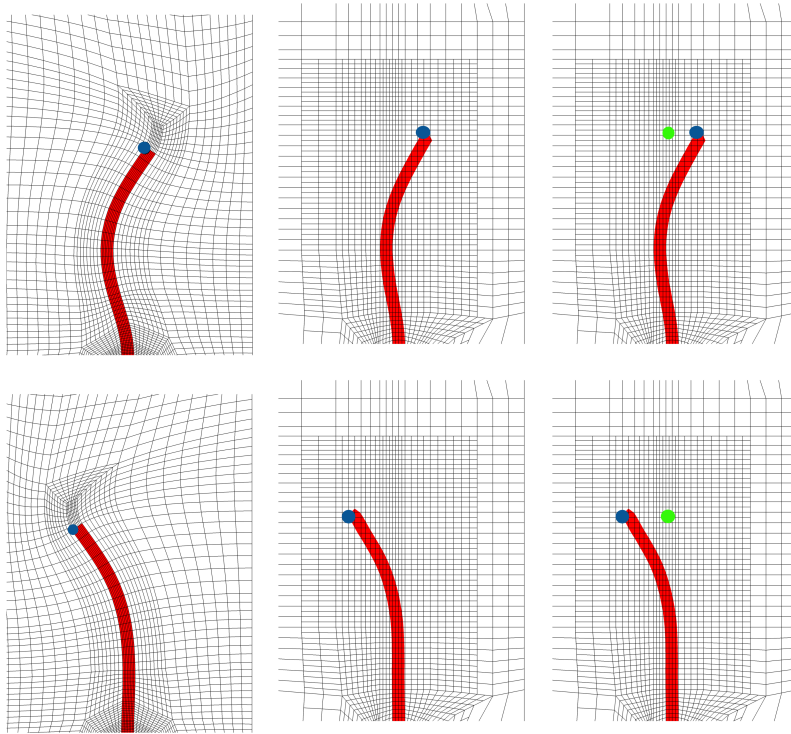


Figure 11: Illustration of a moving point (in blue; part of an elastic body colored in red) for two different times $t^n$ and $t^{n+1}$ in Lagrangian and Eulerian coordinates. In Lagrangian coordinates the point is always associated to the same position in the domain (mesh) - first column. In Eulerian coordinates (second column), the domain (mesh) is fixed and the point is associated at each time step to a new position. Taking the material time derivative of a point (blue) with respect to a fixed position (green) in the Eulerian frame is illustrated in the third column. We finally notice that the Lagrangian result is displayed in the current domain but the computation was performed in the fixed reference configuration as shown in Figure 12.

As we learned for the identification of function values, this specifically applies to the velocities:

$$\partial_t \widehat{T}(t, \hat{x}) = \hat{v}(t, \hat{x}) = \hat{v}(t, \widehat{T}^{-1}(t, x)) = v(t, x). \tag{4}$$

Furthermore, with the help of the chain rule, we then obtain

**Proposition 5.11** (Total/Material time derivative of an Eulerian field)**.** *Let $f(t, x) : \mathbb{R}^m \to \mathbb{R}$ and $x :=$ $(x_1, \ldots, x_{m-1}) \in \mathbb{R}^{m-1}$. Then,*

$$\begin{aligned} D_t f(t, x) &= \partial_t f(t, \widehat{T}(t, \hat{x})) \\ &= \partial_t f(t, x) + \nabla f(t, x) \cdot \partial_t \widehat{T}(t, \hat{x}) \\ &= \partial_t f(t, x) + \nabla f(t, x) \cdot \partial_t x(t, \hat{x}) \\ &= \partial_t f(t, x) + \nabla f(t, x) \cdot v(t, x). \end{aligned}$$

*The material derivative at a fixed material point $\hat{x}$ describes the change of an Eulerian variable $f$ that is at time $t$ at point $x$ and travels with the velocity $v(t, x)$. Here, the first term prescribes the local change whereas the second term, the convective part, is due to the movement of the particle through the domain.* ⋄

*Proof.* The above relation can be proven with the help of the chain rule. Let the functions $g : (a, b) \to \mathbb{R}^m$ and $f : \mathbb{R}^m \to \mathbb{R}$ and its composition $h \in \mathbb{R}$ be given and specifically $g := (t, x) := (t, x_2, x_3, \ldots, x_m)$:

$$\begin{aligned} D_t h(x) = D_t f(g(x)) = D_t f(t, x) &= D_t f(t, x_2, \ldots, x_k) \\ &= \sum_{k=1}^m \partial_k f(g(x)) \cdot \partial_t g_k \\ &= \sum_{k=1}^m \partial_k f(t, x_2, \ldots, x_m) \cdot \partial_t x_k, \quad \text{where } x_1 := t \\ &= \partial_t f \cdot \partial_t t + \sum_{k=2}^m \partial_k f(t, x_2, \ldots, x_k) \cdot \partial_t x_k \\ &= \partial_t f + \nabla f \cdot (\partial_t x_2, \cdots, \partial_t x_m) \\ &= \partial_t f + \nabla f \cdot v. \end{aligned}$$

For instance $m = 4$ means that we deal with a four-dimensional continuum $(t, x, y, z)$. □

**Remark 5.12** (Importance for fluid-structure interaction)**.** *The last time derivative becomes important for fluid-structure interaction in ALE coordinates in which we need to define the ALE time derivative for which we refer to Section 7.3.2.*

**Remark 5.13.** *If $v(t, x) = 0$ for all $x \in \Omega$ and all times $t$, then*

$$\begin{aligned} D_t f(t, x) &= \partial_t f(t, x) + \nabla f(t, x) \cdot v(t, x) \\ &= f(t, x). \end{aligned}$$

*Here, a particle fixed at the current position $x$ is observed and this exactly corresponds to the local time derivative (spatial time derivative of an Eulerian field). This definition makes sense since the partial derivative (in its very mathematical definition) computes the rate of change with respect to a specific variable (here time $t$), while holding all other variables (here the spatial ones) fixed. On the other hand, if both space and time vary we obtain Proposition 5.11.*
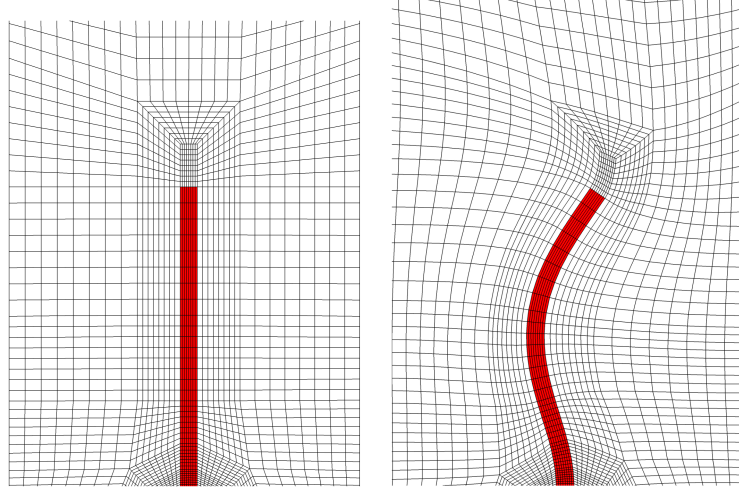
Figure 12: Lagrangian computations: the model and numerical computation of an elastic body (in red color) are defined in the fixed reference domain $\widehat{\Omega}$ (left). The current (physical) domain $\Omega(t)$ of the resulting displacement field is displayed in the right figure.

### 5.1.1 Deformation gradient $\widehat{F}$ and deformation determinant $\hat{J}$

In this section, we introduce two key quantities that are required to transform and formulate equations in different coordinate systems. Specifically, we introduce concepts to further study the changes of size and shape of a body that is moved from the reference configuration $\widehat{\Omega}$ to the current domain $\Omega$.

For simplicity, let a body occupies $\widehat{\Omega}$ at time $t = 0$. It is described by its position vector $\hat{x} = (\hat{x}_1, \hat{x}_2, \hat{x}_3)$ in a Cartesian coordinate system with the orthonormal basis $(\hat{e}_1, \hat{e}_2, \hat{e}_3)$. At time $t$ the body has evolved (and possibly changed its size and shape) and occupies the current domain $\Omega$. Here, the position vector is $x_i(t, \hat{x}_j)$. Consequently:

$$\hat{x} = \hat{x}_i \hat{e}_i, \quad x = x_i(t, \hat{x}_j)\hat{e}_i$$

(using Einstein's sum convention).

In order to define the deformation gradient, let us consider an infinitesimal material vector $d\hat{x}$ in $\widehat{\Omega}$ that displaces the material particle at $\hat{x}$ such that the new position is $\hat{x} + d\hat{x}$. In the current domain, the previous operation yields $x + dx$.

- The key purpose of the deformation gradient $\widehat{F}$ is to link $dx$ and $d\hat{x}$ (see Figure 13).

$\widehat{F}$ is a key principle in continuum mechanics and a primary measure of deformation with nine components at all times. It transports any material vector $d\hat{x}$ to $dx$ onto the current (deformed) configuration.

**Definition 5.14** (Deformation gradient $\widehat{F}$).

$$dx = \widehat{F} \cdot d\hat{x},$$

with $\widehat{F} = \widehat{\nabla} x$, i.e, $\widehat{F}_{ij} = \frac{\partial x_i}{\partial \hat{x}_j}$. $\diamond$

Its inverse and transpose are defined correspondingly:

$$d\hat{x} = \widehat{F}^{-1} \cdot dx, \quad dx = d\hat{x} \cdot \widehat{F}^T.$$
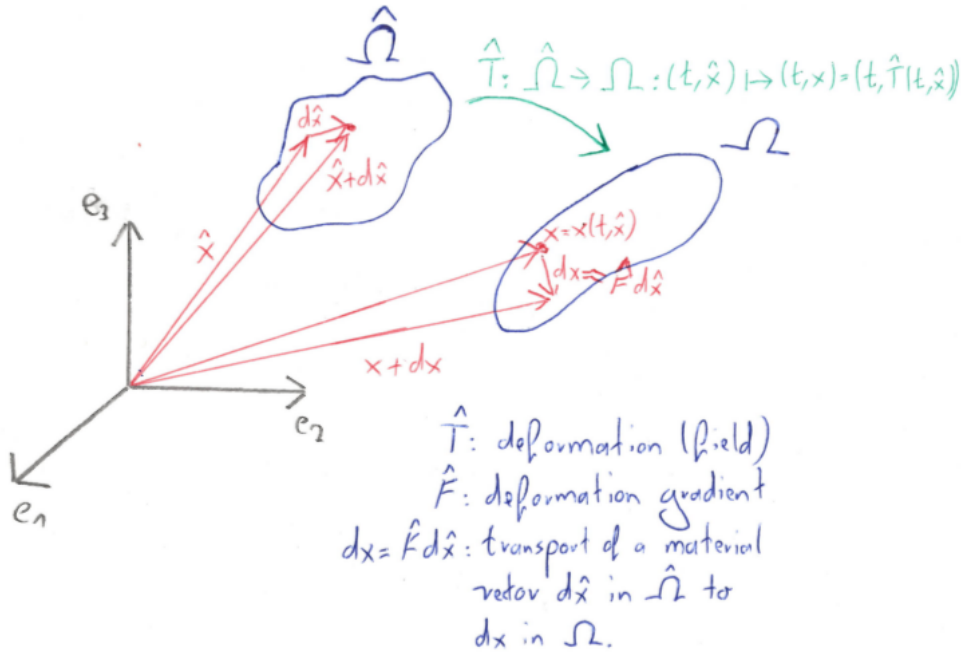
Figure 13: Transport of materials vectors, transformation $\widehat{T}$, and deformation gradient $\widehat{F}$.

**5.1.1.1 Relation of deformation gradient and displacements**  We are now prepared to relate $\widehat{F}$ and the displacement $\hat{u}(t, \hat{x})$. Recall from Definition 5.6

$$x = \hat{x} + \hat{u}.$$

**Definition 5.15** (Deformation and deformation gradient)**.**

$$x := x(t, \hat{x}) = \widehat{T}(t, \hat{x}) = \hat{x} + \hat{u}.$$

*The deformation gradient $\widehat{F}$ can be expressed in terms of $\hat{u}$ as follows:*

$$\widehat{F} = \nabla \widehat{T} = \hat{I} + \widehat{\nabla} \hat{u}.$$

*With the help of the deformation, $\widehat{T}$, we can represent the deformed configuration as $\Omega = \widehat{T}(\widehat{\Omega})$.*

Although we have Definition 5.8, such a relation does not hold for derivatives. Here we have (see also Figure 13):

**Proposition 5.16.** *Let $f(t, x) : \Omega \to \mathbb{R}^n$ be an Eulerian function and let $\hat{f}(t, \hat{x}) : \widehat{\Omega} \to \mathbb{R}^n$ a corresponding Lagrangian function. To compute the Eulerian spatial derivative we have the relation:*

$$\nabla f = \widehat{\nabla} \hat{f} \, \widehat{F}^{-1}.$$

*Proof.* As for the time derivatives, we work with the chain rule. One can proof first that for scalar fields $f$ and $\hat{f}$, we have

$$\widehat{\nabla} \hat{f} = \widehat{F}^T \nabla f.$$

Next, for vector-valued functions, we have:

$$\widehat{\nabla} \hat{f} = \nabla f \widehat{F}.$$

The same holds for tensor-valued functions. $\qquad\qquad\square$

**5.1.1.2 Deformation determinant**  The determinant of the deformation gradient (mathematically-speaking we would call it as the functional determinant or Jacobi determinant) is defined as

**Definition 5.17.**

$$\hat{J} := det(\widehat{F}) > 0,$$

*which is used to relate volume changes between infinitesimal reference and current domains:*

$$d\Omega = \hat{J}d\widehat{\Omega}. \tag{5}$$

◇

For the following, we need another relation

**Proposition 5.18** (Eulerian expansion formula)**.** *It yields*

$$\partial_t \hat{J}(t,\hat{x}) = \nabla \cdot v(t,x)\hat{J}(t,\hat{x})$$

*Proof.* It left as an exercise. □

Extending Relation (5) to the whole domain, we can compute the volume change:

$$|\Omega| = \int_\Omega 1 \, dx = \int_{\widehat{\Omega}} \hat{J}(t,\hat{x}) \, d\hat{x}, \tag{6}$$

which further yields (employing Proposition 5.18)

$$\frac{d}{dt}|\Omega| = \int_\Omega \nabla \cdot v(t,x) \, dx.$$

Consequently, $\hat{J}$ characterizes the volume ratio and is called in *r*-adaptive methods, the *adaptation factor* (Section 7.4). Physically, we do not allow for negative volumes $\hat{J} < 0$, which could be mathematically still allowed. Geometrically, $\hat{J} > 0$ preserves the orientation of $\widehat{T}$ and is also assumed in aller further considerations.

Furthermore, $\hat{J} = 0$ would mean that $\widehat{F}$ is not invertible and has serious consequences in fluid-structure interaction modeling using the ALE approach causing the approach to fail. Consequently, we shall control $\hat{J}$ such that is stays positive during a numerical computation. In the rest of these notes, we always assume that $\hat{J} > 0$.

If a body does not move, we have $\widehat{F} = \hat{I}$ and it follows $\hat{J} = 1$. On the other hand, a motion is called isochoric when $\hat{J} = 1$ with possibly $\widehat{F} \neq \hat{I}$.

### 5.1.2 The Piola transformation

Let $\widehat{T}$ be injective on $\bar{\Omega}$ such that $\widehat{F} = \widehat{\nabla}\widehat{T}$ is invertible at all point in $\widehat{\Omega}$. For sufficient criteria of injectivity conditions, the reader is referred to Section 5.1.3. Let $\sigma := (\sigma_{ij})_{ij=1}^3$ be a tensor in $\Omega$ defined at the point $x = \widehat{T}(t,\hat{x}) \in \Omega$. Then, we are able to define a corresponding tensor $\widehat{\sigma} \in \widehat{\Omega}$ with the help of

**Definition 5.19** (Piola transformation)**.**

$$\widehat{\sigma}(\hat{x}) := \hat{J}(\hat{x})\sigma(x)\widehat{F}^{-T}(\hat{x}) \quad for \ x = \widehat{T}(t,\hat{x}).$$

*In short*

$$\widehat{\sigma} := \hat{J}\sigma\widehat{F}^{-T} \quad for \ x = \widehat{T}(t,\hat{x}).$$

*The Piola transformation relates tensor fields between the deformed and reference configurations and is later used to transform the Cauchy stress tensor from Eulerian coordinates to the Piola-Kirchhoff stress tensor into the Lagrangian framework.*

**Proposition 5.20** (Divergence of the Piola transformation)**.** *Let $\widehat{\sigma} : \bar{\widehat{\Omega}} \to \mathbb{R}^{3\times3}$ be the Piola transformation of $\sigma : \bar{\Omega} \to \mathbb{R}^{3\times3}$. The divergence is then given by:*

$$\widehat{div\,\widehat{\sigma}} = \hat{J}div\,\sigma \quad \forall x = \widehat{T}(\hat{x}), \hat{x} \in \widehat{\Omega}.$$

*Proof.* Exercise. □

**5.1.2.1 Nanson's formula** This formula is a consequence of the Piola transformation and is required to transform normal vectors between both coordinate systems. Let $ds := ds\, n$ and $d\hat{s} := d\hat{s}\, \hat{n}$ be vector elements of infinitesimally small areas and $n$ and $\hat{n}$ the corresponding normal vectors. Then,

**Definition 5.21** (Nanson's formula)**.**

$$ds = \hat{J}\widehat{F}^{-T} d\hat{s}.$$

◇

This derivation is motivated as follows. Consider a surface $d\hat{a}$ with its normal $\hat{n}$. Through $\widehat{T}$, this surface is transformed into $da$ with the normal $n$. However, $\hat{n}$ and $n$ are not material vectors and consequently, the cannot be identified through $\widehat{T}$. In order to justify Definition 5.21, take $\hat{s} \in \widehat{\Omega}$. A cylinder transforms as follows:

$$\hat{n} \cdot \hat{s}\, d\hat{a} \quad \rightarrow \quad n \cdot \widehat{F} \cdot \hat{s}\, da.$$

Using Definition 5.17, we obtain

$$n \cdot \widehat{F} \cdot \hat{s}\, da = \hat{J}\hat{n} \cdot \hat{s}\, d\hat{a}.$$

Since this last expression holds for arbitrary vectors $\hat{s}$, it yields:

$$n \cdot \widehat{F} \cdot \hat{s}\, da = \hat{J}\hat{n} \cdot \hat{s}\, d\hat{a}$$
$$\Rightarrow \quad n\, da = \hat{J}\widehat{F}^{-T}\hat{n}\, d\hat{a}$$
$$\Rightarrow \quad da = \hat{J}\widehat{F}^{-T} d\hat{a},$$

where $da := da\, n$ and $d\hat{a} := d\hat{a}\, \hat{n}$.

### 5.1.3 Mathematical consequences of $\hat{J} > 0$

In view of fluid-structure interaction modeling, let us discuss further consequences of $\hat{J} > 0$ and its importance to require this property.

As previously discussed, $\hat{J} > 0$ keeps the orientation of a mapping $\widehat{T}$ and consequently $\widehat{T}$ is locally invertible. More specifically, each point $\hat{x} \in \widehat{\Omega}$ possesses a neighborhood in which $\widehat{T}$ is injective. This can be established by using the implicit function theorem with the Fréchet derivative $\nabla\widehat{T}$ whose determinant is (after our assumption) positive. However, this idea can not be extended to the entire domain $\widehat{\Omega}$, which means that local invertibility does not imply general injectivity.

Let us look at an (obvious) result that locally holds true:

**Proposition 5.22** (A sufficient condition for orientation-preservation $\hat{J} > 0$ and injectivity of $\widehat{T}$)**.** *As before, let $\widehat{T} : \widehat{\Omega} \to \mathbb{R}^3$ with $\widehat{T} := \hat{x} + \hat{u}$ and differentiable at a point $\hat{x} \in \widehat{\Omega}$. It holds*

$$|\widehat{\nabla} u(x)| < 1 \quad \Rightarrow \quad \hat{J} > 0.$$

*Proof.* Let $\hat{x}$ be a point such that $|\widehat{\nabla}\hat{u}(\hat{x})| < 1$. Here,

$$\det(\hat{I} + t\widehat{\nabla}\hat{u}(\hat{x})) \neq 0 \quad \text{for } 0 \leq t \leq 1$$

and all matrices $(\hat{I} + t\widehat{\nabla}\hat{u}(\hat{x}))$ are consequently invertible. Let us define the function

$$g : t \mapsto g(t) = \det(\hat{I} + t\widehat{\nabla}\hat{u}(\hat{x}))$$
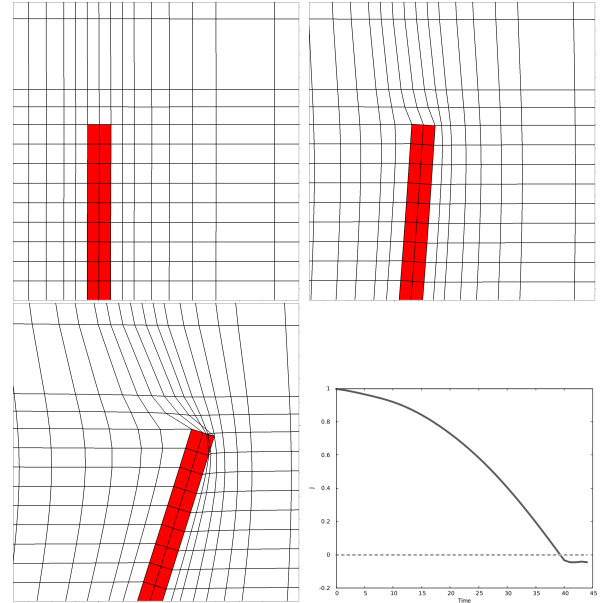


Figure 14: Numerical simulation with finite elements to illustrate violation of $\hat{J} > 0$. A moving (elastic) body (in red color) is immersed in a fluid. Due to the deformation, the orientation preservation gets violated at the tip of the elastic body, which intersects (illegally) the fluid domain. The time evolution of $\hat{J}$ is shown in the bottom right figure.

with

$$g(0) = 1, \quad g(1) = \det(\hat{I} + \widehat{\nabla}\hat{u}(\hat{x}))$$

Obviously, $g$ defines a continuous function but $g(\cdot)$ never yields 0 as result. Consequently, $g > 0$ for $0 \leq t \leq 1$. Q.E.D.

**Remark 5.23** (Global injectivity). *More results including extensions and detailed discussions on global injectivity are discussed in [61].*

**Remark 5.24.** *The previous proposition and remark do only hold true for problems in which $\widehat{T}$ is equal to a known injective mapping on all $\partial\Omega$. This condition is only true for boundary value problems where the boundary is fixed with Dirichlet conditions.*

For problems with a mixture of Dirichlet and Neumann conditions (the solid stress condition in FSI is always of Neumann type!) we have the following results [61](Section 5.6):

**Definition 5.25** (Injectivity condition). *The injectivity condition reads:*

$$\int_{\widehat{\Omega}} \hat{J}\, d\hat{x} = \int_{\widehat{\Omega}} det\,\widehat{\nabla}\widehat{T}\, d\hat{x} \leq |\widehat{T}(\widehat{\Omega})|,$$

*where $|\cdot|$ denotes the volume of the domain $\widehat{T}(\widehat{\Omega})$.*

This condition implies interior injectivity of the mapping $\widehat{T}$:

**Proposition 5.26** (Interior injectivity). *Let $\widehat{\Omega} \subset \mathbb{R}^3$ be a domain and let $\widehat{T} \in C^1(\bar{\Omega})$ such that*

$$\hat{J} > 0 \quad in\ \widehat{\Omega}, \qquad and \qquad \int_{\widehat{\Omega}} \hat{J}\, d\hat{x} \leq |\widehat{T}(\widehat{\Omega})|.$$

*Then, the mapping $\widehat{T}$ is injective on $\widehat{\Omega}$.*

### 5.1.4 Strain tensor

The strain tensor measures changes, caused by the deformation, both in lengths and angels of two material vectors. In this sense, the Green-Lagrange tensor introduced in this section, measures the discrepancy between a given deformation $\widehat{T}$ and a rigid deformation.

There are various definitions for strain tensors [137]. Let us introduce the most important concepts for these lecture notes:

**Definition 5.27** (Right Cauchy-Green tensor $\widehat{C}$).

$$\widehat{C} = \widehat{F}^T\widehat{F},$$

*which is symmetric and positive definite for all $\hat{x} \in \widehat{\Omega}$.* ⋄

In a rigid deformation it holds $\widehat{C} = I$ (where $I$ is the identity).

**Definition 5.28** (Green-Lagrange strain tensor $\widehat{E}$).

$$\widehat{E} = \frac{1}{2}(\widehat{C} - \hat{I}) = \frac{1}{2}(\widehat{F}^T\widehat{F} - \hat{I}) = \frac{1}{2}(\widehat{\nabla}\hat{u} + \widehat{\nabla}\hat{u}^T + \widehat{\nabla}\hat{u} \cdot \widehat{\nabla}\hat{u}^T),$$

*which is again symmetric and positive definite for all $\hat{x} \in \widehat{\Omega}$ since $\widehat{C}$ and of course, $\hat{I}$ have these properties.* ⋄

Performing geometric linearization, which is reasonable for example when $\|\widehat{\nabla}\hat{u}\| \ll 1$, we can work with the linearized Green-Lagrange strain tensor

**Definition 5.29** (Linearized Green-Lagrange strain tensor $\widehat{E}_{lin}$).

$$\widehat{E}_{lin} = \frac{1}{2}(\widehat{\nabla}\hat{u} + \widehat{\nabla}\hat{u}^T).$$

⋄

**5.1.5 Infinitesimal transformation and linearized expressions for $\widehat{E}, \widehat{F}, \hat{J}$**

In many, many problems there is never a distinction between 'had' variables in the reference domain and 'non-hat' functions in the current domain. Actually, both domains are identified. As outlined in the very beginning of these notes, to work with both definitions is one of the characteristics of fluid-structure interaction. In this section, we give brief comments on when the identification is justified. The key idea is to work with first-order approximations under the condition that we deal with a infinitesimal transformation, i.e.,

$$\|\nabla u\| \ll 1.$$

In this limit, we can work with

- $\Omega \approx \widehat{\Omega}$;

- $\widehat{\nabla} \approx \nabla$.

For the strain $\widehat{E}$ we obtain $\widehat{E}_{lin}$ while neglecting the second-order term $\nabla u^T \cdot \nabla u$. Moroever, $\widehat{E}_{lin}$ and $\nabla u$ have the same order, i.e., $\|\nabla u\| \ll 1$ yields $\|E\| \ll 1$. But the other direction does not hold true. In fact, a rigid body motion has $\widehat{E} = \widehat{E}_{lin} = 0$ but the transformation can be arbitrarely large. Furthermore, for $\widehat{F}$ we obtain no specific simplification (except $\widehat{F} \to I$ for $\|\nabla u\| \to 0$) but in $\hat{J}$ some terms cancel:

$$\hat{J} \approx J \approx 1 + \partial_z u_z + \partial_y u_y + \partial_x u_x = 1 + \nabla \cdot u = 1 + (E_{lin})_{ii=1,2,3}.$$

**5.1.6 Reynolds' transport theorem - differentiation under the integral sign**

**Proposition 5.30** (Reynolds' transport theorem). *As before, let $\Omega := \Omega(t)$ be a time-dependent domain and $(t, \hat{x}) \mapsto x(t, \hat{x})$ given and assume Hypothesis 5.4. Furthermore, let the functions $(t, x) \mapsto \partial_t x(t, \hat{x})$ and $(t, x) \mapsto f(t, x)$ be continuously differentiable. Then,*

$$\frac{d}{dt} \int_\Omega f(t, x) \, dx = \int_\Omega \left[ D_t f(t, x) + f(t, x) \nabla \cdot v(t, x) \right] \, dx$$
$$= \int_\Omega \left[ \partial_t f(t, x) + \nabla \cdot (f(t, x) \cdot v(t, x)) \right] \, dx.$$

*Proof.* We first transform back to the reference configuration, employ then the chain rule and Proposition 5.18. The transformation to $\widehat{\Omega}$ is justified with the transformation theorem that is well-known in from real analysis lectures. With this, we calculate

$$\frac{d}{dt} \int_\Omega f(t, x) \, dx = \frac{d}{dt} \int_{\widehat{\Omega}} f(t, x(t, \hat{x})) \, \hat{J} \, d\hat{x}$$
$$= \int_{\widehat{\Omega}} \left( \partial_t f(t, x(t, \hat{x})) + \sum_{k=1}^d \partial_{x_k} f(t, x(t, \hat{x})) \, \hat{v}_k(t, \hat{x}) + f(t, x(t, \hat{x})) \nabla \cdot v(t, x(t, \hat{x})) \right) \hat{J} \, d\hat{x}$$
$$= \int_\Omega \left( \partial_t f(t, x) + \nabla \cdot (f(t, x) \cdot v(t, x)) \right) dx.$$

$\square$

Here, the first term describes the local time evolution of $f$ but irrespectively of the change of $\Omega$. The second term is a result of the changing domain $\Omega$ in time and describes the change of $f$ through the control volume.

## 5.2 Balance principles and conservation equations

The equations in continuum mechanics are based on fundamental physical principles:

- Mass

- Momentum

- Angular momentum

- Energy

These laws are formulated in Eulerian coordinates in the following sections.

### 5.2.1 Conservation of mass - the continuity equation

Let $\rho(t, x)$ be the mass density in Eulerian coordinates.

**Definition 5.31** (Conservation of mass).

$$\frac{d}{dt} \int_\Omega \rho(t, x) \, dx = 0.$$

$\diamond$

Applying Reynolds' transport theorem 5.30, we obtain the integral formulation

$$\int_\Omega \left[ \partial_t \rho(t, x) + \nabla \cdot (\rho(t, x) v(t, x)) \right] \, dx = 0. \tag{7}$$

A more detailed justification is as follows. We now encounter a principle difficulty that the domain $G$ may depend on time and consequently integration and differentiation do not commute. Therefore, in a first step we need to transform the integrand of

$$\frac{d}{dt} \int_G \rho \, dx$$

onto a fixed referene configuration $\hat{G}$ in which we can insert the time derivative under the integral sign. Then we perform the calculation and transform in lastly everything back to the physical domain $G$. Let the mapping between $\hat{G}$ and $G$ be denoted by $T$. Then, it holds:

$$x \in G : x = T(\hat{x}, t), \quad \hat{x} \in \hat{G}.$$

Moreover, $dx = J(\hat{x}, t) d\hat{x}$, where $J := \det(\nabla T)$. Using the substitution rule (change of variables) in higher dimensions yields:

$$\frac{d}{dt} \int_G \rho(x, t) \, dx = \frac{d}{dt} \int_{\hat{G}} \rho(T(\hat{x}, t), t) J(\hat{x}, t) d\hat{x}.$$

We eliminated time dependence on the right hand side integral and thus differentiation and integration commute now:

$$\int_{\hat{G}} \frac{d}{dt} \Big( \rho(T(\hat{x}, t), t) J(\hat{x}, t) \Big) d\hat{x} = \int_{\hat{G}} \Big( \frac{d}{dt} \rho(T(\hat{x}, t), t) \cdot J(\hat{x}, t) + \rho(T(\hat{x}, t), t) \frac{d}{dt} J(\hat{x}, t) \Big) d\hat{x}$$

Here, $\frac{d}{dt} \rho(T(\hat{x}, t), t)$ is the material time derivative of a spatial field (see e.g., [137]), which is <u>not</u> the same as the partial time derivative! In the last step, we need the Eulerian expansian formula

$$\frac{d}{dt} J = \nabla \cdot v \, J.$$

Then:

$$\int_{\hat{G}} \Big( \frac{d}{dt} \rho(T(\hat{x}, t), t) \cdot J(\hat{x}, t) + \rho(T(\hat{x}, t), t) \frac{d}{dt} J(\hat{x}, t) \Big) d\hat{x}$$
$$= \int_{\hat{G}} \Big( \frac{d}{dt} \rho(T(\hat{x}, t), t) \cdot J(\hat{x}, t) + \rho(T(\hat{x}, t), t) \nabla \cdot v \, J \Big) d\hat{x}$$
$$= \int_{\hat{G}} \Big( \frac{d}{dt} \rho(T(\hat{x}, t), t) + \rho(T(\hat{x}, t), t) \nabla \cdot v \Big) J(\hat{x}, t) d\hat{x}$$
$$= \int_G \Big( \frac{d}{dt} \rho(x, t) + \rho(x, t) \nabla \cdot v \Big) dx$$
$$= \int_G \Big( \partial_t \rho(x, t) + \nabla \rho(x, t) \, v + \rho(x, t) \nabla \cdot v \Big) dx$$
$$= \int_G \Big( \partial_t \rho(x, t) + \nabla \cdot (\rho v) \Big) dx.$$

Collecting the previous calculations brings us to:

$$\int_G (\partial_t \rho + \nabla \cdot (\rho v)) \, dx = 0.$$

This equation must hold for each sub-domain of $\Omega$. If $\rho$ and $v$ are sufficiently smooth, we arrive at the differential formulation

$$\partial_t \rho + \nabla \cdot (\rho v) = 0. \tag{8}$$

**Remark 5.32** (Homework). *Make yourself clear how we come from the integral formulation to the differential form.* $\diamond$

**Remark 5.33.** *When changes in density are time-independent, we have*

$$\nabla \cdot (\rho v) = 0.$$

*If the density is also spatially constant, we obtain*

$$\nabla \cdot v = 0.$$

*This is in fact the incompressibility condition for fluid flows; namely the density is constant.* $\diamond$

### 5.2.2 Conservation of momentum

Let $f : \Omega \to \mathbb{R}^d$ be a given force density acting on the volume (for example the gravity $g$); and let $g_t : \partial\Omega \to \mathbb{R}^d$ a surface-related force density (traction force).

Newton's second law states:

$$\frac{d}{dt}(mv) = F,$$

where $F$ is the force that acts on the mass.

In continuum mechanics Newton's second law reads:

$$\frac{d}{dt} \int_\Omega \rho v \, dx = \int_\Omega \rho f \, dx + \int_{\partial\Omega} g_t \, ds.$$

Employing again Reynolds' transport theorem yields:

$$\int_\Omega \left[ \partial_t(\rho v) + \nabla \cdot (\rho v v) \right] dx = \int_\Omega \rho f \, dx + \int_{\partial\Omega} g_t \, ds.$$

Applying Cauchy's existence (from 1827) [46, 60] of the stress tensor,

$$g_t = \sigma \cdot n,$$

further allows to write (and using Gauss' divergence theorem)

$$\int_{\partial\Omega} g_t \, ds = \int_{\partial\Omega} \sigma \cdot n \, ds = \int_\Omega \nabla \cdot \sigma \, dx.$$

We notice that the divergence operator applied to a matrix is calculated component wise and leads to a vector of the form:

$$\nabla \cdot \sigma = \begin{pmatrix} \sum_{j=1}^d \partial_{x_j} \sigma_{1j} \\ \sum_{j=1}^d \partial_{x_j} \sigma_{2j} \\ \vdots \\ \sum_{j=1}^d \partial_{x_j} \sigma_{dj} \end{pmatrix}.$$

We further obtain

$$\int_\Omega (\partial_t(\rho v_j) + \nabla \cdot (\rho v_j v) - \rho f_j - (\nabla \cdot \sigma)_j) \, dx = 0. \tag{9}$$

At this point we now use the product rule and the continuity equation (8) ($\partial_t \rho = -\nabla \cdot (\rho v_j)$) for the first two terms in (9) and calculate

$$\partial_t(\rho v_j) + \nabla \cdot (\rho v_j v) = \rho \partial_t v_j + v_j \partial_t \rho + \nabla \cdot (\rho v_j v) = \rho \partial_t v_j - v_j \nabla \cdot (\rho v_j) + \nabla \cdot (\rho v_j v) = \rho \partial_t v_j + \rho v \cdot \nabla v_j.$$

Therefore,

$$\int_\Omega (\rho \partial_t v_j + \rho v \cdot \nabla v_j - (\nabla \cdot \sigma)_j - \rho f_j) \, dx,$$

and written in compact form:

$$\int_\Omega (\rho \partial_t v + \rho v \cdot \nabla v - (\nabla \cdot \sigma) - \rho f) \, dx.$$

For smooth functions $\rho, v, \sigma$ and arbitray $\Omega$, we obtain the differential form:

$$\rho \partial_t v + \rho(v \cdot \nabla)v - \nabla \cdot \sigma = \rho f.$$

### 5.2.3 Conservation of angular momentum

Let $x$ be the position of a rotating mass point with origin $x_0$. Furthermore, let $\times$ denote the cross product definition; see Section 3. Then, the continuum mechanical description of angular momentum reads:

$$D_t \int_\Omega (x - x^0) \times (\rho v) \, dx = \int_\Omega (x - x^0) \times (\rho f) \, dx + \int_{\partial\Omega} (x - x^0) \times (\sigma n) \, ds.$$

Applying again Reynold's theorem yields (after some calculations)

$$\int_\Omega (x - x^0) \times \left( \partial_t(\rho v) + \sum_{j=1}^3 \partial_{x_j}(\rho v_j v) \right) dx = \int_\Omega (x - x^0) \times (\rho f) \, dx + \int_{\partial\Omega} (x - x^0) \times (\sigma n) \, ds.$$

**Proposition 5.34.** *Let all parameters and data $\rho, v, f, g_t$ be sufficiently smooth. If conservation of momentum and angular momentum are satisfied, then Cauchy's stress tensor $\sigma$ is symmetric; namely*

$$\sigma = \sigma^T.$$

*Proof.* Left as an exercise. $\qquad\square$

**Remark 5.35.** *In formulating the Navier-Stokes equations, we often find a non-symmetric formulation. We strongly emphasize that such a simplification is related to the specific setting and boundary conditions. In general, you must use the symmetric stress tensor. A discussion is provided in Section 6.2.3.*

### 5.2.4 Conservation of energy

The conservation of energy reads:

$$\frac{d}{dt} \int_\Omega \rho(\frac{1}{2}|v|^2 + u) \, dx = \int_\Omega \rho f \cdot v \, dx + \int_{\partial\Omega} \sigma n \cdot v \, ds - \int_{\partial\Omega} g \cdot n \, ds + \int_\Omega \rho h \, dx.$$

This leads into,

$$\rho \partial_t u + \rho v \cdot \nabla u - \sigma : Dv + \nabla \cdot g - \rho h = 0.$$

Here, $u$ is related to the inner energy, $v$ to the kinetic energy, $f$ and $\sigma n$ right hand side source terms, and $g$ and $h$ are related to heat energy terms.

In these notes, we do not further investigate the full system that also accounts explicitly for the conservation of energy.

### 5.2.5 Incompressible, isothermal equations with constant density

If there are no variations in density and temperature, we obtain the following equations for conservation of momentum and mass balance:

$$\rho\partial_t v + \rho(v \cdot \nabla)v - \nabla \cdot \sigma = \rho f,$$
$$\nabla \cdot v = 0.$$

The specification of the stress tensor $\sigma$ follows in Section 5.3.

## 5.3 Modeling fluid flows: constitutive laws and Navier-Stokes equations

The Cauchy stress tensor is not yet specified in Section 5.2.5 and hence the previous equations do hold for all materials; specifically they do not distinguish between fluids, solids, or gas. These properties are fixed by *constitutive* laws that are obtained from measurements, for instance.

### 5.3.1 Constitutive laws

**5.3.1.1 Coincidences between fluids and solids**   Before we dive into details, let us remark that also the constitutive laws for fluids and solids show some remarkable coincides. Under certain properties and assumptions such as material frame-indifference and isotropy, a famous result from Rivlin-Ericksen does hold for both fluids and solids in which a tensor (here the stress) can be decomposed into its principal invariants. More specifically, for a linear material law it can be shown that this can only depent at most on two independent material parameters. These are shear and volume parameters. We state the Rivlin-Ericksen theorem in Section 5.3.1.3.

**5.3.1.2 Constitutive laws for fluids**   We provide two examples for constitutive laws:

- Friction-free fluid flow. Here, only pressure forces are taken into account. The stress tensor reads:

$$\sigma = -pI.$$

- Viscous flow with inner friction:

$$\sigma = -pI + \mu_f(\nabla v + \nabla v^T) + \lambda_f \nabla \cdot vI,$$

  where $\lambda_f$ and $\mu_s$ are volume and shear viscosity, respectively. Fluids with such stress tensors are called *Newtonian fluids*. Inner friction means that particles with different velocities interact on the mirco-scale with each other; namely velocity variations do cause friction.

  In the case of incompressible materials, i.e., $\nabla \cdot v = 0$, this relationship reduces to

$$\sigma = -pI + \mu_f(\nabla v + \nabla v^T).$$

**5.3.1.3 A general form for isotropic materials with frame-indifference - the Rivlin-Ericksen theorem**   As remarked in the introduction of this section, the following theorem does hold for both fluids and solids. In the case of fluids, the principal variable is the velocity whereas in the solids these are the displacements. But the main idea is only based on linear algebra arguments. The resulting stress tensors for fluids and solids then simplify to astonishing expressions.

**Theorem 5.36** (Rivlin-Ericksen)**.** *Let $Q$ be a rotation; namely an orthogonal matrix $(QQ^T = I)$ with $det\,Q = 1$. For a mapping*

$$\tilde{\sigma} : \{A \in \mathbb{R}^{3\times3} | A = A^T, det\,A > 0\} \to \{B \in \mathbb{R}^{3\times3} | B = B^T\}$$

*it holds*

$$\tilde{\sigma}(QAQ^T) = Q\tilde{\sigma}(A)Q^T$$

*for all rotations $Q$, if and only if the mapping has the form*

$$\tilde{\sigma}(A) = a_0(i_A)I + a_1(i_A)A + a_2(i_A)A^2.$$

*Here, $a_0, a_1$ and $a_2$ are real-valued functions of the three principal invariants (definition in Section 3.13 of the matrix $A$.*

*Proof.* Will follow in a later version. □

**Example 5.37.** *Let us now relate this theorem our previous considerations. Let $\sigma = -pI + S$. If the constitutive law for $S$ is material frame-indifferent, isotropic, and linear, then $S$ does only depend on two material parameters and has necessarily the form*

$$S(A) = a_1(i_A)A + a_0(i_A)I = 2\mu A + \lambda tr(A)I.$$

*We emphasize again that in the case of fluids $A := A(v) \sim (\nabla v + \nabla v^T)$ and as we will later see for solids, we have the same form but in terms of displacements, i.e., $A := A(\hat{u}) \sim (\widehat{\nabla}\hat{u} + \widehat{\nabla}\hat{u}^T)$.*

### 5.3.2 The isothermal, incompressible Navier-Stokes equations

Isothermal, incompressible, viscous fluid flow is described by the (nonlinear) Navier-Stokes equations. Find vector-valued velocities $v : \Omega \to \mathbb{R}^3$ and a scalar-valued pressure $p : \Omega \to \mathbb{R}$:

$$\rho\partial_t v + \rho(v \cdot \nabla)v - \nabla \cdot \sigma = \rho f,$$
$$\nabla \cdot v = 0,$$

where

$$\sigma = -pI + \mu_f(\nabla v + \nabla v^T).$$

Here, $\mu_f = \rho_f \nu$ is the dynamic viscosity, whereas $\nu$ is the so-called kinematic viscosity.

A key quantity in fluid flow simulations is the so-called Reynold's number:

**Definition 5.38** (Reynolds' number). *The Reynolds number is a dimensionless parameter and defined as*

$$Re := \frac{LV}{\nu} = \frac{\rho LV}{\mu}.$$

*Here, $L$ is a characteristic length and $V$ is a characteristic velocity. The Reynolds number describes the relationship between friction and inertia forces. The Reynolds number $Re$ does appear as inverse in front of the friction term;*

$$-\frac{1}{Re}\nabla \cdot \sigma.$$

*For small Reynolds numbers $Re \ll 1$ the friction dominates (Navier-Stokes is then a parabolic equation) and the convection term $v \cdot \nabla v$ can be neglected while the flow becomes stationary. On the contrary, the higher the Reynolds number $Re \gg 1$, the more the Navier-Stokes equations become hyperbolic and nonlinearly dominant. First, flow is definitely nonstationary (in a laminar) regime and becomes turbulant for high Reynolds numbers. It is one of the open questions whether turbulant flow can be modeled with the Navier-Stokes equations.*

The main application of the Reynolds number is to relate different scales of, for example, huge experimental set-ups and small-scale model problems. Here, similar characteristic properties; namely length/height and velocity should lead to similar solutions.

**Definition 5.39** (Laminar flow). *Laminar flows may be stationary or nonstationary but **not** turbulent (chaotic behavior). Approximately, the Reynolds number in this regime is in the range of $1 \le Re \le 10^5$ [190].*

**Example 5.40.** *Let $L = 1$ and $V = 1$, then $Re = \nu^{-1}$. For $Re \sim 1 - 10^5$ the flow is laminar and the characteristic time length is $T \sim \nu^{-1}$. This shows the smaller the viscosity, the smaller the characteristic time scale must be chosen, which is a major challenge for flows with very high Reynolds numbers.*

**Remark 5.41** (Nonstationary flow becomes turbulent [190]). *Poisseuille flow (parabolic flow) between to plates (channel flow) is predicted to become turbulent at $Re \sim 5772$. Couette flow (parallel shear flow) is computed to be stable for all $Re > 0$ but experiments show instabilities for $Re \sim 300 - 1500$.*

We have not yet talked about boundary conditions, which are crucial to all equations presented so far. Depending on them and suitable right hand side data, we might obtain existence of a unique solution; for details and discussions we refer to [192, 220] and also to Section 6.

For the full 3d Navier-Stokes equations, the complete proof for smooth solutions is still missing and one of the Millennium prices. Concretely, one has to establish existence and smoothness of solutions in $\mathbb{R}^3$ [80]. This problem is also open for the Euler equations ($\nu = 0$). The 2d solution has been established in [161].

## 5.4 Modeling solids

### 5.4.1 Equations

In these lecture notes, we mainly concentrate on elastic deformations for solid modeling. Specifically, this means that a body under deformation goes back into its initial configuration if forces are removed. So, we work in the linear regime sketched in Figure 15 [8]. When the body does not go back into its initial configuration and a deformed settings remains, we would work in an elasto-plastic regime with plastic deformations. There are huge contributions to hyperelastic materials. We aim to provide a brief overview of basics concepts that help us throughout these lecture notes. For detailed considerations, we refer to [41, 61, 137, 145].
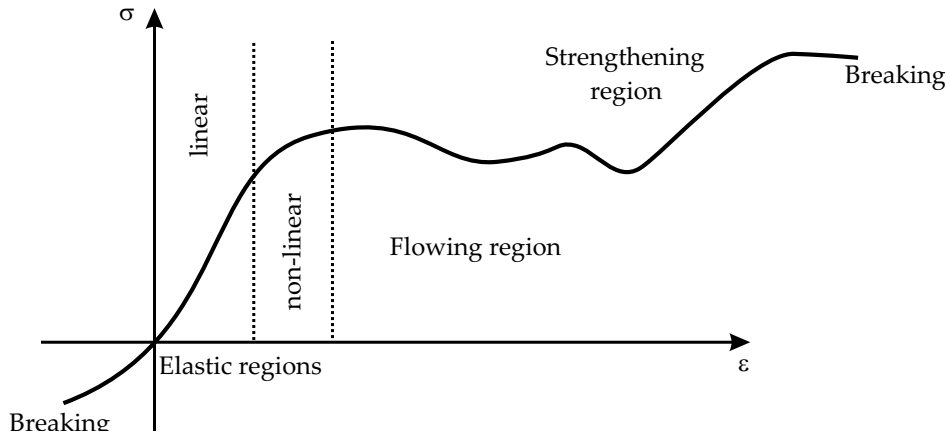


Figure 15: The stress-strain diagram. Here, $\sigma$ is the stress and $\varepsilon$ is the strain.

Typically and in contrast to fluid problems, elasticity is described in Lagrangian coordinates. One reason is related to history-dependent materials. Using Lagrangian coordinates, it facilitates treatment of such laws because each mesh point represents at all times the same material point (for example stress-update procedures in nonlinear elasticity or plasticity). However, it is nevertheless possible to obtain such information in an Eulerian framework; for a discussion, we refer the reader to [41] (chapter 5). Lagrangian coordinates describe a material point $\hat{x}$ in the reference configuration $\widehat{\Omega}$, which is usually the configuration without outer forces (remember in contrast to pre-stressed configurations [137]).

As second reason (that is associated with the first), in solid mechanics we aim to find the resulting deformation field of a body that is subject to given forces. Here, the equations of equilibrium in the deformed configuration are not available because they are formulated in terms of the Eulerian variable $x = \widehat{T}(\hat{x})$. However, the Eulerian variable $x$ is exactly one of the unknowns. For this reason, solid mechanics are treated in Lagrangian coordinates that are associated to a reference configuration.

Since we intend to compute the solution (deformation and stress) in Lagrangian coordinates, but the Cauchy's stress tensor is formulated in the Eulerian framework, we need to transform this tensor back to the reference configuration. This operation is achieved with the so-called Piola-Kirchhoff stress tensor:

**Definition 5.42** (First Piola-Kirchhoff stress tensor). *Applying the Piola transformation of Definition 5.19 to Cauchy's stress tensor yields*

$$\widehat{\Pi} = \hat{J}\sigma_s\widehat{F}^{-T},$$

*where $\sigma_s$ is Cauchy's stress tensor in Eulerian coordinates.* ⋄

With its help, we are able to transform the constitutive laws from $\Omega$ to $\widehat{\Omega}$. We notice that $\widehat{\Pi}$ is in general not symmetric although $\widehat{\sigma}_s$ has this property. However, this is often advantageous and consequently we define a second stress tensor in the reference domain:

---

[8]I took this figure from my Master thesis that was written in German. Bruch = break, damage; Bereich = region; Fließ= flow; Verfestigung = hardening; nicht = non.

**Definition 5.43** (Second Piola-Kirchhoff stress tensor)**.**

$$\widehat{\Sigma} = \widehat{F}^{-1}\widehat{\Pi} = \hat{J}\widehat{F}^{-1}\sigma_s\widehat{F}^{-T}. \tag{10}$$

◇

We are now prepared to formulate the equations for elasticity. As we previously learned, without specifying constitutive laws the conservation equations do hold for all aggregation states. Since we agreed to work for elasticity in the reference configuration, we formulate the following ideas in $\widehat{\Omega}$. We recall the conservation of momentum:

$$\frac{d}{dt}\int_{\widehat{\Omega}} \hat{\rho}\partial_t\hat{u}\,d\hat{x} = \int_{\widehat{\Omega}} \hat{\rho}\hat{f}\,d\hat{x} + \int_{\partial\widehat{\Omega}} \widehat{F}\widehat{\Sigma}\hat{n}\,d\hat{s}.$$

Here, the density $\hat{\rho}$ and the volume force $\hat{f}$ are related to the reference configuration. Further calculation (using Gauss' divergence theorem and Reynolds transport theorem) yields

$$\int_{\widehat{\Omega}} \left(\hat{\rho}\partial_t^2\hat{u} - \widehat{\nabla}\cdot\widehat{F}\widehat{\Sigma}\right)\,d\hat{x} = \int_{\widehat{\Omega}} \hat{\rho}\hat{f}\,d\hat{x}. \tag{11}$$

We notice that the convective term in Reynolds' theorem vanishes since we work in a Lagrangian setting. For sufficiently smooth functions and since (11) holds for each subdomain of $\widehat{\Omega}$, we can write the differential form of the elasto-dynamics equations:

$$\hat{\rho}\partial_t^2\hat{u} - \widehat{\nabla}\cdot\widehat{F}\widehat{\Sigma} = \hat{f}. \tag{12}$$

**Remark 5.44** (A mixed formulation)**.** *We notice that we can split the solid equation into a first order system:*

$$\hat{\rho}\partial_t\hat{v} - \widehat{\nabla}\cdot\widehat{F}\widehat{\Sigma} = \hat{f},$$
$$\hat{\rho}(\partial_t\hat{u} - \hat{v}) = 0.$$

*In fact in Section 7 and 8, we go with this mixed formulation. The main reasons are of numerical nature, i.e., the mixed system is the starting point for a Galerkin time discretization, and further explanation can be found in [13, 121]. Secondly, the mixed formulation allows to apply one-step-$\theta$ finite difference time discretizations and here for $\theta = 0.5$ one can easily obtain a second-order A-stable scheme (many more details will be found in Section 8). In addition, we notice that usually in the solid mechanics community that standard temporal solid discretization is based on the so-called Newmark scheme [141, 251, 252].* ◇

### 5.4.2 A constitutive law: STVK material

In order to specify the properties of a specific material, we again need a constitutive law for the stress tensor. We already discussed the linearized strain tensor if we deal with small strains. In addition, we need a relationship between the stress and strain (we refer to Figure 15). Often, Hooke's law is consulted, which reads:

**Definition 5.45** (Linear stress-strain relationship/Hooke's law)**.**

$$\sigma_{ij} = \sum_{k,l=1}^{d} a_{ijkl}E_{kl}^{lin} \quad for\ i,j = 1,\ldots,d.$$

◇

The tensor $(a_{ijkl})_{ijkl}^{d} \in \mathbb{R}^{d\times d\times d\times d}$ has 81 components in 3$d$. Using symmetry arguments, we obtain

$$a_{ijkl} = a_{jikl} = a_{klij}.$$

Therefore, in 3D we have 21 independent components. Furthermore, the energy density should be positive, i.e. (positive definite)

$$\sum_{ijkl}^{d} a_{ijkl}\xi_{ij}\xi_{kl} \geq a_0|\xi|^2,$$

with $a_0 > 0$. With further assumptions (e.g. isotropy), we arrive at

**Definition 5.46** (Saint Venant-Kirchhoff-Material (STVK) / a large displacement-small strain model). *For an isotropic, homogeneous material for which its reference configuration is a natural state; namely $\widehat{\Sigma}_s(0) = 0$, we obtain*

$$\widehat{\Sigma}_s := \widehat{\Sigma}_s(\hat{u}) = 2\mu\widehat{E} + \lambda tr(\widehat{E})\hat{I},$$

*with the Lamé constants $\mu$ and $\lambda$. In particular, the STVK material is only useful in a neighborhood of the reference configuration $\widehat{C} \approx \hat{I}$ with small strains $\widehat{E}$. We finally mention that the equal sign is (strictly speaking) only an approximation in which higher order terms of $\widehat{E}$ have been neglected.* ◇

The corresponding Hooke tensor reads:

$$a_{ijkl} = \lambda\delta_{ij}\delta_{kl} + \mu(\delta_{ik}\delta_{jl} + \delta_{il}\delta_{jk}).$$

**Remark 5.47** (Homework). *Recall the definitions and properties of*

- *rigid body motion,*

- *material frame-indifference,*

- *an isotropic material,*

- *of an homogeneous material*

- *and find examples for materials that do not satisfy the natural state condition.*

**Remark 5.48.** *Since the STVK material is specifically valid near the reference configuration, we notice that there are limitations for problems that involve large strains [61, 137] for which definitely $\widehat{C} \neq \hat{I}$.* ◇

### 5.4.3 Relationship of $E, \nu_s, \mu_s, \lambda_s$

Often, the elasticity of structures is characterized by the Poisson ratio $\nu_s$ ($\nu_s < \frac{1}{2}$ for compressible materials) and the Young modulus $E_Y$. The relationship to the Lamé coefficients $\mu_s$ and $\lambda_s$ is given by:

$$\nu_s = \frac{\lambda_s}{2(\lambda_s + \mu_s)}, \qquad E_Y = \frac{\mu_s(\lambda_s + 2\mu_s)}{(\lambda_s + \mu_s)}, \tag{13}$$

$$\mu_s = \frac{E_Y}{2(1 + \nu_s)}, \qquad \lambda_s = \frac{\nu_s E_Y}{(1 + \nu_s)(1 - 2\nu_s)}. \tag{14}$$

**Remark 5.49** (Signs of the solid material parameters). *It can be shown that*

$$E_y, \mu_s, \lambda_s > 0 \quad and \quad -1 \leq \nu_s \leq 0.5.$$

*Further calculations (e.g., [192]), yield the refined choice:*

$$-1 \leq \nu_s \leq 0.5, E_y, \mu_s > 0, \quad \lambda_s > -\frac{2}{3}\mu_s. \tag{15}$$

*As background we notice that Poisson's ratio describes the ratio that a compressed material expands into the two directions orthogonal to the compression direction. If $\nu_s \to 0.5$, an elastic material becomes incompressible. For most materials $0.5 \geq \nu_s > 0$. Some polymers have negative $\nu_s$; namely they become thicker when they are stretched.*

**Proposition 5.50.** *For the parameter choice (15), the elasticity tensor $(a_{ijkl})^d_{ijkl}$ for an isotropic material is positive definite for symmetric strain tensors.*

### 5.4.4 Hyperelastic materials

There is a huge body of literature concerned with general laws of hyperelasticity [41, 61, 137, 145] from which the St. Venant-Kirchhoff material is a special case. A material is called hyperelastic, and therefore path-independent, when the applied work during a deformation process does only depend on the initial state and the final configuration. In this case, there exists a potential, the stored strain energy function or elastic potential per unit undeformed volume [137].

In more detail, hyperelastic materials are derived from a stored energy function (or also strain energy function) $W := W(\widehat{F})$ such that the stress can be obtained from the expression:

**Definition 5.51.**

$$\widehat{\Pi} = \frac{\partial W}{\partial \widehat{F}}.$$

With this definition, the total energy of a stationary system with volume forces $f$ and traction forces $g$ for admissible deformations $\widehat{T}$ can be written as:

$$E(\widehat{T}) = \int_{\widehat{\Omega}} W(\widehat{F}) \, dx - \int_{\widehat{\Omega}} f \cdot \widehat{T} \, dx - \int_{\partial\widehat{\Omega}} g \cdot \widehat{T} \, ds.$$

Either this energy functional is now minimized for finding a stationary point of the functional, i.e,

$$\min E(\widehat{T})$$

(following the physical principle that each body tries to find its state of minimal energy). Or, by formally differentiating $E(\widehat{T})$ with respect to $\widehat{T}$, we obtain the Euler-Lagrange equations that correspond to the local equilibrium equations from the previous sections.

Under certain assumptions (see [61, 137]), the stored energy can be expressed in terms of the right Cauchy-Green strain tensor $\widehat{C}$ such that $W := W(\widehat{C}) = W(\widehat{F}^T \widehat{F})$. Then, the second Piola-Kirchhoff stress tensor reads:

$$\widehat{\Sigma}(\widehat{C}) = 2\frac{\partial W}{\partial \widehat{C}}(\widehat{C}),$$

which can be under certain assumptions [61, 137] equivalently written as

$$\widehat{\Sigma}(\widehat{E}) = \frac{\partial W}{\partial \widehat{E}}(\widehat{E}).$$

**Definition 5.52** (Homework). *Show*

$$2\frac{\partial W}{\partial \widehat{C}}(\widehat{C}) = \frac{\partial W}{\partial \widehat{E}}(\widehat{E}).$$

Having these preparations, the previously STVK material satisfies the stored energy:

**Definition 5.53** (Stored energy $W$ of the STVK material).

$$W(\widehat{E}) = \frac{\lambda}{2}(tr\widehat{E})^2 + \mu tr(\widehat{E}^2), \quad with \ \widehat{C} = \hat{I} + 2\widehat{E}.$$

*Then,*

$$\widehat{\Sigma}(\widehat{E}) = \lambda(tr(\widehat{E}))\hat{I} + 2\mu\widehat{E}.$$

An particularly interesting application of the stored energy is for materials with large strains (recall that STVK does not satisfy this property); namely

$$W(\widehat{F}) \to \infty \quad \text{as } \hat{J} \to 0.$$

Physically-speaking, this property reflects the idea that infinite stresses are required to compress a continuum body to a point with vanishing volume. However a major challenge of the mathematical investigation of $W$ is the fact that $W$ is non-convex in general. Here, sophisticated tools (inter alia polyconvexity) from *calculus of variations* are needed. Such topics go much behond the purpose of these lecture notes. For a nice introduction to calculus of variations we refer the reader to [77].

### 5.4.5 Incompressible materials

In solid mechanics the incompressibility of a material (no change in volume) is expressed through

**Definition 5.54** (Incompressible solids)**.**
$$\hat{J} = 1.$$

*In all other cases for positive $\hat{J} > 0$, the material is called compressible.*

A relation to incompressible fluids can be found in Section 5.5.3. Constraints such as the incompressiblity are referred to as *internal constraints.*

In order to formulate constitutive laws for incompressible materials, we work as in the case of fluid dynamics and introduce a Lagrange multiplier $p_s$. As the notation indicates this variable is linked to a pressure and more specifically $p_s$ is the so-called *hydrostatic* pressure. The two simplest constitutive for incompressible, isotropic laws are[9]:

**Remark 5.55** (Incompressible materials: neo-Hookean (INH), Mooney-Rivlin (IMR)[174, 206–208])**.**

$$
\begin{aligned}
\widehat{\Sigma}_s &:= \widehat{\Sigma}_s(\hat{u}) := -\hat{p}_s\hat{I} + \mu_s\hat{F}\hat{F}^{-T}, \\
\widehat{\Sigma}_s &:= \widehat{\Sigma}_s(\hat{u}) := -\hat{p}_s\hat{I} + \mu_1\hat{F}\hat{F}^{-T} + \mu_2\hat{F}^{-T}\hat{F}^{-1},
\end{aligned}
\tag{16}
$$

*with the material coefficients $\mu_s > 0, \mu_1 > 0$ and $\mu_2 > 0$. For instance, the IMR model is as well-known model for incompressible rubber-like materials. Here, the shear modulus is $\mu = \mu_1 - \mu_2$. $\diamond$*

**Remark 5.56.** *A comparison of different nonlinear solid models with application in computational medicine has been carried out in [169].*

### 5.4.6 Nonlinearities in elasticity

We finally summarize possible nonlinearities that are associated with elasticity:

- Geometric nonlinearities in terms of $\hat{u}$: The strain $\widehat{E}$ is nonlinear because of $\widehat{C}$ which results in the terms $\widehat{\nabla}\hat{u} \cdot \widehat{\nabla}^T\hat{u}$;

- The constitutive law might be nonlinear itself, e.g., stress tensors of the form $\widehat{\Sigma} \sim \exp(\widehat{E})$ (see for example Fung [101]);

- Right hand side volume forces that are not dead loads;

- In the case of incompressible solids, the condition $\hat{J} = 1$ makes the system nonlinear.

## 5.5 Summarizing the equations for modeling fluids and solids

In preparation to couple fluids and solids in Section 7 let us summarize our findings from this chapter. As previously mentioned we recapitulate that fluid flows are defined in the Eulerian domain $\Omega$ (i.e., $\Omega_f$) and solid deformations in the reference domain $\widehat{\Omega}$ (i.e., $\widehat{\Omega}_s$).

### 5.5.1 Fluid equations

In a Newtonian incompressible fluid, it holds:

$$
\sigma_f := \sigma_f(v_f, p_f) = -p_f I + 2\rho_f\nu_f D(v_f), \quad D(v_f) := \frac{1}{2}(\nabla v_f + \nabla v_f^T)
\tag{17}
$$

with the velocity $v_f$, the pressure $p_f$, the identity matrix $I$, the density $\rho_f$, and the (kinematic) viscosity $\nu_f$.

---

[9]Since the both models are based on the isotropic material assumption, the Rivlin-Ericksen theorem 5.36 holds true and the final model depends at most on three independent invariants; see Section 3.13.

Using the equations for momentum and continuity together with the Cauchy stress tensor, we obtain the incompressible, isothermal Navier-Stokes equations:

$$\rho_f \partial_t v_f + \rho_f (v_f \cdot \nabla) v_f - 2\text{div}(\rho_f \nu_f D(v_f)) + \nabla p_f = \rho_f f, \quad \text{in } \Omega_f, \, t \in I, \tag{18}$$

$$\text{div } v_f = 0, \quad \text{in } \Omega_f, \, t \in I. \tag{19}$$

These equations are supplemented by appropriate initial and boundary conditions. The initial conditions are prescribed as

$$v(0) = v_0 \quad \text{in } \Omega \times \{t = 0\}.$$

The first type of boundary conditions are Dirichlet conditions (a prescribed velocity):

$$v_f = g \quad \text{on } \Gamma_{f,D} \subset \partial\Omega_f,$$

with a given function $g : \Gamma_{f,D} \times I \to \mathbb{R}^d$. Specifically, such conditions are prescribed on no-slip boundaries and inflow boundaries:

$$v_f = v_{in} \quad \text{on } \Gamma_{f,in}$$
$$v_f = 0 \quad \text{on } \Gamma_{f,D}.$$

No-slip boundaries might be rigid walls for example in modelling channel flow. We also notice that such a Dirichlet condition is seen in the velocity domain on the interface $\Gamma_i$ in the case of a fluid-structure interaction setting, i.e.,

$$v_f = v_s \quad \text{on } \Gamma_i.$$

The second natural type are Neumann boundary conditions (applied stresses):

$$\sigma_f n_f = h \quad \text{on } \Gamma_{f,N} \subset \partial\Omega_f,$$

with a given vector-valued function $h = h(x, t)$.

### 5.5.2 Solid equations

For (nonlinear) elasto-dynamics, we have: Find vector-valued displacements $\hat{u} : \widehat{\Omega} \to \mathbb{R}^3$ such that

$$\hat{\rho}_s \partial_t^2 \hat{u}_s - \widehat{\text{div}}(\widehat{F}\widehat{\Sigma}) = \hat{\rho}_s \hat{f}, \quad \text{in } \widehat{\Omega}_s, \, t \in I, \tag{20}$$

with $\widehat{\Sigma} := \widehat{\Sigma}_s^{STVK}$. This second-order (in time) equation is supplemented by appropriate initial conditions and boundary conditions. As for the fluid equations, we prescribe Dirichlet boundary conditions (fixing the displacements):

$$\hat{u}_s = \hat{g} \quad \text{on } \widehat{\Gamma}_{s,D} \subset \partial\widehat{\Omega}_s,$$

where $\hat{g}$ is a given function. We can also employ Neumann boundary condition (surface stresses):

$$\widehat{F}\widehat{\Sigma}\hat{n}_s = \hat{J}\hat{\sigma}_s \widehat{F}^{-T}\hat{n}_s = \hat{h} \quad \text{on } \widehat{\Gamma}_{s,N} \subset \partial\widehat{\Omega}_s,$$

in which $\hat{h}$ is a given vector-valued function. Such a condition is seen from the structure side on the interface in case of a fluid-structure interaction problem, i.e.,

$$\widehat{F}\widehat{\Sigma}\hat{n}_s = -\hat{J}\hat{\sigma}_f \widehat{F}^{-T}\hat{n}_f \quad \text{on } \widehat{\Gamma}_i.$$

The body (or also volume) force on the right hand side is called a *dead load* if its density per unit volume in $\widehat{\Omega}$ is independent of a particular deformation $\widehat{T}$. An example is the gravity $g$.

In the case of incompressible materials (for example INH), we have the following result:

$$\hat{\rho}_s \partial_t^2 \hat{u}_s - \widehat{\text{div}}(\widehat{F}\widehat{\Sigma}) = \hat{\rho}_s \hat{f}, \quad \text{in } \widehat{\Omega}_s, \, t \in I, \tag{21}$$

$$\hat{J} = 1, \quad \text{in } \widehat{\Omega}_s, \, t \in I, \tag{22}$$

with $\widehat{\Sigma} := \widehat{\Sigma}_s^{INH}$. In the momentum equation, we can calculate specifically

$$-\widehat{\text{div}}(\widehat{F}\widehat{\Sigma}) = -\widehat{\text{div}}(\widehat{F}(-\hat{p}\hat{I} + \mu_s \widehat{F}\widehat{F}^{-T})) = \widehat{\text{div}}(\hat{p}\widehat{F}) - \widehat{\text{div}}(\widehat{F}(\mu_s \widehat{F}\widehat{F}^{-T})).$$

### 5.5.3 Incompressibility link between fluids and solids

Let us finally derive the relationship between incompressible fluids and solids. Recall:

$$\nabla \cdot v = 0 \text{ for fluids} \quad \hat{J} = 1 \text{ for solids} .$$

Since they represent the same physical mechanism; namely mass conservation, they should be the same! We calculate:

$$|\Omega| = \int_{\widehat{\Omega}} \hat{J} \, d\hat{x} \quad \Rightarrow \quad \frac{d}{dt}|\Omega| = \int_{\Omega} \nabla \cdot v \, dx.$$

### 5.5.4 Summary of variables, parameters, and constitutive quantities including their units

| SYMBOL | QUANTITY | UNITY |
|---|---|---|
| $x$ | Position | $m$ |
| $t$ | Time | $s$ |
| $u$ | Displacements | $m$ |
| $\nabla u$ | Gradient of displacements | dimensionless |
| $v$ | Velocity | $m/s$ |
| $\nabla v$ | Gradient of the velocity / inner friction of fluids | $1/s$ |
| $\partial_t v$ | Acceleration ($\partial_t v = \partial_{tt}^2 u$) | $m/s^2$ |
| $v \cdot \nabla v$ | Fluid convection term | $m/s^2$ |
| $p$ | Pressure | $Pa = N/m^2 = kg/ms^2$ |
| $\nabla p$ | Gradient of pressure | $Pa/m = N/m^3 = kg/m^2 s^2$ |
| $\widehat{F}$ | Deformation gradient | dimensionless |
| $\hat{J}$ | Determinant of $F$ | dimensionless |
| $n$ | Normal vector | $m$ |
| $\widehat{C}$ | Right Cauchy-Green tensor | dimensionless |
| $\widehat{E}$ | Green-Lagrange / Green-St. Venant strain tensor | dimensionless |
| $\widehat{E}_{lin}$ | Linearized Green-Lagrange / Green-St. Venant strain tensor | dimensionless |
| $I$ | Identity matrix/tensor | dimensionless |
| $\sigma_f$ | Cauchy fluid stress tensor | $Pa = N/m^2 = kg/ms^2$ |
| $\sigma \cdot n$ | Traction force | $Pa\,m = N/m$ |
| $\rho$ | Density | $kg/m^3$ |
| $\mu_f$ | Dynamic fluid viscosity / shear viscosity | $Pa\,s$ |
| $\nu$ | Kinematic fluid viscosity | $m^2/s$ |
| $\lambda_f$ | Volume viscosity | $Pa\,s$ |
| $Re$ | Reynolds number | dimensionless |
| $g$ | Gravity | $N/kg = m/s^2$ |
| $f$ | Force (such as gravity) | $N/kg = m/s^2$ |
| $\tilde{f}$ | Density of applied body force (in $N$) in per unit volume: $\tilde{f} = \rho f$ | $N/m^3 = kg/m^2 s^2$ |
| $\sigma_s$ | Cauchy solid stress tensor | $Pa/m^2$ |
| $\mu_s$ | Lamé parameter / shear modulus | $Pa = N/m^2 = kg/ms^2$ |
| $\mu_2$ | Material coefficient for Money-Rivlin material | $Pa = N/m^2 = kg/ms^2$ |
| $\lambda_s$ | Lamé parameter | $Pa = N/m^2 = kg/ms^2$ |
| $\kappa$ | Bulk modulus: $\kappa = 1/3(3\lambda + 2\mu)$ | $Pa = N/m^2 = kg/ms^2$ |
| $\nu_s$ | Poisson's ratio | dimensionless |
| $E_Y$ | Young's modulus | $Pa = N/m^2 = kg/ms^2$ |
| $\widehat{\Pi}$ | First Piola-Kirchhoff stress tensor | $Pa/m^2$ |
| $\widehat{\Sigma}$ | Second Piola-Kirchhoff stress tensor | $Pa/m^2$ |
| $W$ | Strain energy density functional per unit volume | $J/m^3 = N/m^2 = Pa$ |

Table 1: Variables and parameters in SI-units (Eulerian description without 'hats' is used when both notations are available).

**Remark 5.57** (Dimension check to verify models and equations). *We can easily check new mathematical models and equations for describing physical phenomena while performing a dimension check.*

# 6 Variational Formulations and Mathematical Analysis

In our three previous sections, we introduced notation and function spaces, mathematical tools (PDEs) and derived the equations for fluids and solids (in strong form). In this section, we work with preparations in order to

- derive the weak forms (separately for fluids and solids);

- establish several mathematical analysis results.

In fact, the first point is then further heavily used in the subsequent section in which fluid-structure interaction is formulated by means of variational coupling techniques. We notice that the equations of equilibrium and their associated weak (i.e., variational) formulations constitute the *principle of virtual work*[10] that is a well-known terminology in mechanics.

## 6.1 Preliminaries to existence and uniqueness

As in general, establishing well-posedness of nonlinear problems is more diffucult than for linear problems. For linear problems, one has for existence and uniquensse (for example)

- the Riesz representation theorem in Hilbert spaces (for symmetric bilinear forms); Theorem 3.44;

- the Lax-Milgram lemma (for symmetric and nonsymmetric bilinear forms); Theorem 3.42.

For nonlinear problems, we might work with combinations of the following key techniques:

- Galerkin methods: show first existence in a discrete setting and pass then to the limit;

- establishing a priori estimates to show boundedness of solutions; we know that bounded sequences (in reflexive spaces) are weakly convergent; by (compact) embedding theorems, weak convergence then leads to strong convergence in larger spaces;

- fixed-point theorems, such as Schauder-Tychonov;

- implicit and inverse function theorems.

**Example 6.1** (Proofing existence). *Let us illustrate these ideas by relating them to our problems:*

- *For Navier-Stokes, we use a combination of the first two techniques;*

- *For nonlinear elasticity, we use a Banach algebra structure and then work with the inverse function theorem;*

- *For fluid-structure interaction, we work a priori estimates, weak convergence, Sobolew embeddings, and the Schauder-Tychnonov fixed-point theorem.*

**Remark 6.2** (Uniqueness). *Uniqueness results often require small data assumptions; such as*

- *for fluids high viscosity, low Reynolds numbers, or small right-hand side forces;*

- *for solids simplifications to slightly nonlinear material behavior, or also small forces.*

*But we emphasize that this is not only a mathematical property but also of physical relevance: often fluid or solid states in nature do exist to certain configurations, forces, and boundary data, but the response is not unique.*

---

[10]For a precise definition and differences between 'principle of virtual work' and 'variational formulation', the reader should consult Ciarlet [61] (chapter 2, Theorem 2.4-1, Theorem 2.6-1 and the Remark on page 288). Additionally, a nice explanation is provided by Rannacher [192].

## 6.2 Weak formulations of Navier-Stokes

**Problem 6.3** (Nonstationary Navier-Stokes). *Find $\{v_f, p_f\} \in \{v_f^D + V_f^0\} \times L_f^0$ (for the definition of $L_f^0$ see Definition 3.21) such that the initial data satisfy $v_f(0) = v_f^0$, and for almost all time steps $t \in I$ holds:*

$$\rho_f(\partial_t v_f, \psi^v)_{\Omega_f} + \rho_f\big(v_f \cdot \nabla v_f, \psi^v\big)_{\Omega_f}$$
$$+(\sigma_f, \nabla \psi^v)_{\Omega_f} - \langle \sigma_f n_f, \psi^v \rangle_{\Gamma_{f,N}} - \rho_f(f, \psi^v)_{\Omega_f} = 0 \quad \forall \psi^v \in V_f^0, \tag{23}$$
$$(\nabla \cdot v_f, \psi^p)_{\Omega_f} = 0 \quad \forall \psi^p \in L_f^0,$$

**Problem 6.4** (Stationary Navier-Stokes). *Find $\{v_f, p_f\} \in \{v_f^D + V_f^0\} \times L_f^0$ such that*

$$\rho_f\big(v_f \cdot \nabla v_f, \psi^v\big)_{\Omega_f}$$
$$+(\sigma_f, \nabla \psi^v)_{\Omega_f} - \langle \sigma_f n_f, \psi^v \rangle_{\Gamma_{f,N}} - \rho_f(f, \psi^v)_{\Omega_f} = 0 \quad \forall \psi^v \in V_f^0, \tag{24}$$
$$(\nabla \cdot v_f, \psi^p)_{\Omega_f} = 0 \quad \forall \psi^p \in L_f^0.$$

To formulate fluid-structure interaction in ALE coordinates, this fluid system is further modified as explained in Section 7.3.3. Please bear in mind that we used the short-hand notation intoduced in Section 3.17 and specifically Definition 3.26.

**Remark 6.5** (At all times / a.e. all times $0 \le t \le T$). *We often use the notation 'for all times' or 'for almost all time steps' or 'a.e. all $0 \le t \le T$'. As alternative, we could have used the notation $L^2(I, X)$ for time-dependent Sobolev spaces. Of course, on the discretized level, we compute at each (discrete) timestep a solution to our problem.* ⋄

Additionally, if $v \in L^2(I, V_f^0)$ the meaning of the initial data needs further explanation. It can be shown that $v_f$ (see Temam [220], p. 253/254 and also Theorem 3.24 of these notes) is a.e. equal to an absolutely continuous function. Consquently, any function satisfying the weak form from above together with $v \in L^2(I, V_f^0)$ is a continuous function from $I$ to $V_f^{0,'}$. Therefore, the initial condition is well-defined. Finally, it is strongly recommended to consult Section 3.16 for the convention of vector-valued spaces and notation.

### 6.2.1 Outflow boundary conditions in channel flow - do-nothing

Let us go back to boundary conditions of the Navier-Stokes system and complement Section 5.5. The principal question we want to address is that the domain of interest might be very large (i.e., unbounded) but needs to be truncated for practical purposes in order to keep the computational cost reasonable; an illustration is provided in Figure 16. The question that comes up is how and what kind of boundary conditions should be described on $\Gamma_{in}$ and $\Gamma_{out}$?

In the variational formulation of Problem 6.3, there is no explicit reference to any kind of additional boundary condition. Let us concentrate on terms in the momentum equation that contribute to boundary integrals after integrating by parts and suppose for the moment that the solution $\{u, p\}$ is smooth enough. Finally, let us work for the moment with the non-symmetric stress tensor[11]:

$$(\sigma_f, \nabla \psi^v)_{\Omega_f} = (-p_f I + \rho_f \nu \nabla v_f, \nabla \psi^v)_{\Omega_f} = (\rho_f \nu \nabla v_f, \nabla \psi^v)_{\Omega_f} - (p_f, \nabla \cdot \psi^v)_{\Omega_f}.$$

Let us now integrate by parts:

$$(\rho \nu \nabla v_f, \nabla \psi^v)_{\Omega_f} - (p_f, \nabla \cdot \psi^v)_{\Omega_f} = \int_{\Gamma_{out}} [\rho \nu \nabla v \cdot n - pn] \, ds - (\rho \nu \Delta v_f, \psi^v) + (\nabla p, \psi^v).$$

If we now do not prescribe any value on $\Gamma_{out}$, we deal with a homogeneous Neumann condition, which leads to a natural boundary condition on the outflow boundary

$$\rho \nu \nabla v \cdot n - pn = 0 \quad \text{on } \Gamma_{out}. \tag{25}$$

---

[11] The non-symmetric version is important here; but below in this section, we augment to the symmetric stress tensor. We also refer to Section 6.2.3 for further comments on this subject.

This condition has been investigated in detail in [132] and since it appears naturally in the variational formulation it is called *do-nothing condition* because nothing needs to be done. Further discussions and references can be found in [190].
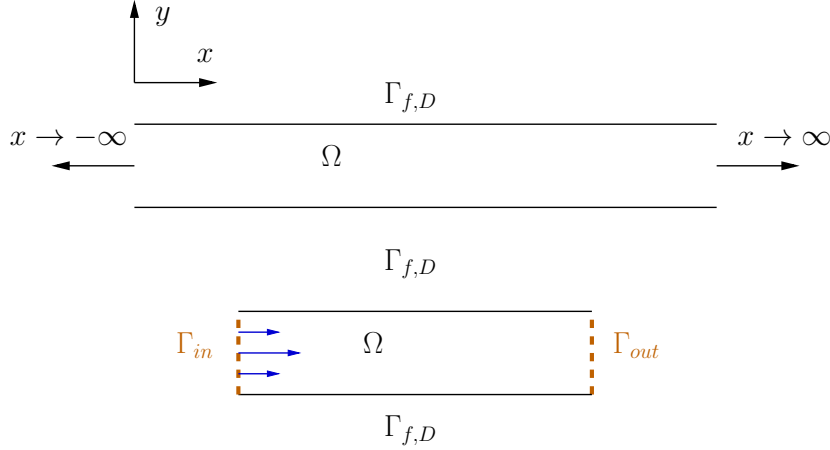


Figure 16: Truncation of an unbounded fluid domain and introducing artificial boundary conditions on $\Gamma_{in}$ and $\Gamma_{out}$. Specifically, the do-nothing condition might be employed on $\Gamma_{out}$ in the case that Dirichlet flow conditions are prescribed on $\Gamma_{in}$. If the model is driven by a pressure conditions on $\Gamma_{in}$ the do-nothing condition must be additionally used at this boundary.

Let us stay here for a moment and explain things in more detail. Usually (always!) the computational domain for a simulation is truncated in order restrict attention to certain parts of interest and to save computational burden. This truncation requires prescription of artificial boundary conditions. We remark that the the do-nothing condition should be taken carefully as we now demonstrate for two situations:

- First, for more than one outlet there are problems because there is a second condition hidden that the mean pressure is zero accross the outflow boundary:

$$\int_{\Gamma_{out}} p \, ds = 0. \tag{26}$$

This is a problem if a bifurcating channel with pipes of different length is considered and changes significantly the flow pattern [190].

- Let us know come to a second (very) important remark and let us work with the (physically correct!) symmetrized stress tensor such $\sigma_f \sim (\nabla v + \nabla v^T)$ (respectively parameters and pressure). Then our above calculation modifies to

$$(\rho\nu(\nabla v_f + \nabla v_f^T), \nabla \psi^v)_{\Omega_f} - (p_f, \nabla \cdot \psi^v)_{\Omega_f}$$
$$= \int_{\Gamma_{out}} [\rho\nu(\nabla v + \nabla v^T) \cdot n - pn] \, ds - (\rho\nu\nabla \cdot (\nabla v + \nabla v^T), \psi^v) + (\nabla p, \psi^v).$$

This modified version however does not anymore yield correct phyisical behavior as shown in the right subfigure of Figure 17; namely a parabolic inflow profile in a channel with straight walls should lead to a parabolic outflow profile. However the streamlines are curved outwards which is not correct. This behavior can be 'repeared' by only imposing the 'true do-nothing condition' (25), which means rather than having

$$\rho\nu(\nabla v + \nabla v^T) \cdot n - pn = 0,$$

we should subtract the symmetric part

$$\rho\nu\nabla v \cdot n - pn = -\rho\nu\nabla v^T \cdot n.$$

This means, everytime when we work with the symmetric stress tensor (in FSI always as we are learning! See also Section 6.2.3, Equation (29).) we need to add a boundary integral to our weak form:

$$- \int_{\Gamma_{out}} \rho \nu \nabla v^T \cdot n \psi^v \, ds,$$

in order to produce a parabolic outflow profile of parabolic inflow (please observe now the left subfigure of Figure 17).
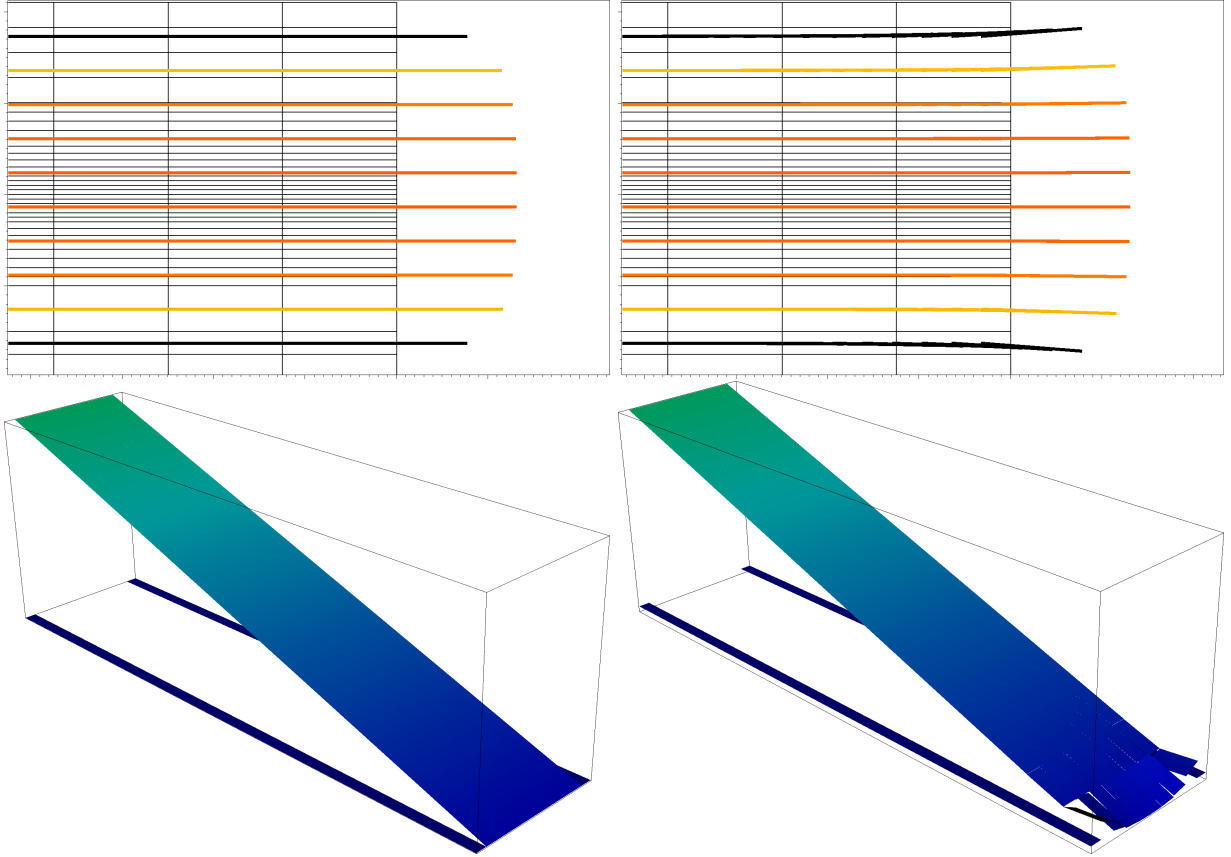


Figure 17: Impact of the correction term on the outflow boundary $\Gamma_{out}$ using the do-nothing [132] condition for Poiseuille flow. On top velocity streamlines are shown and on the bottom the corresponding (linear) pressure profile. In order to get the 'correct' outflow profile using the symmetric stress tensor, we need to subtract the symmetric part $\rho_f \nu_f \nabla v^T n_f$ on the outflow boundary. Otherwise you get non-physical curved streamlines as displayed in the right figure on top or corresponding pressure misbehaving (observed on right bottom). Additionally, the pressure is uniquely determined and fixed (by zero) on $\Gamma_{out}$ by condition (26), which is nicely demonstrated. Further examples and serious consequences are shown in [45].

**Remark 6.6** (do-nothing on the inflow boundary)**.** *If we prescribe on $\Gamma_{in}$ a pressure profile rather than Dirichlet velocities, the do-nothing condition must be also applied to $\Gamma_{in}$. All previous remarks apply analogously.*

**Remark 6.7.** *The do-nothing condition implies a constant pressure on this boundary that might be not physiological in bio-medical applications [95, 187]. Recent advances considering stability and well-posedness of settings including the do-nothing conditions have been obtained in [45]. In particular, the authors propose a modification, the directional do-nothing condition, that is necessary when out- and inflow on one boundary part is involved.*

**Remark 6.8** (Pressure normalization / filtering). *We notice that the pressure appears only in form of a gradient in the Navier-Stokes equations. If the outflow boundary $\Gamma_{out} = \emptyset$, the condition (26) is not implicitly contained since the do-nothing condition does not appear. In this case, the pressure normalization must be explicitly enforced, i.e., the global mean value is zero*

$$\int_\Omega p \, dx = 0. \tag{27}$$

*Then, the corresponding pressure space should be $L_0^2 = L^2/\mathbb{R}$ rather than $L^2$.*

### 6.2.2 Further remarks on flow boundary conditions and illustrations with numerical simulations

Despite the fact that we have advertised the do-nothing condition in Section 6.2.1, this is not the only choice.
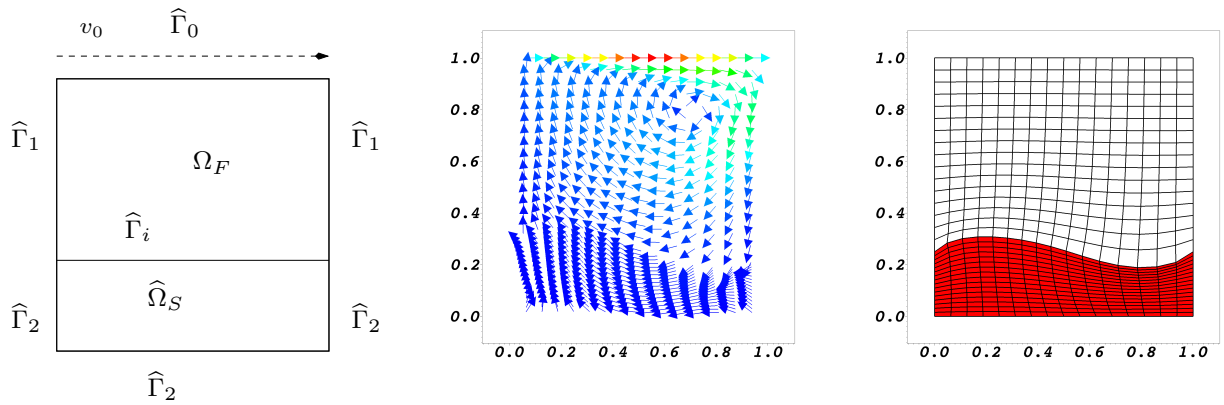


Figure 18: Lid-driven cavity configuration with elasticity: setting (taken from [72, 201]), velocity profile and deformation of the elastic body (in red). The last two figures are visualizations of a numerical FSI simulation with a very smooth solid; $\mu_s = 0.5Pa$ and $\nu_s = 0.4$ using the STVK model.

It is of course possible to set velocity Dirichlet conditions on the outflow boundary in addition to the inflow. However, we have to be careful in nonstationary flow evolutions (oszillatory flow) in which the fluid portion needs time to 'travel' from the inflow to the outflow. Here, the relation between inflow and outflow Dirichlet velocities is not clear and must be carefully derived when intending to employ on both parts Dirichlet conditions.

On the other hand, there are other examples in which the configuration is not channel such as the lid-driven cavity problem as sketched in Figure 18. Here, we prescribe Dirichlet flow $v_0$ on the top boundary $\widehat{\Gamma}_0$ and no-slip (homogeneous Dirichlet) on the other boundaries $\widehat{\Gamma}_1 \cup \widehat{\Gamma}_2$. In this test case, the pressure has been filtered using condition (27) since the pressure is only determined up to a constant.

**6.2.2.1 Prescription of pressure conditions** Alternatively to Dirichlet flow conditions, pressure conditions (of Neumann type) can be prescribed on inflow and outflow in order to cause the fluid to move:

- Prescription of pressure conditions on $\Gamma_{in}$ and $\Gamma_{out}$:

$$\rho\nu\nabla v \cdot n - pn = -\rho\nu\nabla v^T \cdot n + p_{in}n \quad \text{on } \Gamma_{in},$$
$$\rho\nu\nabla v \cdot n - pn = -\rho\nu\nabla v^T \cdot n + p_{out}n \quad \text{on } \Gamma_{out}.$$

- Test 1: $p_{in} = 2.0$ and $p_{out} = 1.0$;

- Test 2: $p_{in} = 1.0$ and $p_{out} = 0.0$;

For clarification let us recapitulate the meaning of these conditions in the weak formulation:

$$\rho_f(\partial_t v_f, \psi^v)_{\Omega_f} + \rho_f\big(v_f \cdot \nabla v_f, \psi^v\big)_{\Omega_f} + (\sigma_f, \nabla \psi^v)_{\Omega_f}$$

$$-\langle -\rho\nu\nabla v^T \cdot n_f + p_{in}n_f, \psi^v\rangle_{\Gamma_{f,in}} - \langle -\rho\nu\nabla v^T \cdot n_f + p_{out}n_f, \psi^v\rangle_{\Gamma_{f,out}} - \rho_f(f, \psi^v)_{\Omega_f} = 0 \quad \forall \psi^v \in V_f^0, \quad (28)$$

$$(\text{div}\, v_f, \psi^p)_{\Omega_f} = 0 \quad \forall \psi^p \in L_f^0.$$

As illustrated in Figure 19, the flow fields are identical because the important property is the pressure difference (which is the same $p_{in} - p_{out} = 1$ in both tests) and not the absolute values of the pressure. We recall that only the pressure gradient appears in the Navier-Stokes equations and thus the pressure is determined up to a constant.
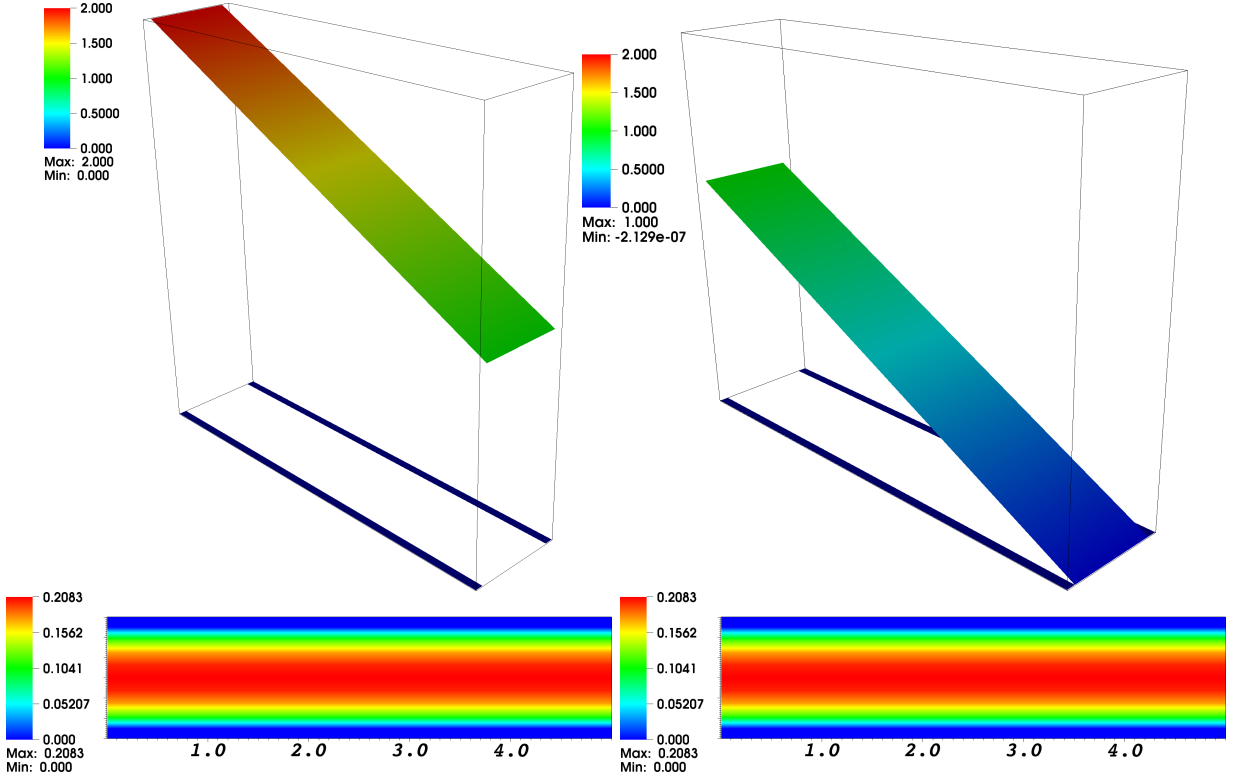


Figure 19: Prescription of pressure conditions on $\Gamma_{in}$ and $\Gamma_{out}$. On the left Test 1 and on the right Test 2. The corresponding flow fields are shown on the bottom. We emphasize that the flow fields are identical because the important property is the pressure difference (which is the same $p_{in} - p_{out} = 1$ in both tests) and not the absolute values of the pressure.

**6.2.2.2 Dirichlet inflow and do-nothing outflow**

- Dirichlet fluid inflow $v_{in}$ on $\Gamma_{out}$ and do-nothing on $\Gamma_{out}$.
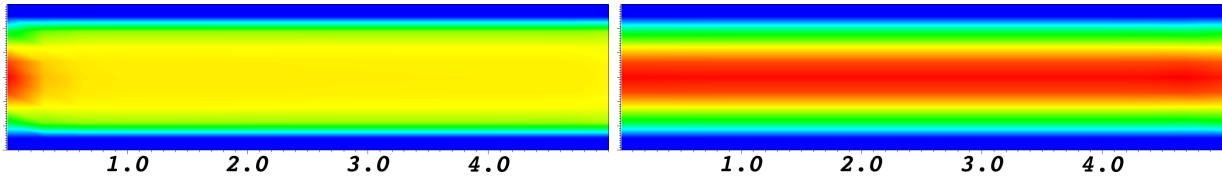


Figure 20: Poiseuille inflow for two different time steps of a numerical simulation. Choosing Dirichlet inflow $v_{in}$ on $\Gamma_{out}$ and do-nothing on $\Gamma_{out}$ is a natural choice. Make a thought experiment and try to imagine how one would describe known Dirichlet velocities on the outflow boundary. This is a priori nearly impossible since the flow field changes over time. Of course, once the flow reaches a steady-state pattern in this example, the outflow velocity is the same as the inflow. However, try to imagine this for oscillating flow.

**6.2.2.3 Limitation of standard do-nothing for pulsatile flow and possible modifications** In channels with elastic walls and pulsatile flow (for example a sinus-like inflow), pressure waves develop as illustrated in Figure 21.

Such a situation might arise using

$$v_{in} = \sin(t) \quad \text{on } \Gamma_{in}$$

as Dirichlet veloctity conditions.

In such situations, the standard do-nothing condition offers an important short-coming because it always normalizes the pressure to zero on $\Gamma_{out}$ as we learned before. However, for pulsatile flow the pressure wave is then reflected on this boundary which is often not desirable. Rather, we might be interested in letting going out this wave. The sequence of time snapshots illustrate this in Figure 22. Such situations are typical in hemodynamics for fluid-wall interactions. Because the outer walls are modeled as an elastic material that is not fixed by Dirichlet boundary conditions, pulse pressure waves propagate with time. In fact, flow simulations in a channel with rigid walls do not induce such behavior. As explained previously, the pressure waves have physical meaning; however, they are reflected at the artificial boundaries ($\widehat{\Gamma}_{in}$ and $\widehat{\Gamma}_{out}$) of the computational domain using standard boundary conditions. These reflections comprise no physics in general. Specifically, a larger artery leads to greater pressure wave propagation, and larger reflections at



Figure 21: Numerical simulation of a pressure wave caused by pulsatile Dirichlet inflow in a channel with elastic walls.

the artificial boundaries. From mathematical and physical point of view, it is a rather complex task to determine the proper boundary conditions and this subject has been investigated for several years. In particular,

the standard do-nothing condition as introduced in Section 6.2.1 needs to be modified so that the pressure is not always constrained to zero on $\Gamma_{out}$.

The *geometrical multiscale approach* (introduced in [90, 93]), is often used to account for this deficiency. With this method, higher-dimensional models (in 3D or 2D) are coupled with lower-dimensional models (in 0D or 1D). The reason to introduce such a coupling originates from the fact that modeling and simulation are too difficult to perform for large systems such as for example, the entire human cardiovascular system. However, because the local flow dynamics in a specific region (for instance inside a blood vessel) are related to global flow dynamics ([95, 172, 187], and the many references cited therein). Consequently, their interaction must not be neglected. Otherwise, only partial information can be extracted from the simulation and be used for further analysis and application to real-life data.

In the following, we briefly recall the concept of *defective* boundary conditions that are well-known in the blood flow community [94, 187]. Using defective boundary conditions, we deal with averaged data (i.e., the mean velocity and the mean pressure instead of vector-like conditions as mentioned above). The mean pressure on each free artificial section can be computed with help of

$$\frac{1}{|\Gamma_{\text{in,out}}|} \int_{\Gamma_{\text{in,out}}} p \ \mathrm{d}s = P_{\Gamma_{\text{in,out}}}(t).$$

The net flux condition reads:

$$\int_{\Gamma_{\text{in,out}}} v_f \cdot n_f \ \mathrm{d}s = Q(t).$$

The difficulty in those cases is to guarantee the well-posedness of the resulting system, which is done for a special configuration in Heywood et al. [132].
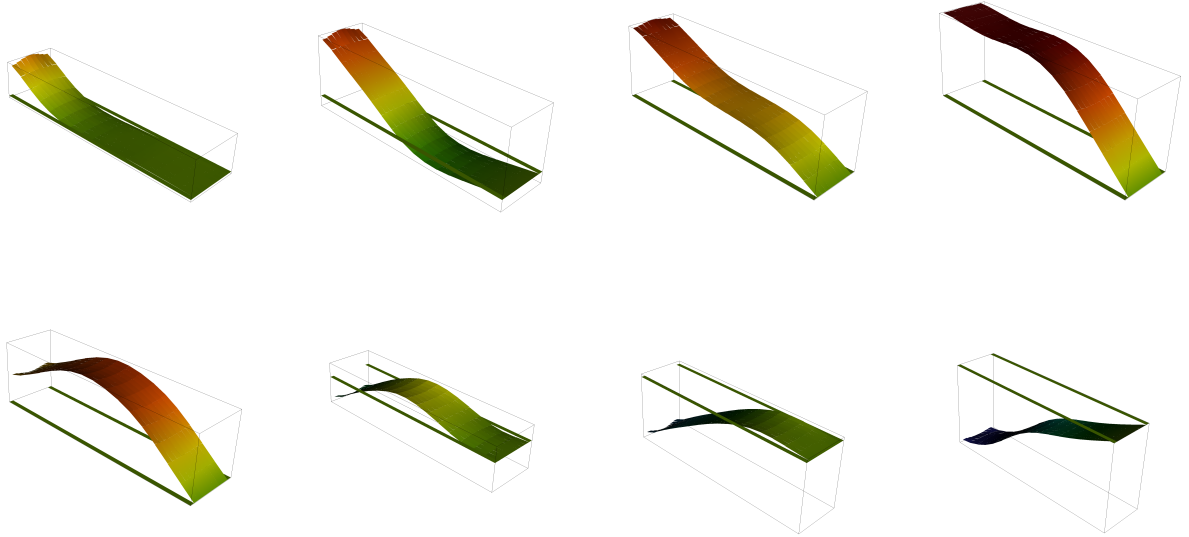


Figure 22: Snapshots of time instances of a numerical simulations that illustrates a short-coming of the standard do-nothing conditions. Pulsatile flow prescribed on $\Gamma_{in}$ causes pressure waves that are reflected on $\Gamma_{out}$ because the do-nothing condition normalizes the pressure to zero.

The geometrical multiscale approach was simplified in [147, 175] to a specific pressure condition on the outflow boundary, i.e., by adding a constant mean pressure value at each time step to the zero mean pressure from the do-nothing condition. This pressure correction is a so-called *absorbing condition* for the fluid problem, that is applied on the artificial outflow boundary $\Gamma_{\text{out}}$ of the domain of interest.

The absorbing condition can be derived from a 1D reduced model (see [147]) for the flow field and it is computed in the reference configuration for each time step $n = 0, 1, 2, \dots$ by

$$\bar{p}^{n+1} \approx \hat{R}\hat{Q}^n \quad \text{on } \widehat{\Gamma}_{\text{out}},$$

where $\bar{p}$ is a mean value for the pressure, $\hat{R}$ (the resistance) is some constant with information on the geometry, structural properties, and fluid properties [147].

The flux value $\hat{Q}^n$ of the velocity is measured on $\widehat{\Gamma}_{\text{out}}$ by:

$$\hat{Q}^n = \int_{\widehat{\Gamma}_{\text{out}}} \hat{v}_f^n \cdot \hat{n}_f \, \mathrm{d}s, \quad n = 0, 1, 2, \dots.$$

This condition accounts for global flow dynamics in the remaining parts of the cardiovascular system.

**Remark 6.9** (Final comments on reflection of pressure waves on $\Gamma_{out}$). *We finally notice that a complete absorption of pressure waves is not necessarily physiological because backflow of waves can be induced by bifurcations, for instance see [95, 175] or other 'obstacles' inside the artery. Consequently, this whole topic on artificial boundary conditions is by far non-trivial.*

**6.2.2.4 Influence of boundary conditions on evaluation of quantities of interest** What is in most cases the purpose of a model and its solutions? Well, we want to gain understanding of certain effects and more specifically, we are interested in evaluating quantities of interest (or mathematically-speaking functionals of interest). In solid mechanics, these are deflections and deformations: what is the displacement of a bridge subject to weather (wind) or forces caused by trucks driving over it. In fluid mechanics, one is often interested in evaluating surface forces such as drag and lift. What have these comments to do with boundary conditions? In addition to our previous considerations, boundary conditions in numerical simulations can have significant influence on quantities of interest - even when these functional evaluations are far away from the boundary. Ideally, the domain should be infinitely large such that boundary conditions do not play a role. However, as explained in the previous sections, this is in most case impossible to achieve. Thus, we have to take care that the error in functionals caused by the boundary is sufficiently small. Let us illustrate these considerations with an example: in channel flow with an elastic beam [140], we want to evaluate the tip-deflection of the beam and also drag and lift forces acting on this beam and the hole. The questions is where to we cut the channel in order to impose artificial boundary conditions. Taking the original FSI-1 benchmark configuration with different channel lengths $5.0m, 2.5m, 1.5m$ and $1.0m$[12] leads to the results presented in Table 2 in which we clearly see that some of the functionals depend significantly on the length of the channel. The original setting in [140] had the length $2.5m$.

Table 2: Dependence of functional evaluations on the length of the channel.

| Length | $u_x(A)[10^{-5}]$ | $u_y(A)[10^{-4}]$ | Drag | Lift |
|--------|-------------------|-------------------|------|------|
| 5.0    | 2.02              | 8.22              | 16.7 | 0.74 |
| 2.5    | 2.27              | 8.22              | 15.3 | 0.74 |
| 1.5    | 2.38              | 8.23              | 14.6 | 0.74 |
| 1.0    | 2.47              | 7.94              | 14.3 | 0.73 |

---

[12] In the last computation displayed in the fourth row of Table 2, even the nonlinear solver for computing the numerical solution had problems to converge.
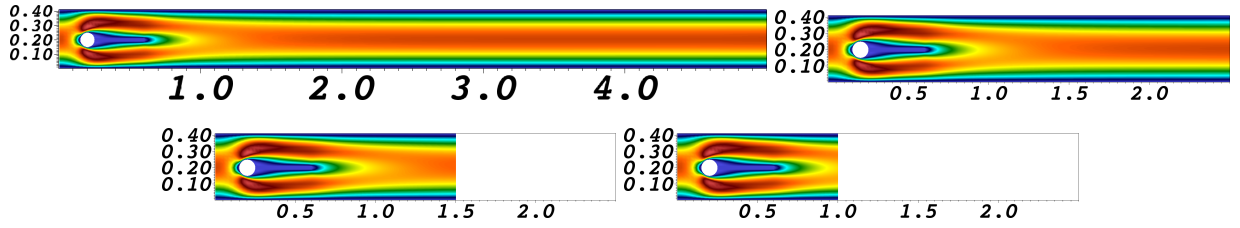
Figure 23: Velocity profile of the FSI 1 benchmark with different channel lengths to illustrate dependence of functional evaluations on boundary conditions.

### 6.2.3 Symmetric versus non-symmetric Cauchy stress in Navier-Stokes

In Navier-Stokes formulations, we often find the non-symmetric version

$$\sigma = -pI + \rho_f \nu \nabla v.$$

This can be reasoned as follows. We have (respectively the pressure):

$$\nabla \cdot \sigma \sim \nabla \cdot (\rho_f \nu (\nabla v + \nabla v^T)).$$

If $\rho_f$ and $\nu$ are constant, we obtain

$$\nabla \cdot (\rho_f \nu (\nabla v + \nabla v^T)) = \rho_f \nu \nabla \cdot (\nabla v + \nabla v^T) = \rho_f \nu (\nabla \cdot \nabla v + \nabla \cdot \nabla v^T) = \rho_f \nu (\Delta v + \nabla \cdot \nabla v^T).$$

The last term can be rewritten as (can be seen if we would write everything component wise and apply vector calculus rules):

$$\rho_f \nu \nabla \cdot \nabla v^T = \rho_f \nu \nabla (\nabla \cdot v).$$

For incompressible fluids, because of $\nabla \cdot v = 0$, it yields

$$\rho_f \nu \nabla (\underbrace{\nabla \cdot v}_{=0}) = 0.$$

Consequently, the symmetric stress tensor could be replaced by the non-symmetric version. Here, we strongly emphasize that

$$\rho_f \nu \nabla (\nabla \cdot v) = 0,$$

does hold in the whole domain $\Omega$ (as global average) and makes use of the divergence operator. Thus, its restriction to a part of the boundary is in general not true,

$$\sigma_f n \sim \rho_f \nu [\nabla v + \nabla v^T] n \neq \rho_f \nu \nabla v\, n. \tag{29}$$

which means that in fluid-structure interaction, where we need $\sigma_f n$ on the interface, we cannot work with this simplification. Possible consequences of symmetric versus non-symmetric Cauchy stress tensors on non-Dirichlet boundary parts are discussed in Section 6.2.1.

## 6.3 Existence, regularity and stability of Navier-Stokes

### 6.3.1 Existence of stationary Navier-Stokes

**Theorem 6.10** ([192, 220])**.** *The stationary Navier-Stokes Problem 6.4 with homoegeneous Dirichlet boundary conditions on $\partial\Omega$ has a solution $\{v, p\} \in V_f^0 \times L_f$ for all Reynolds numbers Re. The solution is unique for sufficiently small data $c_*^2 \nu_f^{-2} \|f\|_{H^{-1}} < 1$, where $c_*^2$ is linked to the continuity of the convection term.*

*Proof.* The outline of the proof is as follows:

- Eliminate the pressure such that we can work (in appropriate spaces!!!) with

$$\rho_f \big( v \cdot \nabla v, \psi^v \big)_{\Omega_f} + (\nabla v, \nabla \psi^v)_{\Omega_f} - \rho_f (f, \psi^v)_{\Omega_f} = 0 \quad \forall \text{ admissible } \psi^v, \tag{30}$$

- Use the Galerkin method and construct an approximate (discrete) solution;

$$\rho_f\big(v_m \cdot \nabla v_m, \psi^v\big)_{\Omega_f} + (\nabla v_m, \nabla \psi^v)_{\Omega_f} - \rho_f(f, \psi^v)_{\Omega_f} = 0 \quad \text{for } m = 1, 2, 3, \ldots.$$

- Proof existence of the approximate system;

- Derive an a priori estimate that makes use of the special structure of the convection term; namely:

$$(u \cdot \nabla v, w) = (v, \nabla(vw)) - (u \cdot \nabla w, v) = -(\nabla \cdot u, vw) - (u \cdot \nabla w, v) = -(u \cdot \nabla w, v). \tag{31}$$

Setting $v = w$ yields $(u \cdot \nabla v, v) = 0$. Then, setting $\psi = v$ in the weak form yields the a priori estimate:

$$\nu\|v\|^2 + (v \cdot \nabla v, v) = (f, v),$$

which is because of (31),

$$\nu\|v\|^2 = (f, v) \leq \|f\|_{V^*}\|v\|,$$

and therefore

$$\nu\|v\| \leq \frac{1}{\nu}\|f\|_{V^*}.$$

Consequently, $v$ is bounded in $V$.

- Use the boundedness to justify weak convergence of a subsequence $v_{m'} \rightharpoonup v$ in $V$.

- Because of the compact embedding $V \hookrightarrow L^2$, we infer $v_{m'} \to v$ in $L^2$. It remains to show that this does also hold for the convection term; i.e., $(v_{m'} \cdot \nabla v_{m'}, \psi) \to (v \cdot \nabla v, \psi)$.

- Pass to the limit $m' \to \infty$:

$$\nu(\nabla v_{m'}, \nabla \psi) + (v_{m'} \cdot \nabla v_{m'}, \psi) = (f, \psi) \quad \to \quad \nu(\nabla v, \nabla \psi) + (v \cdot \nabla v, \psi) = (f, \psi)$$

- Go back to the pressure and show that existence and uniqueness of pressure $p \in L^2$ can be established (uses a result of de Rham from distribution theory). The existence of the pressure and its stability are obtained via the inf-sup condition:

**Proposition 6.11** (inf-sup condition). *For each linear functional $l(\cdot)$ on $H_0^1$ with the property $l(\varphi) = 0$ for $\varphi \in H_{div} := \{\varphi \in H_0^1 : \nabla \cdot \varphi = 0\}$, there exists a unique function $p \in L_f^0$ such that*

$$(p, \nabla \cdot \varphi) = l(\varphi) \quad \forall \varphi \in H_0^1.$$

*Furthermore, to each function $p \in L_f^0$, there exists a $v \in H_0^1$ with*

$$p = \nabla \cdot v, \quad \|\nabla v\| \leq \gamma\|p\|,$$

*with a constant $\gamma$ that is independent of $p$. Finally, it yields the stability estimate (i.e., the continuous inf-sup condition):*

$$\inf_{q \in L_f^0} \sup_{\varphi H_0^1} \frac{(q, \nabla \cdot \varphi)}{\|q\| \|\nabla \varphi\|} \geq \gamma > 0.$$

*Proof.* See for example Rannacher [192]. $\qquad\square$

- Show finally uniqueness of velocities in which we compare two different solution $v_1$ and $v_2$ of the Navier-Stokes problem and use again the a priori estimate together with the special structure of the convection term to obtain (after some calculations):

$$\nu\|v_1 - v_2\|^2 \leq c_*^2\|v_1 - v_2\|^2\|v_1\| \leq \frac{c_*^2}{\nu}\|f\|_{V^*}\|v_1 - v_2\|^2$$

form which follows:

$$\left(\nu - \frac{c_*^2}{\nu}\|f\|_{V^*}\right)\|v_1 - v_2\|^2 \leq 0.$$

Using now the uniquenss condition $c_*^2\nu_f^{-2}\|f\|_{H^{-1}} < 1$, we observe that in this case $\|v_1 - v_2\| = 0$, i.e., $v_1 = v_2$.

---

- Full proofs can be found in [112, 192, 220].

$\square$

**Proposition 6.12** (Homework). *Show that the semi-linear form of Navier-Stokes is non-symmetric.*

### 6.3.2 Regularity of fluid equations

**Problem 6.13** ([220], p. 190). *Let $\hat{f}_f$ and $\hat{v}_f^0$ be given by*

$$\hat{f}_f \in L^2(I; H^{-1}(\widehat{\Omega}_f)), \quad v_f^0 \in \hat{L}(\widehat{\Omega}_f).$$

*Find: $\hat{v}_f \in L^2(I; H^1(\widehat{\Omega}_f))$ such that the standard Navier-Stokes equations (as defined, e.g., by Temam [220]) are solved with the initial data $\hat{v}_f(0) = \hat{v}_f^0$.*

Theorem 3.1 in [220] shows that at least one solution to the previous defined problem exists, i.e., it holds

$$\hat{v}_f \in L^2(I, H^1(\widehat{\Omega}_f)).$$

The main consequence for fluid-structure interaction is that $\hat{v}_f \in H^{1/2}(\widehat{\Gamma}_i)$.

### 6.3.3 Stability of solutions for stationary Navier-Stokes

This section connects the previous theoretical findings with physical observations and addresses the question when stationary flow becomes nonstationary. The presentation follows [192].

**Definition 6.14** (Exponential stability). *Let $w$ be the perturbation of $v - \tilde{v}$ where $v$ is the solution to the stationary NSE problem and $\tilde{v}$ the solution to the nonstarionary NSE problem. Then, exponential stability means:*

$$\|w(t)\| \sim e^{-\alpha t}\|\delta v^0\|, \quad t > 0,$$

*where $\delta v^0$ is a small perturbation from the divergence-free Stokes space.*

**Proposition 6.15** (Hydrodynamical stability). *A solution $v$ to the stationary Navier-Stokes problem on a domain $\Omega$ with Dirichlet conditions on $\partial\Omega$ is exponentially stable if*

$$c_*^2 \nu_f^{-1}\|v\| < 1 \quad i.e., \quad c_*^2 \nu^{-2}\|f\|_{H^{-1}} < 1.$$

*Proof.* See Rannacher [192], p. 128. $\square$

**Remark 6.16.** *We observe that the condition which guaranteed uniqueness of the stationary Navier-Stokes problem also leads to hydrodynamical stability of solutions.*

## 6.4 Weak formulations of elasticity

**Problem 6.17.** *Find $\hat{u} \in V = H_0^1$ such that the initial data satisfy $\hat{u}(0) = \hat{u}_0 \in \hat{V}_s^0$ and $\hat{v}(0) = \hat{v}_0 \in L^2$ and*

$$(\partial_t^2 \hat{u}, \hat{\varphi}) + (\widehat{F\Sigma}, \widehat{\nabla}\hat{\varphi}) = (\hat{f}, \hat{\varphi}) \quad \forall \varphi \in \hat{V}_s^0,$$

*for a.e. all times $0 \le t \le T$. Furthermore, $\partial_t \hat{u} \in L^2$ and $\partial_t^2 \hat{u} \in H^{-1}$ for a.e. all times $0 \le t \le T$.*

**Problem 6.18** (Mixed formulation - first order system in time). *Find $\hat{u} \in \hat{V}_s^0 = H_0^1$ and $\hat{v} \in L^2$ with the initial data $\hat{u}(0) = \hat{u}_0$ and $\hat{v}(0) = \hat{v}_0$ such that*

$$(\partial_t \hat{v}, \hat{\varphi}) + (\widehat{F\Sigma}, \widehat{\nabla}\hat{\varphi}) = (\hat{f}, \hat{\varphi}) \quad \forall \hat{\varphi} \in V$$
$$(\partial_t \hat{u} - \hat{v}, \hat{\chi}) = 0 \quad \forall \hat{\chi} \in L^2$$

*for a.e. all times $0 \le t \le T$. Furthmore, $\partial_t^2 \hat{u} \in H^{-1}$ for a.e. all times $0 \le t \le T$.*

**Problem 6.19** (Stationary elasticity). *Find $\hat{u} \in \hat{V}_s^0 = H_0^1$ such that*

$$(\widehat{F}\widehat{\Sigma}, \widehat{\nabla}\hat{\varphi}) = (\hat{f}, \hat{\varphi}) \quad \forall \hat{\varphi} \in \hat{V}_s^0$$

**Problem 6.20** (Stationary linearized elasticity). *Find $\hat{u} \in \hat{V}_s^0 = H_0^1$ such that*

$$(\widehat{\Sigma}_{lin}, \widehat{\nabla}\hat{\varphi}) = (\hat{f}, \hat{\varphi}) \quad \forall \hat{\varphi} \in \hat{V}_s^0,$$

*where*

$$\widehat{\Sigma}_{lin} = 2\mu\widehat{E}_{lin} + \lambda tr\widehat{E}_{lin}\hat{I}.$$

It remains to justify two things at this moment:

- How are initial conditions prescribed in $L^2$?

- How is the weak formulation related to the strong form?

With regard to the first remark, the initial conditions are justified with the help of Theorem 3.24 that has been already used to justify initial conditions in the Navier-Stokes equations. As an example for the correspondance between weak form und strong equations, let us justify the weak form of Problem 6.20:

**Proposition 6.21.** *Let the following linear boundary value problem be given:*

$$-\nabla \cdot (\widehat{\Sigma}_{lin}) = f \quad in\ \widehat{\Omega}, \tag{32}$$

$$\hat{u} = 0 \quad on\ \partial\widehat{\Omega}_D, \tag{33}$$

$$\widehat{\Sigma}_{lin}\hat{n} = \hat{g} \quad on\ \partial\widehat{\Omega}_N. \tag{34}$$

*Finding a solution $\hat{u}$ of this strong form is formally equivalent to finding a solution of Problem 6.20.*

*Proof.* We employ Green's formula for any sufficiently smooth tensor field $\widehat{\Sigma}$ and vector field $\hat{\varphi}$, we obtain

$$\int_{\widehat{\Omega}} \nabla \cdot \widehat{\Sigma} \cdot \hat{\varphi}\, d\hat{x} = -\int_{\widehat{\Omega}} \widehat{\Sigma} : \widehat{\nabla}\hat{v}\, d\hat{x} + \int_{\partial\widehat{\Omega}_N} \widehat{\Sigma}\hat{n} \cdot \hat{\varphi}\, d\hat{s} = -\int_{\widehat{\Omega}} \widehat{\Sigma} : \widehat{E}_{lin}\, d\hat{x} + \int_{\partial\widehat{\Omega}_N} \widehat{\Sigma}\hat{n} \cdot \hat{\varphi}\, d\hat{s}.$$

The last equal sign is justified with linear algebra arguments, i.e., for a symmetric matrix $A$ is holds:

**Definition 6.22** (Proof is homework).

$$A : B = A : \frac{1}{2}(B + B^T).$$

Furthermore, on the boundary part $\partial\widehat{\Omega}_D$ the vector field $\hat{\varphi}$ vanishes by definition. Thus, the first direction is shown. Conversely, we now assume that the variational equations are satisfied; namely,

$$\int_{\widehat{\Omega}} \widehat{\Sigma} : \widehat{\nabla}\hat{\varphi}\, d\hat{x} = \int_{\widehat{\Omega}} \hat{f} \cdot \hat{\varphi}\, d\hat{x}$$

if $\hat{\varphi} = 0$ on all $\partial\Omega$. By Green's formula we now obtain

$$\int_{\widehat{\Omega}} \widehat{\Sigma} : \widehat{\nabla}\hat{\varphi}\, d\hat{x} = -\int_{\widehat{\Omega}} \widehat{\nabla} \cdot \widehat{\Sigma}\, d\hat{x}.$$

Putting both pieces together and taking into account that the integrals do hold on arbitrary volumes yields

$$-\widehat{\nabla} \cdot \widehat{\Sigma} = \hat{f} \quad in\ \widehat{\Omega}.$$

Considering now the Neumann boundary, we use again Green's formula to see

$$\int_{\partial\widehat{\Omega}_N} \widehat{\Sigma}\hat{n} \cdot \hat{\varphi}\, ds = \int_{\partial\widehat{\Omega}_N} \hat{g}\, ds.$$

This holds for arbitrary boundary parts $\partial\widehat{\Omega}_N$ such that $\widehat{\Sigma}\hat{n} = \hat{g}$ can be inferred and concluded the second part of the proof. □

## 6.5 Existence, damping and regularity of elasticity

### 6.5.1 Existence of stationary linearized elasticity

A general existence theorem for time-dependent, fully nonlinear three-dimensional elasticity does not exist. In order to approach such problems while learning novel techniques and apply results from analysis and functional analysis, we first study a linearized problem. Even so that linearized elasticity is an elliptic problem and has much in common with the scalar-valued Poisson problem, establishing existence and uniquenss for the stationary version is a non-trivial task. Why? Let us work with Problem 6.20 in 3D and since this problem is linear we aim to apply the Riesz representation theorem[13] (or the Lax-Milgram lemma - see Theorem 3.42) and need to check the assumptions:

- Determine in which space $\hat{V}$ we want to work;

- The form $A(\hat{u}, \hat{\varphi})$ is symmetric or non-symmetric

- The form $A(\hat{u}, \hat{\varphi})$ is continuous bilinear w.r.t. to the norm of $\hat{V}$;

- The bilinear form $A(\hat{u}, \hat{\varphi})$ is $V$-elliptic;

- The right-hand side functional $\hat{f}$ is a continuous linear form.

The ingredients to check are:

- From which space must $\hat{f}$ be chosen such that it is continuous? (This leads to Sobolev embedding theorems [61, 77]);

- How do we check the $V$-ellipticity? (This requires the famous Korn inequality as it is stated in a minute below).

For proofing existence of linearized elasticity, we need to check as second contition the $V$-ellipticity which is 'easy for scalar-valued problems' but non-trivial in the case of vector-valued elasticity. The resulting inequalities are named after Korn (1906):

**Theorem 6.23** (1st Korn inequality)**.** *Let us assume displacement Dirichlet conditions on the entire boundary $\partial \Omega$. For vector-fields $\hat{u} \in H_0^1(\widehat{\Omega})^3$ it holds:*

$$\|\nabla \hat{u}\| \leq c_{Korn} \|\widehat{E}_{lin}(\hat{u})\|.$$

*where $\widehat{E}_{lin}(\hat{u}) := \frac{1}{2}(\widehat{\nabla}\hat{u}_s + \widehat{\nabla}\hat{u}_s^T) \in L^2(\widehat{\Omega}_s)$.*

*Proof.* See for example [46, 61, 192]. □

The more general form is as follows:

**Theorem 6.24** (2nd Korn inequality)**.** *Let a part of the boundary of Neumann type, i.e., $\partial \Omega_N \neq 0$ and let the entire boundary be of class $C^1$, or a polygon, or of Lipschitz-type. For vector-fields $\hat{u} \in H^1(\widehat{\Omega})^3$ and $\widehat{E}_{lin} \in L^2$ it holds*

$$\|\hat{u}_s\|_{H^1(\widehat{\Omega}_s)} \leq C_{Korn} \big(|\hat{u}_s|^2_{L^2(\widehat{\Omega}_s)} + |\widehat{E}_{lin}|^2_{L^2(\widehat{\Omega}_s)}\big)^{1/2} \quad \forall \hat{u}_s \in H^1(\widehat{\Omega}_s),$$

*and a positive constant $C_K$ and secondly,*

$$u \mapsto \big(|\hat{u}_s|^2_{L^2(\widehat{\Omega}_s)} + |\widehat{E}_{lin}|^2_{L^2(\widehat{\Omega}_s)}\big)^{1/2}$$

*is a norm that is equivalent to $\|\cdot\|_{H^1}$.*

---

[13] Here, $A(\hat{u}, \hat{\varphi}) = (\widehat{\Sigma}_{lin}, \hat{\varphi})$ is symmetric and the Riesz representation 3.44 is sufficient for existence and uniqeness!

**Theorem 6.25** (Existence of a weak solution of linearized elasticity ). *Let $\widehat{\Omega} \subset \mathbb{R}^3$ and $\widehat{\Gamma}_D > 0$ and $\widehat{\Gamma}_N > 0$ Dirichlet and Neumann boundary respectively. Let the Lamé constants be $\mu > 0$ and $\lambda > 0$ and $\hat{f} \in L^{6/5}(\Omega)$ and $\hat{g} \in L^{4/3}(\widehat{\Gamma}_N)$ be given. Furthermore, let*

$$\hat{V} := \{\hat{\varphi} \in H^1(\widehat{\Omega})| \, \hat{\varphi} = 0 \; on \; \widehat{\Gamma}_D\}.$$

*Then, there exists a unique element $\hat{u} \in \hat{V}$ such that*

$$A(\hat{u}, \hat{\varphi}) = F(\hat{\varphi}) \quad \forall \hat{\varphi} \in \hat{V}.$$

*Here, the bilinear form and the right hand side functional are given by*

$$A(\hat{u}, \hat{\varphi}) = (\widehat{\Sigma}_{lin}, \widehat{\nabla}\hat{\varphi}), \quad and \quad F(\hat{\varphi}) = (\hat{f}, \hat{\varphi}) + \langle\hat{g}, \hat{\varphi}\rangle, \tag{35}$$

*where the linearized STVK model is given by*

$$\widehat{\Sigma}_{lin} := 2\mu\widehat{E}_{lin} + \lambda tr\widehat{E}_{lin}\hat{I}.$$

*The function $\hat{g}$ is a prescribed traction condition on $\widehat{\Gamma}_N$; namely:*

$$[2\mu\widehat{E}_{lin} + \lambda tr\widehat{E}_{lin}I]\,\hat{n} = \hat{g}.$$

*Proof.* The proof is as follows:

- **Continuity of the right hand side functional** $F(\cdot)$. In order to apply Hölder's inequality, we first check the correct Sobolev embedding:

$$H^1 = W^{1,2} \hookrightarrow L^{p^*} \quad \text{with} \quad \frac{1}{p^*} = \frac{1}{p} - \frac{m}{d}$$

for $m < \frac{d}{p}$. Since we work in 3D, $d = 3$. Furthermore, $m = 1, p = 2$ in $W^{m,p}$. It can be inferred that consequently, $p^* = 6$. For the continuity of $F$, we calculate with Hölder's inequality:

$$|(\hat{f}, \hat{\varphi})| \leq \|\hat{f}\|_p \|\hat{\varphi}\|_{q=6}$$

where $\frac{1}{p} + \frac{1}{q} = 1$. Since, $q = 6$, this yields $p = \frac{6}{5}$, i.e., $\hat{f} \in L^{6/5}$. In the same spirit, we obtain $\hat{g} \in L^{4/3}$ while additionally employing the trace inequality. Let us verify this claim: From trace theorems, e.g., [61], p. 280, we know that for $1 \leq p < \infty$ we have

$$tr \in L(W^{1,p}, L^{p^*}) \quad \Leftrightarrow \quad \|\cdot\|_{L^{p^*}} \leq c\|\cdot\|_{W^{1,p}},$$

with $\frac{1}{p^*} = \frac{1}{p} - \frac{1}{(d-1)}(\frac{p-1}{p})$ if $1 \leq p < d$. As before and still, $d = 3$. This means $1 \leq p \leq 2$. Of course we want to work again with $W^{1,2}$, $p = 2$. Then,

$$\frac{1}{p^*} = \frac{1}{p} - \frac{1}{(d-1)}(\frac{p-1}{p}) = \frac{1}{2} - \frac{1}{(3-1)}(\frac{2-1}{2}) = \frac{1}{4}.$$

Consequently, $p^* = 4$. Let us estimate with Hölder's inequality and the trace theorem:

$$\int_{\widehat{\Gamma}_N} \hat{g}\hat{\varphi}\,ds \leq \|\hat{g}\|_{L^q(\widehat{\Gamma}_N)}\|\hat{\varphi}\|_{L^4(\widehat{\Gamma}_N)} \leq \|\hat{g}\|_{L^q(\widehat{\Gamma}_N)}\|\hat{\varphi}\|_{W^{1,2}(\widehat{\Omega})}.$$

In order to be able to apply Hölder's inequality we need to find the correct $q$. This is now easy with

$$\frac{1}{p} + \frac{1}{q} = 1 \quad \Rightarrow q = \frac{4}{3}.$$

Consequently, $\hat{g} \in L^{4/3}$.

- **Symmetry of $A(\hat{u}, \hat{\varphi})$.** Let us now verify if $A(\hat{u}, \hat{\varphi})$ is symmetric:

$$
\begin{aligned}
A(\hat{u}, \hat{\varphi}) &= (\widehat{\Sigma}_{lin}, \widehat{\nabla}\hat{\varphi}) = (2\mu\widehat{E}_{lin}(\hat{u}) + \lambda tr(\widehat{E}_{lin}(\hat{u}))\hat{I}, \widehat{E}_{lin}(\hat{\varphi})) \\
&= 2\mu(\widehat{E}_{lin}(\hat{u}), \widehat{E}_{lin}(\hat{\varphi})) + \lambda(tr(\widehat{E}_{lin}(\hat{u}))\hat{I}, \widehat{E}_{lin}(\hat{\varphi})) \\
&= 2\mu(\widehat{E}_{lin}(\hat{\varphi}), \widehat{E}_{lin}(\hat{u})) + \lambda(tr(\widehat{E}_{lin}(\hat{\varphi}))\hat{I}, \widehat{E}_{lin}(\hat{u})) \\
&= (2\mu\widehat{E}_{lin}(\hat{\varphi}) + \lambda tr(\widehat{E}_{lin}(\hat{\varphi}))\hat{I}, \widehat{E}_{lin}(\hat{u})) \\
&= A(\hat{\varphi}, \hat{u}).
\end{aligned}
$$

Here, we used the relation defined in Definition 6.22.

- **Continuity of $A(\hat{u}, \hat{\varphi})$.** We need to show that

$$
|A(\hat{u}, \hat{\varphi})| \le c\|\hat{u}\|_{H^1}\|\hat{\varphi}\|_{H^1} \quad \forall \hat{u}, \phi \text{ in } \hat{V}.
$$

Let us start with the definition and apply first Cauchy's inequality:

$$
\begin{aligned}
|A(\hat{u}, \hat{\varphi})| &= |(\widehat{\Sigma}_{lin}, \widehat{\nabla}\hat{\varphi})| = |(\widehat{\Sigma}_{lin}, \widehat{E}_{lin}(\hat{\varphi}))| \\
&\le \left(\int |\widehat{\Sigma}_{lin}|^2\right)^{1/2}\left(\int |\widehat{E}_{lin}(\hat{\varphi})|^2\right)^{1/2} \\
&= \left(\int |2\mu\widehat{E}_{lin}(\hat{u}) + \lambda tr(\widehat{E}_{lin}(\hat{u}))\hat{I}|^2\right)^{1/2}\left(\int |\widehat{E}_{lin}(\hat{\varphi})|^2\right)^{1/2}.
\end{aligned}
$$

We use $\|tr(\widehat{E}_{lin}(\hat{u}))\hat{I}\| \le \|E_{lin}(\hat{u})\|$ and $|E(\hat{u})|_{L^2} \le c\|\hat{u}\|_{H^1}$, where the latter one specifically holds for all $\hat{u} \in H^1$. Then,

$$
\begin{aligned}
|A(\hat{u}, \hat{\varphi})| &\le \left(\int |2\mu\widehat{E}_{lin}(\hat{u}) + \lambda tr(\widehat{E}_{lin}(\hat{u}))\hat{I}|^2\right)^{1/2}\left(\int |\widehat{E}_{lin}(\hat{\varphi})|^2\right)^{1/2} \\
&\le \left(\int |2\mu\widehat{E}_{lin}(\hat{u}) + \lambda\widehat{E}_{lin}(\hat{u})|^2\right)^{1/2}\left(\int |\widehat{E}_{lin}(\hat{\varphi})|^2\right)^{1/2} \\
&\le c(\mu, \lambda)\left(\int |\widehat{E}_{lin}|^2\right)^{1/2}\left(\int |\widehat{E}_{lin}(\hat{\varphi})|^2\right)^{1/2} \\
&= c(\mu, \lambda)|E(\hat{u})|_{L^2}\,|E(\hat{\varphi})|_{L^2} \\
&\le c_1\|\hat{u}\|_{H^1}\,\|\hat{\varphi}\|_{H^1}.
\end{aligned}
$$

- *$V$-ellipticity.* First, we observe that

$$
A(\hat{u}, \hat{u}) = (2\mu\widehat{E}_{lin}(\hat{u}) + \lambda tr(\widehat{E}_{lin}(\hat{u}))\hat{I}, \widehat{E}_{lin}(\hat{u})) \ge (2\mu\widehat{E}_{lin}(\hat{u}), \widehat{E}_{lin}(\hat{u})) = 2\mu|\widehat{E}_{lin}|_{L^2}.
$$

because $\mu, \lambda > 0$. The $V$-ellipticity can be inferred if we can show that on the space $\hat{V}_s^0$, the semi-norm

$$
\hat{u} \mapsto |\widehat{E}_{lin}|_{L^2}
$$

is a norm that is equivalant to $\|\cdot\|_{H^1}$. To do so, we proceed in two steps. We now employ the 2nd Korn inequality (first step), see Theorem 6.24. In detail: if $\widehat{\Gamma}_D > 0$ and $c > 0$ a given constant such that (the second step)

$$
c^{-1}\|\hat{u}\|_1 \le |\widehat{E}_{lin}|_{L^2} \le c\|\hat{u}\|_1 \quad \forall \hat{u} \in H^1(\widehat{\Omega}_s),
$$

i.e., on $\hat{V}$, the mapping $u \mapsto |\widehat{E}_{lin}|$ is norm equivalent to $\|\hat{u}\|_1$. (This techniquality requires a seperate proof!)

- **Apply Riesz.** Having proven that $A$ is symmetric, continuous and $V$-elliptic as well as that $F$ is linear continuous, we have checked all assumptions of the Riesz representation Theorem 3.44 and consequently, a unique solution $\hat{u} \in \hat{V}$ does exist.

For further discussions, the reader might consult Ciarlet [61]. $\hfill\square$

---

**Remark 6.26.** *The linearized existence is essential for prooving the nonlinear STVK boundary value problem in Section 6.5.2.*

**Remark 6.27.** *Since this elasticity problem is symmetric, the problem can be also interpreted from the energy minimization standpoint as outlined in Theorem 3.44. In this respect, the weak form considered here corresponds to the first-order necessary condition, i.e., the weak form of the Euler-Lagrange equations.*

### 6.5.2 An existence theorem for the stationary, geometrically-nonlinear STVK solid model

Let us consider the following model in this section:

- The nonlinear STVK model from Definition 5.46, as constitutive law;

- Displacement Dirichlet conditions on the whole boundary;

- The stationary momentum equation

- Enough regularity of the boundary $\partial\Omega$.

Since the resulting PDE is nonlinear (due to the nonlinear STVK model), the proof requires more sophisticated ideas than linearized elasticity as we had in Section 6.5.1.

**Theorem 6.28** ([61]). *Let $\widehat{\Omega} \subset \mathbb{R}^3$ and $\partial\widehat{\Omega}$ of class $C^2$. Then, for each $p > 3$ there exists a neighborhood $F_{rhs}$ of the origin in the space $L^p(\widehat{\Omega})$ and a neighborhood $V_{sol}$ of the origin in the space*

$$V^p(\Omega) := \{v \in W^{2,p}(\Omega)| \, v = 0 \text{ on } \partial\Omega\},$$

*such that for each right hand side $f \in F_{rhs}$, the boundary value problem*

$$L(\hat{u}) := -\widehat{div}(\widehat{F}\widehat{\Sigma}) = \hat{f}$$

*with the (nonlinear) STVK model, defined in 5.46 as constitutive law, has exactly one solution $\hat{u} \in V_{sol}$.*

**Remark 6.29.** *The corresponding weak form of $L(\hat{u}) := -\widehat{div}(\widehat{F}\widehat{\Sigma}) = \hat{f}$ can be found in Problem 6.19.*

*Proof.* The outline of the proof is as follows:

- since the operator $L(\cdot)$ is nonlinear, we use the Banach algebra property in order to determine the image space to work with;

- Having the image space, we check the assumptions of the inverse function theorem in order to establish a locally invertible mapping;

- Within the inverse function theorem, the crucial assumption to be checked is if the derivative $L'$ is an isomporphism (here we apply the closed graph theorem from functional analysis). We observe that the derivative $L'$ solves the linearized elasticity problem that we studied in Section 6.5.1.

For $p > 3$, the Sobolev space $W^{1,p}(\widehat{\Omega})$ is a Banach algebra (i.e., a product of two $W^{m,p}$ functions also belongs to $W^{m,p}$ and $\|\hat{u}\hat{v}\|_{m,p} \leq c\|\hat{u}\|_{m,p}\|\hat{v}\|_{m,p}$ if $mp > d$). Consequently, the nonlinear operator $L(\cdot)$ maps the space $W^{2,p}(\widehat{\Omega})$ into the space $L^p(\widehat{\Omega})$. Furthermore, this operator is infinitely differentiable between these two spaces because it is a combination of continuous linear, bilinear, and trilinear mappings [14] and therefore, all derivatives of order 4 and higher vanish:

$$L \sim \widehat{F}\widehat{\Sigma} \sim \widehat{F}(\widehat{\nabla}\hat{u})^2 \sim (\widehat{\nabla}\hat{u})^3,$$

which yields necessarily $L^{(4)} \equiv 0$. Next, $\hat{f} = 0$ yields $\hat{u} = 0$ (which is obvious). Our goal is to apply the implicit function theorem in order to show that $L$ is locally invertible in a neighborhood of the origin in $V^p \times L^p$. Let us check the assumptions for which all are evident except that we need to check the derivative $L'$

---

[14]Recall fluid's convection term $(u \cdot \nabla v, w)$ that is mathematically also a trilinear mapping.

is an isomorphism between the spaces $V^p$ and $L^p$. Here, we now compute the Fréchet derivative in direction $\delta\hat{u}$, i.e.,

$$
\begin{aligned}
L'(\delta\hat{u})(\hat{u}) &= -\widehat{\mathrm{div}}(\widehat{F}'(\delta\hat{u})\widehat{\Sigma}(u) + \widehat{F}\widehat{\Sigma}'(\delta\hat{u})) \\
&= -\widehat{\mathrm{div}}(\widehat{\nabla}\delta\hat{u}\widehat{\Sigma}(u) + (\hat{I} + \widehat{\nabla}\hat{u})\widehat{\Sigma}'(\delta\hat{u})) \\
&= -\widehat{\mathrm{div}}(\widehat{\nabla}\hat{u}\widehat{\Sigma}(u) + (\hat{I} + \widehat{\nabla}\hat{u})(2\mu(\widehat{\nabla}\delta\hat{u} + \widehat{\nabla}\delta\hat{u}^T + \widehat{\nabla}\delta\hat{u}^T \cdot \widehat{\nabla}\hat{u}^T + \widehat{\nabla}\hat{u}^T \cdot \widehat{\nabla}\delta\hat{u}^T) \\
&\quad + \lambda tr(\widehat{\nabla}\delta\hat{u} + \widehat{\nabla}\delta\hat{u}^T + \widehat{\nabla}\delta\hat{u}^T \cdot \widehat{\nabla}\hat{u}^T + \widehat{\nabla}\hat{u}^T \cdot \widehat{\nabla}\delta\hat{u}^T))).
\end{aligned}
$$

In the orgin $\hat{u} = 0$, we obtain

$$
\begin{aligned}
L'(\delta\hat{u})(0) &= -\widehat{\mathrm{div}}(\hat{I}(2\mu(\widehat{\nabla}\delta\hat{u} + \widehat{\nabla}\delta\hat{u}^T) + \lambda tr(\widehat{\nabla}\delta\hat{u} + \widehat{\nabla}\delta\hat{u}^T))) \\
&= -\widehat{\mathrm{div}}(2\mu(\widehat{\nabla}\delta\hat{u} + \widehat{\nabla}\delta\hat{u}^T) + \lambda tr(\widehat{\nabla}\delta\hat{u} + \widehat{\nabla}\delta\hat{u}^T)) \\
&= -\widehat{\mathrm{div}}(2\mu\widehat{E}_{lin} + \lambda \mathrm{tr}\widehat{E}_{lin}\hat{I}),
\end{aligned}
$$

which is presicely the operator of linearized elasticity defined in Problem 6.20. Since $\partial\widehat{\Omega}$ is of class $C^m$ regularity theory can be applied as follows. For $\hat{f} \in L^p$, $p > 3$, the linearized problem has exactly one solution $\hat{u} \in H_0^1(\widehat{\Omega}) \cap W^{2,p}(\widehat{\Omega})$. Therefore, the continuous linear operator $L'(\delta\hat{u})(0) : V^p \to L^p$ is bijective. From this, we know that the inverse is continuous. Using the closed graph theorem (functional analysis, for example [238])), a continuous, bijective, linear operator between two Banach spaces is an isomorphism, i.e., its inverse is also continuous [238](Satz IV.4.4 and Theorem IV.4.5). Consequently, all assumptions of the implicit function theorem are satisfied and the nonlinear problem has exactly one solution in a neighborhood of the origin. □

### 6.5.3 Damping terms in the solid
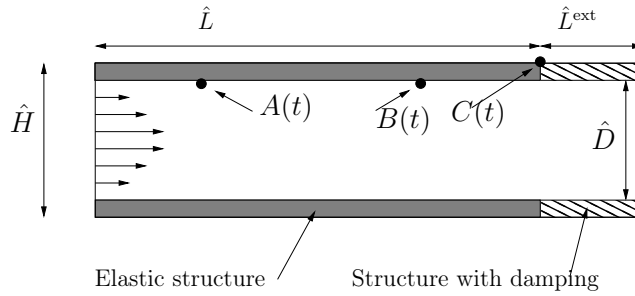


Figure 24: Illustration of a configuration and control points for applying damped solid equations.

Before we consider the regularity of the solid equations, we extend the previously-derived equations. For mathematical and physical reasons, it might be desirable to introduce damping terms.

**Example 6.30** (Physical reason for damping terms). *As example, consider the harmonic oscillator, vibrations or simply a pendular that we let oscillating (remember your physics classes). This pendular will stop at a finite time - otherwise we would have created the famous perpetual motion machine. Correct physical modeling of this process, consequently, requires introducing damping terms (i.e., friction terms).* ◇

**Example 6.31** (Mathematical point of view)*. Damping terms introduce higher regularity into the solid solutions. We see later that this is important in the mathematical analysis of fluid-structure interaction.* ◇

The modified structure problem including damping terms reads:

$$\hat{\rho}_s \partial_t^2 \hat{u}_s - \widehat{\mathrm{div}}(\widehat{F}\widehat{\Sigma}(\hat{u}_s)) + \gamma_w \partial_t \hat{u}_s - \gamma_s \partial_t \widehat{\mathrm{div}}(\hat{\epsilon}(\hat{u}_s)) = \hat{\rho}_s \hat{f}_s \quad (36)$$

$$\mathrm{in}\ \widehat{\Omega}_s,\ t \in I, \quad (37)$$

with $\gamma_s, \gamma_w \geq 0$. The first damping term is referred to as *weak damping* whereas the second damping term is called *strong damping*. Using strong damping, the full operator is used for damping, leading to an additional condition on the interface (because of integration by parts) that has to be considered for the coupling with fluids. Assuming that temporal and spatial differentiation can be changed, we obtain for strong damping:

$$-\gamma_s \partial_t \widehat{\mathrm{div}}(\hat{\epsilon}(\hat{u}_s)) = -\gamma_s \widehat{\mathrm{div}}(\hat{\epsilon}(\partial_t \hat{u}_s)) = -\gamma_s \widehat{\mathrm{div}}(\hat{\epsilon}(\hat{v}_s)),$$

with $\hat{v}_s = \partial_t \hat{u}_s$. The change of temporal and spatial differentiation is invalid for nonlinear strong damping, where we could have been used the full nonlinear operator, i.e.,

$$-\gamma_s \partial_t \widehat{\mathrm{div}}(\widehat{F}\widehat{\Sigma}(\hat{u}_s)) \not\approx -\gamma_s \widehat{\mathrm{div}}(\widehat{F}\widehat{\Sigma}(\hat{v}_s)). \quad (38)$$



Figure 25: Damped elastic equations are employed in $x \geq 6$ as a PML-approach to absorb outgoing elastic waves in the elastic walls.

Such damping strategies have been employed in computational fluid-structure interaction as a perfectly-matched layer (PML) [32] approach to absorb outgoing elastic waves in elastic-wall-fluid-flap simulations [240] as illustrated in Figure 25.

Next, we pose a standard mixed formulation of the structure equations,

$$\hat{\rho}_s \partial_t \hat{v}_s - \widehat{\mathrm{div}}(\widehat{F}\widehat{\Sigma}(\hat{u}_s)) + \gamma_w \hat{v}_s - \gamma_s \widehat{\mathrm{div}}(\hat{\epsilon}(\hat{v}_s)) = \hat{\rho}_s \hat{f}_s \quad \mathrm{in}\ \widehat{\Omega}_s,\ t \in I, \quad (39)$$

$$\hat{\rho}_s(\partial_t \hat{u}_s - \hat{v}_s) = 0 \quad \mathrm{in}\ \widehat{\Omega}_s,\ t \in I, \quad (40)$$

where $\hat{\epsilon}(\hat{v}_s)$ is defined by

$$\hat{\epsilon}(\hat{v}_s) = \frac{1}{2}(\widehat{\nabla}\hat{v}_s + \widehat{\nabla}\hat{v}_s^T). \quad (41)$$

The modified structure problem (40) reduces to the original problem (20) when the damping parameters are set to $\gamma_w = \gamma_s = 0$.

**Problem 6.32** (First order system in time weak formulation of elasticity including damping)*. Find $\hat{u} \in V = H_0^1$ and $\hat{v} \in L^2$ with the initial data $\hat{u}(0) = \hat{u}_0$ and $\hat{v}(0) = \hat{v}_0$ such that*

$$(\partial_t \hat{v}, \varphi) + (\widehat{F}\widehat{\Sigma}, \widehat{\nabla}\varphi) + \gamma_w(\partial_t \hat{u}_s, \varphi) + \gamma_s(\partial_t \hat{\epsilon}(\hat{u}_s), \widehat{\nabla}\varphi) = (\hat{f}, \varphi) \quad \forall \varphi \in V \quad (42)$$

$$(\partial_t \hat{u} - \hat{v}, \chi) = 0 \quad \forall \varphi \in L^2 \quad (43)$$

*for a.e. all times $0 \leq t \leq T$. Furthmore, $\partial_t^2 \hat{u} \in H^{-1}$ for a.e. all times $0 \leq t \leq T$.*

**Remark 6.33.** *Using strong damping requires modification of the continuity of normal stresses at the FSI-interface.*

**Remark 6.34** (Alternative to obtain higher regularity)*. Similar to elliptic and parabolic equations if we assume higher regularity on data and the domain, we obtain higher regularity on the solid solution. For details, I refer to PDE analysis textbooks, e.g., Section 7.2 in [77].*
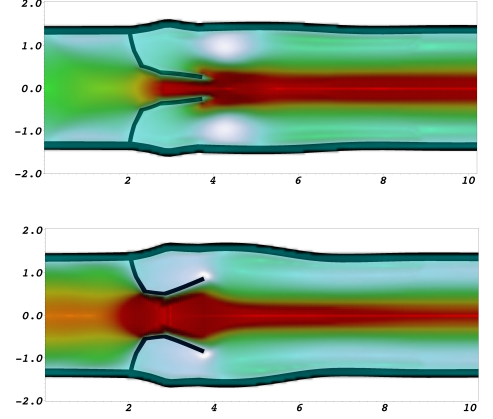
### 6.5.4 Regularity of (linear) solid equations

**Problem 6.35** ([121], p. 351). *Let $\hat{f}_s \in L^2(I, L^2(\widehat{\Omega}_s))$. Find*

$$\hat{u}_s \in L^2(I, H_0^1(\widehat{\Omega}_s)) \quad and \quad \hat{v}_s = d_t\hat{u}_s \in L^2(I, L^2(\widehat{\Omega}_s)),$$

*such that the hyperbolic structure equations*

$$d_t^2\hat{u}_s - \Delta\hat{u}_s = \hat{f}_s \quad in \; I \times \widehat{\Omega}_s,$$
$$\hat{u}_s = 0 \quad on \; I \times \partial\widehat{\Omega}_s,$$

*are solved with the initial data $\hat{u}_s(0) = \hat{u}_s^0$ and $\hat{v}_s(0) = \hat{v}_s^0$.*

In Grossmann and Roos [121], Theorem 5.6 tells us that this problem has a unique solution. The regularity of that solution is given by

$$\hat{u}_s \in L^2(I, H_0^1(\widehat{\Omega}_s)) \quad and \quad \hat{v}_s = d_t\hat{u}_s \in L^2(I, L^2(\widehat{\Omega}_s)).$$

Consequently, we cannot expect $\hat{v}_s \in H^{1/2}(\widehat{\Omega}_s)$. Thus, the FSI velocity coupling condition (51) is only formally valid. For this reason, we assumed a priori enough regularity of the hyperbolic structure equations. This was also observed (and resolved) in theoretically-oriented articles with focus on proofs of existence of fluid-structure interaction problems [8, 64, 65, 146] [15].

The lack of solid-regularity can be resolved by using a vanishing viscosity approach (that acts on the velocity variables) to the structure equations. This coincides with the terms introduced in Equation (36).

To analyze the regularity of structural deformations in more detail, we consider the following hyperbolic equation with weak damping and linear strong damping.

**Problem 6.36** ([105]). *Let $\hat{f}_s$ be sufficient regular. Let $\gamma_s \geq 0$ and $\gamma_w > -\gamma_s\lambda_1$, where $\lambda_1$ is the first eigenvalue of the $-\Delta$ operator under homogeneous Dirichlet boundary conditions. Find*

$$\hat{u}_s \in L^2(I, H_0^1(\widehat{\Omega}_s)) \quad and \quad \hat{v}_s = d_t\hat{u}_s \in L^2(I, L^2(\widehat{\Omega}_s)),$$

*such that the hyperbolic structure equations with weak and strong damping*

$$d_t^2\hat{u}_s - \Delta\hat{u}_s + \gamma_w d_t\hat{u}_s - \gamma_s d_t\Delta\hat{u}_s = \hat{f}_s \quad in \; I \times \widehat{\Omega}_s,$$
$$\hat{u}_s = 0 \quad on \; I \times \partial\widehat{\Omega}_s,$$

*are solved with the initial data $\hat{u}_s(0) = \hat{u}_s^0$ and $\hat{v}_s(0) = \hat{v}_s^0$.*

For example, in the work from Gazzola and Squassina [105], the first statement on p. 189 explains that this problem has a unique solution. In particular, the regularity of $\hat{v}_s$ is given by

$$\hat{v}_s = d_t\hat{u}_s \in L^2(I, H_0^1(\widehat{\Omega}_s)),$$

for arbitrary $\gamma_s > 0$; hence, $\hat{v}_s \in H^{1/2}(\widehat{\Gamma}_i)$. Thus, linear strong damping provides more regularity of the solution, specifically for $\hat{v}_s$, such that the coupling FSI condition (51) holds true. We finally notice that we only consider regularity properties of linear structure equations. Thus, typical nonlinearities of the structural operators are neglected.

---

[15]In this sense, we would like to point to two other important contributions analyzing FSI from the theoretical point of view: [219] investigate time-dependent FSI flow-elastic-shell coupling with small displacements; and [118] existence of a stationary FSI problem formulated in ALE coordinates.

### 6.5.5 Additional regularity of (stationary) elasticity

Let us close this chapter by briefly accounting for additional regularity of stationary elasticity.

- Pure Dirichlet displacement problems: if $\partial\widehat{\Omega}_S = \widehat{\Gamma}_D$, the solution $\hat{u}_s$ possesses additional regularity provided that data and the boundary do so:

$$m > 0 : \widehat{\Gamma}_D \in C^{m+2}, \hat{f} \in W^{m,p} \quad \Rightarrow \quad \hat{u}_s \in W^{m+2,p}$$

- Pure Neumann problems (traction):

$$m > 0 : \widehat{\Gamma}_N \in C^{m+2}, \hat{f} \in W^{m,p}, \hat{g} \in W^{1-(1/p),p}(\widehat{\Gamma}_N) \quad \Rightarrow \quad \hat{u}_s \in W^{m+2,p}$$

- Mixed Dirichlet and Neumann conditions: Above results only hold true if the closures of the two sets $\widehat{\Gamma}_D$ and $\widehat{\Gamma}_N$ do not intersect;

- In all other cases, the weak solution still possesses interior regularity but lacks regularity at the intersecting points where the boundary conditions change their type.

**Example 6.37.** *The latter condition constitutes indeed a challenge in fluid-structure interaction since different boundary conditions intersect on $\widehat{\Gamma}_D, \widehat{\Gamma}_N$ and $\widehat{\Gamma}_i$. For this reason, in [248], we assumed that the solid is completely contained (as a ball for example) in the fluid such that $\widehat{\Gamma}_i$ never touches $\widehat{\Gamma}_{D,f}$ and never $\widehat{\Gamma}_{D,s}$.*
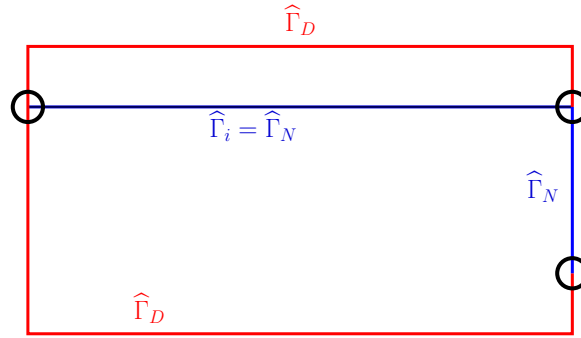


Figure 26: Intersection of different boundaries of Dirichlet and Neumann type. Here, the solution lacks additional regularity.

**Remark 6.38.** *Further literature and references on the intersection of boundaries and their regularity can be found in Ciarlet [61], p.298.*

# 7 Fluid-Structure Interaction Modeling

In Section 5, we have prepared ourselves with modeling of physics in terms of conservation laws and partial differential equations. In this section, we shall couple these equations into one common framework. The principal challenges are listed in Challenge 2.2. We discuss different coupling algorithms and concentrate on two of them on which I have been working in the last few years.

The procedure of FSI-coupling is as follows: Let us say, we are given fluid equations in Eulerian coordinates and solid equations in a Lagrangian framework. The first questions we need to pose are:

- How to we couple or combine the coordinate systems?

- Once we decided for a technique, we further ask ourselves which amount of information needs to be transferred to the other problem; i.e, do we need weak or strong coupling? This question might be posed from an application viewpoint but also from a mathematical perspective (as example to the latter aspect: a consistent Galerkin formulation for gradient-based sensitivity analysis would require a monolithic coupling).

- Can we establish a under certain conditions priori estimates, or even well-posedness?

This information guides us through the discretization and the solution algorithm. We particularly focus on consistent variational-monolithic coupling.

## 7.1 Techniques for coupling fluids and solids

In this first subsection, we provide an overview of possible coupling techniques.

### 7.1.1 Choosing frameworks for the coupled fluid-solid system

- **Immersed boundary (IB) method:**
  References [129, 184].
  This method was specifically designed for applications in hemodynamics and heart valve simulations. It keeps the Eulerian and Lagrangian coordinate systems and the coupling is achieved by a Dirac delta function that can be seen as a momentum forcing source term of the fluid equations. Consequently, the discretization uses two different meshes. Temporal discretization can be carried out with finite difference schemes such as first-order backward Euler or higher-order Runge-Kutta. Closely related is the immersed finite element method [257].

- **Immersed structural potential method:**
  References: [110].
  As the name indicates, this method is related to the IB method. Since numerical diffusion is a challenge in the original IB-method the current method mainly tries to reduce these errors. In addition, it allows to employ state-of-the-art fiber-reinforced solid models.

- **Fictious domain method (FD):**
  References: [9, 113–115].
  As in immersed boundary methods, two meshes (possibly nonmatching) are used and the kinematic coupling condition is imposed with Lagrange multipliers and possibly with mortar coupling. Again, the fluid is treated in the Eulerian framework and the solid in Lagrangian coordinates.

- **Arbitrary Lagrangian-Eulerian (ALE):**
  References: [31, 70, 97, 135, 144, 180].
  The ALE method is perhaps the oldest approach. Here, Eulerian and Lagrangian frameworks are combined without changing the mesh topology. One needs to solve or prescribe the mesh movement of the fluid mesh. Difficult for large deformations if no remeshing is used. The key advantage is that the interface aligns with mesh edges and interface-terms such as traction forces can be computed with high accuracy.

- **Fixed mesh ALE (FM-ALE):**
  References: [63].
  Here, an ALE approach is used in which at each time step, the problem is projected on a fixed background mesh. In other words: in each time step remeshing is performed. The method was in particular developed for solid mechanics with large strains in which the elements stretch.

- **Universal mesh method:**
  References: [104].
  This method has similarities to the FM-ALE method and tries again to combine advantages from Eulerian and Lagrangian representations. In particular, large deformations are possible. The key difference to FM-ALE is that during temporal integration element splitting as in FM-ALE is avoided.

- **Hybrid level-set/front-tracking approach:**
  References: [18].
  The idea behind this approach is similar to the universal mesh method: roughly-speaking, Eulerian and Lagrangian frameworks are combined. A level-set approach (interface-capturing) method is used to detect the interface, then the mesh nodes are shifted in order to align the interface with mesh edges.

- **Fully Eulerian FSI:**
  References: [72, 200].
  This approach belongs to the fixed-mesh interface-capturing[16] approaches but in contrast to IB and FD methods, solid mechanics is formulated in terms of Eulerian coordinates. Therefore, the coupled system can be computed on a single mesh. Coupling is achieved by a variational monolithic formulation. As in the previous methods, the interface is first captured (here with the initial-point set method rather than a level-set approach). For the cut-cells a locally modified FEM method has been proposed and is currently under further development [99, 197].

- **Discontinuous Galerkin (DG):**
  References: [81, 122, 123, 125, 237].
  A specific proposed a method is by [237] in which again the fluid is kept in Eulerian coordinates and the solid is modeled in a Lagrangian setting. This specific formulation is closely related to the IB method. Application to standard ALE schemes is straightforward and performed in [122, 123]. In [81, 125], compressible Navier-Stokes equations in ALE form are coupled with solid mechanics.

- **XFEM /GFEM fixed-grid approach, Eulerian-Lagrangian coupling with level-sets, mortar coupling**
  References: [109, 130, 163, 236].
  The key idea is to compute the fluid in an Eulerian framework and to couple it to the Lagrangian structure. The interface (again) cuts the mesh cells and is not anymore aligned with mesh faces. In order to represent jumps of the velocity, pressure and stress fields, the extended/generalized finite element (XFEM/GFEM) scheme is used. Recently, it has been shown that both approaches are equivalent [100]. The approach is that the shape functions are enriched by using additional degrees of freedom together with special enrichment functions that are designed according to the solution form (its characteristics are generally known). Mortar coupling [109] and mortar with domain decomposition [130] allow for non-matching meshes on the interface. A Lagrange multiplier is introduced to satisfy the coupling conditions.

- **Isogeometric analysis (IGA):**
  References: [19, 142].
  In IGA, the test and ansatz functions are not anymore polynomials but splines: e.g., non-uniform rational B-Splines. The main purpose of IGA is to combine geometry representation and discretization. In particular, higher order discretization require less degrees of freedom (for example for $C^1$ implementations) as a standard finite element model.

- **Deforming spatial domain/stabilized space-time (DSD/SST):**
  References: [221, 222]:

---

[16]An interface-capturing method implicitly represents the interface which is typically immersed in the (fixed) computational domain. In contrast to interface-tracking approaches, the accuracy is however less accurate.

This method is an interface-tracking method and moves the mesh similar to an ALE approach. The problem is written in terms of a space-time discretization rather than splitting into spatial Galerkin finite elements combined with finite differences in time (Rothe method or the other way around method of lines).

- **Lattice Boltzmann (LBM):**
  References: [159, 160].
  Lattice Boltzmann methods have been introduced for computational fluid dynamics simulations. Rather than using continuum mechanics equations, the fluid is represented by particles on a so-called lattice mesh. Has been successfully applied for fluid-structure interaction.

- **The particle finite element method (PFEM):**
  References: [181].
  The PFEM method is based on a particle representation in which both continua (fluid and solid) are modeled in Lagrangian coordinates. The nodes (the particles) are connected in order to build a mesh that serves as computational domain. The resulting triangulation can be used for a finite element discretization. The method is capable to treat large deformations and free surface problems (e.g. water waves). Again, this approach has been successfully applied for fluid-structure interaction.

In addition to the primer coupling techniques, we briefly mention examples of hybrid techniques that couple two of the primal techniques in different parts of the domain:

- IB-Lattice Boltzmann for solving fluid-particle interaction problems [82];

- FD-ALE: [124, 212];

- Fluid-solid interface-tracking/interface-capturing technique (MITICT - FSITICT) [3, 225];

- Coupling of fully-Eulerian/ALE (EALE) - FSITICT [243, 245].

### 7.1.2 Combining the underlying frameworks: FSI coupling algorithms

The key question we have to pose is:

- Do we satisfy the energy balance on the interface:

$$\hat{v}_f = \hat{v}_s,$$
$$\hat{J}\hat{\sigma}_f \widehat{F}^{-T}\hat{n}_f = \widehat{F}\widehat{\Sigma}_s \hat{n}_s$$
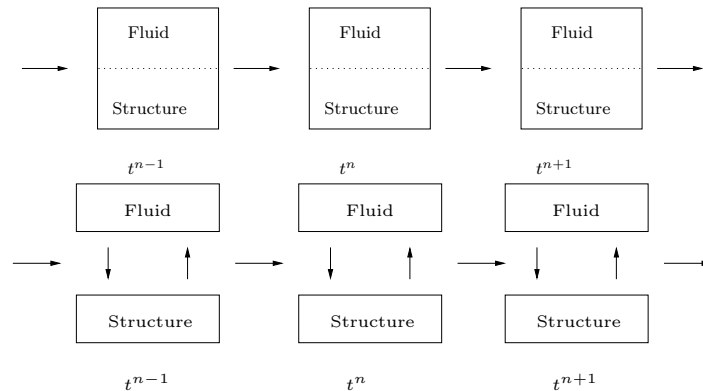
at each time step?



Figure 27: Monolithic and paritioned coupling of FSI. In monolithic coupling, the coupled system is solved all-at-once whereas in the paritioned scheme subiterations are required to enforce the force balance on the interface.

Several algorithms have been proposed and they can be roughly divided into the following concepts (see also [84] or [87]):

- Strongly-coupled (or implicit) schemes preserve the coupling conditions after time discretization. Monolithic methods are strongly-coupled by construction or partitioned approaches with several subiterations between both subsystems.

- Weakly-coupled (or loosely, explicit, staggered) schemes do not 'exactly' satisfy the coupling conditions in each time step. Partitioned approaches with few subiterations are weakly-coupled. Famous examples where these algorithms have been applied are problems in aero-elasticity.

- Semi-implicit schemes, e.g. [6, 7, 10, 85], are a comprise of the previous two schemes with respect to computational cost and stability.

- Coupling via an optimization algorithm [155].

**Remark 7.1** (Added-mass effect [59, 235])**.** *In several studies it has been shown that weakly-coupled schemes introduce instabilities when both densities such as in hemodynamic problems are of similar order; consequently, strongly-coupled schemes are required. In fact, it can be shown that certain explicit schemes are unconditionally unstable [59]. Roughly speaking, weak coupling is sufficient in most cases if the density ratio is large:*

$$\frac{\rho_s}{\rho_f} \gg 1.$$

*Strong coupling is required if*

$$\frac{\rho_s}{\rho_f} \sim 1.$$

*This is only a rough idea and in [59] is has also been shown that the added-mass effect depends on the geometry of the domain. Consequently for all details we refer to that work. Various stabilization techniques have been investigated to make weakly-coupled schemes stable [57, 85, 102, 165, 235].* ⋄

It is very important to notice that all coupling schemes have their justification. In particular, partitioned schemes are often preferred in engineering because (for example):

- For decades a fluid flow code has been developed in a group, which is now intended to be coupled with other equations (such as solids). Here, it is much easier to extend the existing code by coupling explicitly via a partitioned algorithm;

- Due to too many equations or physical laws, derivation and implementation of monolithic schemes is a big challenge [17];

- Partitioned schemes allow to employ sophisticated solvers for each subproblem without taking care of cross-coupling terms that arise in monolithic schemes;

- In several applications (e.g., aero-elasticity in which the solid density is much larger than the fluid density; see added-mass effect) and explicit schemes might work well with sufficient accuracy and robustness.

Reasons for monolithic techniques are:

1. High accuracy of coupling conditions;

2. Numerical stability and implicit discretizations (e.g., in FSI - added-mass effect);

3. Consistent numerical modeling/solution of gradient-based optimization; a

4. Consistent numerical modeling/solution of dual-weighted error estimation;

5. Space-time formulations.

---

[17]See for example coupling of elasticity and multi-phase flow in subsurface modeling and geomechanics. Here, a famous partitioned scheme is called fixed-stress splitting [170, 216]. However, in those applications a typical FSI-difficulty does a priori not appear that the equations are formulated in different parts of the domain.

### 7.1.3 Regularity of interface coupling in fluid-structure

Apart from practical aspects, there are some theoretical findings that should be taken into account:

- The regularity gap between $v_f \in H^1$ and $v_s \in L^2$. Might be overcome by backward difference discretization of $v_s$ [155]. Or by a viscosity method by adding additional viscous terms to the structure equation [64, 65, 146]. Basically, if we add structural damping (might be also physically taking place; and refer to our discussion in Section 6.5.4), we obtain higher spatial regularity for $v_s$.

## 7.2 Lagrangian, Eulerian, ALE

As we learned in Section 5, Eulerian and Lagrangian approaches are the classical ways to describe problems in continuum mechanics. The so-called arbitrary-Eulerian-Lagrangian (ALE) approach is an intermediate method to overcome some of the shortcomings of the Eulerian and Lagrangian frameworks as we described above. Despite possible drawbacks (mesh degeneration for large deformations; mesh tangling, mesh racing), we focus on this approach in the following sections. The reasons are:

- It is one of the oldest and possibly (still) most widely-used algorithms.

- It is relatively easy to implement.

- It is an interface-tracking approach in which the interface is aligned with mesh edges at all times and allows for a sharp and accurate representation of the interface. Thus, this approach allows for accurate measurements of quantities of interest on the interface as for instance traction forces.

- It combines Lagrangian and Eulerian coordinate systems and we naturally learn to work with the transformation rules from continuum mechanics (see Chapter 5), which are (partially) indispensable for other (but younger) approaches.

- Implemented correctly (which is always assumed), it is an efficient, robust, and accurate method in terms of a single consistent variational form and therefore allows for trustable extensions towards sensitivity analysis and optimization [18] In this respect, our view in these lecture notes is directed to classical numerical topics such as convergence studies, stability, and error estimation.

Let us recapitulate:

- Lagrangian methods: mainly designed for problems in structural mechanics, allows easy tracking of surfaces and interfaces between different materials, also appropriate for materials with history dependent constitutive relations (such as plasticity); but has difficulties for problems with large mesh deformations;

- Eulerian methods: used in fluid mechanics, the mesh is fixed and the body moves with respect to the mesh, consequently, mesh deformations do not appear here; but the interface is allowed to cut through cells, which requires adapted discretization techniques in order to keep accuracy and robustness,

- ALE methods (between Lagrangian and Eulerian). We deal with two motions: first the physical motion and the motion of the computational domain due to the moving interface $\widehat{\Gamma}$ caused by the solid deformation. The mesh moves (in the extreme case as in an Lagrangian setting; on the other extreme: it is not moved at all and we recover an Eulerian approach), this flexibility is the major advantage and specifically for fluid-structure interaction it leads to moving meshes around the interface and a fixed mesh far away (see Figure 30).

Generally-speaking the ALE approach tries to conserve mesh regularity and equidistribution (the optimal mesh geometry) of mesh vertices while keeping the mesh topology. Essentially, we shall control size, shape, and orientation of mesh cells. The location of new vertices or the velocity of mesh points is usually determined by solving an additional partial differential equation: the moving mesh equation. In addition, a scalar (or vector) valued monitor function is used to determine the optimal mesh vertices distribution. From the mathematical viewpoint, the ALE-transformation maps one domain into another and are therefore linked to geometry aspects. Furthermore, they have common features with differential geometry (i.e., optimal transport) and mean curvature flows.

---

[18] This does not mean that the other approaches are not capable of doing this, but first we have to trust our forward solver before we can go with adjoint formulations.

## 7.3 ALE-FSI

In the present chapter, we discuss fluid-structure interaction problems in ALE coordinates. The ALE mapping is defined by solving an additional partial differential equation, for which we present three possibilities. With the help of this mapping, we realize the fluid mesh motion, which means to displace the vertices of the computational domain (either explicitly or implicitly). Next, the coupled framework is described in terms of a coupled fashion, leading to a variationally-coupled monolithic representation of fluid-structure interaction in the reference configuration $\widehat{\Omega}$. Here, the domain movement is contained implicitly. Our terminology to describe the monolithic approach is based on [72–74, 138, 139, 200].

### 7.3.1 Defining the ALE transformation

The idea of ALE - roughly speaking - is pretty simple:

**Definition 7.2** (Rough idea of ALE and its definition using the concepts from continuum mechanics). *As learned in Section 7.2, ALE is an intermediate state in which the fluid domain is moved according to the solid. This requires a mapping between the deformed state and a reference configuration. However, this is exactly how we worked in Chapter 5 to introduce the concepts of continuum mechanics. In the following we are going to use $\hat{\mathcal{A}} := \widehat{T}$ and recapitulate all definitions we already have had so far.*
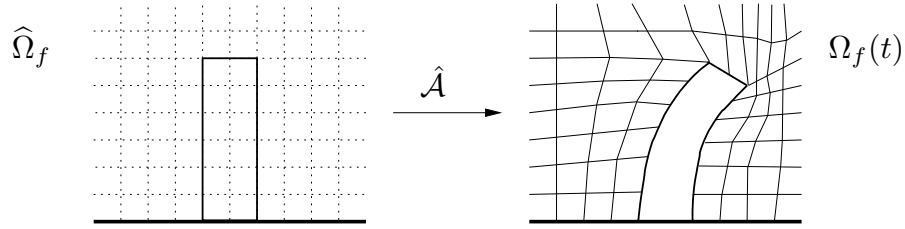


Figure 28: Defining the ALE transformation.

Firstly, we need to define the ALE transformation:

**Definition 7.3.** *The ALE mapping is defined in terms of the fluid mesh displacement $\hat{u}_f$ such that*

$$\hat{\mathcal{A}}(\hat{x}, t) : \widehat{\Omega}_f \times I \to \Omega_f, \quad with \ \hat{\mathcal{A}}(\hat{x}, t) = \hat{x} + \hat{u}_f(\hat{x}, t). \tag{44}$$

*It is specified through the deformation gradient and its determinant*

$$\widehat{F} := \widehat{\nabla}\hat{\mathcal{A}} = \hat{I} + \widehat{\nabla}\hat{u}, \quad \hat{J} := det(\widehat{F}). \tag{45}$$

*Furthermore, function values in Eulerian and Lagrangian coordinates are identified by*

$$u_f(x) =: \hat{u}_f(\hat{x}), \quad with \ x = \hat{\mathcal{A}}(\hat{x}, t). \tag{46}$$

*The mesh velocity is defined by $\hat{w} := \partial_t \hat{\mathcal{A}}$; similarly to $\partial_t \widehat{T}$ defined in Equation (4). The mesh velocity is numerically realized as $\hat{w} = \partial \hat{\mathcal{A}} = \frac{\hat{u}_f - \hat{u}_f^{n-1}}{k}$, where the fluid mesh displacements are computed with the help of an additional PDE (the so-called mesh motion or MMPDE); we refer the reader to the Sections 7.3.5 and 7.3.6.* ⋄

To formulate FSI in ALE coordinates, there are two possible ways presented in the literature:

**Definition 7.4.** *Fluid-structure interaction in ALE coordinates can be realized in two ways:*

- *$ALE_{dm}$ (explicit mesh moving): the fluid equations are computed on the deformed configuration $\Omega$ and the mesh is moved explicitely.*

- *$ALE_{fx}$ (implicit mesh moving): all fluid equations are transformed onto the fixed reference configuration $\widehat{\Omega}$ and the mesh movement is 'hidden' in the transformations $\widehat{F}$ and $\hat{J}$.*

*In our work, we prefer this second possibility; namely $ALE_{fx}$. Examples of computational domains of both approaches are shown in Figure 30.*

### 7.3.2 The ALE time derivative

The derivation of both approaches follows the same rules that we sketch in the following. Let us briefly explain the relations between different time derivatives for different frameworks (such as the Lagrangian, the Eulerian, and the ALE frameworks). In a Lagrangian setting, the total and the partial derivatives coincide:

$$d_t \hat{f}(\hat{x}, t) = \partial_t \hat{f}(\hat{x}, t).$$

In an Eulerian framework, we find the following standard relation between the *material time-derivative* (the total time derivative) $d_t f$ and the partial time derivative $\partial_t f$:

$$d_t f(x, t) = v \cdot \nabla f + \partial_t f(x, t),$$

where the additional term $v \cdot \nabla f$ is referred to as a transport term. In an analogous fashion, we extend this concept to define the

**Definition 7.5** (ALE time derivative). *Taking the Definition 5.11, the ALE time derivative is defined as*

$$\hat{\partial}_t f(x, t) := \partial_t|_{\hat{\mathcal{A}}} f(x, t) = w \cdot \nabla f + \partial_t f(x, t), \tag{47}$$

*where the transport term appears due to the motion of the computational domain. Moreover (see additionally Figure 29),*

- *In a Lagrangian description, we have $w = v$, i.e., the domain is moving with the fluid velocity $v$;*

- *In a fixed Eulerian setting, it holds $w = 0$, i.e., the domain is fixed.*

- *In ALE, we have $0 \leq w \leq v$. Later we will see that $v = w$ at the FSI-interface $\widehat{\Gamma}_i$ and a bit away, we have $0 < w < v$, while far away $w = 0$ (the mesh is not moving anymore). Thus, in ALE, depending on the location in the domain, we use both Eulerian and Lagrangian frameworks with a smooth transition between them.*
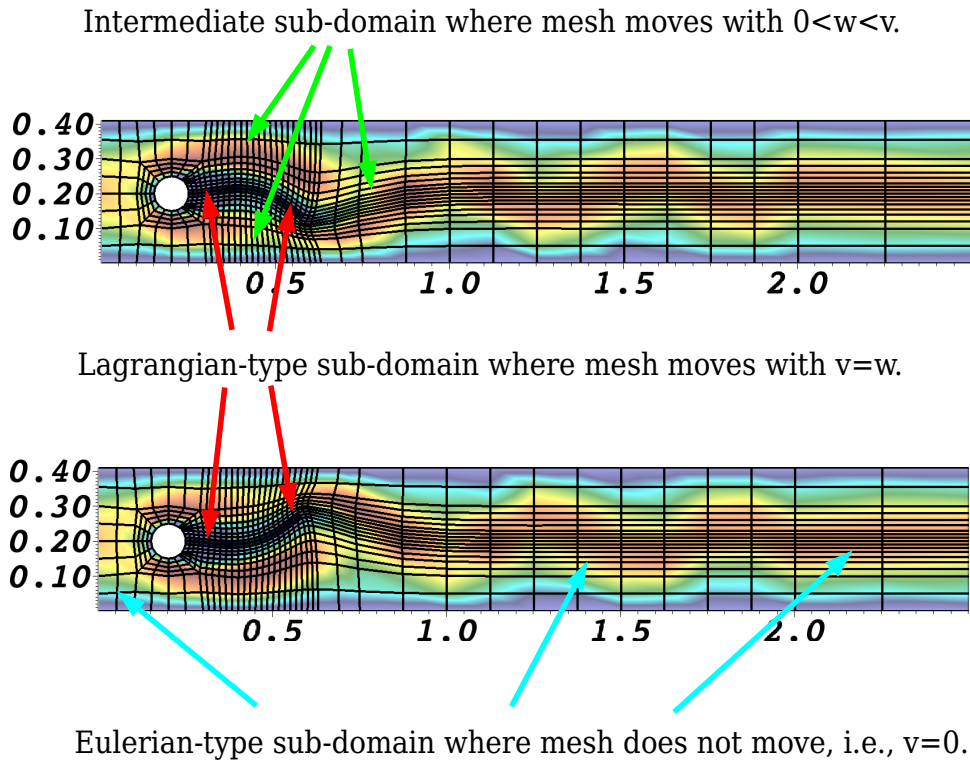
Figure 29: Explanation of the ALE-approach with the help of snapshots at two different times of a FSI-simulation: consequences of the mesh velocity $w$ on the domain (mesh) movement. In regions where $w = 0$ the domain does not move and is fixed. The solid and the interface $\widehat{\Gamma}_i$ both move with $w = v$. In between (green arrows) the domain moves with $0 < w < v$. A zoom-in to better localize the solid is provided in Figure 30. In summary: using ALE, the transition between Lagrangian parts and Eulerian parts occurs automatically and is covered by the formulation; see also Section 7.3.3 how the ALE-idea is represented in the Navier-Stokes equations.

*The ALE time-derivative has important ramifications for the numerical discretization of ALE equations; for a deeper discussion, we refer to [94], p. 88 and [91, 92].*
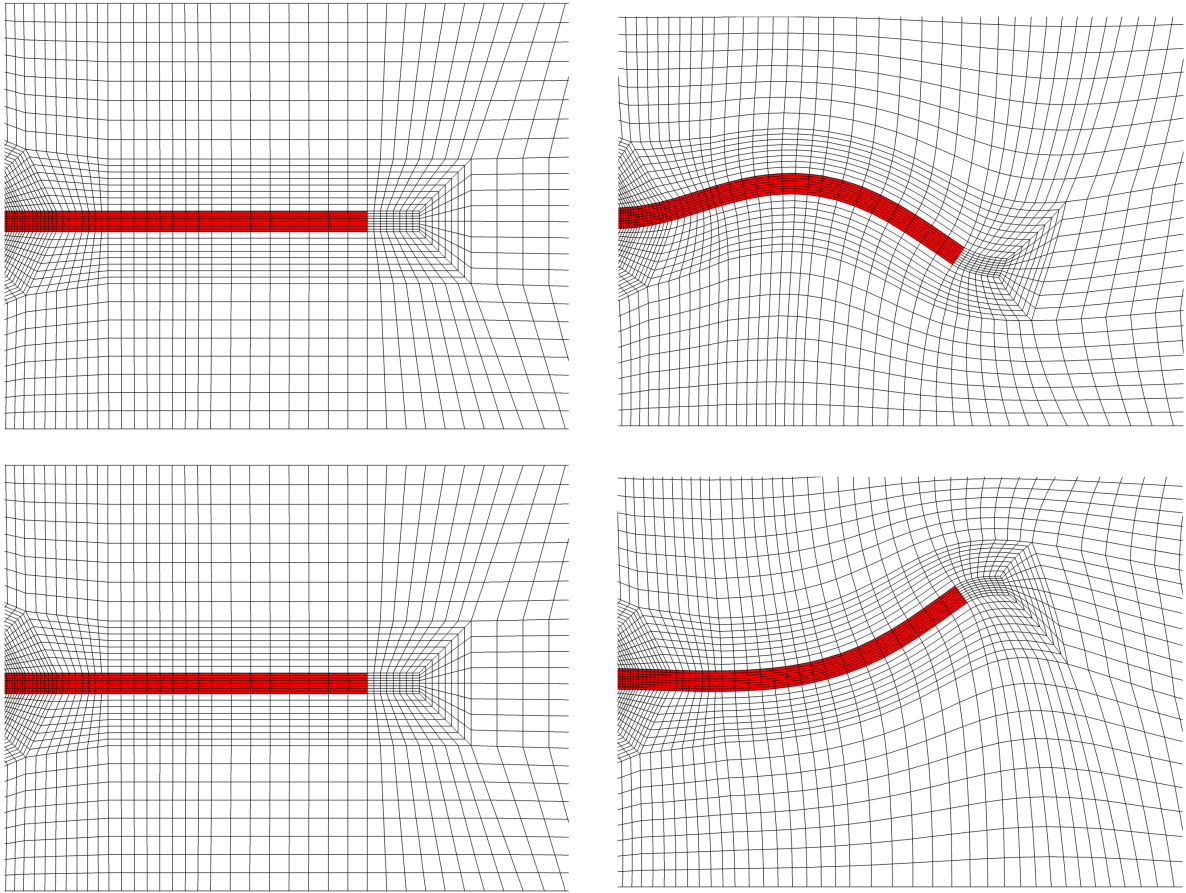
Figure 30: Comparison computational domains for two time steps between the $\text{ALE}_{fx}$ and $\text{ALE}_{dm}$. In $\text{ALE}_{fx}$, all computations are done in the same fixed reference domain $\widehat{\Omega}$ (left). In particular, a specific cell remains all times the same material (here, an elastic structure in red), i.e., $\Omega_f$ and $\Omega_s$ are time-independent. The mesh movement is hidden in the transformation $\vec{F}$ and $J$. The physical (current) ALE domain $\Omega(t)$ including the mesh movement is displayed in on the right, which also corresponds to the computational domain of the $\text{ALE}_{dm}$ approach. As explained, using $\text{ALE}_{dm}$, the mesh is moved explicitly such that the fluid is still computed in an Eulerian-like fashion. Figures partially taken from [243].

### 7.3.3 Navier-Stokes in ALE coordinates

**7.3.3.1 Navier-Stokes in ALE$_{dm}$ coordinates**    Inserting now the ALE time derivative into the Navier-Stokes equations, we obtain:

**Problem 7.6** (ALE$_{dm}$ fluid problem). *Find*
$\{v_f, p_f\} \in \{v_f^D + V_f^0\} \times L_f^0$ *such that the initial data satisfy $v_f(0) = v_f^0$, and for almost all time steps $t \in I$ holds:*

$$\rho_f(\hat{\partial}_t v_f, \psi^v)_{\Omega_f} + \rho_f\big((v_f - w) \cdot \nabla v_f, \psi^v\big)_{\Omega_f}$$
$$+(\sigma_f, \nabla \psi^v)_{\Omega_f} - \langle \sigma_f n_f, \nabla \psi^v \rangle_{\Gamma_{f,N} \cup \Gamma_i} - \rho_f(f, \psi^v)_{\Omega_f} = 0 \quad \forall \psi^v \in V_f^0, \tag{48}$$
$$(div\, v_f, \psi^p)_{\Omega_f} = 0 \quad \forall \psi^p \in L_f^0,$$

*with the Cauchy stress tensor*

$$\sigma_f = -p_f I + 2\rho_f \nu_f D(v_f) = -p_f I + \rho_f \nu_f (\nabla v_f + \nabla v_f^T),$$

*and a correction term on the outflow boundary ([132]):*

$$g := -\rho_f \nu_f \nabla v_f^T \quad on\ \Gamma_{f,N} = \Gamma_{out}.$$

**Remark 7.7.** *We observe in Problem 7.6 that the standard Eulerian framework is recovered if $w = 0$.*

This is now the place in which ALE$_{fx}$ and ALE$_{dm}$ differ.  Working with ALE$_{dm}$, we keep the above equations and solve these equations on the current domain $\Omega$ with appropriate discretization of the ALE time derivatives[19]:

$$\hat{\partial}_t v_f = \frac{1}{k}(v_f^n - v_f^{n-1} \circ \hat{\mathcal{A}}^{n-1} \circ (\hat{\mathcal{A}}^n)^{-1}).$$

Here, we work with an ALE map $\hat{\mathcal{A}}$ which is defined from the previous time step $t_{n-1}$ to the the present time step $t_n$. Thus, the reference configuration at time step $t_n$ is denoted by $\Omega^n$. Moreover, $v^n \in \Omega^n$ is used as an approximation to $v(t_n)$, which is transported from $\Omega^n$ to any other configuration $\Omega^l$ (for $l \neq n$) through the ALE map ([176]):

$$\hat{\mathcal{A}}_{n,l} = \hat{\mathcal{A}}_l \circ \hat{\mathcal{A}}_n^{-1}.$$

On the other hand, in ALE$_{fx}$, we use the fundamental theorem of calculus [154] in higher dimensions, and we obtain the Navier-Stokes equations on a fixed domain. This formulation introduces additional geometric nonlinearities in the equations (rather than in terms of the mesh) and they are formulated in terms of $\widehat{F}$ and $\hat{J}$.

**Remark 7.8.** *Reading the literature, it seems that more people use $ALE_{dm}$ to formulate fluid-structure inter-action problems. Of course, the equations look much nicer than introducing all transformation rules. However, we want to emphasize that in our taste, the $ALE_{fx}$ approach follows the Lagrangian idea by transforming all equations onto the refererence configuration leading to a consistent variational-monolithic coupling scheme. From the computational viewpoint it is maybe just a matter of taste.* $\diamond$

**7.3.3.2 Navier-Stokes in ALE$_{fx}$ coordinates**    Let us know work with ALE$_{fx}$ and explain things in more detail.  In addition to the ALE-time derivative transformation, we map (and solve!)  all equations to an (arbitrary) reference configuration $\widehat{\Omega}_f$. Consequently, the realization of the mesh movement appears not any more in the function spaces defined on moving domains, but now the function spaces are fixed and the domain movement is introduced via the transformation rules $\widehat{F}$ and $\hat{J}$, where $\hat{J}$ enters due to the transformation theorem (real analysis) and $\widehat{F}$ because of re-writing derivatives as explained in Section 5.1.1.

Using the concepts from continuum mechanics, it is clear how gradients and integrals are transformed to the reference configuration. For the incompressibility condition, $\nabla \cdot v = 0$, the transformation is a bit tricky and a property of the Piola transformation. It holds:

$$\hat{J}\mathrm{tr}(\widehat{\nabla}\hat{v}\widehat{F}^{-1}) = \widehat{\nabla} \cdot (\hat{J}\widehat{F}^{-1}\hat{v}).$$

---

[19]Many thanks to my present colleague Huidong Yang for fruitful discussions!

This is a rather surprising result since on the first view the right hand side should contain second-order derivatives of the displacements $\hat{u}_f$. However, the calculation shows (e.g., component-wise) that second-order derivatives cancel out and all regularity requirements that be made on $\hat{u}_f$ and $\widehat{F}$ are still valid.

As before, the boundary of $\widehat{\Omega}_f$ is divided into three non-overlapping parts $\partial\widehat{\Omega}_f = \widehat{\Gamma}_{f,D} \cup \widehat{\Gamma}_{f,N} \cup \widehat{\Gamma}_i$, where $\widehat{\Gamma}_i$ denotes later the interface and it coincides with $\widehat{\Gamma}_{f,N}$ in the case of pure fluid problems. We prescribe

$$\hat{u} = \hat{u}_D, \quad \text{and} \quad \hat{v} = \hat{v}_D \quad \text{on } \widehat{\Gamma}_{f,D},$$
$$\hat{J}\widehat{\sigma}_f\widehat{F}^{-T}\hat{n}_f = \hat{g} \quad \text{on } \widehat{\Gamma}_{f,N}.$$

Let $\hat{v}_f^D$ a suitable extension of Dirichlet inflow data. Then, the variational form in $\widehat{\Omega}_f$ reads:

**Problem 7.9** (ALE$_{fx}$ fluid problem). *Find*
$\{\hat{v}_f, \hat{p}_f\} \in \{\hat{v}_f^D + \hat{V}_f^0\} \times \hat{L}_f^0$ *such that the initial data* $\hat{v}_f(0) = \hat{v}_f^0$ *are satisfied, and for almost all time steps* $t \in I$ *holds:*

$$\hat{\rho}_f(\hat{J}\partial_t\hat{v}_f, \hat{\psi}^v)_{\widehat{\Omega}_f} + \hat{\rho}_f(\hat{J}\widehat{F}^{-1}(\hat{v}_f - \hat{w}) \cdot \widehat{\nabla}\hat{v}_f, \hat{\psi}^v)_{\widehat{\Omega}_f} + (\hat{J}\widehat{\sigma}_f\widehat{F}^{-T}, \widehat{\nabla}\hat{\psi}^v)_{\widehat{\Omega}_f}$$
$$- \langle \hat{J}\hat{g}_f\widehat{F}^{-T}\hat{n}_f, \hat{\psi}^v \rangle_{\widehat{\Gamma}_{f,N}} - \langle \hat{J}\widehat{\sigma}_f\widehat{F}^{-T}\hat{n}_f, \hat{\psi}^v \rangle_{\widehat{\Gamma}_i} - \hat{\rho}_f(\hat{J}\hat{f}_f, \hat{\psi}^v)_{\widehat{\Omega}_f} = 0,$$
$$(\widehat{div}(\hat{J}\widehat{F}^{-1}\hat{v}_f), \hat{\psi}^p)_{\widehat{\Omega}_f} = 0,$$

*for all* $\hat{\psi}^v \in \hat{V}_f^0$ *and* $\hat{\psi}^p \in \hat{L}_f^0$, *and with the transformed Cauchy stress tensor*

$$\widehat{\sigma}_f = -\hat{p}_f\hat{I} + 2\hat{\rho}_f\nu_f\widehat{D}(\hat{v}_f) = -\hat{p}_f\hat{I} + 2\hat{\rho}_f\nu_f(\widehat{\nabla}\hat{v}_f\widehat{F}^{-1} + \widehat{F}^{-T}\widehat{\nabla}\hat{v}_f^T). \tag{49}$$

As before, $\hat{g}_f$ accounts for (possible) Neumann data, for instance, a correction term for the do-nothing outflow condition (see Figure 17 if this correction term is not applied):

$$\hat{g}_f = -\hat{\rho}_f\nu_f\widehat{F}^{-T}\widehat{\nabla}\hat{v}_f^T \quad \text{on } \widehat{\Gamma}_{f,N} = \widehat{\Gamma}_{\text{out}}. \tag{50}$$

**Remark 7.10** (Variational-monolithic coupling; see also Section 7.3.8). *Coupling fluid flows with structural deformations along an interface* $\widehat{\Gamma}_i$ *requires the fulfillment of two coupling conditions. Fluid flows require a Dirichlet condition on* $\widehat{\Gamma}_i$, *i.e., the continuity of the velocities is strongly enforced in the corresponding Sobolev spaces. The structural problem is driven by the normal stresses that act on* $\widehat{\Gamma}_i$ *caused by the fluid. These normal stresses are achieved with the boundary term:*

$$\langle \hat{J}\widehat{\sigma}_f\widehat{F}^{-T}\hat{n}_f, \hat{\psi}^v \rangle_{\widehat{\Gamma}_i} \quad on \ \widehat{\Gamma}_i.$$

$\diamond$

Let us pause for a moment and have a closer look to the transformation of derivatives. With regard to the stress term $(\hat{J}\widehat{\sigma}_f\widehat{F}^{-T}, \widehat{\nabla}\hat{\psi}^v)_{\widehat{\Omega}_f}$ there exist two equivalent derivations. We explain the situation for the following problem:

$$-\nabla \cdot \sigma(u) = f \quad \text{in } \Omega_f,$$
$$u = 0 \quad \text{on } \partial\Omega_f.$$

As before, the weak form is obtained by multiplying with a test function and partial integration:

$$(-\nabla \cdot \sigma(u), \varphi)_\Omega = (f, \varphi)_\Omega \quad \forall\varphi \in H_0^1(\Omega),$$
$$\Rightarrow \quad (\sigma(u), \nabla\varphi)_\Omega = (f, \varphi)_\Omega \quad \forall\varphi \in H_0^1(\Omega),$$

Transforming to the reference domain $\widehat{\Omega}$ requires two operations employing Theorem 3.41:

$$\nabla\varphi \to \widehat{\nabla}\hat{\varphi}\widehat{F}^{-1}, \quad (x, y)_\Omega \to (\hat{J}\hat{x}, \hat{y})_{\widehat{\Omega}},$$

which yield for the above problem:

$$(\hat{J}\hat{\sigma}(\hat{u}), \widehat{\nabla}\hat{\varphi}\widehat{F}^{-1})_{\widehat{\Omega}} = (\hat{J}\hat{f}, \hat{\varphi})_{\widehat{\Omega}} \quad \forall \hat{\varphi} \in H_0^1(\widehat{\Omega}),$$
$$\Rightarrow \quad (\hat{J}\hat{\sigma}(\hat{u})\widehat{F}^{-T}, \widehat{\nabla}\hat{\varphi})_{\widehat{\Omega}} = (\hat{J}\hat{f}, \hat{\varphi})_{\widehat{\Omega}} \quad \forall \hat{\varphi} \in H_0^1(\widehat{\Omega}),$$

On the other hand, we can apply the Piola transformation to the strong-form operator and consider the weak form directly in $\widehat{\Omega}$. That is:

$$-\nabla \cdot \sigma(u) = f,$$
$$\Rightarrow \quad -\widehat{\nabla} \cdot (\hat{J}\hat{\sigma}(\hat{u})\widehat{F}^{-T}) = \hat{J}\hat{f}.$$

Since the strong-form operator is now already defined in the reference coordinates, we can formulate the weak form immediately in $\widehat{\Omega}$:

$$-\widehat{\nabla} \cdot (\hat{J}\hat{\sigma}(\hat{u})\widehat{F}^{-T}) = \hat{J}\hat{f},$$
$$\Rightarrow \quad (-\widehat{\nabla} \cdot (\hat{J}\hat{\sigma}(\hat{u})\widehat{F}^{-T}), \hat{\varphi})_{\widehat{\Omega}} = (\hat{J}\hat{f}, \hat{\varphi})_{\widehat{\Omega}} \quad \forall \hat{\varphi} \in H_0^1(\widehat{\Omega}),$$
$$\Rightarrow \quad (\hat{J}\hat{\sigma}(\hat{u})\widehat{F}^{-T}, \widehat{\nabla}\hat{\varphi})_{\widehat{\Omega}} = (\hat{J}\hat{f}, \hat{\varphi})_{\widehat{\Omega}} \quad \forall \hat{\varphi} \in H_0^1(\widehat{\Omega}).$$

### 7.3.4 On the regularity of the ALE mapping

Revisiting Chapter 5, we need $C^1$ regularity for the transformation map. In this section, we first recall the findings from [91, 176] who gave conditions for the regularity of the ALE mapping as well as requirements to transform functions between $\Omega$ and $\widehat{\Omega}$.

**Problem 7.11.** *The ALE mapping $\hat{\mathcal{A}}$ has to be defined such that $\hat{v} \in H^1(\widehat{\Omega})$ if and only if $v = \hat{v} \circ \hat{\mathcal{A}}^{-1} \in H^1(\Omega)$.*

Using classical function spaces, a sufficient condition is that $\hat{\mathcal{A}}$ is a $C^1$-diffeomorphism:

$$\hat{\mathcal{A}} \in C^1(\overline{\widehat{\Omega}}), \quad \hat{\mathcal{A}}^{-1} \in C^1(\overline{\Omega}),$$

and

$$\widehat{F} \in L^\infty(\widehat{\Omega}), \quad F \in L^\infty(\Omega).$$

This requirement must be weakened because classical function spaces are inappropriate when approximate solutions with help of a Galerkin finite element scheme are computed.

**Proposition 7.12.** *Let $\widehat{\Omega}$ be a bounded domain with $C^{1,1}$-boundary (see, e.g., [250]). Let $\hat{\mathcal{A}}$ be invertible in the closure of $\widehat{\Omega}$ and there holds for each $t \in I$ the two conditions*

- *$\Omega = \hat{\mathcal{A}}(\widehat{\Omega})$ is bounded and $\partial\Omega$ is Lipschitz-continuous.*

- *Let $\hat{\mathcal{A}} \in W^{1,\infty}(\widehat{\Omega})$ and $\hat{\mathcal{A}}^{-1} \in W^{1,\infty}(\Omega)$.*

*Then, $v \in H^1(\Omega)$ if and only if $\hat{v} = v \circ \hat{\mathcal{A}} \in H^1(\widehat{\Omega})$. Moreover, the corresponding norms are equivalent.*

For a proof of this Lemma, we refer to [176].

**Remark 7.13** (Accessing the ALE mapping regularity). *As previously explained, as quantity to measure the ALE regularity, we can consult the determinant $\hat{J}$ of the deformation gradient. In particular, $\hat{J} > 0$ if $\|\hat{u}_f\|_{W^{2,p}(\widehat{\Omega}_f;\mathbb{R}^d)}$ is sufficiently small, which implies $\widehat{\mathcal{A}}$ and $\widehat{\mathcal{A}}^{-1} \in W^{1,\infty}(\widehat{\Omega};\mathbb{R}^{d\times d})$; the reader is also referred to Section 5.1.3). Furthermore, the more we bound $\hat{J}$ away from zero, the better the regularity. In other words, all mesh motion models aim to control $\hat{J}$ and try to bound this quantity away from zero. Here, it is clear from the theoretical standpoint (and numerical tests displayed in Figure 32 confirm the theory) that biharmonic mesh motion leads to higher regularity than harmonic or linear-elastic models. A computational analysis is provided in Section 7.3.7.* ◇

### 7.3.5 Interface coupling conditions

In this section, we state the interface coupling conditions for fluid-structure interaction. The coupling of the fluid with the structure equations must satisfy three conditions:

- continuity of velocities;

- continuity of normal stresses;

- continuity of displacements (geometrical coupling of phyiscal solids and fluid mesh motion).

The first two conditions are of physical nature whereas the latter one has geometrical meaning. Mathematically, the first and third condition can be classified as (non-homogeneous) Dirichlet conditions and the second condition is a (non-homogeneous) Neumann condition.
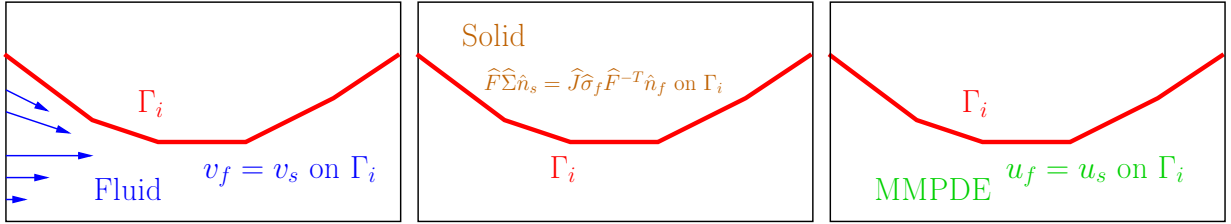


Figure 31: Illustration of the three coupling conditions on $\Gamma_i$ (respectively its corresponding definition on the fixed $\widehat{\Gamma}_i$): $v_f$ is required to solve the fluid system, $\widehat{F}\Sigma_s\hat{n}_s$ is required for the solid system, and $u_f$ is necessary for the MMPDE (fluid mesh motion).

**7.3.5.1 Physical conditions: continuity of velocity and normal stresses** The velocity field must be continuous on the interface (which is a Dirichlet-like condition seen from the fluid side). Sufficient regularity for the structure velocity is taken as assumption, such that this velocity can be given to the fluid problem. In detail, we have

$$v_f = v_s \quad \text{on } \Gamma_i, \tag{51}$$

i.e.,

$$v_f = w = v_s \quad \text{on } \Gamma_i. \tag{52}$$

To complete the structure problem, we must enforce the balance of the normal stresses on the interface:

$$\hat{J}\hat{\sigma}_f\widehat{F}^{-T}\hat{n}_f + \widehat{F}\widehat{\Sigma}\hat{n}_s = 0 \quad \text{on } \widehat{\Gamma}_i. \tag{53}$$

This condition corresponds to a Neumann-like boundary condition for the structure subsystem.

**Remark 7.14.** *Condition* (53) *is formulated for the standard solid equation. Including strong damping of solid equations; namely the term* $\gamma_s\hat{\epsilon}(\hat{v}_s)\hat{n}_s$ *brings us to*

$$\hat{J}\hat{\sigma}_f\widehat{F}^{-T}\hat{n}_f + \widehat{F}\widehat{\Sigma}\hat{n}_s + \gamma_s\hat{\epsilon}(\hat{v}_s)\hat{n}_s = 0 \quad on \ \widehat{\Gamma}_i. \tag{54}$$

$\diamond$

**7.3.5.2 Geometric coupling (the third condition)** The MMPDE problem requires as interface condition that the displacements of the fluid mesh motion follow the solid:

$$\hat{u}_f = \hat{u}_s \quad \text{on } \widehat{\Gamma}_i, \tag{55}$$

from which we obtain immediately $\hat{w} = \hat{v}_s$ with temporal differentiation.

Here, for fluid-structure interaction based on the 'arbitrary Lagrangian-Eulerian' framework (ALE), the choice of appropriate a fluid mesh movement PDE (MMPDE) is important in order to guarantee $\hat{J} > 0$. In order to move the mesh and to determine the new location of mesh vertices, an effective and automated techique is based on solving an auxiliary PDE that keeps good mesh quality. Often in these cases, an additional elasticity equation is solved [56, 217, 226]. For moderate deformations, one can pose an auxiliary Laplace problem [52, 70, 249] that is known as harmonic mesh motion. More advanced equations from linear elasticity (including Jacobi-based stiffening) are also available [210, 226]. A comparison of such models has been performed in [255]. In Jacobi-based stiffening, the resulting PDE becomes nonlinear. Thirdly, we also use (for mesh moving) the fourth-order biharmonic equation that others have studied for fluid flows in ALE coordinates [128]. It was also shown there, that using the biharmonic model provides greater freedom in the choice of boundary and interface conditions. In general, the biharmonic mesh motion model leads to a smoother mesh (and larger deformations of the structure) compared to the mesh motion models based on second order partial differential equations [241]. Although the mesh behavior of the harmonic and the biharmonic mesh motion models were analyzed in [128] for different applications, we upgrade these concepts to fluid-structure interaction



Figure 32: Computational structure mechanics (CSM 4) test [241] with harmonic and linear-elastic mesh motion models on top. Both models lead to mesh distortion close to the lower boundary. At the bottom, meshes using biharmonic mesh motion are displayed, which perform significantly better near the tip of the beam. In addition, we observe node-clustering that is a typical result of mesh motion. In the final figure, function plots of $\min(\hat{J})$ for the mesh motion models of the CSM 4 test. Degeneration of mesh cells corresponds to negative values of $\hat{J}$, arising in the first three models.

problems. Quantitative comparisons are shown in the Figure 32 (taken from [241]).

We define the ALE mapping in terms of the displacement variable, such that we obtain

$$\hat{u}(\hat{x}) = \hat{\mathcal{A}}(\hat{x}) - \hat{x}.$$

In the following, we discuss the three possible partial differential equations in detail, which can be used for fluid mesh moving. In two dimensional configurations, the mesh moves in $x$- and $y$-direction, which allows us to find a vector-valued artificial displacement variable

$$\hat{u}_f := (\hat{u}_f^{(1)}, \hat{u}_f^{(2)}, \hat{u}_f^{(3)}) := (\hat{u}_f^{(x)}, \hat{u}_f^{(y)}, \hat{u}_f^{(z)}).$$

We need the single components of $\hat{u}_f$ below to apply different types of boundary conditions to the biharmonic mesh motion model. In the following, the formal description of the first two mesh motion models coincides and only differ in the definition of the stress tensors $\hat{\sigma}_{\text{mesh}}$.
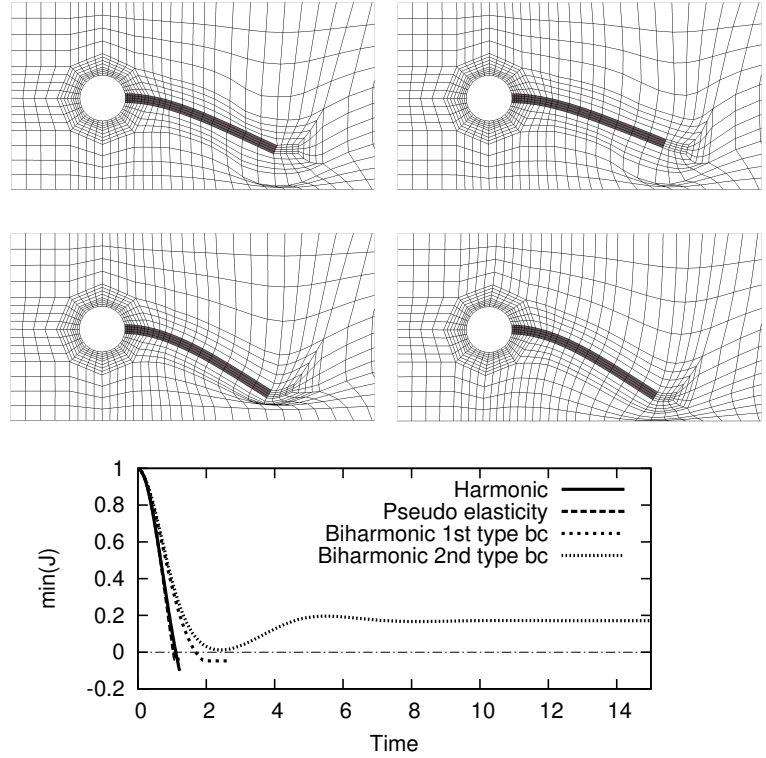
### 7.3.6 Mesh motion models (MMPDEs)

**7.3.6.1 Mesh motion with a harmonic model**  The simplest model is based on the harmonic equation, which reads in strong formulation:

$$-\widehat{\operatorname{div}}(\hat{\sigma}_{\mathrm{mesh}}) = 0, \tag{56}$$

$$\hat{u}_f = \hat{u}_s \text{ on } \widehat{\Gamma}_i, \tag{57}$$

$$\hat{u}_f = 0 \text{ on } \partial\widehat{\Omega}_f \setminus \widehat{\Gamma}_i, \tag{58}$$

with

$$\widehat{\sigma}_{\mathrm{mesh}} = \alpha_u \widehat{\nabla}\hat{u}_f.$$

The monitor function $\alpha_u := \alpha_u(\hat{x})$ (for a solid equation, we would just call it diffusion parameter) is chosen such that a good fluid mesh quality is guaranteed. The oldest idea steems from [249]. As second idea, we can choose

$$\alpha_u(\hat{x}) = a + b\exp(-c\hat{d}), \tag{59}$$

with certain constants $a, b, c > 0$. The Euclidian distance of a point $\hat{x}$ to the interface $\widehat{\Gamma}_i$ is denoted by $\hat{d} = |\hat{x} - \widehat{\Gamma}_i|$ . Another, even simpler, strategy was proposed by Tezduyar et al. [226], which was further developed by Stein et al. [217]. They propose to choose as monitor function:

$$\alpha_u(\hat{x}) = \hat{J}^{-1}. \tag{60}$$

This choice works well because mesh cell distortion appears in the vicinity of $\widehat{\Gamma}_i$. That means $\hat{J} \searrow 0$ near $\widehat{\Gamma}_i$, and consequently $\alpha_u(\hat{x}) \gg 0$ near $\widehat{\Gamma}_i$. By reason that high diffusion causes low mesh movement, the quality of the fluid mesh is maintained. For a comparison of different choices of $\alpha_u := \alpha_u(\hat{x})$, we refer to [241].

**Remark 7.15.** *Using model* (60) *leads to a nonlinear equation for* $\widehat{\sigma}_{mesh}$ *since* $\hat{u}$ *is used to define* $\hat{J}$. $\diamond$

**7.3.6.2 Mesh motion with a linear elastic model**  The equation of linear elasticity is formally based on the well-known momentum equations from structural mechanics as introduced previously. In a steady-state regime, we obtain the following equation defining a static equilibrium:

$$-\widehat{\operatorname{div}}(\widehat{\sigma}_{\mathrm{mesh}}) = 0, \quad \hat{u}_f = \hat{u}_s \text{ on } \widehat{\Gamma}_i, \quad \hat{u}_f = 0 \text{ on } \partial\widehat{\Omega}_f \setminus \widehat{\Gamma}_i,$$

where $\widehat{\sigma}_{\mathrm{mesh}}$ is formally equivalent to the STVK constitutive tensor in Equation (5.46). It is given by

$$\widehat{\sigma}_{\mathrm{mesh}} := \alpha_\lambda(\operatorname{tr}\widehat{E}_{lin})\hat{I} + 2\alpha_\mu\widehat{E}_{lin}, \tag{61}$$

where $\widehat{E}_{lin}$ was defined in Definition 5.29. The mesh monitor parameters $\alpha_\lambda := \alpha_\lambda(\hat{x})$ and $\alpha_\mu := \alpha_\mu(\hat{x})$ are chosen in a way, such that a good fluid mesh quality is guaranteed. By virtue of (13), we compute $\alpha_\lambda$ and $\alpha_\mu$ from the Young modulus $E_Y$ and the Poisson ration $\nu_s$. Therefore, we choose $E_Y$ according to (59) or (60). Further, we choose a negative Poisson ratio (recall that $\nu_s \in (-1, 0.5]$). Materials with negative Poisson ratio belongs to auxetic materials and they become thinner in the perpendicular direction, when they are compressed. This is a useful property for the evolution of the fluid mesh. We refer the reader again to [217] (and references cited therein) for other choices of $\alpha_\lambda$ and $\alpha_\mu$.

**7.3.6.3 Mesh motion with a biharmonic model**  Using the biharmonic mesh model provides much more freedom in choosing boundary conditions [62, 128]. In these notes, solving the biharmonic equation is introduced as a third possible fluid mesh deformation:

$$\widehat{\Delta}^2\hat{u}_f = 0 \quad \text{in } \widehat{\Omega}_f, \tag{62}$$

$$\hat{u}_f = \hat{u}_s \text{ and } \partial\hat{u}_f = \partial\hat{u}_s \quad \text{on } \widehat{\Gamma}_i, \tag{63}$$

$$\hat{u}_f = \partial\hat{u}_f = 0 \quad \text{on } \partial\widehat{\Omega}_f. \tag{64}$$

This model is considered in a mixed formulation in the sense of Ciarlet [62]. As before, a control parameter is used to steer the mesh motion. Then, we deduce

$$\hat{\eta}_f = -\alpha_u \hat{\Delta} \hat{u}_f \quad \text{and} \quad -\alpha_u \hat{\Delta} \hat{\eta}_f = 0. \tag{65}$$

It is more convenient to consider the single component functions $\hat{u}_f^{(1)}, \hat{u}_f^{(2)}$ and $\hat{u}_f^{(3)}$,

$$\hat{\eta}_f^{(1)} = -\alpha_u \hat{\Delta} \hat{u}_f^{(1)} \quad \text{and} \quad -\alpha_u \hat{\Delta} \hat{\eta}_f^{(1)} = 0, \tag{66}$$

$$\hat{\eta}_f^{(2)} = -\alpha_u \hat{\Delta} \hat{u}_f^{(2)} \quad \text{and} \quad -\alpha_u \hat{\Delta} \hat{\eta}_f^{(2)} = 0, \tag{67}$$

$$\hat{\eta}_f^{(3)} = -\alpha_u \hat{\Delta} \hat{u}_f^{(3)} \quad \text{and} \quad -\alpha_u \hat{\Delta} \hat{\eta}_f^{(3)} = 0. \tag{68}$$

We utilize two types of boundary conditions. First, we pose the *first type of boundary conditions* (that corresponds to conditions of a clamped plate)

$$\hat{u}_f^{(k)} = \partial_n \hat{u}_f^{(k)} = 0 \quad \text{on } \partial\widehat{\Omega}_f \setminus \widehat{\Gamma}_i, \quad \text{for } k = 1, 2, 3. \tag{69}$$

Second, we are concerned with a mixture of boundary conditions

$$\hat{u}_f^{(1)} = \partial_n \hat{u}_f^{(1)} = 0 \quad \text{and} \quad \hat{\eta}_f^{(1)} = \partial_n \hat{\eta}_f^{(1)} = 0 \quad \text{on } \widehat{\Gamma}_{\text{in}} \cup \widehat{\Gamma}_{\text{out}}, \tag{70}$$

$$\hat{u}_f^{(2)} = \partial_n \hat{u}_f^{(2)} = 0 \quad \text{and} \quad \hat{\eta}_f^{(2)} = \partial_n \hat{\eta}_f^{(2)} = 0 \quad \text{on } \widehat{\Gamma}_{\text{wall}}, \quad \text{on } \widehat{\Gamma}_{\text{in}} \cup \widehat{\Gamma}_{\text{out}}, \tag{71}$$

$$\hat{u}_f^{(3)} = \partial_n \hat{u}_f^{(3)} = 0 \quad \text{and} \quad \hat{\eta}_f^{(3)} = \partial_n \hat{\eta}_f^{(3)} = 0 \quad \text{on } \widehat{\Gamma}_{\text{wall}}. \tag{72}$$

which we call *second type of boundary conditions*. In particular, the conditions

$$\hat{\eta}_f^{(k)} = \partial_n \hat{\eta}_f^{(k)} = 0 \quad \text{on } \widehat{\Gamma}_{\text{in}} \cup \widehat{\Gamma}_{\text{out}}, \quad \text{for } k = 1, 2, 3, \tag{73}$$

mean, that a plate is left free along this boundary part. Using biharmonic mesh motion, we also must enforce two conditions on the interface:

$$\hat{u}_f = \hat{u}_s \quad \text{and} \quad \partial_n \hat{u}_f = \partial_n \hat{u}_s \quad \text{on } \widehat{\Gamma}_i.$$

**Remark 7.16.** *Using the second type of boundary conditions in a rectangular domain where the coordinate axes match the Cartesian coordinate system, leads to mesh movement only in the tangential direction. This effect reduces mesh cell distortion because only the perpendicular directions of $\hat{u}_f$ and $\hat{\eta}_f$ are constrained to zero at the different parts of $\partial\widehat{\Omega}$. The effects of these boundary conditions are examined in Figure 32* ⋄

**Remark 7.17** (Mixed system on non-convex domains)**.** *It has been shown in [258], that the solutions of the biharmonic problem do not correspond (in general) to the mixed system if the problem is considered on a non-convex domain. This is exactly the case in our situations. However, we emphasize that the mesh motion problem is an artificial problem and we are not interested in its accurate physical solution but rather in a reasonable approximation in order to move the mesh. Recent findings from [107] confirm [258] and the authors even outline that in some cases with re-entrant corners, there might be not even a solution to the mixed problem. However, numerical algorithms converge.* ⋄

**Remark 7.18** (Tolerance of the numerical solution)**.** *We notice again that the moving mesh equations are auxiliary equations to move the mesh. This means in particular, we are still mainly interested in the solution of the physical equations (fluid and solid). Consequently, for the numerical solution of the mesh moving equations a much lower tolerance can be employed for the nonlinear and/or linear solver.* ⋄
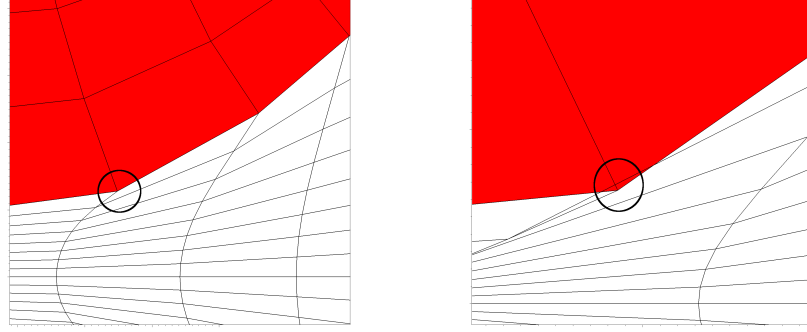
Figure 33: Mesh tangling/degeneration in which the inner angle 180 degree opening (left) and mesh racing in which solid mesh cells (in red) intersect illegally with fluid cells (in white) - right figure.

### 7.3.7 Computational analysis and comparison of three MMPDEs for the FSI-2 benchmark

**7.3.7.1 The idea** This section is motivated by [241] but all following results in this part have been recently reported in [246]. We adopt the three previously discussed mesh motion models; namely nonlinear harmonic and nonlinear elastic models and compare them with the (linear) biharmonic MMPDE. Of course, the biharmonic equation is much more expensive to solve since either $C^1$ continuous finite elements are required or Ciarlet's splitting into a first order system. However, in [241], it was never systematically analyzed that the 4th order biharmonic equation is linear but the 2nd order models are, firstly, nonlinear, and secondly, have worse regular ALE mappings. Consequently, it is a priori not clear if the biharmonic MMPDE is really (always) inferior in terms of computational cost because the linear solve is indeed more expensive but it might have less Newton steps per time step due to a better ALE regularity. To answer this key question, the present study addresses:

- Computational analysis of the regularity of the ALE mapping (observing $min(\hat{J})$);

- Observation of the number of Newton steps at each time step for (very) large deformations for a long-term FSI computation;

- Relation of the ALE-regularity and number of Newton steps with conclusions on the total computational cost for a serial programming code.

We emphasize that the findings of this study hold for a challenging FSI benchmark test FSI-2 [140] computed on a relatively coarse mesh but more than thousand time steps. For other applications and configurations with smaller solid deformations, less time steps and much finer grids, the results might differ significantly.

As three models in this study, we consult two nonlinear second-order models and a linear biharmonic equation:

$$-\widehat{\mathrm{div}}(\widehat{\sigma}_{\mathrm{mesh}}) = 0 \quad \text{in } \widehat{\Omega}_f, \quad \hat{u}_f = \hat{u}_s \text{ on } \widehat{\Gamma}_i, \quad \hat{u}_f = 0 \text{ on } \partial\widehat{\Omega}_f, \tag{74}$$

with

$$\widehat{\sigma}_{\mathrm{mesh}}^{harmonic} = \frac{\alpha_u}{\hat{J}} \widehat{\nabla} \hat{u}_f, \qquad \widehat{\sigma}_{\mathrm{mesh}}^{elastic} = \alpha_\lambda (\mathrm{tr}\, \widehat{E}_{lin}) \hat{I} + 2\alpha_\mu \widehat{E}_{lin}, \tag{75}$$

and

$$\alpha_\mu = \frac{\alpha_u}{2\hat{J}(1+\nu_s)}, \quad \alpha_\lambda = \frac{\nu_s \alpha_u}{\hat{J}(1+\nu_s)(1-2\nu_s)}, \quad \nu_s = -0.1, \quad \widehat{E}_{lin} = \frac{1}{2}(\widehat{\nabla}\hat{u}_f + \widehat{\nabla}\hat{u}_f^T).$$

Thirdly, the linear 4th-order biharmonic model reads:

$$\alpha_u \widehat{\Delta}^2 \hat{u}_f = 0 \quad \text{in } \widehat{\Omega}_f, \quad \hat{u}_f = \hat{u}_s \text{ and } \partial\hat{u}_f = \partial\hat{u}_s \quad \text{on } \widehat{\Gamma}_i, \qquad \hat{u}_f = \partial\hat{u}_f = 0 \quad \text{on } \partial\widehat{\Omega}_f,$$

and a (small) constant $\alpha_u > 0$ that is independent of $\hat{u}_f$.

**7.3.7.2 Numerical test: the FSI-2 benchmark [140]** In this section, a numerical example shows that 4th-order biharmonic mesh motion is not always more expensive than 2nd order MMPDEs.

*Configuration*

The computational domain has length $L = 2.5m$ and height $H = 0.41m$. The circle center is positioned at $C = (0.2m, 0.2m)$ with radius $r = 0.05m$. The elastic beam has length $l = 0.35m$ and height $h = 0.02m$. The right lower end is positioned at $(0.6m, 0.19m)$, and the left end is attached to the circle.

*Boundary conditions*

For the upper, lower, and left boundaries, the 'no-slip' conditions for velocity and no zero displacement for structure are given. At the outlet $\hat{\Gamma}_{out}$, the 'do-nothing' outflow condition [132] is imposed leading to a zero mean value, i.e., $\int_{\hat{\Gamma}_{out}} p\, ds$ of the pressure at this part of the boundary.

A parabolic inflow velocity profile is given on $\hat{\Gamma}_{in}$ by



Figure 34: Flow around cylinder with elastic beam with circle-center $C = (0.2, 0.2)$ and radius $r = 0.05$.

$$v_f(0, y) = 1.5\bar{U}\frac{4y(H - y)}{H^2}, \quad \bar{U} = 1.0ms^{-1}.$$

*Initial conditions*

For the non-steady tests one should start with a smooth increase of the velocity profile in time. We use

$$v_f(t; 0, y) = \begin{cases} v_f(0, y)\frac{1 - \cos(\frac{\pi}{2}t)}{2} & \text{if } t < 2.0\text{s} \\ v_f(0, y) & \text{otherwise.} \end{cases}$$

The term $v_f(0, y)$ is already explained above.

*Quantities of comparison and their evaluation*

1) The $y$-deflection of the beam at $A(t)$.

2) The minimal $\hat{J}$.

3) Number of Newton iterations for both low deformations and largest deformations.

4) Total computational cost, total matrix assemblings and total linear solves.

*Model and material Parameters*

For the fluid we use $\varrho_f = 10^3 kgm^{-3}$, $\nu_f = 10^{-3}m^2s^{-1}$. The elastic structure is characterized by $\varrho_s = 10^4 kgm^{-3}$, $\nu_s = 0.4$, $\mu_s = 5 * 10^5 kgm^{-1}s^{-2}$. The Reynold's number is

$$Re = \frac{L\bar{V}}{\nu} = \frac{0.1 \times 1}{10^{-3}} = 100,$$

where we choose the diameter of the cylinder as characteristic length, $D = 2r = 0.1m$. As characteristic velocity, we take the mean velocity, $\bar{V} = \frac{2}{3}V(0, H/2, t)$ where $V$ is just the parabolic inflow profile from above and evaluated in the middle $H/2$ with the highest velocity:

$$V = v_f(0, H/2) = 1.5 \times 1.0\frac{4y(H - H/2)}{H^2} = 1.5 \quad \Rightarrow \quad \bar{V} = 1.5 \times V = \frac{2}{3}1.5 = 1.$$

The (absolute) Newton tolerance is chosen as $10^{-8}$. The shifted Crank-Nicolson scheme [131, 189] is used for time integration with a time step size $k = 10^{-2}s$ and total time $T = 15$ such that 1500 time steps are computed. The initial mesh is one-time globally refined with 748 cells and 14740 (6248 + 6248 + 2244) degrees of freedom for the second order models and 20988 (6248 + 6248 + 2244 + 6248) degrees of freedom for the biharmonic MMPDE. The Jacobian matrix (left hand side of Newton's method) is only build if the ratio between the new newton residual and the previous one, is larger than 0.1.
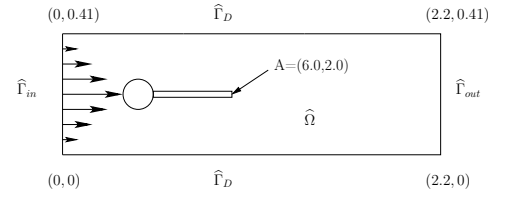
*Programming code and computing machine*

As programming code, the serial open-source code published in [244] has been employed for the biharmonic MMPDE with four basic unknowns $\{\hat{v}, \hat{p}, \hat{u}, \hat{\eta}\}$. For the 2nd order models, this code has been modified for solving second order models with three basic unknowns $\{\hat{v}, \hat{p}, \hat{u}\}$. The examples were run on a Intel(R) Core(TM) i5-3320M CPU 2.60GHz machine.

*Discussion of the results*
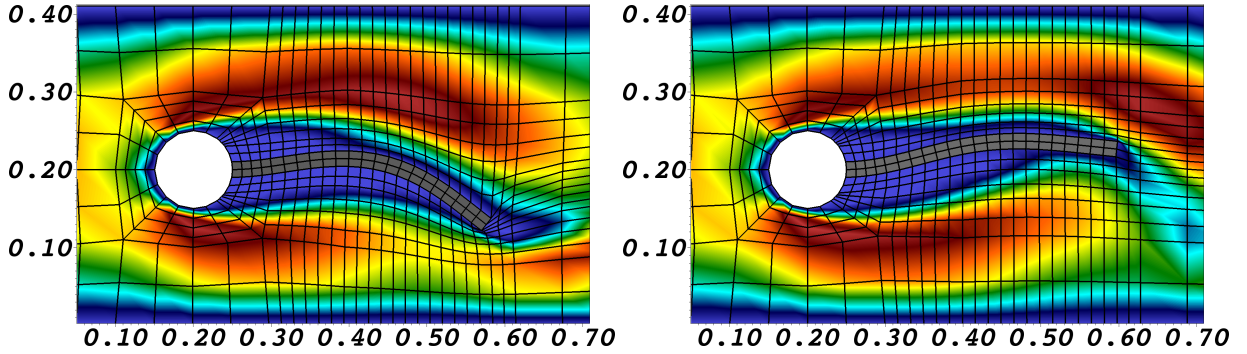


Figure 35: Velocity field and mesh deformation at two snapshots using the harmonic MMPDE. The displacement extremum is displayed at left and a small deformation is shown at right. These two time instances also refer to Table 3, where the respective Newton iterations are measured.
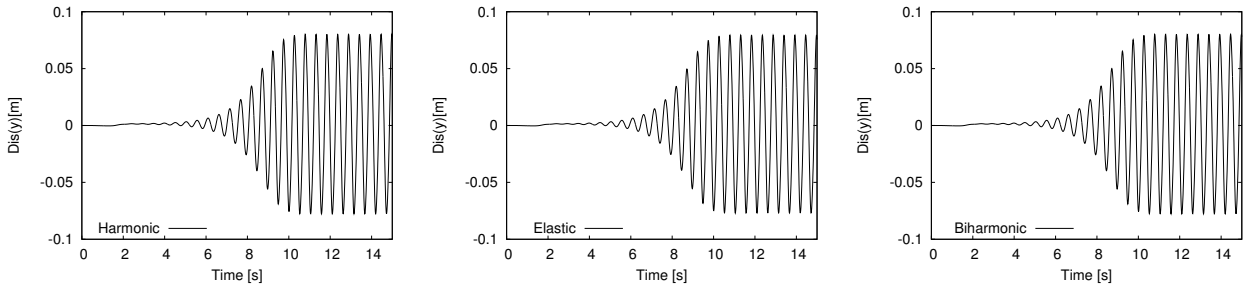


Figure 36: Comparison of the $u_y$ for nonlinear harmonic, nonlinear elastic and linear biharmonic mesh motion.
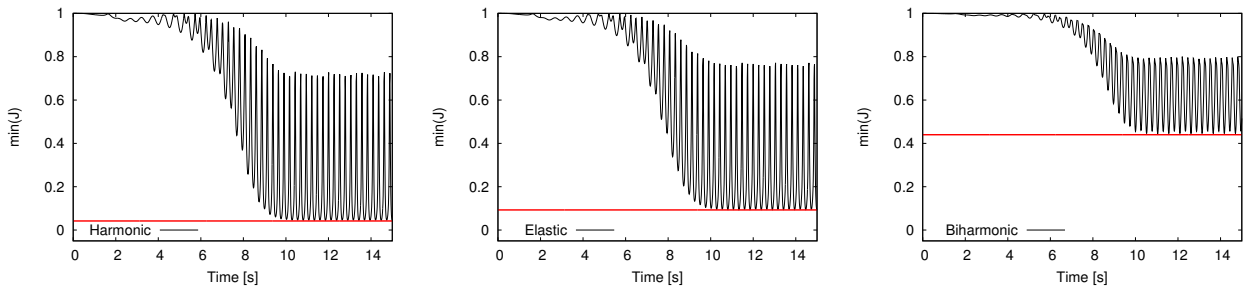


Figure 37: Comparison of the mesh regularity in terms of $\min(\hat{J})$ for nonlinear harmonic, nonlinear elastic and linear biharmonic mesh motion.

In our findings, we observe in Figure 36 that the $u_y$ displacements are similar. The mesh regularity becomes better using a more sophisticated MMPDE as displayed in Figure 37. First, the nonlinear harmonic model is still able to compute this test with a minimal $\hat{J} = 0.045$ compared to a twice better $\hat{J} = 0.094$ (using the elastic MMPDE) and a 10 times better $\hat{J} = 0.445$ using biharmonic mesh motion (see also Table 3). These differences

are reflected in the number of Newton iterations which in the extremum points with largest solid deformations are two times higher for the second order models compared to the biharmonic MMPDE. Assembling the Jacobian matrix is almost three times higher using the second order models. The total computational cost differs slightly between the second order models (here the nonlinear elastic model performs worst because of additional nonlinearities compared to harmonic mesh motion) and is approximately around $9h$ CPU time (see Table 3). The biharmonic MMPDE performs better with a total CPU time of $7.25h$. Our findings indicate that for this FSI benchmark, the biharmonic mesh motion model is competitive due to better regularity of the ALE mapping and less Newton iterations despite higher cost in each linear solve.

Table 3: Comparison of Newton iterations, the minimal $\hat{J}$, number of assembling the Jacobian, solving the linear system, and the total computational cost.

|  | Harmonic | Elastic | Biharmonic |
|---|---|---|---|
| Newton iter (extremum; Fig. 35 (left)) | 39 | 39 | 17 |
| Newton iter (small deform.; Fig. 35 (right)) | 9 | 9 | 8 |
| $\min(\hat{J})$ | 0.045 | 0.094 | 0.445 |
| Assembling the Jacobian matrix (total no.) | 18893 | 18357 | 6746 |
| Solve linear system (total no.) | 20987 | 20457 | 10747 |
| Computational cost (total CPU time) | $3.183 \times 10^4 s$ | $3.304 \times 10^4 s$ | $2.609 \times 10^4 s$ |

In conclusion, we found that biharmonic mesh motion for ALE-FSI has competitive computational cost for long-term simulations with many time steps. Using biharmonic mesh motion, the higher fluid-mesh regularity for large solid deformations does lead to much less Newton iterations per time step and consequently the higher cost in the linear solver is compensated. On the other hand, for moderate deformations, it is still absolutely sufficient to use a (linear) second order mesh motion model rather than a 4th order equation.

### 7.3.8 Variational-monolithic coupling

Before we state the coupled FSI problem, let us briefly recapitulate our philosophy for coupling. In these notes, we aim for a consistent variational-monolithic coupling scheme in which we need all equations defined in the same domain; therefore, $\mathrm{ALE}_{fx}$ was introduced. In variational monolithic coupling, Neumann-like interface conditions, like the continuity of normal stresses are fulfilled exactly in a weak sense on the continuous level:

$$\langle \hat{J}\hat{\sigma}_f \widehat{F}^{-T}\hat{n}_f, \varphi \rangle + \langle \widehat{F}\widehat{\Sigma}\hat{n}_s, \varphi \rangle = 0 \quad \forall \varphi \in V, \tag{76}$$

and they are realized through interface integrals (but actually disappear in the later models because of their contiuity in the weak (variational) sense).

**Remark 7.19.** *Using strong damping leads to the modified interface condition:*

$$\langle \hat{J}\hat{\sigma}_f \widehat{F}^{-T}\hat{n}_f, \varphi \rangle + \langle \widehat{F}\widehat{\Sigma}\hat{n}_s, \varphi \rangle + \langle \gamma_s \hat{\epsilon}(\hat{v}_s)\hat{n}_s, \varphi \rangle = 0 \quad \forall \varphi \in V, \tag{77}$$

The continuity of flow conditions,

$$v_f = v_s,$$

and the geometric coupling

$$u_f = u_s,$$

are incorporated directly in the Sobolev spaces as usually done for Dirichlet conditions:

$$\hat{V}_{f,\hat{v}}^0 := \{\hat{v}_f \in H_0^1(\widehat{\Omega}_f) : \hat{v}_f = \hat{v}_s \text{ on } \widehat{\Gamma}_i\},$$
$$\hat{V}_{f,\hat{u}}^0 := \{\hat{u}_f \in H_0^1(\widehat{\Omega}_f) : \hat{u}_f = \hat{u}_s \text{ on } \widehat{\Gamma}_i\}.$$

### 7.3.9 A variational-monolithic FSI-formulation using ALE$_{fx}$

With the previous preparations at hand, in this section, we define the monolithically coupled fluid-structure interaction problems employing the ALE$_{fx}$ approach. Thus, we define the setting in a fixed domain and formulate the equations in a fashion that can be used in a straightforward way for the implementation. The coupled strong problem (with the fluid equations defined in a moving domain $\Omega$) can be formulated as illustrated previously, see [94], p. 120-121, and [19]. The corresponding weak formulations have also been derived elsewhere [19, 175].

The definitions of the fully coupled problems include three (or four) types of nonlinearities that are divided into two groups:

- The physical nonlinearities includes the convection term for the fluid;

- and the nonlinear structure model;

- an additional nonlinearity induced by the ALE transformation is a so-called geometric nonlinearity;

- and possibly a fourth condition in case of a nonlinear MMPDE if $\alpha_u(\hat{x}) = 1/\hat{J}$.

In order to derive the weak form a the FSI model, we now put our different pieces together:

**Definition 7.20** (Collecting all pieces for variational-monolithic FSI in $ALE_{fx}$). *To build the FSI model, we use:*

- *Fluid momentum and mass conservation: the weak form of Navier-Stokes in $ALE_{fx}$; namely Problem 7.9;*

- *Solid momentum in mixed form: the weak form of elasticity Problem 6.18; possibly with damping terms as defined in Problem 6.32;*

- *Solid volume conservation: only in the case of incompressible solids;*

- *Fluid mesh motion: the weak form $(\widehat{\sigma}_{mesh}, \widehat{\nabla}\hat{\psi}^u)_{\widehat{\Omega}_f}$ of one of the second-order MMPDEs or alternatively a fourth-order MMPDE from Section 7.3.6.*

Then, the weak form of the coupled FSI model reads:

**Problem 7.21** (ALE$_{fx}$ FSI with harmonic and linear-elastic mesh motion). *Find*
$\{\hat{v}_f, \hat{v}_s, \hat{u}_f, \hat{u}_s, \hat{p}_f, \hat{p}_s\} \in \{\hat{v}_f^D + \hat{V}_{f,\hat{v}}^0\} \times \hat{L}_s \times \{\hat{u}_f^D + \hat{V}_{f,\hat{u}}^0\} \times \{\hat{u}_s^D + \hat{V}_s^0\} \times \hat{L}_f^0 \times \hat{L}_s^0$, *such that* $\hat{v}_f(0) = \hat{v}_f^0$, $\hat{v}_s(0) = \hat{v}_s^0$,
$\hat{u}_f(0) = \hat{u}_f^0$, *and* $\hat{u}_s(0) = \hat{u}_s^0$ *are satisfied, and for almost all time steps* $t \in I$ *holds:*

$$\textit{Fluid momentum} \begin{cases} (\hat{J}\hat{\rho}_f \partial_t \hat{v}_f, \hat{\psi}^v)_{\widehat{\Omega}_f} + (\hat{\rho}_f \hat{J}(\widehat{F}^{-1}(\hat{v}_f - \hat{w}) \cdot \widehat{\nabla})\hat{v}_f), \hat{\psi}^v)_{\widehat{\Omega}_f} \\ + (\hat{J}\widehat{\sigma}_f \widehat{F}^{-T}, \widehat{\nabla}\hat{\psi}^v)_{\widehat{\Omega}_f} - \langle \hat{g}_f, \hat{\psi}^v \rangle_{\widehat{\Gamma}_N} - (\hat{\rho}_f \hat{J}\hat{f}_f, \hat{\psi}^v)_{\widehat{\Omega}_f} \quad = 0 \quad \forall \hat{\psi}^v \in \hat{V}_{f,\widehat{\Gamma}_i}^0, \end{cases}$$

$$\textit{Solid momentum, 1st eq.} \begin{cases} (\hat{\rho}_s \partial_t \hat{v}_s, \hat{\psi}^v)_{\widehat{\Omega}_s} + (\widehat{F}\widehat{\Sigma}, \widehat{\nabla}\hat{\psi}^v)_{\widehat{\Omega}_s} \\ + \gamma_w(\hat{v}_s, \hat{\psi}^v)_{\widehat{\Omega}_s} + \gamma_s(\hat{\epsilon}(\hat{v}_s), \widehat{\nabla}\hat{\psi}^v)_{\widehat{\Omega}_s} - (\hat{\rho}_s \hat{f}_s, \hat{\psi}^v)_{\widehat{\Omega}_s} \quad = 0 \quad \forall \hat{\psi}^v \in \hat{V}_s^0, \end{cases}$$

$$\textit{Fluid mesh motion} \begin{cases} (\widehat{\sigma}_{mesh}, \widehat{\nabla}\hat{\psi}^u)_{\widehat{\Omega}_f} \quad = 0 \quad \forall \hat{\psi}^u \in \hat{V}_{f,\hat{u},\widehat{\Gamma}_i}^0, \end{cases}$$

$$\textit{Solid momentum, 2nd eq.} \begin{cases} \hat{\rho}_s(\partial_t \hat{u}_s - \hat{v}_s, \hat{\psi}^u)_{\widehat{\Omega}_s} \quad = 0 \quad \forall \hat{\psi}^u \in \hat{L}_s, \end{cases}$$

$$\textit{Fluid mass conservation} \begin{cases} (\widehat{div}(\hat{J}\widehat{F}^{-1}\hat{v}_f), \hat{\psi}^p)_{\widehat{\Omega}_f} \quad = 0 \quad \forall \hat{\psi}^p \in \hat{L}_f^0, \end{cases}$$

$$\textit{Solid volume conservation} \begin{cases} (\hat{P}_s, \hat{\psi}^p)_{\widehat{\Omega}_s} \quad = 0 \quad \forall \hat{\psi}^p \in \hat{L}_s^0, \end{cases}$$

*with $\hat{\rho}_f$, $\hat{\rho}_s$, $\nu_f$, $\mu_s$, $\lambda_s$, $\widehat{F}$, and $\hat{J}$ as defined before. The stress tensors $\widehat{\sigma}_f$, $\widehat{\Sigma}$, and $\widehat{\sigma}_{mesh}$ are defined in the Equations (49), (16), (5.46), and in (74) and (61), respectively. The pressure-related quantity in the last equation is determined by $\hat{P}_s = \hat{J} - 1$ (volume conserving), using incompressible materials, such as the INH or the IMR material. In the case of the STVK material, the last term is not present.*

Recall that we use the mixed form of the wave equation, for this reason we have a decomposition of the momentum equation into two subequations.

The previous problem can be formulated in terms of semi-linear forms that allow later for compact notation:

**Problem 7.22** (ALE$_{fx}$ FSI with harmonic and linear-elastic mesh motion). *Find*
$\hat{U} := \{\hat{v}_f, \hat{v}_s, \hat{u}_f, \hat{u}_s, \hat{p}_f, \hat{p}_s\} \in \hat{X}_D^0 := \{\hat{v}_f^D + \hat{V}_{f,\hat{v}}^0\} \times \hat{L}_s \times \{\hat{u}_f^D + \hat{V}_{f,\hat{u}}^0\} \times \{\hat{u}_s^D + \hat{V}_s^0\} \times \hat{L}_f^0 \times \hat{L}_s^0$, *such that*
$\hat{v}_f(0) = \hat{v}_f^0$, $\hat{v}_s(0) = \hat{v}_s^0$, $\hat{u}_f(0) = \hat{u}_f^0$, *and* $\hat{u}_s(0) = \hat{u}_s^0$ *are satisfied, and for almost all time steps* $t \in I$ *holds:*

*Fluid momentum*
$$\begin{cases} \hat{A}_1(\hat{U})(\hat{\psi}^v) = (\hat{J}\hat{\rho}_f \partial_t \hat{v}_f, \hat{\psi}^v)_{\hat{\Omega}_f} + (\hat{\rho}_f \hat{J}(\widehat{F}^{-1}(\hat{v}_f - \hat{w}) \cdot \widehat{\nabla})\hat{v}_f), \hat{\psi}^v)_{\hat{\Omega}_f} \\ +(\hat{J}\hat{\sigma}_f \widehat{F}^{-T}, \widehat{\nabla}\hat{\psi}^v)_{\hat{\Omega}_f} - \langle \hat{g}_f, \hat{\psi}^v \rangle_{\hat{\Gamma}_N} - (\hat{\rho}_f \hat{J}\hat{f}_f, \hat{\psi}^v)_{\hat{\Omega}_f} \qquad = 0 \quad \forall \hat{\psi}^v \in \hat{V}_{f,\hat{\Gamma}_i}^0, \end{cases}$$

*Solid momentum, 1st eq.*
$$\begin{cases} \hat{A}_2(\hat{U})(\hat{\psi}^v) = (\hat{\rho}_s \partial_t \hat{v}_s, \hat{\psi}^v)_{\hat{\Omega}_s} + (\widehat{F}\widehat{\Sigma}, \widehat{\nabla}\hat{\psi}^v)_{\hat{\Omega}_s} \\ +\gamma_w(\hat{v}_s, \hat{\psi}^v)_{\hat{\Omega}_s} + \gamma_s(\hat{\epsilon}(\hat{v}_s), \widehat{\nabla}\hat{\psi}^v)_{\hat{\Omega}_s} - (\hat{\rho}_s \hat{f}_s, \hat{\psi}^v)_{\hat{\Omega}_s} \quad = 0 \quad \forall \hat{\psi}^v \in \hat{V}_s^0, \end{cases}$$

*Fluid mesh motion* $\left\{ \hat{A}_3(\hat{U})(\hat{\psi}^u) = (\hat{\sigma}_{mesh}, \widehat{\nabla}\hat{\psi}^u)_{\hat{\Omega}_f} \quad = 0 \quad \forall \hat{\psi}^u \in \hat{V}_{f,\hat{u},\hat{\Gamma}_i}^0, \right.$

*Solid momentum, 2nd eq.* $\left\{ \hat{A}_4(\hat{U})(\hat{\psi}^u) = \hat{\rho}_s(\partial_t \hat{u}_s - \hat{v}_s, \hat{\psi}^u)_{\hat{\Omega}_s} \quad = 0 \quad \forall \hat{\psi}^u \in \hat{L}_s, \right.$

*Fluid mass conservation* $\left\{ \hat{A}_5(\hat{U})(\hat{\psi}^p) = (\widehat{div}(\hat{J}\widehat{F}^{-1}\hat{v}_f), \hat{\psi}^p)_{\hat{\Omega}_f} \quad = 0 \quad \forall \hat{\psi}^p \in \hat{L}_f^0, \right.$

*Solid volume conservation* $\left\{ \hat{A}_6(\hat{U})(\hat{\psi}^p) = (\hat{P}_s, \hat{\psi}^p)_{\hat{\Omega}_s} \quad = 0 \quad \forall \hat{\psi}^p \in \hat{L}_s^0. \right.$

*Consequently, we can write in short form: Find* $\hat{U} \in \hat{X}_0^D$ *such that* $\hat{v}_f(0) = \hat{v}_f^0$, $\hat{v}_s(0) = \hat{v}_s^0$, $\hat{u}_f(0) = \hat{u}_f^0$, *and* $\hat{u}_s(0) = \hat{u}_s^0$ *are satisfied, and for almost all time steps* $t \in I$ *holds:*

$$\hat{A}(\hat{U})(\hat{\Psi}) = 0 \quad \text{for all } \hat{\Psi} \in \hat{X} \tag{78}$$

*with* $\hat{\Psi} = \{\hat{\psi}_f^v, \hat{\psi}_s^v, \hat{\psi}_f^u, \hat{\psi}_s^u, \hat{\psi}_f^p, \hat{\psi}_s^p\}$ *and* $\hat{X} = \hat{V}_{f,\hat{v}}^0 \times \hat{L}_f \times \hat{V}_{f,\hat{u},\hat{\Gamma}_i}^0 \times \hat{V}_s^0 \times \hat{L}_f^0 \times \hat{L}_s^0$ *and*

$$\hat{A}(\hat{U})(\hat{\Psi}) := \hat{A}_1(\hat{U})(\hat{\psi}^v) + \hat{A}_2(\hat{U})(\hat{\psi}^v) + \hat{A}_3(\hat{U})(\hat{\psi}^u) + \hat{A}_4(\hat{U})(\hat{\psi}^u) + \hat{A}_5(\hat{U})(\hat{\psi}^p) + \hat{A}_6(\hat{U})(\hat{\psi}^p).$$

Recapitulating the previous system, let us explicitely count for how many equations and variables we must solve in FSI. We consider fluid mass, fluid momentum, solid momentum, and the MMPDE, which are 4 basic equations. Splitting the solid momentum into a first order in time system, leads to 5 basic equations. If the solid is assumed to be incompressible we need additionally account for the incompressibility constraint $\hat{J} = 1$, which then requires to solve 6 equations. Moreover, the equations for velocities and displacements are vector-valued. This means for example that in the 6 basic equations, we actually solve in 2D for $2+1+2+2+1+2 = 10$ unknowns and in 3D for $3 + 1 + 3 + 3 + 1 + 3 = 14$ unknowns.

**Remark 7.23.** *The semi-linear form (78) is the starting point for temporal and spatial discretization schemes.*

**Remark 7.24.** *Alternatively, the spatial semi-linear form (78) could have been formulated in terms of a time-dependent form: Find* $\hat{U} \in \hat{X}_0^D$ *such that* $\hat{v}_f(0) = \hat{v}_f^0$, $\hat{v}_s(0) = \hat{v}_s^0$, $\hat{u}_f(0) = \hat{u}_f^0$, *and* $\hat{u}_s(0) = \hat{u}_s^0$ *are satisfied and*

$$\underline{\hat{A}}(\hat{U})(\hat{\Psi}) := \int_0^T \hat{A}(\hat{U})(\hat{\Psi}) = 0 \quad \text{for all } \hat{\Psi} \in \hat{X} \tag{79}$$

*with* $\hat{\Psi} = \{\hat{\psi}_f^v, \hat{\psi}_s^v, \hat{\psi}_f^u, \hat{\psi}_s^u, \hat{\psi}_f^p, \hat{\psi}_s^p\}$ *and* $\hat{X} = \hat{V}_{f,\hat{v}}^0 \times \hat{L}_f \times \hat{V}_{f,\hat{u},\hat{\Gamma}_i}^0 \times \hat{V}_s^0 \times \hat{L}_f^0 \times \hat{L}_s^0$ *and*

$$\hat{A}(\hat{U})(\hat{\Psi}) := \hat{A}_1(\hat{U})(\hat{\psi}^v) + \hat{A}_2(\hat{U})(\hat{\psi}^v) + \hat{A}_3(\hat{U})(\hat{\psi}^u) + \hat{A}_4(\hat{U})(\hat{\psi}^u) + \hat{A}_5(\hat{U})(\hat{\psi}^p) + \hat{A}_6(\hat{U})(\hat{\psi}^p).$$

Next, we state the monolithic setting for fluid-structure interaction with a biharmonic mesh motion model utilizing the first type of boundary conditions. To do so, we first formulate the weak form of the biharmonic system:

**Problem 7.25** (Weak form of the mixed biharmonic system). *Find $\hat{\eta}_f \in H^1(\widehat{\Omega})$ and $\hat{u}_f \in H^1_0(\widehat{\Omega})$ such that*

$$(\hat{\eta}_f, \hat{\psi}^\eta) - (\widehat{\nabla}\hat{u}_f, \widehat{\nabla}\hat{\psi}^\eta) = 0 \quad \forall \hat{\psi}^\eta \in H^1(\widehat{\Omega}),$$

$$(\widehat{\nabla}\hat{\eta}_f, \widehat{\nabla}\hat{\hat{\psi}}^u) = 0 \quad \forall \hat{\psi}^u \in H^1_0(\widehat{\Omega}).$$

With these preparations, we now come to the full problem:

**Problem 7.26** (ALE$_{fx}$ FSI with biharmonic mesh motion). *Find*
$\{\hat{v}_f, \hat{v}_s, \hat{u}_f, \hat{u}_s, \hat{\eta}_f, \hat{\eta}_s, \hat{p}_f, \hat{p}_s\} \in \{\hat{v}_f^D + \hat{V}_{f,\hat{v}}^0\} \times \hat{L}_s \times \{\hat{u}_f^D + \hat{V}_{f,\hat{u}}^0\} \times \{\hat{u}_s^D + \hat{V}_s^0\} \times \hat{V}_f \times \hat{V}_s \times \hat{L}_f^0 \times \hat{L}_s^0$, *such that*
$\hat{v}_f(0) = \hat{v}_f^0$, $\hat{v}_s(0) = \hat{v}_s^0$, $\hat{u}_f(0) = \hat{u}_f^0$, $\hat{u}_s(0) = \hat{u}_s^0$ *are satisfied, for almost all time steps $t \in I$, and*

$$(\hat{J}\hat{\rho}_f \partial_t \hat{v}_f, \hat{\psi}^v)_{\widehat{\Omega}_f} + (\rho_f \hat{J}(\widehat{F}^{-1}(\hat{v}_f - \hat{w}) \cdot \widehat{\nabla})\hat{v}_f), \hat{\psi}^v)_{\widehat{\Omega}_f}$$

$$+ (\hat{J}\hat{\sigma}_f \widehat{F}^{-T}, \widehat{\nabla}\hat{\psi}^v)_{\widehat{\Omega}_f} - \langle \hat{g}_f, \hat{\psi}^v \rangle_{\widehat{\Gamma}_N} - (\hat{\rho}_f \hat{J}\hat{f}_f, \hat{\psi}^v)_{\widehat{\Omega}_f} = 0 \quad \forall \hat{\psi}^v \in \hat{V}_{f,\widehat{\Gamma}_i}^0,$$

$$(\hat{\rho}_s \partial_t \hat{v}_f, \hat{\psi}^v)_{\widehat{\Omega}_s} + (\widehat{F}\hat{\Sigma}, \widehat{\nabla}\hat{\psi}^v)_{\widehat{\Omega}_s}$$

$$+ \gamma_w(\hat{v}_s, \hat{\psi}^v)_{\widehat{\Omega}_s} + \gamma_s(\hat{\epsilon}(\hat{v}_s), \widehat{\nabla}\hat{\psi}^v)_{\widehat{\Omega}_s} - (\hat{\rho}_s \hat{f}_s, \hat{\psi}^v)_{\widehat{\Omega}_s} = 0 \quad \forall \hat{\psi}^v \in \hat{V}_s^0,$$

$$(\alpha_u \hat{\eta}_f, \hat{\psi}^\eta)_{\widehat{\Omega}_f} - (\alpha_u \widehat{\nabla}\hat{u}_f, \widehat{\nabla}\hat{\psi}^\eta)_{\widehat{\Omega}_f} = 0 \quad \forall \hat{\psi}^\eta \in \hat{V}_f,$$

$$(\alpha_u \hat{\eta}_s, \hat{\psi}^\eta)_{\widehat{\Omega}_s} - (\alpha_u \widehat{\nabla}\hat{u}_s, \widehat{\nabla}\hat{\psi}^\eta)_{\widehat{\Omega}_s} = 0 \quad \forall \hat{\psi}^\eta \in \hat{V}_s,$$

$$(\alpha_u \widehat{\nabla}\hat{\eta}_f, \widehat{\nabla}\hat{\psi}^u)_{\widehat{\Omega}_f} = 0 \quad \forall \hat{\psi}^u \in \hat{V}_{f,\hat{u},\widehat{\Gamma}_i}^0,$$

$$\hat{\rho}_s(\partial_t \hat{u}_s - \hat{v}_s, \hat{\psi}^u)_{\widehat{\Omega}_s} = 0 \quad \forall \hat{\psi}^u \in \hat{L}_s,$$

$$(\widehat{div}(\hat{J}\widehat{F}^{-1}\hat{v}_f), \hat{\psi}^p)_{\widehat{\Omega}_f} = 0 \quad \forall \hat{\psi}^p \in \hat{L}_f^0,$$

$$(\hat{P}_s, \hat{\psi}^p)_{\widehat{\Omega}_s} = 0 \quad \forall \hat{\psi}^p \in \hat{L}_s^0,$$

*with all quantities as defined in Problem 7.21 and the monitor parameter $\alpha_u$ defined in (65).*

**Remark 7.27.** *The monolithic variational formulation for the second type of boundary conditions is formally equivalent as demonstrated in Problem 7.26. Only the definition of the function spaces for trial and test functions of the displacement variables $\hat{u}$ and $\hat{\eta}$ changes.* ◇

For later purposes and also the existence of stationary ALE-FSI in Section 7.3.14), we also state a stationary version of the coupled equations:

**Problem 7.28** (Stationary FSI with harmonic and linear-elastic mesh motion). *Find $\{\hat{v}_f, \hat{u}_f, \hat{u}_s, \hat{p}_f, \hat{p}_s\} \in \{\hat{v}_f^D + \hat{V}_{f,\hat{v}}^0\} \times \{\hat{u}_f^D + \hat{V}_{f,\hat{u}}\} \times \{\hat{u}_s^D + \hat{V}_s^0\} \times \hat{L}_f^0$, such that*

$$(\hat{\rho}_f \hat{J}(\widehat{F}^{-1}\hat{v}_f \cdot \widehat{\nabla})\hat{v}_f), \hat{\psi}^v)_{\widehat{\Omega}_f}$$

$$+ (\hat{J}\hat{\sigma}_f \widehat{F}^{-T}, \widehat{\nabla}\hat{\psi}^v)_{\widehat{\Omega}_f} - \langle \hat{g}_f, \hat{\psi}^v \rangle_{\widehat{\Gamma}_N} - (\hat{\rho}_f \hat{J}\hat{f}_f, \hat{\psi}^v)_{\widehat{\Omega}_f} = 0 \quad \forall \hat{\psi}^v \in \hat{V}_{f,\hat{v}}^0,$$

$$(\widehat{F}\hat{\Sigma}, \widehat{\nabla}\hat{\psi}^v)_{\widehat{\Omega}_s} - (\hat{\rho}_s \hat{f}_s, \hat{\psi}^v)_{\widehat{\Omega}_s} = 0 \quad \forall \hat{\psi}^v \in \hat{V}_s^0,$$

$$(\hat{\sigma}_{mesh}, \widehat{\nabla}\hat{\psi}^u)_{\widehat{\Omega}_f} = 0 \quad \forall \hat{\psi}^u \in \hat{V}_{f,\hat{u},\widehat{\Gamma}_i}^0,$$

$$(\widehat{div}(\hat{J}\widehat{F}^{-1}\hat{v}_f), \hat{\psi}^p)_{\widehat{\Omega}_f} = 0 \quad \forall \hat{\psi}^p \in \hat{L}_f^0,$$

*with all quantities as defined in Problem 7.21.*

Problem 7.28 offers further insight of key differences between stationary and nonstationary fluid-structure interactions. We do not search any longer for a velocity solution $\hat{v}_s$ in the structure because it is zero in a stationary setting. Consequently, the damping terms vanish because they are defined by means of $\hat{v}_s$. Likewise, the fluid domain velocity $\hat{w}$ vanishes too.

**Remark 7.29** (On the Neumann FSI coupling conditions). *The weak continuity of the normal stresses of Equation (53) that is required on $\widehat{\Gamma}_i$ becomes an implicit condition computing nonstationary fluid-structure interactions:*

$$(\hat{J}\hat{\sigma}_f \widehat{F}^{-T}\hat{n}_f, \hat{\psi}^v)_{\widehat{\Gamma}_i} + (\widehat{F}\hat{\Sigma}\hat{n}_s, \hat{\psi}^v)_{\widehat{\Gamma}_i} + \gamma_s(\hat{\epsilon}(\hat{v}_s)\hat{n}_s, \hat{\psi}^v)_{\widehat{\Gamma}_i} = 0 \quad \forall \hat{\psi}^v \in \hat{V}^0.$$

*In stationary settings, we deal with*

$$(\hat{J}\widehat{\sigma}_f \widehat{F}^{-T}\hat{n}_f, \hat{\psi}^v)_{\widehat{\Gamma}_i} + (\widehat{F}\widehat{\Sigma}\hat{n}_s, \hat{\psi}^v)_{\widehat{\Gamma}_i} = 0 \quad \forall \hat{\psi}^v \in \hat{V}^0.$$

**Remark 7.30** (Discretizing solid's stress tensor in terms of velocities). *An alternative way (and this seems more natural in fluid-structure interaction, see, e.g., [136]) is to take the time derivative on solid's stress tensor, e.g.,*

$$\partial_t \widehat{\sigma}_s(\hat{u}_s) = \partial_t(2\mu \widehat{E}_{lin}(\hat{u}) + \lambda tr(\widehat{E}(\hat{u}))\hat{I}) = 2\mu \widehat{E}_{lin}(\hat{v}) + \lambda tr(\widehat{E}(\hat{v}))\hat{I}.$$

*This has the advantage that both stress tensors can be formally combined into one global stress tensor $\widehat{\sigma} = \chi_f\widehat{\sigma}_f + \chi_s\widehat{\sigma}_s$. To the best of my knowledge it is not yet clear which formulation (our or the the unified one) is preferrable from computational cost point of view.* ⋄

### 7.3.10 A monolithic ALE$_{dm}$-FSI formulation

In this section, we consider monolithic formulations for ALE$_{dm}$-FSI. One idea (this in fact could also have been applied to ALE$_{fx}$ is based on splitting of the physical and the geometry problem:

- Solve the geometry problem;

- Solve the FSI problem.

Consequently, monolithic refers here 'only' to the physical part of the FSI problem; which however is the primal goal. In ALE$_{dm}$, we work with ALE form of Navier-Stokes on $\Omega(t)$, here the ALE mapping appears still in form of the ALE time derivative but all the transformations in form of $\widehat{F}$ and $\hat{J}$ disappear since they represented at each time step by a new domain $\Omega(t)$ - and this is the most prominent difference between ALE$_{dm}$ and ALE$_{fx}$.

### 7.3.11 A priori energy estimates for monolithic ALE$_{dm}$-FSI with damped solid equations.

One of the key advantages of monolithic solution approaches is their robustness with respect to numerical stability. In this section, we show that our coupled problem is indeed stable in the energy norm. The proof follows the philosophy of Fernández and Gerbeau [84]; their statement was derived for a coupling between one single structure model and the fluid equations. We extend their result to the case of a coupling with damped structure equations.

The energy loss of the systems originates from the viscosity of the fluid and the damping terms that have been added to the structure. The energy exchanged over the interface is exactly balanced, due to the coupling conditions for the velocity and the stresses (see the Relations (51) and (53)).

For the Dirichlet velocity conditions (51), we assume sufficient regularity in the case $\gamma_w = \gamma_s = 0$. Moreover, we neglect the do-nothing outflow condition and the right-hand-side forces, and we assume that the system is isolated, i.e., $v_f = \hat{u}_s = 0$ on $\partial\Omega$.

For the first result, we employ the damped structure equations in the whole subdomain $\widehat{\Omega}_s$. The total energy of the coupled system at time step $t$ is denoted by $E(t)$ with

$$E(t) := \frac{\rho_f}{2}||v_f||^2_{\Omega_f} + \frac{\hat{\rho}_s}{2}||\hat{v}_s||^2_{\widehat{\Omega}_s} + \int_{\widehat{\Omega}_s} W(\hat{E})\, d\hat{x}.$$

For (linear) strong damping with the help of $\hat{\epsilon}(\hat{v}_s)$, the scalar product induces the energy norm

$$||\hat{\epsilon}(\cdot)||^2_E := (\hat{\epsilon}(\cdot), \widehat{\nabla}\cdot)_{\widehat{\Omega}_s}. \tag{80}$$

The right term is positive thanks to the Korn inequality.

**Theorem 7.31.** *Let the coupled fluid-structure problem be isolated, i.e., $v_f = 0$ on $\partial\Omega_f \setminus \Gamma_i$ and a stress-free state $\widehat{F}\widehat{\Sigma}\hat{n}_s = 0$ on $\partial\widehat{\Omega}_s \setminus \widehat{\Gamma}_i$ and (if $\gamma_s > 0$) $\hat{\epsilon}(\hat{v}_s)\hat{n}_s = 0$ on $\partial\widehat{\Omega}_s \setminus \widehat{\Gamma}_i$. Then, the following a priori energy estimate holds true:*

$$\frac{d}{dt}\Big[\frac{\rho_f}{2}||v_f||^2_{\Omega_f} + \frac{\hat{\rho}_s}{2}||\hat{v}_s||^2_{\widehat{\Omega}_s} + \int_{\widehat{\Omega}_s} W(\hat{E})\, d\hat{x}\Big] + 2\rho_f\nu_f||D(v_f)||^2_{\Omega_f} + \gamma_w||\hat{v}_s||^2_{\widehat{\Omega}_s} + \gamma_s||\hat{\epsilon}(\hat{v}_s)||^2_E = 0.$$

*That implies the following energy decay property:*

$$E(t) = E(0) - \int_0^t \left[ \gamma_w ||\hat{v}_s(\tau)||_{\widehat{\Omega}_s}^2 + \gamma_s ||\hat{\epsilon}(\hat{v}_s)(\tau)||_E^2 + 2\rho_f \nu_f ||D(v_f)(\tau)||_{\Omega_f}^2 \right] d\tau.$$

*Proof.* We proof the argument with a standard energy technique. The outline is analogous to [84]. The equations are multiplied through by $v_f$ and $\hat{v}_s$, respectively. We start with the fluid equations, defined in the weak formulation in Problem 7.6. We use $\psi^v = v_f$ and $\psi^p = p_f$, and obtain for the first term:

$$\rho_f(\hat{\partial}_t v_f, v_f)_{\Omega_f} = \rho_f(\hat{J}\partial_t \hat{v}_f, \hat{v}_f)_{\widehat{\Omega}_f} \tag{81}$$

$$= \frac{\rho_f}{2} \int_{\widehat{\Omega}_f} \partial_t[\hat{J}\,|\hat{v}_f|^2]\,\mathrm{d}\hat{x} - \frac{\rho_f}{2}\int_{\widehat{\Omega}_f} \hat{J}\,\widehat{\mathrm{div}}\,\hat{w}\,|\hat{v}_f|^2\,\mathrm{d}\hat{x} \tag{82}$$

$$= d_t \frac{\rho_f}{2}||v_f||_{\Omega_f}^2 - \frac{\rho_f}{2}\int_{\Omega_f} \mathrm{div}\,w\,|v_f|^2\,\mathrm{d}x. \tag{83}$$

The second term (the ALE convection term) is treated as follows (using integration by parts):

$$\rho_f\big((v_f - w)\cdot\nabla v_f, v_f\big)_{\Omega_f} = \frac{\rho_f}{2}\int_{\Omega_f}(v_f - w)\cdot\nabla\,|v_f|^2\,\mathrm{d}x \tag{84}$$

$$= \frac{\rho_f}{2}\int_{\Gamma_{f,N}}(v_f - w)\,n_f\,|v_f|^2\,\mathrm{d}s - \frac{\rho_f}{2}\int_{\Omega_f}\nabla\cdot(v_f - w)\,|v_f|^2\,\mathrm{d}x. \tag{85}$$

Now, we use $v_f = w$ on $\Gamma_i$ and $v_f = 0$ on $\partial\Omega_f \setminus \Gamma_i$. Furthermore, we use the incompressibility of the fluid, i.e., $\nabla \cdot v_f = 0$ on the continuous level. This implies

$$\rho_f\big((v_f - w)\cdot\nabla\,v_f, v_f\big)_{\Omega_f} = \frac{\rho_f}{2}\int_{\Omega_f}\nabla\cdot w\,|v_f|^2\,\mathrm{d}x. \tag{86}$$

This term cancels with the last term of the first relation (83). Next, we treat the term including the Cauchy stress tensor (using again the incompressibility of the fluid) and the symmetry of $D(v_f)$:

$$-(\nabla\cdot\sigma_f, v_f)_{\Omega_f} = -\langle\sigma_f n_f, v_f\rangle_{\Gamma_{f,N}\cup\Gamma_i} + (\sigma_f, \nabla v_f)_{\Omega_f} \tag{87}$$

$$= -\langle\sigma_f n_f, v_f\rangle_{\Gamma_{f,N}\cup\Gamma_i} + (-p_f, \nabla\cdot v_f)_{\Omega_f} + 2\rho_f \nu_f\big(D(v_f), \nabla v_f\big)_{\Omega_f} \tag{88}$$

$$= -\langle\sigma_f n_f, v_f\rangle_{\Gamma_{f,N}\cup\Gamma_i} + 2\rho_f \nu_f\big(D(v_f), D(v_f)\big)_{\Omega_f}. \tag{89}$$

Summarizing (83), (86), and (87), gives us:

$$d_t\frac{\rho_f}{2}||v_f||_{\Omega_f}^2 + 2\rho_f \nu_f ||D(v_f)||_{\Omega_f}^2 - \langle\sigma_f n_f, v_f\rangle_{\Gamma_{f,N}\cup\Gamma_i}. \tag{90}$$

In a fully isolated system, i.e. , $\Gamma_{f,N} = \emptyset$, the following boundary term in Equation (90) remains on the interface $\Gamma_i$:

$$-\langle\sigma_f n_f, v_f\rangle_{\Gamma_{f,N}\cup\Gamma_i} = -\langle\sigma_f n_f, v_f\rangle_{\Gamma_i}. \tag{91}$$

We continue with the mass term of the structure. We multiply in Equation (36) through by $\hat{v}_s = \partial_t \hat{u}_s$ and integrate over $\widehat{\Omega}_s$. Then, we deduce

$$\hat{\rho}_s(\partial_t^2 \hat{u}_s, \partial_t \hat{u}_s)_{\widehat{\Omega}_s} = d_t\frac{\hat{\rho}_s}{2}||\hat{v}_s||_{\widehat{\Omega}_s}^2. \tag{92}$$

The second term is treated as follows (using partial integration):

$$-(\widehat{\nabla}\cdot(\widehat{F}\widehat{\Sigma}), \hat{v}_s)_{\widehat{\Omega}_s} = (\widehat{F}\widehat{\Sigma}, \widehat{\nabla}\hat{v}_s)_{\widehat{\Omega}_s} - \int_{\widehat{\Gamma}_{s,N}\cup\widehat{\Gamma}_i} \widehat{F}\widehat{\Sigma}\hat{n}_s\cdot\hat{v}_s\,\mathrm{d}s \tag{93}$$

$$= (\widehat{F}\widehat{\Sigma}, \widehat{\nabla}\hat{v}_s)_{\widehat{\Omega}_s} - \int_{\widehat{\Gamma}_i} \widehat{F}\widehat{\Sigma}\hat{n}_s\cdot\hat{v}_s\,\mathrm{d}s. \tag{94}$$

In the last term of Equation (93), we use the boundary condition $\widehat{F}\widehat{\Sigma}\hat{n}_s = 0$ on $\partial\widehat{\Omega}_s \setminus \widehat{\Gamma}_i$ that was part of our assumptions. We rearrange the first term as follows with the help of the component-wise multiplication operator (for second order tensors $A$ and $B$ holds $A : B = \sum_{ij} A_{ij}B_{ij}$):

$$\widehat{F}\widehat{\Sigma} : \widehat{\nabla}\hat{v}_s = \widehat{F}\widehat{\Sigma} : \widehat{\nabla}\partial_t\hat{u}_s = \widehat{F}\widehat{\Sigma} : \partial_t\widehat{\nabla}\hat{u}_s \tag{95}$$

$$= \widehat{F}\widehat{\Sigma} : \partial_t[\widehat{\nabla}\hat{u}_s + \hat{I}] = \widehat{F}\widehat{\Sigma} : \partial_t\widehat{F} \tag{96}$$

$$= \widehat{\Sigma} : \partial_t\widehat{F}\widehat{F} = \widehat{\Sigma} : \partial_t\widehat{E}, \quad \text{with } \widehat{E} = \frac{1}{2}(\widehat{F}^T\widehat{F} - \hat{I}) \tag{97}$$

$$= \partial_E W : \partial_t\widehat{E}, \quad \text{with } \widehat{\Sigma} = \partial_E W \tag{98}$$

$$= \partial_t W(\widehat{E}), \tag{99}$$

where we use the Green-Lagrange tensor and the definition of hyperelasticity of the material model in Section 5.4.4. The definitions of the time derivative of material tensors can be found in Holzapfel [137]. We plug the previous relation into (93):

$$(\widehat{F}\widehat{\Sigma}, \widehat{\nabla}\hat{v}_s)_{\widehat{\Omega}_s} - \int_{\widehat{\Gamma}_i} \widehat{F}\widehat{\Sigma}\hat{n}_s \cdot \hat{v}_s \, \mathrm{d}\hat{s} = \int_{\widehat{\Omega}_s} \partial_t W(E) \, \mathrm{d}\hat{x} - \int_{\widehat{\Gamma}_i} \widehat{F}\widehat{\Sigma}\hat{n}_s \cdot \hat{v}_s \, \mathrm{d}\hat{s} \tag{100}$$

$$= d_t \int_{\widehat{\Omega}_s} W(E) \, \mathrm{d}\hat{x} - \int_{\widehat{\Gamma}_i} \widehat{F}\widehat{\Sigma}\hat{n}_s \cdot \hat{v}_s \, \mathrm{d}\hat{s}. \tag{101}$$

Summarizing (92) and (100), we finally get:

$$d_t\frac{\hat{\rho}_s}{2}||\hat{v}_s||^2_{\widehat{\Omega}_s} + d_t \int_{\widehat{\Omega}_s} W(\widehat{E}) \, \mathrm{d}\hat{x} - \int_{\widehat{\Gamma}_i} \widehat{F}\widehat{\Sigma}\hat{n}_s \cdot \hat{v}_s \, \mathrm{d}\hat{s}.$$

Combining this result with the fluid equations, we obtain

$$d_t\left[\frac{\rho_f}{2}||v_f||^2_{\Omega_f} + \frac{\hat{\rho}_s}{2}||\hat{v}_s||^2_{\widehat{\Omega}_s} + \int_{\widehat{\Omega}_s} W(\widehat{E}) \, \mathrm{d}\hat{x}\right]$$
$$+ 2\rho_f\nu_f||D(v_f)||^2_{\Omega_f} - \langle\sigma_f n_f, v_f\rangle_{\Gamma_i} - \langle\widehat{F}\widehat{\Sigma}\hat{n}_s, \hat{v}_s\rangle_{\widehat{\Gamma}_i}.$$

The both interface terms cancel, thanks to the coupling conditions, such that

$$\langle\sigma_f n_f, v_f\rangle_{\Gamma_i} + \langle\widehat{F}\widehat{\Sigma}\hat{n}_s, \hat{v}_s\rangle_{\widehat{\Gamma}_i} = \langle\hat{J}\hat{\sigma}_f\widehat{F}^{-T}\hat{n}_f, \hat{v}_f\rangle_{\widehat{\Gamma}_i} + \langle\widehat{F}\widehat{\Sigma}\hat{n}_s, \hat{v}_s\rangle_{\widehat{\Gamma}_i} = 0.$$

It remains to consider the damping terms of the structure Equation (36). We multiply again by $\partial_t\hat{u}_s = \hat{v}_s$. Using integration by parts for strong damping, we obtain

$$\gamma_w(\partial_t\hat{u}_s, \partial_t\hat{u}_s)_{\widehat{\Omega}_s} - \gamma_s(\nabla\cdot\hat{\epsilon}(\partial_t\hat{u}_s), \partial_t\hat{u}_s)_{\widehat{\Omega}_s}$$
$$= \gamma_w||\hat{v}_s||^2_{\widehat{\Omega}_s} + \gamma_s(\hat{\epsilon}(\hat{v}_s), \widehat{\nabla}\hat{v}_s)_{\widehat{\Omega}_s} - \gamma_s\langle\hat{\epsilon}(\hat{v}_s)\hat{n}_s, \hat{v}_s\rangle_{\widehat{\Gamma}_i}.$$

The middle term is positive thanks to the Korn inequality. Thus, the scalar product induces the norm (an energy norm)

$$(\hat{\epsilon}(\hat{v}_s), \widehat{\nabla}\hat{v}_s)_{\widehat{\Omega}_s} =: ||\hat{\epsilon}(\hat{v}_s)||^2_E.$$

Moreover, the incorporation the strong damping induces an additional term on the interface. That means, for $\gamma_s > 0$, we get a modification of the coupling conditions on the interface. It holds:

$$(\hat{J}\hat{\sigma}_f\widehat{F}^{-T}\hat{n}_f, \hat{v}_f)_{\widehat{\Gamma}_i} + (\widehat{F}\widehat{\Sigma}\hat{n}_s, \hat{v}_s)_{\widehat{\Gamma}_i} + \gamma_s(\hat{\epsilon}(\hat{v}_s)\hat{n}_s, \hat{v}_s)_{\widehat{\Gamma}_i} = 0 \quad \text{on } \widehat{\Gamma}_i,$$

which corresponding strong form is stated in Equation (53). This concludes the proof of the first assertion. The energy decay (the second argument) can be proven by integration over the time interval, which immediately shows the assertion. $\qquad\square$

Indeed, it can be inferred from the energy decay property in Theorem (7.31) that:

- For $\gamma_w, \gamma_s \to 0$ the artificial energy dissipation gets lost.

- For $\gamma_w, \gamma_s \to \infty$ the structure system tends to freeze in $\widehat{\Omega}_s^{\text{ext}}$.

In fact, for $\gamma_w, \gamma_s \to 0$ it only remains a natural energy dissipation that comes through the Cauchy stress term in the fluid domain. A deeper analysis for the (qualitatively) *best* damping of a super-linear hyperbolic equation was made by Gazzola and Squassina [105] (see Theorem 3.8).

### 7.3.12 A partitioned approach using ALE$_{fx}$

In this partitioned coupling algorithm, we solve subsequently for three problems:

- The fluid mesh (mesh motion problem);

- Solving the fluid problem in $\widehat{\Omega}$;

- Solving the solid problem.

The most prominent technique is based on a Dirichlet-Neumann (DN) coupling: the velocity interface condition is imposed as a Dirichlet condition and the stress condition for the solid is imposed as Neumann condition.

The weak form reads:

**Problem 7.32** (Partioned FSI with harmonic and linear-elastic mesh motion). *Given the initial conditions* $\hat{v}_f(0) = \hat{v}_f^0$, $\hat{v}_s(0) = \hat{v}_s^0$, $\hat{u}_f(0) = \hat{u}_f^0$, *we compute for almost all time steps* $t \in I$ *the following problems.*

- *Find* $\{\hat{u}_f\} \in \{\hat{u}_f^D + \hat{V}_{f,\hat{u}}^0\}$,

$$(\widehat{\sigma}_{mesh}, \widehat{\nabla}\hat{\psi}^u)_{\widehat{\Omega}_f} = 0 \quad \forall \hat{\psi}^u \in \hat{V}_{f,\hat{u},\widehat{\Gamma}_i}^0,$$

- *Find* $\{\hat{v}_f, \hat{p}_f\} \in \{\hat{v}_f^D + \hat{V}_{f,\hat{v}}^0\} \times \hat{L}_f^0$,

$$(\hat{J}\hat{\rho}_f \partial_t \hat{v}_f, \hat{\psi}^v)_{\widehat{\Omega}_f} + (\hat{\rho}_f \hat{J}(\widehat{F}^{-1}(\hat{v}_f - \hat{w}) \cdot \widehat{\nabla})\hat{v}_f), \hat{\psi}^v)_{\widehat{\Omega}_f}$$
$$+(\hat{J}\widehat{\sigma}_f \widehat{F}^{-T}, \widehat{\nabla}\hat{\psi}^v)_{\widehat{\Omega}_f} - \langle \hat{g}_f, \hat{\psi}^v \rangle_{\widehat{\Gamma}_N} - (\hat{\rho}_f \hat{J}\hat{f}_f, \hat{\psi}^v)_{\widehat{\Omega}_f} = 0 \quad \forall \hat{\psi}^v \in \hat{V}_{f,\widehat{\Gamma}_i}^0,$$
$$(\widehat{div}(\hat{J}\widehat{F}^{-1}\hat{v}_f), \hat{\psi}^p)_{\widehat{\Omega}_f} = 0 \quad \forall \hat{\psi}^p \in \hat{L}_f^0,$$

- *Find* $\{\hat{v}_s, \hat{u}_s\} \in \hat{L}_s \times \{\hat{u}_s^D + \hat{V}_s^0\}$,

$$(\hat{\rho}_s \partial_t \hat{v}_s, \hat{\psi}^v)_{\widehat{\Omega}_s} + (\widehat{F}\widehat{\Sigma}, \widehat{\nabla}\hat{\psi}^v)_{\widehat{\Omega}_s}$$
$$+\gamma_w(\hat{v}_s, \hat{\psi}^v)_{\widehat{\Omega}_s} + \gamma_s(\hat{\epsilon}(\hat{v}_s), \widehat{\nabla}\hat{\psi}^v)_{\widehat{\Omega}_s} - (\hat{\rho}_s \hat{f}_s, \hat{\psi}^v)_{\widehat{\Omega}_s} = 0 \quad \forall \hat{\psi}^v \in \hat{V}_s^0,$$
$$\hat{\rho}_s(\partial_t \hat{u}_s - \hat{v}_s, \hat{\psi}^u)_{\widehat{\Omega}_s} = 0 \quad \forall \hat{\psi}^u \in \hat{L}_s,$$

*with* $\hat{\rho}_f$, $\hat{\rho}_s$, $\nu_f$, $\mu_s$, $\lambda_s$, $\widehat{F}$, *and* $\hat{J}$ *as defined before. The stress tensors* $\widehat{\sigma}_f$, $\widehat{\Sigma}$, *and* $\widehat{\sigma}_{mesh}$ *are defined in the Equations (49), (16), (5.46), and in (74) and (61), respectively.*

### 7.3.13 A partitioned approach using ALE$_{dm}$

We solve in the same order as in Section 7.3.12 but now the fluid equations on the current (deformed) domain $\Omega$.

The weak form reads:

**Problem 7.33** (Partitioned FSI with harmonic and linear-elastic mesh motion). *Given the initial conditions* $v_f(0) = v_f^0$, $\hat{v}_s(0) = \hat{v}_s^0$, *we compute for almost all time steps* $t \in I$ *the following problems.*

- *Find* $\{\hat{u}_f\} \in \{\hat{u}_f^D + \hat{V}_{f,\hat{u}}^0\}$,

$$(\widehat{\sigma}_{mesh}, \widehat{\nabla}\hat{\psi}^u)_{\widehat{\Omega}_f} = 0 \quad \forall \hat{\psi}^u \in \hat{V}_{f,\hat{u},\widehat{\Gamma}_i}^0,$$

- *Find* $\{v_f, p_f\} \in \{v_f^D + V_{f,v}^0\} \times L_f^0$,

$$(\rho_f \hat{\partial}_t v_f, \psi^v)_{\Omega_f} + (\rho_f (v_f - w) \cdot \nabla) v_f, \psi^v)_{\Omega_f}$$
$$+ (\sigma_f, \nabla \psi^v)_{\Omega_f} - \langle g_f, \psi^v \rangle_{\Gamma_N} - (\rho_f f_f, \psi^v)_{\Omega_f} = 0 \quad \forall \psi^v \in V_{f,\Gamma_i}^0,$$
$$(div(\hat{v}_f), \psi^p)_{\Omega_f} = 0 \quad \forall \psi^p \in L_f^0,$$

- *Find* $\{\hat{v}_s, \hat{u}_s\} \in \hat{L}_s \times \{\hat{u}_s^D + \hat{V}_s^0\}$,

$$(\hat{\rho}_s \partial_t \hat{v}_s, \hat{\psi}^v)_{\widehat{\Omega}_s} + (\widehat{F}\widehat{\Sigma}, \widehat{\nabla}\hat{\psi}^v)_{\widehat{\Omega}_s}$$
$$+ \gamma_w (\hat{v}_s, \hat{\psi}^v)_{\widehat{\Omega}_s} + \gamma_s (\hat{\epsilon}(\hat{v}_s), \widehat{\nabla}\hat{\psi}^v)_{\widehat{\Omega}_s} - (\hat{\rho}_s \hat{f}_s, \hat{\psi}^v)_{\widehat{\Omega}_s} = 0 \quad \forall \hat{\psi}^v \in \hat{V}_s^0,$$
$$\hat{\rho}_s (\partial_t \hat{u}_s - \hat{v}_s, \hat{\psi}^u)_{\widehat{\Omega}_s} = 0 \quad \forall \hat{\psi}^u \in \hat{L}_s,$$

*with* $\hat{\rho}_f$, $\hat{\rho}_s$, $\nu_f$, $\mu_s$, $\lambda_s$, $\widehat{F}$, *and* $\hat{J}$ *as defined before. The stress tensors* $\hat{\sigma}_f$, $\widehat{\Sigma}$, *and* $\hat{\sigma}_{mesh}$ *are defined in the Equations (49), (16), (5.46), and in (74) and (61), respectively.*

**Remark 7.34** (Iteration loop / Fix point iteration). *In the implementation, we add iteration indices k to all equations and produce sequences of solutions*

$$u_f^1, u_f^2, u_f^3, \ldots \quad \text{Mesh motion}$$
$$v_f^1, v_f^2, v_f^3, \ldots \quad \text{Fluid}$$
$$p_f^1, p_f^2, p_f^3, \ldots \quad \text{Fluid}$$
$$\hat{v}_s^1, \hat{v}_s^2, \hat{v}_s^3, \ldots \quad \text{Solid}$$
$$\hat{u}_s^1, \hat{u}_s^2, \hat{u}_s^3, \ldots \quad \text{Solid}.$$

*A loosely-coupled scheme would terminate (or be forced to stop) after a few iterations. A strongly-coupled algorithms solves up to a tolerance and based a stopping criterion that is based on the Steklov-Operator, i.e., find* $\hat{u}$ *on* $\widehat{\Gamma}_i$ *such that the stress condition* $\hat{\sigma}_f \hat{n}_f = \hat{\sigma}_s \hat{n}_s$ *is satisfied.* ◇

**Remark 7.35** (Solution of the mesh motion problem). *In the partitioned approach different solution techniques can be easily employed to solve the three subproblems (mesh, fluid, solid). Here, we emphasize that the mesh motion equation is purely artificial without physical relevance and it can be solved without satisfying a low tolerance. So, its solution can be achieved in a fast way.* ◇

**Remark 7.36** (Decoupling in time). *In the partitioned approach it is obvious (under the condition that certain relationships and additional information are known) that we can decouple in time. For instance, we have seen in [203] that the FSI-benchmark requires smaller time steps than the pure fluid benchmark. An open question is if we could use a partitioned solver in which we solve the fluid equations and mesh motion problem only at every 10th time step.* ◇

### 7.3.14 Existence of a stationary ALE-FSI problem in the $ALE_{fx}$ framework

In this section, we establish existence of an stationary ALE-FSI problem in the $ALE_{fx}$ framework. Clearly, stationary FSI is much different (easier) than nonstationary FSI still very sophisticated and consequently sufficient for these notes. The ideas of this chapter follow Grandmont [118] and the basic idea is to combine the fluid flow ALE version of Theorem 6.10 and the existence Theorem 6.28 for nonlinear elasticity.

We make the following assumptions:

- We assume all assumptions made in Theorem 6.10 and Theorem 6.28;

- The boundaries of $\Omega_s$ and $\Omega_f$ as well as the interface are sufficiently smooth;

- The interface does not touch the fluid boundary; namely $\Gamma_i \cap \partial\Omega = \emptyset$[20];

---

[20]This is exactly one of the obstacles outlined in Challange 2.2 in FSI because this restriction contradicts most of the practical FSI problems

- For the solid, an additional injectivity condition (because we also deal with Neumann conditions in addition to Dirichlet) is required, i.e.,

$$\int_{\Omega_s} \hat{J}\, dx = |\Omega_s|;$$

for which we also refer to Definition 5.25. For a detailed discussion on this condition we refer the reader to [61](Section 5.6);

- Additionally,

$$\int_{\Omega_f} \hat{J}\, dx = |\Omega_f|.$$

**Theorem 7.37** (Existence of stationary ALE-FSI in the $ALE_{fx}$ framework)**.** *Let $3 < p < \infty$. Let $\hat{f}_f \in L^p(\Omega_f)$ and $\hat{f}_s \in L^p(\Omega_s)$ be given. Assume that $\hat{f}_f$ and $\hat{f}_s$ are sufficiently small such that*

$$C_s \|\hat{f}_s\|_{L^p} + C_f \|\hat{f}_f\|_{L^p} \le C$$

*for $C > 0$. Furthermore, let us assume $\|\hat{f}_f\|_{H^{-1}} \le c_*^2 \nu_f^2$ (see Theorem 6.10). Then, there exists a solution $\{\hat{v}, \hat{p}, \hat{u}, c\}$ with*

$$(\hat{v}, \hat{p}, \hat{u}) \in W_0^{1,p}(\widehat{\Omega}_f) \cap W^{2,p}(\widehat{\Omega}_f) \times W^{1,p}(\widehat{\Omega}_f) \times W_{0,\Gamma_i}^{1,p}(\widehat{\Omega}_s) \cap W^{2,p}(\widehat{\Omega}_s),$$

*and $c$ is a Lagrange multiplier associated with the volume conservation constraint.*

**Remark 7.38.** *A recent (nontrivial) extension of Theorem 7.37 to show uniqueness and differentiability of the FSI solution map has been estabilished in [248].*

*Proof.* (of Theorem 7.37)
The key idea is to employ the Schauder-Tychonov fixed point theorem. $\qquad\square$

## 7.4 A larger perspective: Connecting ALE schemes and r-adaptivity (moving mesh methods)

It is interesting to notice that ALE-schemes can be connected to a larger class of mesh-adaption procedures that are known as r-adaptivity methods (a nice overview is provided in [52]). In particular, they are used to improve the finite element discretization accuracy, which is known as *r*-adaptivity (beyond usual $h$ and $p$ adaptivity). This is slightly different from moving boundary problems, since here, as in fluid-structure interaction, you *must* move the mesh according to the interface. Whereas in other applications it is a powerful method that complements other techniques to improve the accuracy of the solution.

In extension to our explanations in Section 7.2, moving mesh methods can be decomposed into two different sub-classes:

- Location-based methods: the new mesh points are directly obtained from the solution of the auxiliary PDE. Typically, such methods cluster mesh points (see Figure 32).

- Velocity-based methods: the auxiliary PDE computes a mesh-velocity that is then integrated in order to obtain new mesh points. It is clear that such methods are prone to mesh tangling since we work in a Lagrangian-based setting for solving fluid flows and consequently, if we transport the mesh in a setting with high fluid vorticity, mesh faces might intersect. (see, e.g., Figure 33).

**Remark 7.39** (Mesh moving in non-convex domains)**.** *In fluid-structure interaction, there is the inherent problem that the moving mesh equations must be solved in non-convex domains, which might lead to additional complications due to re-entrant corners. For brief discussions, we refer to [75, 107]. However, we observed in several numerical tests [241] that biharmonic mesh motion offers interesting features, and very smooth meshes in non-convex domains. We recall that the second equation is related to the bending moment (in solid mechanics) or the vorticity in fluid dynamics. $\diamond$*

Since the ALE method can be identified as a moving mesh method, the following theorem from measure theory builds the ground of mesh moving and equidistribution:

**Theorem 7.40** (Radon-Nikodym). *Let $\hat{\mathcal{A}}$ be an invertible mapping that maps $\hat{A} \subset \widehat{\Omega}$ to $\hat{\mathcal{A}}(A) \subset \Omega$. The Borel measure is $\nu(\hat{\mathcal{A}}(A)) = |A|$, where $|\cdot|$ denotes the Lebuesgue measure. If $\nu$ is a well-defined Borel measure on $\Omega$, then there exists a non-negative function $M : \Omega \to \mathbb{R}$ such that*

$$\nu(\hat{\mathcal{A}}(A)) = \int_{\hat{\mathcal{A}}(A)} M(x)\,dx,$$

*for any $\hat{\mathcal{A}}(A) \subset \Omega$. Additionally, $M$ is unique up to a Lebuesgue measure zero.*

This theorem ensures that for any invertible mapping $\hat{\mathcal{A}}$, we can find a unique function $M$ such that

$$\int_A dx = \int_{\hat{\mathcal{A}}(A)} M(x)\,dx.$$

The function $M$ is usually called a monitor function that should be large when mesh points are required to be clustered or mesh tangling is likely to occur.

**Example 7.41.** *The simplest and oldest example is Winslow's variable diffusion method [249]:*

$$M = \sqrt{1 + \omega^2 |\widehat{\nabla}\hat{u}|^2}, \quad \omega > 0.$$

*Another example is given by setting*

$$\alpha = \frac{1}{M} = \frac{1}{\hat{J}}$$

*as done by employing Jacobi-based stiffening. We refer to Figure 32 for visualization.*

**Remark 7.42** (Matrix-valued monitor functions). *We notice that the concept of the monitor function is straightforward to apply to matrix-valued monitor functions [52].* ◇

**Remark 7.43** (Viewpoint of energy minimization). *The mesh motion equations can be interpreted as the Euler-Lagrange equations of a corresponding energy functional. With this step, mesh moving strategies can be embedded into calculus of variations. As simplest example, we may write harmonic mesh motion as*

$$\min I(\hat{x}),$$

*with*

$$I(\hat{x}) = \int_{\widehat{\Omega}} \alpha |\widehat{\nabla}\hat{u}|^2\,d\hat{x}.$$

◇

**Remark 7.44** (Extension to time-dependent mesh motion equations). *One might think that a time-dependent mesh motion model would produce more reliable results since fluid-structure interaction is itself time-dependent. Carrying out several numerical tests by using a heat-type equation,*

$$\partial_t \hat{u} - \widehat{\nabla} \cdot (\alpha \widehat{\nabla} \hat{u}) = 0, \quad in\ \widehat{\Omega}_f,$$

*or*

$$\partial_t \hat{u} - \widehat{\nabla} \cdot \hat{\sigma}_{mesh} = 0, \quad in\ \widehat{\Omega}_f,$$

*we never could produce better results than with a pure stationary method as described in the previous sections.* ◇

# 8 Temporal and Spatial Discretization

In this part, we mostly concentrate on the $\mathrm{ALE}_{fx}$ framework and we focus on

- the Rothe method (first time, then space);

- Time discretization based on finite differences: first-order backward Euler, second order Crank-Nicolson, second-order shifted Crank-Nicolson, second-order Fractional-Step-$\theta$;

- Spatial discretization based on inf-sup stable Galerkin finite elements;

- Newton's method with simple line search backtracking;

- Solution of the linear equations;

- To discuss a 'simple' problem showing that our approach is easy to realize with pre-understanding of a class such as numerical methods for partial differential equations;

Due to the fact that traditionally, fluids and solids have been formulated in different frameworks, their respective discretization reflected these differences.

Before, we start let us briefly provide reasons why we want to work with the Rothe method (horizontal method of lines). The traditional way of discretizing time-dependent problems is the (vertical) method of lines in which first spatial discretization is performed and subsequently temporal treatment. The advantage is that we have simple data structures and matrix assembly. This leads to a (large) ODE system, which can be treated by (well-known) standard methods from ODE analysis (ordinary differential equations) can be employed for time discretization. The major disadvantage is that the spatial mesh is fixed (since we first discretize space) and it is then difficult to represent or compute time-varying features such as certain target functionals (e.g., drag or lift). In contrast, the Rothe method allows for dynamic spatial mesh adaptation with the price that data structures and matrix assembly are more costly. As third possibility a full space-time formulation can be formulated, which is however difficult to implement.

## 8.1 Time stepping

### 8.1.1 Basics

In order to discretize nonstationary FSI, we follow the Rothe method and first discretize in time and later in space. Therefore, we begin by briefly explaining the derivation of One-Step-$\theta$ schemes (see, e.g., [229, 232]) for parabolic problems (here in terms of the heat equation). Let

$$\partial_t u - \Delta u = f,$$

be given. Time discretization yields: Find $u := u^n$:

$$\frac{u - u^{n-1}}{\delta t} - \theta \Delta u - (1-\theta)\Delta u^{n-1} = \theta f + (1-\theta)f^{n-1}.$$

Thus,

$$u - \delta t \theta \Delta u = u^{n-1} + \delta t(1-\theta)\Delta u^{n-1} + \delta t \theta f + \delta t(1-\theta)f^{n-1}.$$

**8.1.1.1 One-step-$\Theta$ time-stepping for Navier-Stokes** Let us know briefly extend this idea to Navier-Stokes to point an important property. Setting $N(v) := v \cdot \nabla v - \nabla \cdot (\nabla v + \nabla v^T)$, we write

$$\partial_t v + N(v) + \nabla p = f, \quad \nabla \cdot v = 0$$

be given. In the time discretization, the pressure term in the momentum equation is treated fully implicity such that we seek $v := v^n, p := p^n$:

$$\frac{v - v^{n-1}}{\delta t} + \theta N(v) + (1-\theta)N(v^{n-1}) + \nabla p = \theta f + (1-\theta)f^{n-1}, \quad \nabla \cdot v = 0.$$

Finally, a fully nonlinear (because of $N(v)$) scheme reads

$$v + \delta t\theta N(v) + \delta t\nabla p = v^{n-1} - \delta t(1-\theta)N(v^{n-1})\delta t\theta f + \delta t(1-\theta)f^{n-1}, \quad \nabla \cdot v = 0.$$

This time stepping scheme is generically implicit (independendly of the choice of $\theta$ because of the incompressibility constraint.

**8.1.1.2 One-step-$\Theta$ time-stepping for the mixed form of elasticity**   As advertised in Remark 5.44, the mixed form of elasticity can be directly treated with a One-step-$\Theta$ scheme as well. We are given:

$$\hat{\rho}\partial_t\hat{v} - \widehat{\nabla} \cdot \widehat{F}\widehat{\Sigma} = \hat{f},$$
$$\hat{\rho}(\partial_t\hat{u} - \hat{v}) = 0.$$

Let $\hat{u}^{n-1}, \hat{v}^{n-1}, \widehat{F}^{n-1} := \widehat{F}(\hat{u}^{n-1})$ and $\widehat{\Sigma}^{n-1} := \widehat{\Sigma}(\hat{u}^{n-1})$ be given. We seek for the time-discretized $\hat{u}$ and $\hat{v}$ such that:

$$\hat{\rho}\hat{v} - \delta t\theta\widehat{\nabla} \cdot \widehat{F}\widehat{\Sigma} = \hat{\rho}\hat{v}^{n-1} + \delta t(1-\theta)\widehat{\nabla} \cdot \widehat{F}^{n-1}\widehat{\Sigma}^{n-1} + \delta t\theta\hat{f} + \delta(1-\theta)\hat{f}^{n-1},$$
$$\hat{\rho}\hat{u} - \delta t\theta\hat{v} = \hat{u}^{n-1} + \delta t(1-\theta)\hat{v}^{n-1}.$$

**8.1.1.3 On the choice of $\theta$**

**Definition 8.1** (Choice of $\theta$). *By the choice of $\theta$, we obtain the following time-stepping schemes:*

- *$\theta = 0$: 1st order explicit Euler time stepping;*

- *$\theta = 0.5$: 2nd order Crank-Nicolson (trapezoidal rule) time stepping;*

- *$\theta = 0.5 + k_n$: 2nd order shifted Crank-Nicolson which is shifted by the time step size $k$ towards the implicit side;*

- *$\theta = 1$: 1st order implicit Euler time stepping.*

*Properties of these schemes are listed in Definition 8.5.*

From linear stability analysis in ODEs (ordinary differential equations), we recapitulate 'numerical stability', 'absolute stability' and 'A-stability'. From the model problem

$$u'(t) = \lambda u(t), \quad u(t_0) = u_0, \ \lambda \in \mathbb{C},$$

we know the solution $u(t) = u_0 \exp(\lambda t)$. For $t \to \infty$ the solution is characterized by the sign of $Re\,\lambda$:

$$Re\,\lambda < 0 \quad \Rightarrow |u(t)| = |u_0|\exp(Re\,\lambda) \to 0,$$
$$Re\,\lambda = 0 \quad \Rightarrow |u(t)| = |u_0|\exp(Re\,\lambda) = |u_0|,$$
$$Re\,\lambda > 0 \quad \Rightarrow |u(t)| = |u_0|\exp(Re\,\lambda) \to \infty.$$

For a 'good' numerical scheme, the first case is particularly interesting whether such a scheme can produce a bounded discrete solution when the continuous solution has this property.

**Definition 8.2** (Absolute stability). *A (one-step) method is absolute stable for $\lambda\delta t \neq 0$ if its application to the model problem produces in the case $Re\,\lambda \leq 0$ a sequence of bounded discrete solutions: $\sup_{n\geq 0}|u_n| < \infty$. To find the stability region, we work with the stability function $R(z)$ where $z = \lambda\delta t$. The region of absolute stability is defined as:*

$$SR = \{z = \lambda\delta t \in \mathbb{C} : |R(z)| \leq 1\}.$$

**Example 8.3.** *For the simplest time-stepping schemes forward Euler ($\theta = 0$), backward Euler ($\theta = 1$) and the trapezoidal rule ($\theta = 0.5$), the stability functions $R(z)$ read:*

$$R(z) = 1 + z,$$

$$R(z) = \frac{1}{1-z},$$

$$R(z) = \frac{1 + \frac{1}{2}z}{1 - \frac{1}{2}z}.$$

*They are obtained by applying the temporal difference quotients to the above model problem. We see that for stiff problems (here $\lambda$ is large), we need very small steps $\delta t$ in order to guarantee $R(z) \leq 1$ for the case $\theta = 0$. On the other hand, the case $\theta = 1$ will work for arbitrary high $\lambda$.*

**Definition 8.4** (A-stability). *A difference method is A-stable if its stability region is part of the absolute stability region:*

$$\{z \in \mathbb{C} : Re\, z \leq 0\} \subset SR.$$

To have good stability properties (namely A-stability) of the time-stepping scheme is important for temporal discretization of partial differential equations. Often (in fluid-structure interaction in nearly all equations!) we deal with second-order operators in space, such PDE-problems are generically (very) stiff with the order $O(h^{-2})$, where $h$ is the spatial discretization parameter. Additionally, material parameters for fluids and solids differ of several orders of magnitude.

**Definition 8.5** (Stability and properties of time stepping schemes ). *A good time stepping scheme for time-discretizing partial differential equations should satisfy:*

- *A-stability (local convergence): an example is the Crank-Nicolson scheme (trapezoidal rule);*

- *strict A-stability (global convergence): an example is the shifted Crank-Nicolson scheme;*

- *strong A-stability (smoothing property): examples are backward Euler (in particular even L-stable[21]) and Fractional-step-$\theta$ schemes;*

- *small dissipation (energy conservation).*

$\diamond$

**Remark 8.6** (BDF schemes - backward differentiation formula). *Another class of schemes that are often used are the so-called BDF schemes. For instance, application of BDF(2) to Navier-Stokes in Eulerian coordinates and strong form reads:*

$$\frac{\frac{3}{2}v_n - 2v_{n-1} + \frac{1}{2}v_{n-2}}{\delta t} + v_n \cdot \nabla v_n - \nabla \cdot \sigma(v_n, p_n) = f_n.$$

*Here, we need two start values $v_0$ and $v_1$, where $v_0$ is given as initial value and $v_1$ is computed with a one-step method. The two lowest order schemes BDF(1) and BDF(2) are A-stable as their one-step-$\theta$ counterparts. We notice that BDF schemes of order $> 2$ cannot be A-stable.*

Let us now describe the properties of the previous schemes in more detail:

- The explicit Euler scheme is cheap in the computational cost since no equation system needs to be solved. However, in order to be numerically stable (very, very) small time steps must be employed, which makes this scheme infeasible for fluid-structure interaction problems.

- A classical scheme for problems with a stationary limit is the (implicit) backward Euler scheme (BE), which is strongly A-stable (but only from first order), robust and dissipative. It is used in numerical Examples, where a stationary limit must be achieved. However, due to its dissipativity this schemes dampes high-frequent temporal parts of the solution too much and for this reason this scheme is not recommended for nonstationary flow or FSI (see Figure 47 for a comparison of BE and CN).

---

[21] A time-stepping scheme is L-stable if it is A-stable and the stability function satisfies $|R(z)| \to 0$ for $z \to \infty$. In this respect the Crank-Nicolson scheme is not L-stable since $R(z) \to 1$ for $z \to -\infty$.

- In contrast, the (implicit) Crank-Nicolson scheme is of second order, A-stable, and has very little dissipation but suffers from case-to-case instabilities caused by rough initial and/or boundary data. These properties are due to weak stability (it is not *strongly* A-stable). A variant of the Crank-Nicolson scheme is called *shifted* Crank-Nicolson scheme, is analyzed in Rannacher et al. [131, 189], which allows for global stability of the solution [22]. In particular, Rannacher analyzed in [188] the shifted Crank-Nicolson scheme for linear evolution equations and how they can be modified in order to make them suitable for long-term computations (without reducing second order accuracy!!). In [203, 239], it has been shown that these ideas apply also to (nonlinear) fluid-structure interaction problems by demonstrating computational evidence. More details are addressed below in Section 8.1.3.

- The fourth scheme summarizes the advantages of the previous two and is known as the Fractional-Step-$\theta$ scheme for computing unsteady-state simulations [116]. Roughly-speaking it consists of summarizing three Crank-Nicolson steps and has therefore the same accuracy and compuational cost as the Crank-Nicolson scheme. However, it is more robust, i.e., it is strongly A-stable (as backward Euler) but has 2nd order accuracy as Crank-Nicolson, and is therefore well-suited for computing solutions with rough initial data and long-term computations for problems. This property also holds for ALE-transformed fluid equations, which is demonstrated in a numerical test below. We also refer the reader to a modification of the Fractional-Step-$\theta$ scheme [232].

### 8.1.1.4 Time stability of second-order hyperbolic equations: revisiting the solid equations
In fluid-structure interaction, the solid equation is of hyperbolic type and satisfies an energy conservation law on the continuous level. That means that our time-discretization scheme should reproduce this property; see fourth point in Definition 8.5.

We recall findings (neglecting the damping terms) from the theory [13, 33, 121]:

- *Stability in the $L^2$-norm:* the One-Step-$\theta$ scheme (112) is unconditionally stable, i.e., there is no time step restriction on $k$ if and only if $\theta \in [\frac{1}{2}, 1]$.

- *Energy conservation:* the one-step-$\theta$ scheme (112) preserves energy only for the choice $\theta = \frac{1}{2}$. For $\theta > \frac{1}{2}$ (e.g., the implicit Euler scheme for the choice $\theta = 1$) the scheme dissipates energy.

Consequently, the Crank-Nicolson scheme is an optimal time-stepping scheme for hyperbolic equations. Possible restrictions with respect to the time-step size are weaker for hyperbolic problems than for parabolic differential equations [121]; namely

**Definition 8.7** (Courant-Friedrichs-Levy - CFL). *A necessary condition for explicit time stepping schemes is the Courant-Friedrichs-Levy (CFL) condition, i.e., the time step size $k$ is dependent on material parameters and the spatial discretization parameter $h$:*

- *Parabolic problems: $k \leq \frac{1}{2}ch^2$;*

- *Hyperbolic problems: $k \leq a^{-1}h$, where $a$ is of order of the elasticity constant in the wave operator.*

To bring it to the point: issues of numerical stability of the coupled problem are of utter importance, as it consists of a combined consideration of two different types of equations:

- the incompressible Navier-Stokes equations which is of parabolic type and that comes with smoothing properties; and the hyperelastic solid equation of hyperbolic type, which requires good conservation properties with very little numerical dissipation.

By these considerations, the Crank-Nicolson scheme and its variants like shifted versions [131, 167, 189] or the fractional step theta scheme [49, 232], appear to be ideal candidates.

---

[22] A famous alternative to the shifted Crank-Nicolson scheme is Rannacher's time-marching technique in which the unshifted Crank-Nicolson scheme is augmented with backward Euler steps for stabilization and in particular for irregular initial data [188]. Adding backward Euler steps within Crank-Nicolson does also stabilize during long-term computations [131, 188].

**8.1.1.5 Consequences of energy conservation in pipes/tubes/arteries with moving elastic walls** Let us briefly illustrate practical consequences associated with hyperbolic (non-damping) solid equations. Assuming we have *optimal* conservation properties using a Crank-Nicolson-type scheme for temporal discretization. As we mentioned in the introduction, hemodynamical applications are often subject of research. Here, blood flows in a veine or artery. Due to its enormous computational cost, we can not simulate the whole circulatory system and we need to *cut* the computational domain. Blood flow is a pulsating fluid and introduces waves and in particular these waves can be observed in the arterial wall (see a snapshot at time $t^*$ in Figure 38). Using standard Dirichlet or Neumann conditions on the structural boundary conditions (inlet and outlet), elastic waves are reflected. This is non-physical behavior and is subject of present research [54, 96, 108, 176]. Our conclusion that is inferred from these observations is that correct numerical discretization does not necessarely result in the correct physical answer.
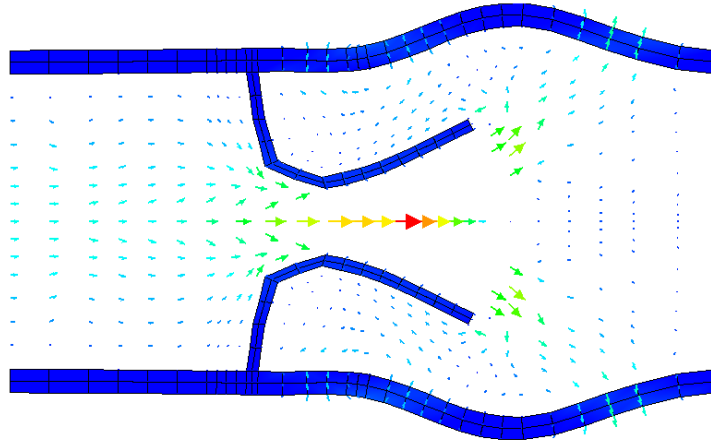


Figure 38: Snapshot at time step $t^*$ of flapping simulation with moving elastic boundaries.

### 8.1.2 Temporal discretization of fluid-structure interaction by the Rothe method

We now concentrate on temporal discretization of fluid-structure interaction. Here, use

**Proposition 8.8.** *Applying the one-step-$\theta$ scheme to the strong form and then taking the weak formulation is formally equivalent to first writing the weak formulation and then time-discretizing this scheme.*

*Proof.* A check is left as an exercise. □

In the domain $\widehat{\Omega}$ and the time interval $I = [0, T]$, we consider the fluid-structure interaction Problem 7.21 with harmonic or linear-elastic mesh motion in an abstract setting (the biharmonic problem is straightforward):

**Definition 8.9.** *Find* $\hat{U} = \{\hat{v}_f, \hat{v}_s, \hat{u}_f, \hat{u}_s, \hat{p}_f, \hat{p}_s\} \in \widehat{X}_D^0$, *where* $\widehat{X}_D^0 := \{\hat{v}_f^D + \hat{V}_{f,\hat{v}}^0\} \times \hat{L}_f \times \{\hat{u}_f^D + \hat{V}_{f,\hat{u}}^0\} \times \{\hat{u}_s^D + \hat{V}_s^0\} \times \hat{L}_f^0 \times \hat{L}_s^0$, *such that*

$$\int_0^T \hat{A}(\hat{U})(\hat{\Psi}) \, dt = 0 \quad \forall \hat{\Psi} \in \widehat{X}, \tag{102}$$

*where* $\hat{\Psi} = \{\hat{\psi}_f^v, \hat{\psi}_s^v, \hat{\psi}_f^u, \hat{\psi}_s^u, \hat{\psi}_f^p, \hat{\psi}_s^p\}$ *and* $\widehat{X} = \hat{V}_{f,\hat{v}}^0 \times \hat{L}_f \times \hat{V}_{f,\hat{u},\widehat{\Gamma}_i}^0 \times \hat{V}_s^0 \times \hat{L}_f^0 \times \hat{L}_s^0$ *and*

$$\hat{A}(\hat{U})(\hat{\Psi}) := \hat{A}_1(\hat{U})(\hat{\psi}^v) + \hat{A}_2(\hat{U})(\hat{\psi}^v) + \hat{A}_3(\hat{U})(\hat{\psi}^u) + \hat{A}_4(\hat{U})(\hat{\psi}^u) + \hat{A}_5(\hat{U})(\hat{\psi}^p) + \hat{A}_6(\hat{U})(\hat{\psi}^p).$$

*as defined in Problem 7.22.*

The abstract problem (102) can either be treated by a full time-space Galerkin formulation, which was investigated previously for fluid problems in Besier et al. [35, 36, 215]. Alternatively, the Rothe method can be used in cases where the time discretization is based on finite difference schemes.

To sum-up: After semi-discretization in time, we obtain a sequence of generalized steady-state fluid-structure interaction problems that are completed by appropriate boundary values at every time step. Let us now go into detail and let

$$I = \{0\} \cup I_1 \cup \ldots \cup I_N$$

be a partition of the time interval $I = [0, T]$ into half open subintervals $I_n := (t_{n-1}, t_n]$ of (time step) size $k_n := t_n - t_{n-1}$ with

$$0 = t_0 < \cdots < t_N = T.$$

**Definition 8.10** (Arranging of the FSI semi-linear form into groups). *We formally define the following semi-linear forms and group them into four categories:*

- *time equation terms (including the time derivatives);*

- *implicit terms (e.g., the incompressibility of the fluid);*

- *pressure terms;*

- *all remaining terms (stress terms, convection, damping, etc.);*

*such that*

$$\hat{A}_T(\hat{U})(\hat{\Psi}) = (\hat{J}\hat{\rho}_f \partial_t \hat{v}_f, \hat{\psi}_f^v)_{\widehat{\Omega}_f} - (\hat{\rho}_f \hat{J}(\widehat{F}^{-1}\hat{w} \cdot \widehat{\nabla})\hat{v}_f), \hat{\psi}_f^v)_{\widehat{\Omega}_f} + (\hat{\rho}_s \partial_t \hat{v}_s, \hat{\psi}_s^v)_{\widehat{\Omega}_s} + (\hat{\rho}_s \partial_t \hat{u}_s, \hat{\psi}_s^u)_{\widehat{\Omega}_s}, \tag{103}$$

$$\hat{A}_I(\hat{U})(\hat{\Psi}) = (\alpha_u \widehat{\nabla}\hat{u}_f, \widehat{\nabla}\hat{\psi}_f^u)_{\widehat{\Omega}_f} + (\widehat{div}(\hat{J}\widehat{F}^{-1}\hat{v}_f), \hat{\psi}_f^p)_{\widehat{\Omega}_f} + (\hat{P}_s, \hat{\psi}_s^p)_{\widehat{\Omega}_s}, \tag{104}$$

$$\hat{A}_E(\hat{U})(\hat{\Psi}) = (\hat{\rho}_f \hat{J}(\widehat{F}^{-1}\hat{v}_f \cdot \widehat{\nabla})\hat{v}_f), \hat{\psi}_f^v)_{\widehat{\Omega}_f} + (\hat{J}\widehat{\sigma}_{f,vu}\widehat{F}^{-T}, \widehat{\nabla}\hat{\psi}_f^v)_{\widehat{\Omega}_f} - \langle \rho_f \nu \widehat{F}^{-T} \widehat{\nabla}v^T \hat{n}, \hat{\psi}_f^v \rangle_{\widehat{\Gamma}_{out}} \tag{105}$$

$$+ (\widehat{F}\widehat{\Sigma}, \widehat{\nabla}\hat{\psi}_s^v)_{\widehat{\Omega}_s} - (\hat{\rho}_s \hat{v}_s, \hat{\psi}_s^u)_{\widehat{\Omega}_s}, \tag{106}$$

$$\hat{A}_P(\hat{U})(\hat{\Psi}) = (\hat{J}\widehat{\sigma}_{f,p}\widehat{F}^{-T}, \widehat{\nabla}\hat{\psi}_f^v)_{\widehat{\Omega}_f} + (\hat{J}\widehat{\sigma}_{s,p}\widehat{F}^{-T}, \widehat{\nabla}\hat{\psi}_s^v)_{\widehat{\Omega}_s}, \tag{107}$$

*where the reduced stress tensors $\widehat{\sigma}_{f,vu}$, $\widehat{\sigma}_{f,p}$, and $\widehat{\sigma}_{s,p}$ are defined as:*

$$\widehat{\sigma}_{f,p} = -\hat{p}_f \hat{I}, \quad \widehat{\sigma}_{f,vu} = \rho_f \nu_f (\widehat{\nabla}\hat{v}_f \widehat{F}^{-1} + \widehat{F}^{-T}\widehat{\nabla}\hat{v}_f^T), \tag{108}$$

$$\widehat{\sigma}_{s,p} = -\hat{p}_s \hat{I}, \quad \textit{(if we deal with the INH or IMR material)}, \tag{109}$$

*and $\widehat{\Sigma}$ denotes as usual the structure tensor of the INH, IMR, or STVK material. The time derivative in $\hat{A}_T(\hat{U})(\hat{\Psi})$ is approximated by a backward difference quotient. For the time step $t_n \in I$ for $n = 1, 2, \ldots, N$ ($N \in \mathbb{R}$), we compute $\hat{v}_i := \hat{v}_i^n, \hat{u}_i := \hat{u}_i^n$ ($i = f, s$) via*

$$\hat{A}_T(\hat{U}^{n,k})(\hat{\Psi}) \approx \frac{1}{k}\big(\rho_f \hat{J}^{n,\theta}(\hat{v}_f - \hat{v}_f^{n-1}), \hat{\psi}^v\big)_{\widehat{\Omega}_f} - \frac{1}{k}\big(\rho_f (\hat{J}\widehat{F}^{-1}(\hat{u}_f - \hat{u}_f^{n-1}) \cdot \widehat{\nabla})\hat{v}_f, \hat{\psi}^v\big)_{\widehat{\Omega}_f} \tag{110}$$

$$+ \frac{1}{k}\big(\hat{\rho}_s(\hat{v}_s - \hat{v}_s^{n-1}), \hat{\psi}^v\big)_{\widehat{\Omega}_s} + \big(\hat{u}_s - \hat{u}_s^{n-1}, \hat{\psi}^u\big)_{\widehat{\Omega}_s}, \tag{111}$$

*where we introduce a parameter $\theta$, which is clarified below. Furthermore, we use*

$$\hat{J}^{n,\theta} = \theta \hat{J}^n + (1 - \theta)\hat{J}^{n-1},$$

*and $\hat{u}_i^n := \hat{u}_i(t_n)$, $\hat{v}_i^n := \hat{v}_i(t_n)$, and $\hat{J} := \hat{J}^n := \hat{J}(t_n)$. The former time step is given by $\hat{v}_i^{n-1}$, etc. for $i = f, s$.*

**Remark 8.11.** *Working with damped solid equations, one needs to add two terms such that:*

$$\hat{A}_E(\hat{U})(\hat{\Psi}) = \ldots + \gamma_w(\hat{v}_s, \hat{\psi}_s^v)_{\widehat{\Omega}_s} + \gamma_s(\hat{\epsilon}(\hat{v}_s), \widehat{\nabla}\hat{\psi}_s^v)_{\widehat{\Omega}_s}.$$

### 8.1.2.1 The One-Step-$\theta$ scheme

**Definition 8.12.** *Let the previous time step solution*
$\hat{U}^{n-1} = \{\hat{v}_f^{n-1}, \hat{v}_s^{n-1}, \hat{u}_f^{n-1}, \hat{u}_s^{n-1}, \hat{p}_f^{n-1}, \hat{p}_s^{n-1}\}$ *and the time step* $k := k_n = t_n - t_{n-1}$ *be given.*
  *Find* $\hat{U}^n = \{\hat{v}_f^n, \hat{v}_s^n, \hat{u}_f^n, \hat{u}_s^n, \hat{p}_f^n, \hat{p}_s^n\}$ *such that*

$$\hat{A}_T(\hat{U}^{n,k})(\hat{\Psi}) + \theta\hat{A}_E(\hat{U}^n)(\hat{\Psi}) \tag{112}$$

$$+\hat{A}_P(\hat{U}^n)(\hat{\Psi}) + \hat{A}_I(\hat{U}^n)(\hat{\Psi}) = -(1-\theta)\hat{A}_E(\hat{U}^{n-1})(\hat{\Psi}) \tag{113}$$

$$+\theta\widehat{F}^n(\hat{\Psi}) + (1-\theta)\widehat{F}^{n-1}(\hat{\Psi}), \tag{114}$$

*where* $\widehat{F}^n(\hat{\Psi}) = (\hat{\rho}_s\hat{f}_s^n, \hat{\psi}_s^v)_{\widehat{\Omega}_s}$ *with* $\hat{f}_s^n := \hat{f}_s(t_n)$. *The concrete scheme depends on the choice of the parameter* $\theta$ *as defined in Definition 8.1.*
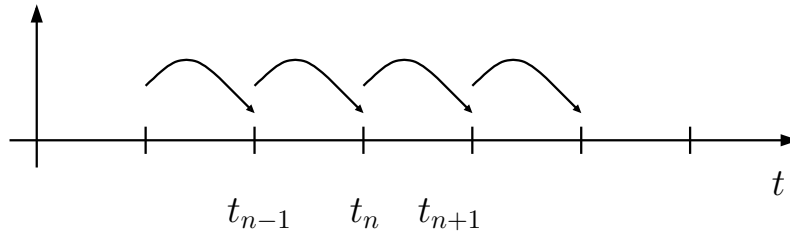


Figure 39: Time step computation using One-Step-$\theta$ schemes.

We notice that for problems with large time steps ($k \geq 0.5$), we need to normalize/non-dimensionalize the equations in order to get the characteristic time step size that can be used for the shifted variant. Otherwise, you have $\theta > 1$, which is senseless. As alternative, one can use the Rannacher time-stepping by adding backward Euler steps on a regular basis [188].

### 8.1.2.2 The Fractional-Step-$\theta$ scheme

**Definition 8.13.** *Let us choose* $\theta = 1 - \frac{\sqrt{2}}{2}, \theta' = 1 - 2\theta$, *and* $\alpha = \frac{1-2\theta}{1-\theta}, \beta = 1 - \alpha$. *The time step is split into three consecutive sub-time steps. Let* $\hat{U}^{n-1} = \{\hat{v}_f^{n-1}, \hat{v}_s^{n-1}, \hat{u}_f^{n-1}, \hat{u}_s^{n-1}, \hat{p}_f^{n-1}, \hat{p}_s^{n-1}\}$ *and the time step* $k := k_n = t_n - t_{n-1}$ *be given.*
  *Find* $\hat{U}^n = \{\hat{v}_f^n, \hat{v}_s^n, \hat{u}_f^n, \hat{u}_s^n, \hat{p}_f^n, \hat{p}_s^n\}$ *such that*

$$\hat{A}_T(\hat{U}^{n-1+\theta,k})(\hat{\Psi}) + \alpha\theta\hat{A}_E(\hat{U}^{n-1+\theta})(\hat{\Psi}) \tag{115}$$

$$+\theta\hat{A}_P(\hat{U}^{n-1+\theta})(\hat{\Psi}) + \hat{A}_I(\hat{U}^{n-1+\theta})(\hat{\Psi}) = -\beta\theta\hat{A}_E(\hat{U}^{n-1})(\hat{\Psi}) + \theta\hat{F}^{n-1}(\hat{\Psi}), \tag{116}$$

$$\tag{117}$$

$$\hat{A}_T(\hat{U}^{n-\theta,k})(\hat{\Psi}) + \beta\theta'\hat{A}_E(\hat{U}^{n-\theta})(\hat{\Psi}) \tag{118}$$

$$+\theta'\hat{A}_P(\hat{U}^{n-\theta})(\hat{\Psi}) + \hat{A}_I(\hat{U}^{n-\theta})(\hat{\Psi}) = -\beta\theta'\hat{A}_E(\hat{U}^{n-1+\theta})(\hat{\Psi}) + \theta'\hat{F}^{n-\theta}(\hat{\Psi}), \tag{119}$$

$$\tag{120}$$

$$\hat{A}_T(\hat{U}^{n,k})(\hat{\Psi}) + \alpha\theta\hat{A}_E(\hat{U}^n)(\hat{\Psi}) \tag{121}$$

$$+\theta\hat{A}_P(\hat{U}^n)(\hat{\Psi}) + \hat{A}_I(\hat{U}^n)(\hat{\Psi}) = -\beta\theta\hat{A}_E(\hat{U}^{n-1})(\hat{\Psi}) + \theta\hat{F}^{n-\theta}(\hat{\Psi}). \tag{122}$$
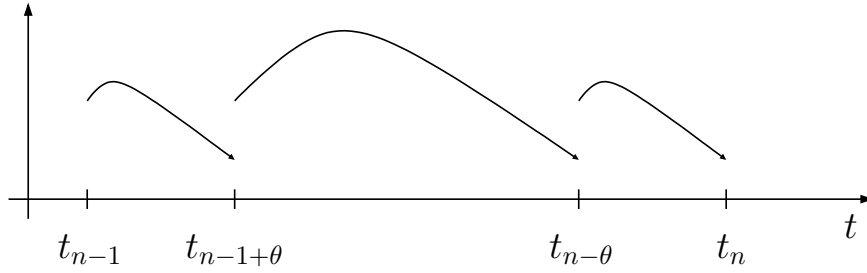
Figure 40: Time step computation using the Fractional-Step-$\theta$ scheme.

**8.1.2.3 Resulting time discretized problems**   With the help of the previous considerations, we formulate a statement for the time-discretized equations:

**Problem 8.14.** *Let the semi-linear form $\hat{A}(\cdot)(\cdot)$ be formulated in terms of the previous arrangement, such that*

$$\hat{A}(\hat{U})(\hat{\Psi}) := \hat{A}_T(\hat{U})(\hat{\Psi}) + \hat{A}_I(\hat{U})(\hat{\Psi}) + \hat{A}_E(\hat{U})(\hat{\Psi}) + \hat{A}_P(\hat{U})(\hat{\Psi}).$$

*After time discretization, let the time derivatives are approximated with*

$$\hat{A}_T(\hat{U})(\hat{\Psi}) \approx \hat{A}_T(\hat{U}^{n,k})(\hat{\Psi}),$$

*such that the time-discretized semi-linear form reads*

$$\hat{A}(\hat{U}^n)(\hat{\Psi}) := \hat{A}_T(\hat{U}^{n,k})(\hat{\Psi}) + \hat{A}_I(\hat{U}^n)(\hat{\Psi}) + \hat{A}_E(\hat{U}^n)(\hat{\Psi}) + \hat{A}_P(\hat{U}^n)(\hat{\Psi}).$$

*Then, we aim to find $\hat{U}^n = \{\hat{v}_f^n, \hat{v}_s^n, \hat{u}_f^n, \hat{u}_s^n, \hat{p}_f^n, \hat{p}_s^n\} \in \widehat{X}_D^0$, where $\widehat{X}_D^0 := \{\hat{v}_f^D + \hat{V}_{f,\hat{v}}^0\} \times \hat{L}_s \times \{\hat{u}_f^D + \hat{V}_{f,\hat{u}}^0\} \times \{\hat{u}_s^D + \hat{V}_s^0\} \times \hat{L}_f^0 \times \hat{L}_s^0$ and $\widehat{X} = \hat{V}_{f,\hat{v}}^0 \times \hat{L}_s \times \hat{V}_{f,\hat{u},\widehat{\Gamma}_i}^0 \times \hat{V}_s^0 \times \hat{L}_f^0 \times \hat{L}_s^0$, for all $n = 1, 2, \ldots, N$ such that*

$$\hat{A}(\hat{U}^n)(\hat{\Psi}) = \widehat{F}(\hat{\Psi}) \quad \forall \hat{\Psi} \in \widehat{X},$$

*where this equation is treated with one specific time-stepping scheme as introduced previously.*

**Remark 8.15.** *Detailed discussions and a nice overview on time-stepping schemes for flow problems (incompressible Navier-Stokes) and their formulations in terms of One-Step-$\theta$ schemes and Fractional-Step-$\theta$ are provided in [229], pp. 161ff.*

**Remark 8.16** (Newmark scheme [141, 251, 252] for temporal solid discretization)**.** *We notice that the standard discretization for solid equations is based on the so-called Newmark scheme, which avoids splitting into a first-order mixed system. The relation to special cases of One-Step-$\theta$ schemes (in particular Crank-Nicolson) is discussed in [13].* ⋄

**Remark 8.17** (Geometrical conservation law)**.** *Using the $ALE_{dm}$ scheme for time discretization, there have been studies [79, 91, 92, 176] that convergence is influenced by the discretization of the mesh motion velocity and also depends if ALE conservative schemes are used. Such studies are open questions for $ALE_{fx}$ schemes. Several examples and ideas are presented in [176], p. 71.* ⋄

## 8.1.3 Numerical observations for long-term FSI computations using the FSI 2 benchmark [140]

Let us substantiate the previous algorithms with numerical examples. Specifically, we study the fluid-structure interaction benchmark test FSI 2 [140]. To detect numerical artefacts is a delicate task, therefore, we study (qualitative) convergence with respect to space and time on three different (globally-refined) mesh levels with $1914, 7176$ and $27744$ degrees of freedom using the $Q_2^c/P_1^{dc}$ element (which is introduced in the next section). Moreover, we use three different time levels with the time steps $k = 0.01, 0.005$ and $0.001$. It is sufficient to study the results for the drag evaluation because we observed the same qualitative behavior for all the four quantities of interest (the $x$- and the $y$-displacement, the drag, and the lift).

**Remark 8.18** (FSI 1,2,3). *As important notice we remark that there have been three benchmarks suggested FSI 1, FSI 2 and FSI 3. The first test is stationary can be either computed with a stationary code or a nonstationary code using the implicit Euler scheme. The second and third benchmarks are nonstationary. Here, FSI 2 has a lower Reynold's number and would lead without an elastic beam also to a stationary solution whereas FSI 3 has high inflow. The particular difficulty in FSI 2 is that the beam leads to larger deformations (good MMPDE necessary!) than FSI 3 and the coupling conditions are very important since the oscillations are only caused the fluid-structure interaction. In FSI 3, the beam ocsillationsa are mainly caused by the non-symmetric cylindric boundary though.*

Specifically, we are interested in the following:

- The detection of instabilities (or even the blow-up of solutions in finite time) for the ordinary (i.e., unstabilized) Crank-Nicolson scheme. If we observe any, we are able to resolve them by the choice of a sufficiently small time step.

- Finally, we compare the standard second-order time-stepping schemes for the simulation of nonstationary fluid flows/fluid-structure interactions such as the Crank-Nicolson scheme, the shifted Crank-Nicolson scheme, and the Fractional-Step-$\theta$ scheme.
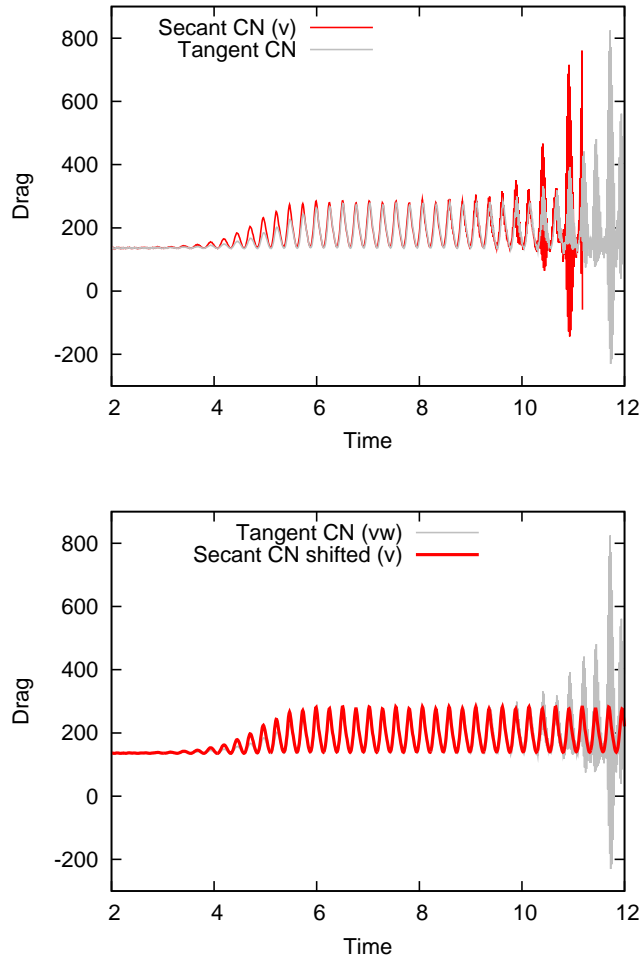


Figure 41: Blow-up (using the time step $k = 0.01$) of the unstabilized Crank-Nicolson schemes (secant and tangent) whereas the shifted Crank-Nicolson schemes is stable throughout the whole time interval. We notice that the secant Crank-Nicolson scheme exhibits the instabilities earlier than the tangent version. The unit of the time axis is $s$, whereas the drag unit is $kg/m\,s^2$. Related figures published in [203].

*Configuration*

The computational domain has length $L = 2.5m$ and height $H = 0.41m$. The circle center is positioned at $C = (0.2m, 0.2m)$ with radius $r = 0.05m$. The elastic beam has length $l = 0.35m$ and height $h = 0.02m$. The right lower end is positioned at $(0.6m, 0.19m)$, and the left end is attached to the circle.
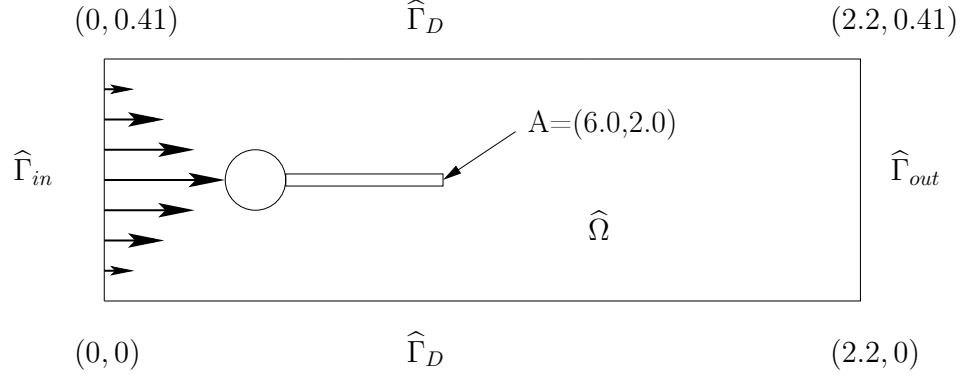
$(0, 0.41)$ $\widehat{\Gamma}_D$ $(2.2, 0.41)$

$\widehat{\Gamma}_{in}$

A=(6.0, 2.0)

$\widehat{\Omega}$

$\widehat{\Gamma}_{out}$

$(0, 0)$ $\widehat{\Gamma}_D$ $(2.2, 0)$

Figure 42: Flow around cylinder with elastic beam with circle-center $C = (0.2, 0.2)$ and radius $r = 0.05$.

*Boundary conditions*

For the upper, lower, and left boundaries, the 'no-slip' conditions for velocity and no zero displacement for structure are given. At the outlet $\hat{\Gamma}_{out}$, the 'do-nothing' outflow condition is imposed leading to a zero mean value, i.e., $\int_{\widehat{\Gamma}_{out}} p\,ds$ of the pressure at this part of the boundary.

A parabolic inflow velocity profile is given on $\hat{\Gamma}_{in}$ by

$$v_f(0, y) = 1.5\bar{U}\frac{4y(H - y)}{H^2}, \quad \bar{U} = 1.0ms^{-1}.$$

*Initial conditions*

For the non-steady tests one should start with a smooth increase of the velocity profile in time. We use

$$v_f(t; 0, y) = \begin{cases} v_f(0, y)\frac{1 - \cos(\frac{\pi}{2}t)}{2} & \text{if } t < 2.0s \\ v_f(0, y) & \text{otherwise.} \end{cases}$$

The term $v_f(0, y)$ is already explained above.

*Quantities of comparison and their evaluation*

1) $x$- and $y$-deflection of the beam at $A(t)$.

2) The forces exerted by the fluid on the whole body, i.e., drag force $F_D$ and lift force $F_L$ on the rigid cylinder and the elastic beam. They form a closed path in which the forces can be computed with the help of line integration. The formula is evaluated on the fixed reference domain $\hat{\Omega}$ and reads:

$$(F_D, F_L) = \int_{\hat{S}} \hat{J}\hat{\sigma}_{all}\hat{F}^{-T} \cdot \hat{n}\,d\hat{s} = \int_{\hat{S}(\text{circle})} \hat{J}\hat{\sigma}_f\hat{F}^{-T} \cdot \hat{n}_f\,d\hat{s} + \int_{\hat{S}(\text{beam})} \hat{J}\hat{\sigma}_f\hat{F}^{-T} \cdot \hat{n}_f\,d\hat{s}. \tag{123}$$

The quantities of interest for this time dependent test case are represented by the mean value, amplitudes, and frequency of $x$- and $y$-deflections of the beam in one time period $T$ of oscillations.

*Parameters*

We choose for our computation the following parameters. For the fluid we use $\varrho_f = 10^3 kgm^{-3}$, $\nu_f = 10^{-3}m^2s^{-1}$. The elastic structure is characterized by $\varrho_s = 10^4 kgm^{-3}$, $\nu_s = 0.4$, $\mu_s = 5 * 10^5 kgm^{-1}s^{-2}$.

**Example 8.19** (Computation of the Reynolds number for FSI 2). *As small example, let us compute the Reynolds number defined in 5.38 of this test. As characteristic lenght, we choose the diameter of the cylinder,*

*D = 2r = 0.1m. As characteristic velocity, we take the mean velocity, $\bar{V} = \frac{2}{3}V(0, H/2, t)$ where V is just the parabolic inflow profile from above and evaluated in the middle H/2 where we have the hightest velocity:*

$$V = v_f(0, H/2) = 1.5 \times 1.0 \frac{4y(H - H/2)}{H^2} = 1.5,$$

*where we set $\bar{U} = 1.0$. Then,*

$$\bar{V} = 1.5 \times V = \frac{2}{3}1.5 = 1.$$

*This yields the Reynolds number*
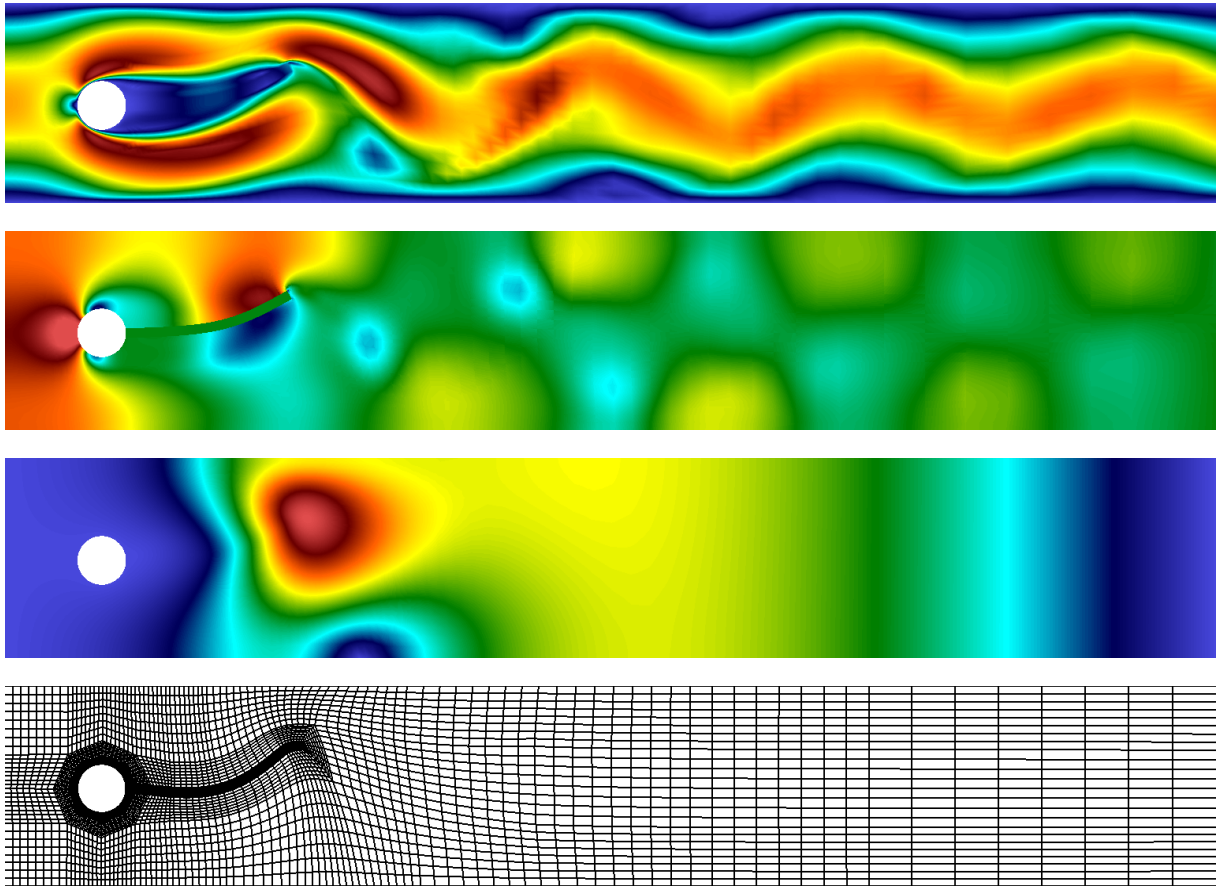
$$Re = \frac{LV}{\nu} = \frac{0.1 \times 1}{10^{-3}} = 100.$$



Figure 43: Numerical simulation of the FSI 2 benchmark problem: magnitude of the velocity field (displaying the van Karman vorticity street), pressure field, and magnitude of the displacement field and deformed mesh $\Omega(t)$. In all figures, red indicates high values and blue low values.
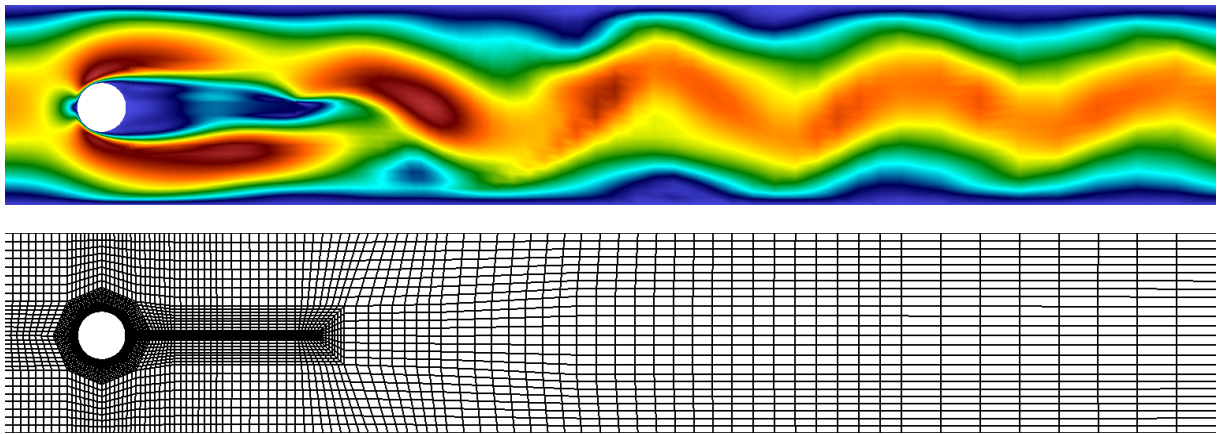
Figure 44: Magnitude of the velocity field and mesh of the reference domain $\widehat{\Omega}$ in which the computation was performed using the $\text{ALE}_{fx}$ approach. In order to display these findings in the deformed (physical) domain $\Omega$ as shown in Figure 43, the operation $\hat{\mathcal{A}}(\hat{x}, t) = x = \hat{x} + \hat{u}(\hat{x}, t)$ must be applied; either in your simulator or in the visualization program.
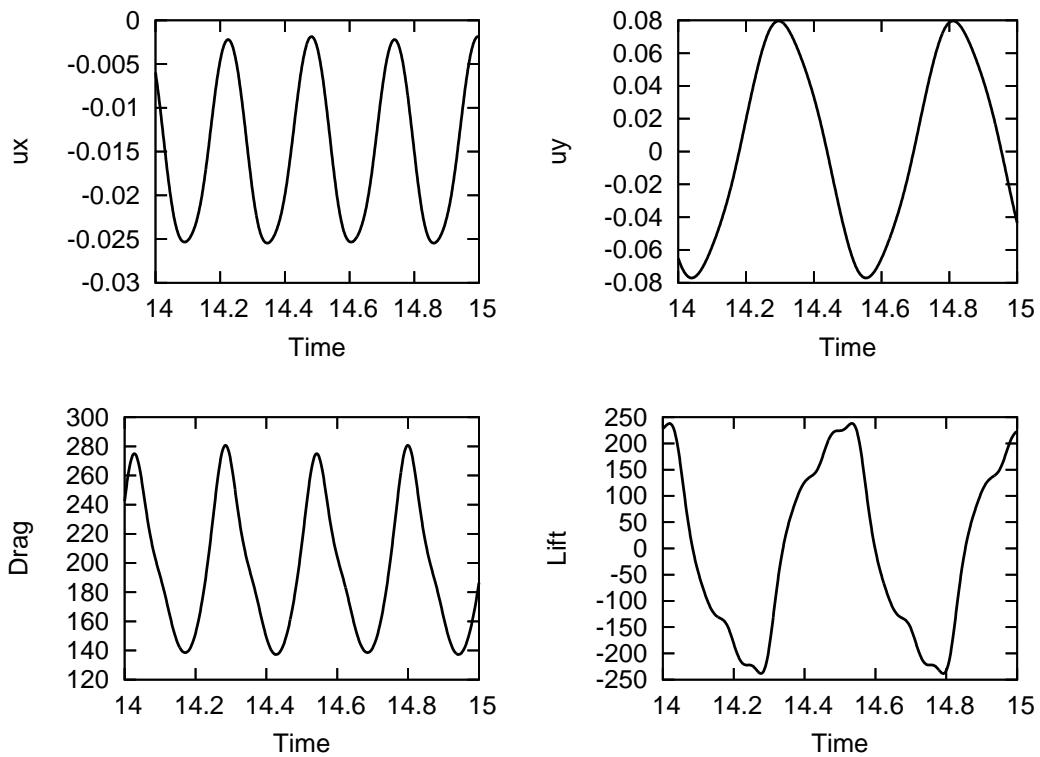


Figure 45: FSI 2. Top: the deflections of the beam, $u_x(A)$ and $u_y(A)$. Bottom: the drag and the lift computations over the path $S$ of the cylinder and the interface between the fluid and the structure.
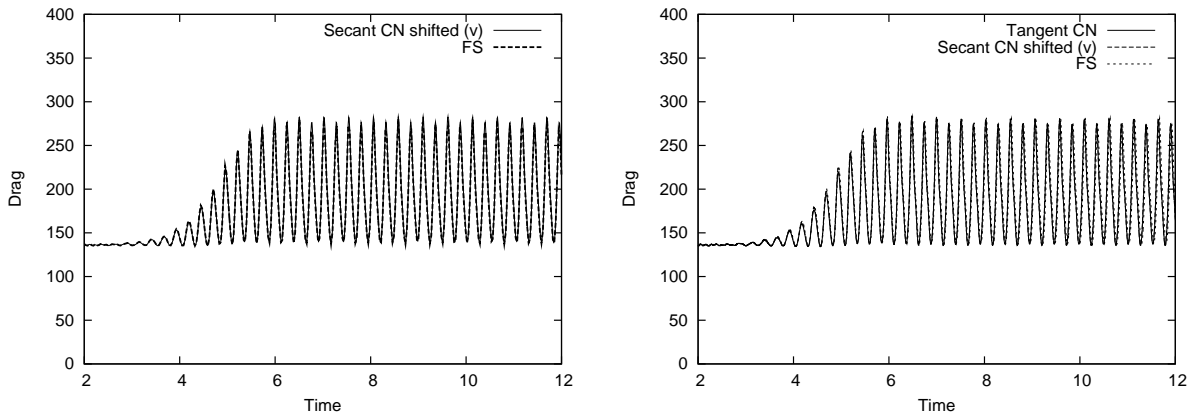
Figure 46: Top: stable solution (using the large time step $k = 0.01$) computed with the shifted Crank-Nicolson and the Fractional-Step-$\theta$ scheme. Recall the blow-up of the unstabilized Crank-Nicolson scheme in this case. Right: using a smaller time step $k = 0.001$ yields stable solutions for any time-stepping scheme. The unit of the time axis is $s$, whereas the drag unit is $kg/m\,s^2$.

**Observation 1**

We observed in our computations that there are only minor differences in the drag evaluation computed with the unstabilized Crank-Nicolson scheme using the different ALE convection term discretizations defined in the problems above. Specifically, we observed unstable behavior (blow-up) for computations over long-term intervals, as illustrated in Figure 41. Naturally, we expected this behavior from our previous numerical analysis.

**Observation 2**

As expected, the shifted Crank-Nicolson scheme and the Fractional-Step-$\theta$ scheme showed no stability problems in long-term computations, even for the large time step $k = 0.01$ (see the top of Figure 46). This result indicates that the instabilities induced by the ALE convection term have minor consequences, and our observation is in agreement with the statement in [92]. Furthermore, all time-stepping schemes are stable over the entire time interval for a sufficiently small time step $k = 0.001$; (see the bottom Figure 46).

**Observation 3**

We finally compare in Figure 47 the shifted Crank-Nicolson scheme and the backward Euler scheme in order to show that the latter time-stepping method is too dissipative and will not cause the elastic beam to keep periodic-in-time oscillations.
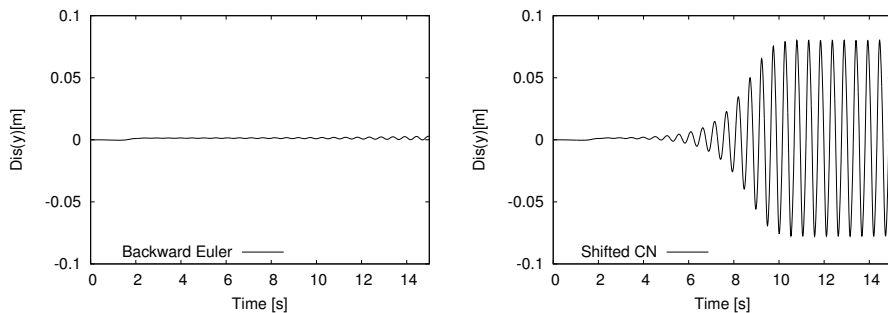


Figure 47: Comparison of the $u_y$ displacement using the backward Euler scheme (left) and the shifted Crank-Nicolson scheme (right). These findings show that it is important to choose the 'correct' time-stepping scheme. For nonstationary flow, the backward Euler scheme is too dissipative and is not able to compute oscillatory flow as the shifted CN scheme does.

### 8.1.4 Time stability for fluid-structure interaction

In the following, we consider the stability of the monolithically coupled problem.

Following Formaggia and Nobile [92], we consider the following modification of the classical Crank-Nicolson scheme (i.e., it is a Gauss-Legendre implicit second-order Runge-Kutta method)

$$v_f^{n+1} - v_f^n = kg\left(t_{n+\frac{1}{2}}, \frac{v_f^{n+1} + v_f^n}{2}\right), \tag{124}$$

where $g(t, v_f(t))$ denotes the right-hand-side of a differential equation. This modified scheme can be reduced to the classical scheme for a linear advection-diffusion problem on a fixed domain and time-independent coefficients. Moreover, the *geometric conservation law* is satisfied for this scheme in two-dimensional domains [92, 176] if the ALE transformation is reconstructed linearly in time (i.e., using a constant in time-mesh velocity $w$). We consider this aspect in more detail below.

To derive a stability result for the Crank-Nicolson scheme, we provide some further notation. In the rest of this section, we are going to work with an ALE mapping that is defined from the previous time step $t_{n-1}$ to the the present time step $t_n$. This is an extension to our previous definitions, where the reference configuration coincided with the configuration at the initial time step, i.e., $\Omega^0 = \widehat{\Omega}$. In the following, we denote by $\Omega^n$ the reference configuration at time step $t_n$ and we use $v^n \in \Omega^n$ as an approximation of $v(t_n)$. This value is transported from $\Omega^n$ to any other configuration $\Omega^l$ (for $l \neq n$) through the ALE mapping ([176]):

$$\hat{\mathcal{A}}_{n,l} = \hat{\mathcal{A}}_l \circ \hat{\mathcal{A}}_n^{-1}.$$

For the sake of notation, we omit the explicit representation of the ALE mapping when we work with the value $v^n$ in a domain $\Omega_l$ with $n \neq l$, i.e.,

$$\int_{\Omega_l} v^n \, dx := \int_{\Omega_l} v^n \circ \hat{\mathcal{A}}_{n,l} \, dx, \quad \text{and} \quad ||v^n||_{\Omega^l} := ||v^n \circ \hat{\mathcal{A}}_{n,l}||_{\Omega^l},$$

which we use frequently in the following.

With these preparations, the application of the relation (124) to the Navier-Stokes equations in a moving domain reads in the weak formulation:

**Problem 8.20.** *Find $\{v_f, p_f\} \in \{v_f^D + V_f^0\} \times L_f^0$, such that $v_f(0) = v_f^0$ is satisfied, and for $n = 0, 1, 2, \ldots, N$ holds:*

$$\rho_f\left(v_f^{n+1} - v_f^n, \psi^v\right)_{\Omega_f^{n+1}} + k\rho_f\left(\left[v_f^{n+\frac{1}{2}} - w^{n+1}\right] \cdot \nabla\left(\frac{v_f^{n+1} + v_f^n}{2}\right), \psi^v\right)_{\Omega_f^{n+1}} \tag{125}$$

$$+ 2k\rho_f\nu_f\left(D\left(\frac{v_f^{n+1} + v_f^n}{2}\right), \nabla\psi^v\right)_{\Omega_f^{n+1}} - k\left(\frac{p_f^{n+1} + p_f^n}{2}, \nabla \cdot \psi^v\right)_{\Omega_f^{n+1}} = 0 \quad \forall \psi^v \in V_f^0, \tag{126}$$

$$\left(\nabla \cdot \left(\frac{v_f^{n+1} + v_f^n}{2}\right), \psi^p\right)_{\Omega_f^{n+1}} = 0 \quad \forall \psi^p \in L_f^0, \tag{127}$$

*where $v_f^{n+\frac{1}{2}}$ can be chosen as $v_f^{n+\frac{1}{2}} = 2^{-1}(v_f^{n+1} + v_f^n)$ to obtain a fully implicit nonlinear convection term. Otherwise, one can approximate $v_f^{n+\frac{1}{2}}$ by extrapolating the former time steps $v_f^{n-1}$ and $v_f^{n-2}$ such that $v_f^{n+\frac{1}{2}} = \frac{1}{2}\left(3v_f^{n-1} - v_f^{n-2}\right)$.*

We supplement this scheme with homogeneous boundary conditions and admissible initial conditions:

$$v_f^n = 0 \quad \text{on } \partial\Omega_f, \quad n = 1, 2, \ldots, N+1 \tag{128}$$

$$v_f^0 = v_0 \quad \text{in } \Omega_f^0 = \widehat{\Omega}_f. \tag{129}$$

In the case of Neumann conditions, we add in the first equation of (125) the term

$$2k\rho_f\nu_f\left\langle D\Big(\frac{v_f^{n+1}+v_f^n}{2}\Big)n_f,\psi^v\right\rangle_{\Gamma_{f,N}^{n+1}}. \tag{130}$$

As usual, this is the outcome of partial integration of the stress term. This term must be incorporated in the case of fluid-structure interaction problems because it contributes to the energy exchange on the interface.

For the structure subproblem, we also use the Crank-Nicolson scheme. First, we state the following weak form of the structure Equations (40):

**Problem 8.21.** *Find* $\{\hat{v}_s,\hat{u}_s\}\in\hat{L}_s\times\{\hat{u}_s^D+\hat{V}_s^0\}$, *such that* $\hat{v}_s(0)=\hat{v}_s^0$ *and* $\hat{u}_s(0)=\hat{u}_s^0$ *are satisfied, and for almost all time steps* $t\in I$ *holds:*

$$\hat{\rho}_s(\partial_t\hat{v}_s,\hat{\psi}^v)_{\widehat{\Omega}_s}+(\widehat{F\Sigma},\widehat{\nabla}\hat{\psi}^v)_{\widehat{\Omega}_s}-\langle\widehat{F\Sigma}\hat{n}_s,\hat{\psi}^v\rangle_{\widehat{\Gamma}_{s,N}} \tag{131}$$

$$+\gamma_w(\hat{v}_s,\hat{\psi}^v)_{\widehat{\Omega}_s}+\gamma_s(\hat{\epsilon}(\hat{v}_s),\widehat{\nabla}\hat{\psi}^v)_{\widehat{\Omega}_s}-\gamma_s\langle\hat{\epsilon}(\hat{v}_s)\hat{n}_s,\hat{\psi}^v\rangle_{\widehat{\Gamma}_{s,N}}=0 \quad\forall\hat{\psi}^v\in\hat{V}_s^0, \tag{132}$$

$$\hat{\rho}_s(\partial_t\hat{u}_s,\hat{\psi}^u)_{\widehat{\Omega}_s}-\hat{\rho}_s(\hat{v}_s,\hat{\psi}^u)_{\widehat{\Omega}_s}=0 \quad\forall\hat{\psi}^u\in\hat{L}_s. \tag{133}$$

*Problem 8.21 is obtained from the weak STVK solid problem, neglecting volume forces.*

Temporal discretization of the structure Problem 8.21 with the Crank-Nicolson scheme yields:

**Problem 8.22.** *Find* $\{\hat{v}_s^{n+1},\hat{u}_s^{n+1}\}\in\hat{L}_s\times\{\hat{u}_s^D+\hat{V}_s^0\}$ *for* $n=0,1,2,\ldots,N$:

$$\hat{\rho}_s\frac{1}{k}\Big(\hat{v}_s^{n+1}-\hat{v}_s^n,\hat{\psi}^v\Big)_{\widehat{\Omega}_s}+\theta\big(\widehat{F\Sigma}(\hat{u}_s^{n+1}+\hat{u}_s^n),\widehat{\nabla}\hat{\psi}^v\big)_{\widehat{\Omega}_s} \tag{134}$$

$$-\theta\big\langle\widehat{F\Sigma}(\hat{u}_s^{n+1}+\hat{u}_s^n)\hat{n}_s,\hat{\psi}^v\big\rangle_{\widehat{\Gamma}_{s,N}}+\gamma_w\theta\big(\hat{v}_s^{n+1}+\hat{v}_s^n,\hat{\psi}^v\big)_{\widehat{\Omega}_s} \tag{135}$$

$$+\gamma_s\theta\big(\hat{\epsilon}(\hat{v}_s^{n+1}+\hat{v}_s^n),\widehat{\nabla}\hat{\psi}^v\big)_{\widehat{\Omega}_s}-\gamma_s\theta\big\langle\hat{\epsilon}(\hat{v}_s^{n+1}+\hat{v}_s^n)\hat{n}_s,\hat{\psi}^v\big\rangle_{\widehat{\Gamma}_{s,N}}=0 \quad\forall\hat{\psi}^v\in\hat{V}_s^0, \tag{136}$$

$$\hat{\rho}_s\frac{1}{k}\Big(\hat{u}_s^{n+1}+\hat{u}_s^n,\hat{\psi}^u\Big)_{\widehat{\Omega}_s}-\hat{\rho}_s\theta\big(\hat{v}_s^{n+1}+\hat{v}_s^n,\hat{\psi}^u\big)_{\widehat{\Omega}_s}=0 \quad\forall\hat{\psi}^u\in\hat{L}_s, \tag{137}$$

*with* $\theta=0.5$.

First, we recall the coupling conditions that are required for an implicit solution algorithm:

$$\hat{u}_f^{n+1}=\hat{u}_s^{n+1}\quad\text{on }\widehat{\Gamma}_i,\qquad\hat{w}^{n+1}=\frac{1}{k}(\hat{u}_f^{n+1}-\hat{u}_f^n)\quad\text{in }\widehat{\Omega}_f, \tag{138}$$

$$2^{-1}(v_f^{n+1}+v_f^n)=w_f^{n+1}\quad\text{on }\Gamma_i,\qquad\hat{u}_s^{n+1}=0\quad\text{on }\widehat{\Gamma}_{s,D}. \tag{139}$$

Using the Crank-Nicolson scheme for temporal discretization, the second relation in (138), can be further developed into

$$\hat{w}^{n+1}=\frac{1}{k}(\hat{u}_f^{n+1}-\hat{u}_f^n)=\frac{1}{2}(\hat{v}_f^{n+1}+\hat{v}_f^n). \tag{140}$$

Using these coupling conditions with a slight modification of the second term,

$$v_f^{n+1}=w_f^{n+1}\quad\text{on }\Gamma_i,$$

an unconditioned stability (without restrictions on the time-step size) was obtained by Fernández and Gerbeau [84]. In their study, the authors use the backward Euler scheme to discretize the fluid. The structure is discretized using a second-order mid-point rule. In this thesis, we upgrade these findings to a stability result in which the Crank-Nicolson time discretization scheme is performed for the both subproblems. Moreover, we incorporate the damping of the structure equations.

To get an analogous stability result for the time-discretized Crank-Nicolson scheme on moving domains, we use the methodology used in [91, 92, 176]. It holds:

**Lemma 8.23.** *For the time-discretized solution of the Crank-Nicolson scheme* (125) *holds:*

$$\rho_f||v_f^{n+1}||_{\Omega_f^{n+1}}^2 + k\rho_f\nu_f||D(v_f^{n+1}+v_f^n)||_{\Omega_f^{n+1}}^2 + \frac{k\rho_f}{4}\int_{\Omega_f^{n+1}}\nabla\cdot w^{n+\frac{1}{2}}\,|v_f^{n+1}+v_f^n|^2\,\mathrm{d}x$$

$$= \rho_f||v_f^n||_{\Omega_f^{n+1}}^2,$$

*For* $\nabla\cdot w > 0$ *for all* $x \in \Omega_f$ *and for all* $t \in I$ *(a uniform contraction of the mesh), the CN scheme is unconditionally stable. Otherwise, the ALE convection term causes instabilities that restricts the choice of the time step size. Specifically, it holds:*

$$k \leq \frac{1}{\delta_w}.$$

*Proof.* To proof the assertion, we use the arguments presented in [92, 176]. In Problem 8.20, we take the test functions $\psi^v = v_f^{n+1} + v_f^n$ and $\psi^p = p_f^{n+1} + p_f^n$. We observe that with this choice, the pressure term in the first equation can be removed thanks to the incompressibility condition. The mass term can be written as

$$\rho_f(v_f^{n+1} - v_f^n, v_f^{n+1} + v_f^n)_{\Omega_f^{n+1}} = \rho_f||v_f^{n+1}||_{\Omega_f^{n+1}}^2 + \rho_f||v_f^n||_{\Omega_f^{n+1}}^2. \tag{141}$$

Using the identity

$$\left(D(v_f^{n+1}),\nabla v_f^{n+1}\right)_{\Omega_f^{n+1}} = \left(D(v_f^{n+1}),D(v_f^{n+1})\right)_{\Omega_f^{n+1}} \quad \forall n = 0,1,2,\ldots,$$

brings us to

$$2k\rho_f\nu_f\left(D\left(\frac{v_f^{n+1}+v_f^n}{2}\right),D(v_f^{n+1}+v_f^n)\right)_{\Omega_f^{n+1}} = k\rho_f\nu_f||D(v_f^{n+1}+v_f^n)||_{\Omega_f^{n+1}}^2. \tag{142}$$

So far, we assume that homogenous Dirichlet conditions are prescribed on the outer boundaries. Otherwise, the following term would remain on Neumann parts:

$$-\frac{k}{2}\langle\sigma(v_f^{n+1}+v_f^n)n_f, v_f^{n+1}+v_f^n\rangle_{\Gamma_{f,N}^{n+1}}. \tag{143}$$

It remains to consider the convection term using the fully nonlinear discretization $v_f^{n+\frac{1}{2}} = 2^{-1}(v_f^{n+1}+v_f^n)$. We plug-in the test function $\psi^v = v_f^{n+1} + v_f^n$, which gives us:

$$k\rho_f\left(\left[\left(\frac{v_f^{n+1}+v_f^n}{2}\right)-w^{n+1}\right]\cdot\nabla\left(\frac{v_f^{n+1}+v_f^n}{2}\right), v_f^{n+1}+v_f^n\right)_{\Omega_f^{n+1}}$$

$$= \frac{k\rho_f}{4}\int_{\Omega_f^{n+1}}\left[(v_f^{n+1}+v_f^n)-w^{n+1}\right]\cdot\nabla\,|v_f^{n+1}+v_f^n|^2\,\mathrm{d}x.$$

Using the explicit representation of the integral and using integration by parts, yields

$$\frac{k\rho_f}{4}\int_{\Omega_f^{n+1}}\left[(v_f^{n+1}+v_f^n)-w^{n+1}\right]\cdot\nabla\,|v_f^{n+1}+v_f^n|^2\,\mathrm{d}x \tag{144}$$

$$= \frac{k\rho_f}{4}\int_{\Gamma_{f,N}^{n+1}}\left[(v_f^{n+1}+v_f^n)-w^{n+1}\right]\cdot n_f\,|v_f^{n+1}+v_f^n|^2\,\mathrm{d}x \tag{145}$$

$$- \frac{k\rho_f}{4}\int_{\Omega_f^{n+1}}\nabla\cdot\left[(v_f^{n+1}+v_f^n)-w^{n+1}\right]\,|v_f^{n+1}+v_f^n|^2\,\mathrm{d}x. \tag{146}$$

The boundary term vanishes, thanks again to the homogeneous Dirichlet boundary conditions. Using the incompressibility of the fluid, brings us to

$$\frac{k\rho_f}{4}\int_{\Omega_f^{n+1}}\nabla\cdot[w^{n+1}]\,|v_f^{n+1}+v_f^n|^2\,\mathrm{d}x. \tag{147}$$

126

We note that the last step is admissible because we are still working in spatially infinite-dimensional spaces, where the incompressibility of the fluid is satisfied in each time step. This property gets lost after spatial discretization and the incompressibility term requires attention (see e.g., [176]). Adding the contributions (141), (142), and (147) finishes the proof. □

We emphasize, that fluid flows on moving meshes with a Crank-Nicolson time discretization only serve for a conditioned stability (see Lemma 8.23). Consequently, we cannot expect a better result for the overall problem.

We use the Equations (125) with the stability result proven in Lemma 8.23. For fluid-structure interaction, we must consider the interface term (we refer to the term (143)):

$$-\frac{k}{2}\langle \sigma_f(v_f^{n+1}+v_f^n)n_f, v_f^{n+1}+v_f^n \rangle_{\Gamma_i^{n+1}}. \tag{148}$$

The coupling term on the interface that is needed for the next statement reads:

$$\sigma_f(v_f^{n+1}+v_f^n)n_f + \widehat{F}\widehat{\Sigma}(\hat{u}_s^{n+1}+\hat{u}_s^n)\hat{n}_s + \gamma_s\hat{\epsilon}(\hat{v}_s^{n+1}+\hat{v}_s^n)\hat{n}_s = 0. \tag{149}$$

**Theorem 8.24.** *Let the fluid-structure interaction problem be coupled via an implicit solution algorithm and let both subproblems be time-discretized with the second order Crank-Nicolson scheme. The coupled problem is assumed to be isolated, i.e., $v_f^{n+1} = 0$ on $\partial\Omega_f \setminus \Gamma_i$ and $\widehat{F}\widehat{\Sigma}(\hat{u}_s^{n+1})\hat{n}_s = 0$ on $\partial\widehat{\Omega}_s \setminus \widehat{\Gamma}_i$. Further, in the case of strong damping $\gamma_w > 0$, let $\hat{\epsilon}(\hat{v}_s^{n+1})\hat{n}_s = 0$ on $\partial\widehat{\Omega}_s \setminus \widehat{\Gamma}_i$. Then,*

$$\rho_f||v_f^{n+1}||^2_{\Omega_f^{n+1}} + \hat{\rho}_s||\hat{v}_s^{n+1}||^2_{\widehat{\Omega}_s} + \int_{\widehat{\Omega}_s} W\big(\widehat{F}(\hat{u}_s^{n+1})\big)\,\mathrm{d}x$$

$$+ k\rho_f\nu_f||D(v_f^{n+1}+v_f^n)||^2_{\Omega_f^{n+1}} + \frac{k\rho_f}{4}\int_{\Omega_f^{n+1}} \nabla\cdot w^{n+1}|v_f^{n+1}+v_f^n|^2\,\mathrm{d}x$$

$$+ \frac{k\gamma_w}{2}||\hat{v}_s^{n+1}||^2_{\widehat{\Omega}_s} + \frac{k\gamma_s}{2}||\hat{\epsilon}(\hat{v}_s^{n+1})||^2_E$$

$$\leq \rho_f||v_f^n||^2_{\Omega_f^{n+1}} + \rho_s||\hat{v}_s^n||^2_{\widehat{\Omega}_s} + \int_{\widehat{\Omega}_s} W\big(\widehat{F}(\hat{u}_s^n)\big)\,\mathrm{d}x$$

$$+ \frac{k\gamma_w}{2}||\hat{v}_s^n||^2_{\widehat{\Omega}_s} + \frac{k\gamma_s}{2}||\hat{\epsilon}(\hat{v}_s^n)||^2_E.$$

*Proof.* The fluid subproblem is attacked with the help of Lemma 8.23 and by taking the test functions $\psi_f^v = \frac{1}{2}(v_f^{n+1}+v_f^n)$ and $\psi_f^p = \frac{1}{2}(p_f^{n+1}+p_f^n)$. With this choice, the following two terms remain on the interface $\Gamma_i$:

$$-\frac{k}{2}\langle \sigma_f(v_f^{n+1}+v_f^n)n_f, v_f^{n+1}+v_f^n \rangle_{\Gamma_i^{n+1}},$$

$$\frac{k\rho_f}{4}\int_{\Gamma_i^{n+1}} \big[(v_f^{n+1}+v_f^n) - w^{n+1}\big]\cdot n_f|v_f^{n+1}+v_f^n|^2\,\mathrm{d}x.$$

The first term appears due to integration by parts of the fluid stress term and it becomes part of the coupling condition on $\Gamma_i$. The second term is obtained in (144) by using partial integration in the convection term. This term vanishes on the interface because we require the coupling condition (see (138)):

$$\frac{1}{2}(v_f^{n+1}+v_f^n) - w^{n+1} = 0 \quad \text{on } \Gamma_i^{n+1}.$$

In the following, we consider the structure subproblem 8.22. We take as test functions $\hat{\psi}^v := \hat{\psi}_s^v = \frac{1}{k}(\hat{u}_s^{n+1}-\hat{u}_s^n)$ and $\hat{\psi}^u := \hat{\psi}_s^u = \frac{1}{k}(\hat{v}_s^{n+1}-\hat{v}_s^n)$ in the Equations (134). This choice of test functions is admissible, thanks to the coupling conditions (138). This choice implies $\hat{\psi}_f^v = \hat{\psi}_s^v$ on $\widehat{\Gamma}_i$, i.e.,

$$\hat{\psi}_s^v = \frac{1}{k}(\hat{u}_s^{n+1}-\hat{u}_s^n) = \frac{1}{2}(\hat{v}_f^{n+1}+\hat{v}_f^n) = \hat{\psi}_f^v.$$

Subtraction of the second equation from the first equation in Problem 8.22 and multiplication through by $k$ leads to

$$
\begin{aligned}
&\hat{\rho}_s(\hat{v}_s^{n+1} + \hat{v}_s^n, \hat{v}_s^{n+1} - \hat{v}_s^n)_{\widehat{\Omega}_s} \\
&+ \frac{1}{2}\big(\widehat{F}\widehat{\Sigma}(\hat{u}_s^{n+1} + \hat{u}_s^n), \widehat{\nabla}(\hat{u}_s^{n+1} - \hat{u}_s^n)\big)_{\widehat{\Omega}_s} \\
&- \frac{1}{2}\langle\widehat{F}\widehat{\Sigma}(\hat{u}_s^{n+1} + \hat{u}_s^n)\hat{n}_s, \hat{u}_s^{n+1} - \hat{u}_s^n\rangle_{\widehat{\Gamma}_{s,N}} \\
&= 0.
\end{aligned}
$$

For the moment, we omit the damping terms. The mass term reads:

$$
\hat{\rho}_s||\hat{v}_s^{n+1}||_{\widehat{\Omega}_s}^2 - \hat{\rho}_s||\hat{v}_s^n||_{\widehat{\Omega}_s}^2 = 0. \tag{150}
$$

To treat the stress term, we use

$$
\frac{1}{2}\big(\widehat{F}\widehat{\Sigma}(\hat{u}_s^{n+1} + \hat{u}_s^n), \widehat{\nabla}(\hat{u}_s^{n+1} - \hat{u}_s^n)\big)_{\widehat{\Omega}_s} = \frac{1}{2}\big(\widehat{F}\widehat{\Sigma}(\hat{u}_s^{n+1} + \hat{u}_s^n), \widehat{F}(\hat{u}_s^{n+1} - \hat{u}_s^n)\big)_{\widehat{\Omega}_s}. \tag{151}
$$

With this, we proceed as in [84], to deduce:

$$
\frac{1}{2}\big(\widehat{F}\widehat{\Sigma}(\hat{u}_s^{n+1} + \hat{u}_s^n), \widehat{\nabla}(\hat{u}_s^{n+1} - \hat{u}_s^n)\big)_{\widehat{\Omega}_s} \tag{152}
$$

$$
= \frac{1}{2}\big(\partial_F W(\widehat{F}(\hat{u}_s^{n+1} + \hat{u}_s^n)), \widehat{F}(\hat{u}_s^{n+1} - \hat{u}_s^n)\big)_{\widehat{\Omega}_s} \tag{153}
$$

$$
= \int_{\widehat{\Omega}_s} W\big(\widehat{F}(\hat{u}_s^{n+1} - \hat{u}_s^n)\big)\,\mathrm{d}x \tag{154}
$$

$$
= \int_{\widehat{\Omega}_s} W\big(\widehat{F}(\hat{u}_s^{n+1})\big) - W\big(\widehat{F}(\hat{u}_s^n)\big)\,\mathrm{d}x. \tag{155}
$$

It remains to discuss the boundary terms. The data on outer boundaries vanish due to our assumption that we work in an isolated system. Thus, it remains to consider the interface term:

$$
-\frac{1}{2}\langle\widehat{F}\widehat{\Sigma}(\hat{u}_s^{n+1} + \hat{u}_s^n)\hat{n}_s, \hat{u}_s^{n+1} - \hat{u}_s^n\rangle_{\widehat{\Gamma}_i}. \tag{156}
$$

We remind the reader to recall the interface condition that is seen from the fluid side. Now we employ (140), such that

$$
-\frac{k}{2}\langle\sigma_f(v_f^{n+1} + v_f^n)n_f, v_f^{n+1} + v_f^n\rangle_{\Gamma_i^{n+1}} = -\frac{1}{2}\langle\sigma_f(v_f^{n+1} + v_f^n)n_f, u_f^{n+1} - u_f^n\rangle_{\Gamma_i^{n+1}}. \tag{157}
$$

Thus, by adding (156) and (157), we get

$$
-\frac{1}{2}\langle\sigma(v_f^{n+1} + v_f^n)n_f, u_f^{n+1} - u_f^n\rangle_{\Gamma_i^{n+1}} - \frac{1}{2}\langle\widehat{F}\widehat{\Sigma}(\hat{u}_s^{n+1} + \hat{u}_s^n)\hat{n}_s, \hat{u}_s^{n+1} - \hat{u}_s^n\rangle_{\widehat{\Gamma}_i} = 0, \tag{158}
$$

which corresponds to the already introduced strong form of the coupling conditions (except of the damping interface term). Finally, we consider the damping terms of the structure equations:

$$
\frac{\gamma_w}{2}\big(\hat{v}_s^{n+1} + \hat{v}_s^n, \hat{\psi}^v\big)_{\widehat{\Omega}_s} + \frac{\gamma_s}{2}\big(\hat{\epsilon}(\hat{v}_s^{n+1} + \hat{v}_s^n), \widehat{\nabla}\hat{\psi}^v\big)_{\widehat{\Omega}_s} - \frac{\gamma_s}{2}\big(\hat{\epsilon}(\hat{v}_s^{n+1} + \hat{v}_s^n)\hat{n}_s, \hat{\psi}^v\big)_{\widehat{\Gamma}_{s,N}} = 0.
$$

Taking again $\hat{\psi}_s^v = \frac{1}{k}(\hat{u}_s^{n+1} - \hat{u}_s^n)$ yields:

$$
\frac{\gamma_w}{2}\big(\hat{v}_s^{n+1} + \hat{v}_s^n, \hat{u}_s^{n+1} - \hat{u}_s^n\big)_{\widehat{\Omega}_s} + \frac{\gamma_s}{2}\big(\hat{\epsilon}(\hat{v}_s^{n+1} + \hat{v}_s^n), \widehat{\nabla}(\hat{u}_s^{n+1} - \hat{u}_s^n)\big)_{\widehat{\Omega}_s} = 0.
$$

Estimating the both terms by using the relation between the velocities and the displacements (i.e., (143)):

$$
\frac{\hat{u}_s^{n+1} - \hat{u}_s^n}{k} = \frac{1}{2}(\hat{v}_s^{n+1} + \hat{v}_s^n),
$$

yields for the first term (using the Young inequality):

$$\frac{\gamma_w}{2}(\hat{v}_s^{n+1} + \hat{v}_s^n, \hat{u}_s^{n+1} - \hat{u}_s^n)_{\widehat{\Omega}_s} \tag{159}$$

$$= \frac{k\gamma_w}{4}(\hat{v}_s^{n+1} + \hat{v}_s^n, \hat{v}_s^{n+1} + \hat{v}_s^n)_{\widehat{\Omega}_s} \tag{160}$$

$$= \frac{k\gamma_w}{4}||\hat{v}_s^{n+1} + \hat{v}_s^n||_{\widehat{\Omega}_s}^2 \tag{161}$$

$$\leq \frac{k\gamma_w}{2}(||\hat{v}_s^{n+1}||_{\widehat{\Omega}_s}^2 + ||\hat{v}_s^n||_{\widehat{\Omega}_s}^2). \tag{162}$$

The second term is treated in a similar fashion by using the definition of the energy norm (80):

$$\frac{\gamma_s}{2}\big(\hat{\epsilon}(\hat{v}_s^{n+1} + \hat{v}_s^n), \widehat{\nabla}(\hat{u}_s^{n+1} - \hat{u}_s^n)\big)_{\widehat{\Omega}_s} \tag{163}$$

$$= \frac{k\gamma_s}{4}\big(\hat{\epsilon}(\hat{v}_s^{n+1} + \hat{v}_s^n), \widehat{\nabla}(\hat{v}_s^{n+1} + \hat{v}_s^n)\big)_{\widehat{\Omega}_s} \tag{164}$$

$$= \frac{k\gamma_s}{4}||\hat{\epsilon}(\hat{v}_s^{n+1} + \hat{v}_s^n)||_E^2 \tag{165}$$

$$\leq \frac{k\gamma_s}{2}(||\hat{\epsilon}(\hat{v}_s^{n+1})||_E^2 + ||\hat{\epsilon}(\hat{v}_s^n)||_E^2). \tag{166}$$

It remains to discuss the interface term of strong damping on $\widehat{\Gamma}_i$:

$$-\gamma_s \frac{1}{2}\big\langle \hat{\epsilon}(\hat{v}_s^{n+1} + \hat{v}_s^n)\hat{n}_s, \hat{u}_s^{n+1} - \hat{u}_s^n \big\rangle_{\widehat{\Gamma}_i}.$$

Together with (158), this gives immediately the interface condition for the balance of the coupling (see Equation (149)). By adding (150), (152), (159), (163), with Lemma 8.23, we achieve the desired result. $\qquad\square$

In a similar way as already illustrated for the continuous case (see Theorem 7.31), we derive from Theorem 8.24 an adequate result for damping in an artificial domain. Thus, we formulate the stress coupling conditions on $\widehat{\Gamma}_i^{\text{in}} = \widehat{\Omega}_s^{\text{phys}} \cap \widehat{\Omega}_s^{\text{ext}}$:

$$\widehat{F}\widehat{\Sigma}_s(\hat{u}_s^{n+1} + \hat{u}_s^n)\hat{n}_s = \widehat{F}\widehat{\Sigma}_s^{\text{ext}}(\hat{u}_s^{n+1} + \hat{u}_s^n)\hat{n}_s^{\text{ext}} + \gamma_s \hat{\epsilon}_s(\hat{v}_s^{n+1} + \hat{v}_s^n)\hat{n}_s^{\text{ext}} \quad \text{on } \widehat{\Gamma}_i^{\text{in}}. \tag{167}$$

## 8.2 Space

The time-discretized equations are the starting point for a finite element Galerkin discretization method in space.

### 8.2.1 Galerkin approximations

Our goal is to approximate the weak solutions by using finite-dimensional subspaces. So far, the equations still contain the continuous spatial spaces $\hat{V}$, $\hat{V}^0$ and $\hat{L}^0$. In the following, we discuss the spatial discretization of the semi-discrete problems obtained in the previous section. To this end, we construct finite dimensional subspaces $\hat{V}_h \subset \hat{V}$, $\hat{V}_h^0 \subset \hat{V}^0$, $\hat{L}_h^0 \subset \hat{L}^0$. If indeed the discrete spaces are contained in their continuous spaces, we call the spatial discretization scheme a conforming method. For a Galerkin approximation, the specific form of the basis functions does not matter. A concrete realization can be performed in terms of a Galerkin finite element method (in short FEM). Or, if the problem is symmetric (not the case of course in fluid-structure) then the FEM scheme is a Ritz (or Ritz-Galerkin) approximation.

The basic idea of a FEM-Galerkin scheme is to start with the continuous semi-linear form[23]: Find $U \in V$ such that

$$A(U, \Phi) = F(\Phi) \quad \forall \Phi \in V,$$

and to seek an approximation $U_h \in V_h$ such that

$$A(U_h, \Phi_h) = F(\Phi_h) \quad \forall \Phi_h \in V_h.$$

---

[23]Here, we either think of a pure stationary problem or even the time-discretized equations.

Despite the fact that error estimates for nonlinear problems are (very) difficult and we do not focuses that much on them, we recapitulate Cea's lemma for linear problems, which is well-known and the basis for most convergence results for Galerkin methods. Furthermore, the discretization error and best approximation error are linked through this lemma. Finally, we work there with the so-called Galerkin orthogonality which is of utter importance.

**Theorem 8.25** (Cea's lemma; holds for example for linearized elasticity (Section 6.5.1))**.** *Let $A(U, \Phi)$ be a continuous, V-elliptic bilinear form. Then, an elliptic problem (such as linearized elasticity for example) has a unique solution $U \in V$ and the corresponding discrete problem has a unique solution $U_h \in V_h$. The error $\|U - U_h\|$ satisfies the estimate:*

$$\|U - U_h\| \le \frac{M}{\gamma} \inf_{W_h \in V_h} \|U - W_h\|.$$

*Proof.* Existence and uniqueness for the continuous problem have been discussed in Theorem 6.25. Similarly, the same arguments can be used for showing existence and uniqueness for the discrete system. Since the method is conforming; namely $V_h \subset V$, we can clearly insert the discrete test function into the continuous problem:

$$A(U, \Phi_h) = F(\Phi_h) \quad \forall \Phi_h \in V_h.$$

By linearity, we can now subtract the fully discrete version from the previous form:

$$A(U, \Phi_h) - A(U_h, \Phi_h) = A(U - U_h, \Phi_h) = 0 \quad \forall \Phi_h \in V_h.$$

This is the so-called Galerkin orthogonality, which means that the error $U - U_h$ is orthogonal in a certain sense to the discrete space $V_h$. We proceed as with the energy norm and want to employ, the continuity of the bilinear form and its V-ellipticity:

$$
\begin{aligned}
\|U - U_h\|^2 &= A(U - U_h, U - U_h) \\
&= A(U - U_h, U - \Phi_h + \Phi_h - U_h) \\
&= A(U - U_h, U - \Phi_h) + A(U - U_h, \Phi_h - U_h)
\end{aligned}
$$

Here, the latter term is zero thanks to Galerkin's orthogonality. Then,

$$\|U - U_h\|^2 = A(U - U_h, U - U_h) = A(U - U_h, U - \Phi_h) \le \alpha \|U - U_h\| \, \|U - \Phi_h\|$$

It follows:

$$\|U - U_h\| \le \alpha \|U - \Phi_h\|$$

Going to the infimum yields:

$$\|U - U_h\| \le \frac{\alpha}{\beta} \inf_{\Phi_h \in V_h} \|U - \Phi_h\|,$$

where $\alpha$ is the constant from the continuity and $\beta$ the V-ellipticity constant. $\qquad \square$

Before, we specify the basis functions of $V_h$ (and the other spaces), let us briefly show how we come then to a linear equation system. Let $V_h := \{\phi_1, \dots, \phi_N\}$. Then each vector in $V_h$ can be represented as

$$\phi = \sum_{j=1}^{N} v_j \phi_j, \quad v_j \in \mathbb{R}.$$

In particular, an approximation $U_h$ to $U$ is represented as

$$U_h = \sum_{j=1}^{N} U_j \phi_j, \quad U_j \in \mathbb{R}.$$

Plugging this into the bilinear form $A(U_h)(\Phi_i)$ for $i = 1, \ldots, N$ yields

$$A(U_h, \Phi_i) = (f, \Phi_i) \tag{168}$$

$$\Leftrightarrow A(\sum_{j=1}^{N} U_j \Phi_j, \Phi_i) = (f, \Phi_i) \tag{169}$$

$$\Leftrightarrow \sum_{j=1}^{N} U_j A(\Phi_j, \Phi_i) = (f, \Phi_i) \tag{170}$$

for all $i = 1, \ldots, N$. The solution is achieved by solving a linear equation system $Mx = b$ with:

$$x^T = (U_1, \ldots, U_N), \quad b^T = (b_1, \ldots, b_N), b_i = (f, \Phi_i), \quad M = A(\Phi_j, \Phi_i), M \in \mathbb{R}^{\mathbb{N} \times \mathbb{N}}.$$

Be careful with the matrix $M$ and its entries: the test function determines the row and the ansatz function the column and this matters in non-symmetric problems!

### 8.2.2 Finite element spaces

In order to realize the Galerkin scheme, we need to specify basis functions of the finite dimensional space $V_h$. Here, we employ piecewise polynomial functions up to order $l$. The spatial terms are computed in a fixed reference configuration. This is the characteristic feature of the ALE$_{fx}$ approach. The computational domain $\widehat{\Omega}$ is partitioned into open cells $\hat{K}$ that depend on the spatial dimension $d$. A mesh consists of quadrilateral or hexahedron cells $\hat{K}$. They perform a non-overlapping cover of the computation domain $\widehat{\Omega} \subset \mathbb{R}^d$, $d = 2, 3$. The mesh $\hat{\mathcal{T}}_h = \{\hat{K}\}$ of $\widehat{\Omega}$ is formed by taking all cells. The cell parameter $\hat{h}$ is given as a cell-wise constant function $\hat{h}_K := \mathrm{diam}(\hat{K})$ (where $\mathrm{diam}(\hat{K})$ denotes the diameter $\hat{h}_K$ of a cell $\hat{K}$). The maximum diameter is denoted by $\hat{h} := \max_{\hat{K} \in \hat{\mathcal{T}}_h} \hat{h}_k$.

We follow the standard literature ([46, 47, 62]) to formulate the following statements:

**Definition 8.26** (Regularity)**.** *A mesh $\hat{\mathcal{T}}_h = \{\hat{K}\}$ is called regular if the following conditions are fulfilled:*

*1)* $\overline{\widehat{\Omega}} = \bigcup_{\hat{K} \in \hat{\mathcal{T}}_h} \overline{\hat{K}}$.

*2)* $\hat{K}_1 \cap \hat{K}_2 = \emptyset$ *for all cells* $\hat{K}_1, \hat{K}_2 \in \hat{\mathcal{T}}_h$ *with* $\hat{K}_1 \neq \hat{K}_2$.

*3) Any face of any cell* $\hat{K}_1 \in \hat{\mathcal{T}}_h$ *is either a subset of the boundary* $\partial\widehat{\Omega}$ *or a face of another cell* $\hat{K}_2 \in \hat{\mathcal{T}}_h$.

$\diamond$

The last condition is too restrictive for our purposes and is weakened for the following reason. To facilitate adaptive mesh refinement and to avoid connecting elements, we use the concept of *hanging nodes*. Cells are allowed to have nodes that lie on the midpoints of the faces or edges of neighboring cells. At most, one hanging node is allowed on each face or edge. In three dimensions, this concept is generalized to subplanes and faces because we must deal with two types of lower manifolds.

We define continuous $H^1$-conforming finite element spaces $\hat{V}_h^l$ by (see [47, 62, 152]):

$$\hat{V}_h^l := \left\{ \hat{v}_h \in C(\overline{\widehat{\Omega}}) | \quad \hat{v}_h|_{\hat{K}} \in \mathcal{Q}(\hat{K}) \quad \forall \hat{K} \in \hat{\mathcal{T}}_h \right\} \subseteq H^1(\widehat{\Omega}).$$

Here, $\mathcal{Q}(\hat{K})$ denotes the space of polynomial-like functions on $\hat{K} \in \hat{\mathcal{T}}_h$. In the following, we introduce the space $\mathcal{Q}_l(\hat{K})$ of tensor product polynomials up to degree $l$. On the reference cell $\hat{K}_{\mathrm{unit}} = (0,1)^d$ they are defined as

$$\hat{\mathcal{Q}}_l(\hat{K}_{\mathrm{unit}}) := \mathrm{span}\left\{ \prod_{i=1}^{d} \hat{x}_i^{\alpha_i} | \alpha_i \in \{0, 1, \ldots, l\} \right\}.$$

**Definition 8.27.** *We consider for each $\hat{K} \in \hat{\mathcal{T}}_h$ the bilinear transformation $\hat{\sigma}_K : \hat{K}_{unit} \to \hat{K}$.*
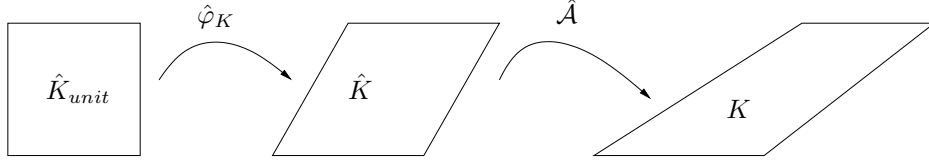
Figure 48: Transformation $\hat{\varphi}_K$ from the unit cell $\hat{K}_{unit}$ to the ALE cell $\hat{K}$ and from that cell via the ALE mapping $\hat{\mathcal{A}}$ to the physical cell $K$.

**Remark 8.28** (Transformations $\widehat{T}, \hat{\mathcal{A}}$ and $\hat{\sigma}_K$). *It is worthy to emphasize that the definition of the transformation from the reference cell (master cell) to the physical cell is formally equivalent to the definition of the transformation $\widehat{T}$ in continuum mechanics and consequently also equivalent to the ALE mapping $\hat{\mathcal{A}}$.*

In the following, we want to understand better the meaning of the transformation $\hat{\sigma}_K$. The main purpose is that we want to be independent from a fixed coordinate system. This might be a problem when cells are stretched or rotated. Here, a fixed coordinate system would not allow to use the same ansatz (e.g., for bilinear quadrilaterals). A second reason of the master element is that on general quadrilaterals and hexahydra it is then easier to construct *conforming* finite elements.

**Example 8.29** (Construction of $\hat{\sigma}_K$ on a triangle). *We define the unit triangle $E$ as the reference element. Let $\sigma_T : E \to T$ be affine-linear mapping of $E$ onto the triangle $T$. Then we have the properties*

$$x = \sigma_T(\hat{x}) = B_T \hat{x} + b_T, \quad x \in T, \, \hat{x} \in E$$
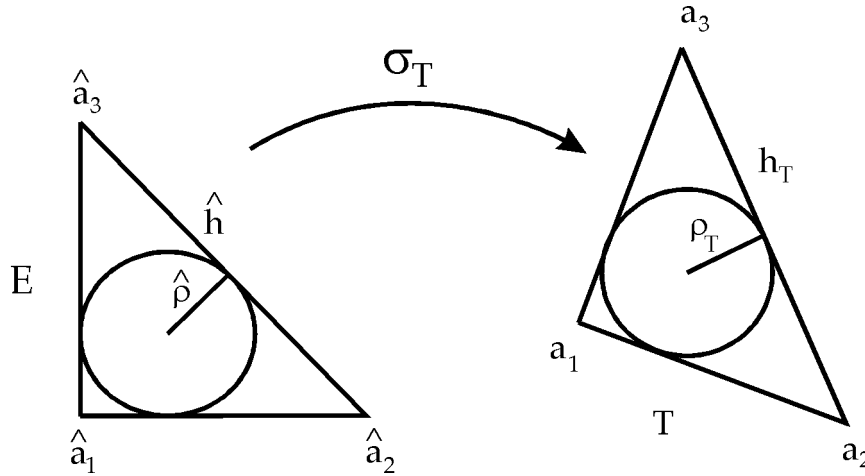
*with the functional matrix $B_T$.*



Figure 49: Reference element $E$ and physical cell (here a triangle) $T$.

Let $E = conv\{\hat{a}_1, \hat{a}_2, \hat{a}_3\}$ with $\hat{a}_1 = (0,0)^T, \hat{a}_2 = (1,0)^T, \hat{a}_3 = (0,1)^T$. The triangle $T$ has the coordinates $a_1 = (3, 1/4), a_2 = (4, -1/2), a_3 = (17/4, 1)$.

A bijective mapping between $E$ and a triangle $T$ is given by $\sigma_T : E \to T$ with $\sigma_T(\hat{x}) = B_T \hat{x} + b$, where $b = a_1$. The functional matrix is defined by

$$B_T = (a_2 - a_1, a_3 - a_1) = \begin{pmatrix} 1 & \frac{5}{4} \\ -\frac{3}{4} & \frac{3}{4} \end{pmatrix}$$

The determinant of $B_T$ is of order $h^2$. That means $det B_T = \mathcal{O}(h^2)$. Additional details can be found in [121], p. 207ff. The corresponding definitions and computations for finite elements on quadrilaterals can be found for example in [89].

With the help of $\widehat{\sigma}_K$, the $Q_1^c$ element is defined as

$$Q_1^c(\hat{K}) = \{\hat{q} \circ \hat{\sigma}_K^{-1} : \hat{q} \in \text{span} < 1, \hat{x}, \hat{y}, \hat{x}\hat{y} >\} \qquad (d = 2),$$

$$Q_1^c(\hat{K}) = \{\hat{q} \circ \hat{\sigma}_K^{-1} : \hat{q} \in \text{span} < 1, \hat{x}, \hat{y}, \hat{z}, \hat{x}\hat{y}, \hat{x}\hat{z}, \hat{y}\hat{z}, \hat{x}\hat{y}\hat{z} >\} \qquad (d = 3),$$

with dim $Q_1^c = 4$ (in 2D) and $Q_1^c = 8$ (in 3D) in which the dimension denotes the local degrees of freedom on a single cell. The $Q_2^c$ element (in two dimensions) is defined as

$$Q_2^c(\hat{K}) = \{\hat{q} \circ \hat{\sigma}_K^{-1} : \hat{q} \in \text{span} < 1, \hat{x}, \hat{y}, \hat{x}\hat{y}, \hat{x}^2, \hat{y}^2, \hat{x}^2\hat{y}, \hat{y}^2\hat{x}, \hat{x}^2\hat{y}^2 >\},$$

with dim $Q_2^c = 9$. Finally, the $P_1^{dc}$ element is defined with the help of linear functions and it reads

$$P_1^{dc}(\hat{K}) = \{\hat{q} \circ \hat{\sigma}_K^{-1} : \hat{q} \in \text{span}, < 1, \hat{x}, \hat{y} >\}$$

with dim $P_1^{dc}(\hat{K}) = 3$. In addition to these polynomial spaces, we need a set of *node* functionals $\{\chi_r\}$ to determine uniquely a polynomial function on an element $\hat{K}$. For instance for the $Q_1^c$ spaces we choose the node functionals

$$\{\chi_i(p) = p(a_i), i = 1, \ldots, 4\}.$$

**Example 8.30.** *On the master element in 2D, we can construct a bilinear function by*

$$p(x, y) = a \cdot 1 + bx + cy + dxy, \quad a, b, c, d \in \mathbb{R}.$$

*As node functionals, we choose:*

$$\chi_1(p) = p(0,0) = 1, \quad \chi_2(p) = p(1,0) = 0, \quad \chi_3(p) = p(0,1) = 0, \quad \chi_4(p) = p(1,1) = 0.$$

*On each edge the $Q_1^c$ function is linear.*

**Remark 8.31.** *If the transformation $\widehat{\sigma}_K$ itself is an element of $\hat{\mathcal{Q}}_l(\hat{K})^d$ , the corresponding finite element space is called* isoparametric.

Extending these concepts to finite element spaces in the case of hanging nodes requires some remarks. To enforce global continuity (i.e., global conformity), the degrees of freedom located on the interface between different refinement levels have to satisfy additional constraints. They are determined by interpolation of neighboring degrees of freedom. Therefore, hanging nodes do not carry any degrees of freedom. For more details on this, we refer to [58].

To ensure the approximation properties of the finite element spaces, additional conditions on the geometry of the cells are required. The two classical assumptions from the literature ([46, 47]) are the so-called *uniformity* and the weaker *quasi-uniformity*:

**Definition 8.32** (Quasi-Uniformity). *A family of meshes $\{\hat{\mathcal{T}}_h | h \searrow 0\}$ is called quasi-uniform if there is a constant $\kappa$ such that the following two conditions are fulfilled:*

*1) For each transformation $\widehat{\sigma}_K : \hat{K}_{unit} \to \hat{K}$ it holds*

$$\frac{\sup\{||\nabla\widehat{\sigma}_K(\hat{x})\hat{x}|| \; |\hat{x} \in \hat{K}, \, ||\hat{x}|| = 1\}}{\inf\{||\nabla\widehat{\sigma}_K(\hat{x})\hat{x}|| \; |\hat{x} \in \hat{K}, \, ||\hat{x}|| = 1\}} \le \kappa, \qquad \hat{K} \in \bigcup_h \hat{\mathcal{T}}_h. \tag{171}$$

*2) It holds*

$$\frac{\hat{h}_K}{\hat{\rho}_K} \le \kappa \quad \forall \hat{K} \in \bigcup_h \hat{\mathcal{T}}_h.$$

◇

### 8.2.3 Spatial discretization of incompressible fluids

To compute fluid problems, we prefer the biquadratic, discontinuous-linear $Q_2^c/P_1^{dc}$ element. The definitions of the spaces for the unknowns $\hat{v}_h$ and $\hat{p}_h$ read:

$$\hat{V}_h := \{\hat{v}_h \in [C(\hat{\Omega}_h)]^d, \hat{v}_h|_{\hat{K}} \in [Q_2(\hat{K})]^d \quad \forall \hat{K} \in \hat{\mathcal{T}}_h, \hat{v}_h|_{\hat{\Gamma}\setminus\hat{\Gamma}_i} = 0\},$$

$$\hat{P}_h := \{\hat{p}_h \in [\hat{L}^2(\hat{\Omega}_h)], \hat{p}_h|_{\hat{K}} \in [P_1(\hat{K})] \quad \forall \hat{K} \in \hat{\mathcal{T}}_h\}.$$

**Remark 8.33.** *Other choices for inf-sub stable elements would be the classical Taylor-Hood element $Q_2^c/Q_1^c$ or also $Q_2^c/P_0^{dc}$.* ⋄
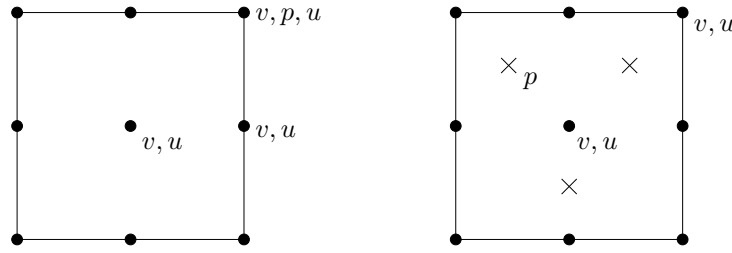


Figure 50: Taylor Hood element $Q_2^c/Q_1^c$ (left) and $Q_2^c/P_1^{dc}$ element (right).

The continuity of the velocity values across different mesh cells is one property of the $Q_2^c/P_1^{dc}$ element. In contrast, the pressure is allowed to be discontinuous across faces because it is defined utilizing discontinuous test functions. In addition, this element preserves local mass conservation, is of low order, gains the *inf-sup stability*, and it is therefore an optimal choice for both fluid problems and fluid-structure interaction problems.

In fact, for the choice of finite element pairs for the spatial discretization of incompressible flow, it is very important that the discrete inf-sup condition is satisfied. We need to check two things: first, a discrete pressure $p_f^h$ does exist and secondly, $p_f^h$ is suitable approximation to $p_f$. This means the pressure be uniquely (up to a constant) determined, it should depend continuously on the problem data and it should satisfy a stability estimate. All these requirements are achieved by the discrete inf-sup condition:

$$\min_{q_h \in L_0^f} \{\max_{\varphi_h \in H_h} \frac{(q_h, \nabla \cdot \varphi_h)}{\|q_h\| \, \|\nabla\varphi_h\|}\} \geq \beta_h \geq \beta > 0,$$

which should go uniformly for $h \to 0$. It is important that the discrete stability constant $\beta_h$ is bounded from below by the continuous stability constant $\beta$. The discrete inf-sup condition is also known as the Babuska-Brezzi (BB) or also Ladyshenskaja-Babuska-Brezzi (LBB) condition. With the discrete inf-sup condition, we obtain a unique pressure $p_f^h$ and the a priori estimates:

$$\|\nabla v_h\| \leq \|f\|_{-1}, \quad \|p_h\| \leq 2\beta^{-1}\|f\|_{-1}.$$

The crucial part is now that the stability estimate requires a careful choice of the pressure space. This space should be not too large compared to the velocity space. Violation is illustrated in Figure 51.

**Remark 8.34.** *The LBB condition does not only hold for incompressible flow but in general for mixed problems and saddle-point problems of similar type; see for example [121]. Consequently, incompressible solids have to satisfy the LBB condition, too.*

In remains the specific questions of how many degrees of freedom have to dealt with in the case of the Navier-Stokes? Using the $Q_2^c/P_1^{dc}$ element in 2D, leads to $9 + 9 + 3 = 21$ local degrees of freedom on each mesh cell.
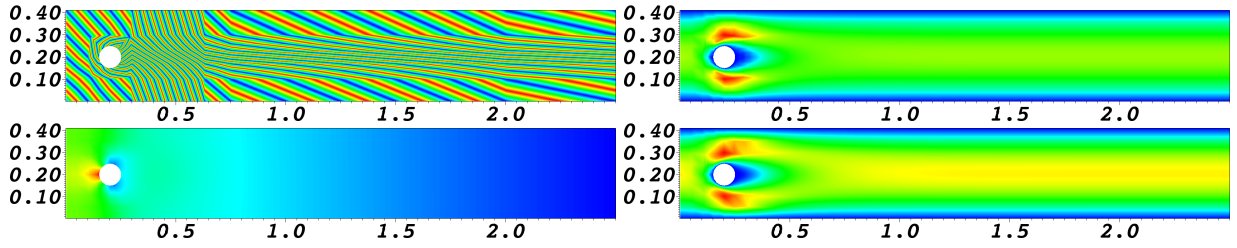
Figure 51: Fluid flow in channel with a hole: Illustration of the violation of the inf-sup condition using the unstable $Q_1^c/Q_1^c$ discretization: the pressure field oscillates (top left) whereas the corresponding velocity field (top right) is 'more or less' okay in the picture norm. On the bottom, the inf-sup stable Taylor-Hood element $Q_2^c/Q_1^c$ results in a smooth pressure field (bottom left). The corresponding flow field is shown at bottom right. *(As footnote: The picture norm does only provide a rough idea of a sitation. It is neither a proof nor computational evidence nor evidence of numerical convergence or rigorous correctness of a result!)*

In the case of equal-order discretizations, a pressure can be obtained nonetheless if a pressure stabilization is added. The first results have been published in [50, 143]. Here, we deal with certain parameters, where details reasons for certain choices are explained for example in [42]. An interesting pressure stabilization is based on the so-called local projection stabilization (LPS) [25]. There are good reasons to do so. First, low-order equal-order elements are less computationally costly than the Taylor-Hood element. Second, equal-order discretizations allow for easier data structures in programming codes and consequently also allow an easier construction of good iterative linear solvers such as multigrid solvers.

### 8.2.4 Spatial discretization of solids

The definition of the displacement space reads:

$$\hat{W}_h := \{\hat{u}_h \in [C(\hat{\Omega}_h)]^d, \hat{u}_h|_{\hat{K}} \in [Q_2(\hat{K})]^d \quad \forall \hat{K} \in \hat{\mathcal{T}}_h, \hat{u}_h|_{\Gamma_0} = 0\}.$$

**8.2.4.1 Compressible solids - STVK**   For compressible solids, we discretize the displacements and the velocities with equal-order finite elements; thus $\{\hat{v}, \hat{u}\} \in Q_1^c \times Q_1^c$ or $\{\hat{v}, \hat{u}\} \in Q_2^c \times Q_2^c$.

**8.2.4.2 Incompressible and nearly incompressible solids - INH and IMR**   In compressible solids, we deal again with the inf-sup condition in the relationship between displacements and pressure. Here, one has to use equal-order for the velocity-displacement discretization. This pair should be from a 'larger' space than the pressure. For example, we could use $\{\hat{v}, \hat{u}, \hat{p}\} \in Q_2^c \times Q_2^c \times Q_1^c$.

### 8.2.5 Spatial discretization of fluid-structure interaction

Summarizing the previous considerations, we need to discretize the following unknowns:

- Velocities in the fluid and the solid;

- Displacements in the solid;

- Displacements for mesh motion in the fluid domain;

- Pressures for incompressible Navier-Stokes and in case of incompressible solids.

In summary, we need to solve for

$$\hat{v}_f, \hat{v}_s, \hat{u}_s, \hat{u}_f, \hat{p}_f, (\hat{p}_s),$$

using second order MMPDEs. Employing the biharmonic MMPDE, we need additionally to solve for

- $\hat{w}_f$.

Bearing the three mesh motion models in mind, the computation of fluid-structure interaction with biharmonic mesh motion incurs a greater computational cost at each time step than using only a harmonic model or the equations of linear elasticity because an additional equation is added to the problem (see Problem 7.26). In the context of a Galerkin finite element scheme, the spatial discretization of the mixed biharmonic equation is stable for equal-order discretization on polygonal domains, which is one of our assumptions. In this lecture notes, we work with $Q_2^c$ elements for $\hat{u}_h$ and $\hat{\eta}_h$.

For the next statement, let $\hat{v}_{f,h}^D$, $\hat{u}_{f,h}^D$, and $\hat{v}_{s,h}^D$ be suitable extensions of Dirichlet inflow data. Having these preparations, the spatially (and temporal) discretized problem of (102) reads:

**Problem 8.35.** *Let the semi-linear form be composed as shown in Problem 8.14.*
*Find $\hat{U}_h^n = \{\hat{v}_{f,h}^n, \hat{v}_{s,h}^n, \hat{u}_{f,h}^n, \hat{u}_{s,h}^n, \hat{p}_{f,h}^n, \hat{p}_{s,h}^n\} \in \hat{X}_{h,D}^0$, where $\hat{X}_{h,D}^0 := \{\hat{v}_{f,h}^D + \hat{V}_{f,\hat{v},h}^0\} \times \hat{L}_{s,h} \times \{\hat{u}_{f,h}^D + \hat{V}_{f,\hat{u},h}^0\} \times \{\hat{u}_{s,h}^D + \hat{V}_{s,h}^0\} \times \hat{L}_{f,h}^0 \times \hat{L}_{s,h}^0$, for all $n = 1, 2, \ldots, N$ such that*

$$\hat{A}(\hat{U}_h^n)(\hat{\Psi}_h) = \hat{F}(\hat{\Psi}_h) \quad \forall \hat{\Psi}_h \in \hat{X}_h,$$

*with $\hat{\Psi}_h = \{\hat{\psi}_{f,h}^v, \hat{\psi}_{s,h}^v, \hat{\psi}_{f,h}^u, \hat{\psi}_{s,h}^u, \hat{\psi}_{f,h}^p, \hat{\psi}_{s,h}^p\}$ and $\hat{X}_h = \hat{V}_{f,\hat{v},h}^0 \times \hat{L}_{s,h} \times \hat{V}_{f,\hat{u},\hat{\Gamma}_i,h}^0 \times \hat{V}_{s,h}^0 \times \hat{L}_{f,h}^0 \times \hat{L}_{s,h}^0$.*

In Section 8.2.7, two tables show how many degrees of freedom have to dealt while considering this FSI problem.

### 8.2.6 Stabilization for convection-dominated flows

In the case of higher Reynolds numbers the flow becomes convection dominated and needs to be stabilized. Residual based stabilization is first introduced in Brooks and Hughes [50] and is intensively analyzed in Wall [235]. Our method of choice is a rough simplification of the streamline upwind Petrov-Galerkin (SUPG) method.

We start with a consistent formulation for the fluid problem that is given on the continuous level in a time-dependent domain $\Omega_f$. Then, the stabilization term reads (in which we omit for the moment the subscripts 'h' and 'n' in the equations):

$$S_{\text{stab}}(U_h^n)(\Psi) := \sum_{K \in \mathcal{T}_h} (\rho_f \hat{\partial}_t v_f + \rho_f(v_f - w) \cdot \nabla v_f - \text{div} \sigma_f, \delta_{K,n}(v_f \cdot \nabla)\psi_f^v)_K$$

with

$$\delta_{K,n} = \delta_0 \frac{h_K^2}{6\nu_f + h_K ||v_h^n||_K}, \quad \delta_0 = 0.1.$$

For more details on the choice of these parameters, we refer the reader to [42].

From the computational point of view, the major disadvantage comes from the necessity of computing second derivatives contained in the stress tensor $\sigma_f$, because we must consider the strong formulation. Specifically, in the case of fluid-structure interaction problems, this formulation is a serious drawback. To this end, we only use a nonconsistent simplified version (in $\Omega_f$):

$$S_{\text{stab}}(U_h^n)(\Psi) := \sum_{K \in \mathcal{T}_h} (\rho_f v_f \cdot \nabla v_f, \delta_{K,n}(v_f \cdot \nabla)\psi_f^v)_K.$$

This term can be rewritten in the reference configuration $\hat{\Omega}_f$ and reads:

$$\hat{S}_{\text{stab}}(\hat{U}_h^n)(\hat{\Psi}) := \sum_{\hat{K} \in \mathcal{T}_h} (\hat{\rho}_f(\hat{J}\hat{F}^{-1}\hat{v}_f \cdot \hat{\nabla})\hat{v}_f, \delta_{K,n}(\hat{F}^{-1}\hat{v}_f \cdot \hat{\nabla})\hat{\psi}_f^v)_{\hat{K}}. \tag{172}$$

**Problem 8.36.** *Let the semi-linear form be composed as shown in Problem 8.14.*
*Find $\hat{U}_h^n = \{\hat{v}_{f,h}^n, \hat{v}_{s,h}^n, \hat{u}_{f,h}^n, \hat{u}_{s,h}^n, \hat{p}_{f,h}^n, \hat{p}_{s,h}^n\} \in \hat{X}_{h,D}^0$, where $\hat{X}_{h,D}^0 := \{\hat{v}_{f,h}^D + \hat{V}_{f,\hat{v},h}^0\} \times \hat{L}_{s,h} \times \{\hat{u}_{f,h}^D + \hat{V}_{f,\hat{u},h}^0\} \times \{\hat{u}_{s,h}^D + \hat{V}_{s,h}^0\} \times \hat{L}_{f,h}^0 \times \hat{L}_{s,h}^0$, for all $n = 1, 2, \ldots, N$ such that*

$$\hat{A}(\hat{U}_h^n)(\hat{\Psi}_h) + \hat{S}_{stab}(\hat{U}_h^n)(\hat{\Psi}) = \hat{F}(\hat{\Psi}_h) \quad \forall \hat{\Psi}_h \in \hat{X}_h,$$

*with $\hat{\Psi}_h = \{\hat{\psi}_{f,h}^v, \hat{\psi}_{s,h}^v, \hat{\psi}_{f,h}^u, \hat{\psi}_{s,h}^u, \hat{\psi}_{f,h}^p, \hat{\psi}_{s,h}^p\}$ and $\hat{X}_h = \hat{V}_{f,\hat{v},h}^0 \times \hat{L}_{s,h} \times \hat{V}_{f,\hat{u},\hat{\Gamma}_i,h}^0 \times \hat{V}_{s,h}^0 \times \hat{L}_{f,h}^0 \times \hat{L}_{s,h}^0$.*

**Remark 8.37.** *An elegant alternative has been investigated in [157] (and further references of the same author) in recent years. This scheme belongs to flux-corrected transport algorithms and can be applied to convection-dominated transport problems.* ⋄

### 8.2.7 Comparison of number of degrees of freedom

A table is provided that illustrates how much the computational cost in terms of local number of degrees of freedom varies depending on the dimension and the order of the polynomial degree. This information is then used to display the development of the global numbers of degrees of freedom under uniform (global) mesh refinement.

Table 4: Comparison of local number of degrees of freedom on a cell.

| Problem | Variable(s) | FE | 2D (d=2) | 3D (d=3) |
|---|---|---|---|---|
| Poisson | $u$ | $Q_1^c$ | 4 | 8 |
| Poisson | $u$ | $Q_2^c$ | 9 | 27 |
| Elasticity | $u = (u)^d$ | $(Q_1^c)^d$ | 8 (4+4) | 24 (8+8+8) |
| Elasticity | $u = (u)^d$ | $(Q_2^c)^d$ | 18 (9+9) | 81 (27+27+27) |
| Navier-Stokes | $\{v^d, p\}$ | $(Q_2^c)^d/Q_1^c$ | 22 (18+4) | 89 (81+8) |
| Navier-Stokes | $\{v^d, p\}$ | $(Q_2^c)^d/P_1^{dc}$ | 21 (18+3) | 85 (81+4) |
| FSI | $\{v_f^d, p_f, u_s^d\}$ | $(Q_2^c)^d/P_1^{dc}, (Q_1^c)^d, (Q_1^c)^d$ | 37 (18+3+8+8) | 123 (81+4+24+24) |
| FSI (el.mix) | $\{v_f^d, p_f, u_f^d, v_s^d, u_s^d\}$ | $(Q_2^c)^d/P_1^{dc}, (Q_1^c)^d, (Q_1^c)^d, (Q_1^c)^d$ | 45 (18+3+8+8+8) | 157 (81+4+24+24+24) |
| FSI (el.mix) | $\{v_f^d, p_f, u_f^d, v_s^d, u_s^d\}$ | $(Q_2^c)^d/P_1^{dc}, (Q_2^c)^d, (Q_2^c)^d, (Q_2^c)^d$ | 75 (18+3+18+18+18) | 328 (81+4+81+81+81) |
| FSI (biharm) | $\{v_f^d, p_f, u_f^d, v_s^d, u_s^d, \eta_s^d\}$ | $(Q_2^c)^d/P_1^{dc}, (Q_1^c)^d, (Q_1^c)^d, (Q_1^c)^d, (Q_1^c)^d$ | 53 (18+3+8+8+8+8) | 181 (81+4+24+24+24+24) |
| FSI (biharm) | $\{v_f^d, p_f, u_f^d, v_s^d, u_s^d, \eta_s^d\}$ | $(Q_2^c)^d/P_1^{dc}, (Q_2^c)^d, (Q_2^c)^d, (Q_2^c)^d, (Q_2^c)^d$ | 93 (18+3+18+18+18+18) | 409 (81+4+81+81+81+81) |

The table demonstrates how much the local number of degrees varies (specifically in FSI) depending the formulation, MMPDE, choice of the finite element and the problem dimension. For instance, to test a new code with an academic example, a 2D version without splitting the elasticity equation into a mixed system has 37 local DoFs. In contrast, a 3D version including elasticity splitting and higher order elements for the solid with a standard 2nd order MMPDE has 328 DoFs (this is 9-times higher!!!).

Table 5: Comparison of global number of degrees of freedom using uniform mesh refinement.

| Level | Cells (d=2) | $Q_1^c$ | $(Q_2^c)^{d=2}$ | Cells (d=3) | $Q_1^c$ | $(Q_2^c)^{d=3}$ |
|---|---|---|---|---|---|---|
| 0 | 1 | 4 | 18 (9+9) | 1 | 8 | 81 (27+27+27) |
| 1 | 4 | 9 | 50 (25+25) | 8 | 27 | 375 (125+125+125) |
| 2 | 16 | 25 | 162 (81+81) | 64 | 125 | 2187 (729+729+729) |
| 3 | 64 | 81 | 578 (289+289) | 512 | 729 | 14739 (4913+4913+4913) |
| 4 | 256 | 289 | 2178 (1089+1089) | 4096 | 4913 | 107811 (35937+35937+35937) |

In Table 5, we present exemplary how the numbers of DoFs increase for scalar-valued $Q_1^c$ discretizations and a vector-valued $Q_2^c$ discretization. Here, we observe that the $Q_2^c$ element on level $L = n$ has as many DoFs as a $Q_1^c$ element one level higher $L = n + 1$. Uniform mesh refinement in 2D is obtained by dividing a cell into 4 children; thus at each step, we increase the number of cells by a factor of 4. In 3D, a hexahydra is divided into 8 children.

# 9 Numerical Solution Algorithms

## 9.1 Nonlinear solution: Newton's method

### 9.1.1 Classical Newton's method

Let $f \in C^1[a,b]$ and $x_0 \in [a,b]$ be an intial value. The tangent (based for instance on a Taylor expension) of $f$ is given by

$$t(x) = f(x_k) + (x - x_k)f'(x_k), \quad k = 0, 1, 2, \dots.$$

A root is then given by:

$$x_{k+1} = x_k - \frac{f(x_k)}{f'(x_k)}, \quad k = 0, 1, 2, \dots. \tag{173}$$

This iteration is possible as long as $f'(x_k) \neq 0$.

This is iteration terminates if a stopping criterium

$$|x_{k+1} - x_k| < TOL, \tag{174}$$

or

$$|f(x_k)| < TOL. \tag{175}$$

is fulfilled. Or (better!), the relative stopping criteria may be used:

$$\frac{|x_{k+1} - x_k|}{|x_k|} < TOL, \tag{176}$$

or

$$|f(x_k)| < TOL|f(x_0)| \tag{177}$$
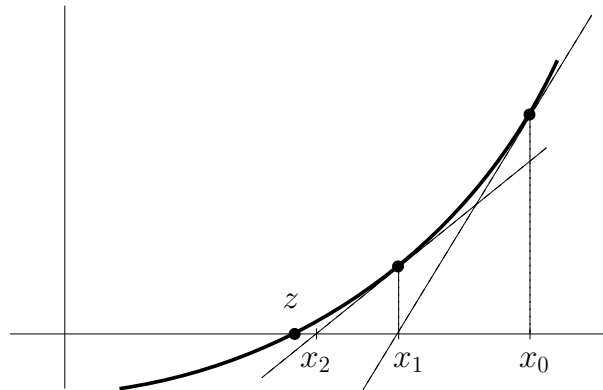


Figure 52: Geometrical interpretation of Newton's method.

**Remark 9.1.** *Newton's method belongs to fix-point iteration schemes with the iteraction function:*

$$F(x) := x - \frac{f(x)}{f'(x)}. \tag{178}$$

*For a fix-point $\hat{x} = F(\hat{x})$ it holds: $f(\hat{x}) = 0$ ◇*

Often (and in particular for higher-dimensional problems such as fluid-structure interaction), Newton's method is formulated in terms of a defect-correction scheme.

**Definition 9.2** (Defect)**.** *Let $\tilde{x} \in \mathbb{R}$ an approximation of the solution $f(x) = y$. The defect (or similarly the residual) is defined as*

$$d(\tilde{x}) = y - f(\tilde{x}).$$

◇

For the sake of presentation, let the right hand side be $y = 0$. For the approximation $x_k$, the defect $d_k := 0 - f(x_k)$ is given by and we write:

**Definition 9.3** (Newton's method as defect-correction scheme)**.**

$$f'(x_k)\delta x = d_k, \quad d_k := -f(x_k),$$
$$x_{k+1} = x_k + \delta x, \quad k = 0, 1, 2, \ldots.$$

*The iteration is finished with the same stopping criterium as for the classical scheme.* ⋄

### 9.1.2 Residual-based Newton methods

We present a classical residual-based method in this section.

**Algorithm 9.4** (Residual-based Newton's method)**.** *In this type of methods, the main criterion is a decrease of the residual in each step:*

$$F'(x^k)\delta x^k = -F(x^k),$$
$$x^{k+1} = x^k + \lambda_k \delta x^k$$

*The criterion for convergence is contractions of the residuals:*

$$\|F(x^{k+1})\| < \|F(x^k)\|$$

*In order to accelerate Newton's method close to the solution $x^*$ we can use intermediate quasi-Newton steps. In the case of $\lambda_k = 1$ we observe*

$$\theta_k = \frac{\|F(x^{k+1})\|}{\|F(x^k)\|} \leq \theta_{max} < 1,$$

*where e.g. $\theta \approx 0.1$. Finally the stopping criterion is*

$$\|F(x^{k+1})\| < TOL.$$

*If fulfilled, set $x^* := x^{k+1}$.*

### 9.1.3 Extension to PDEs (higher-dimensional problems)

Time and spatial discretization end at each single time step in a nonlinear quasi-stationary problem

$$\hat{A}(\hat{U}_h^n)(\hat{\Psi}) = \hat{F}(\hat{\Psi}) \quad \forall \hat{\Psi} \in \hat{X}_h,$$

which is solved with a Newton-like method. As done in the previous section, we can express this relation in terms of the defect:

$$d := \hat{F}(\hat{\Psi}) - \hat{A}(\tilde{U}_h^n)(\hat{\Psi}) = 0 \quad \forall \hat{\Psi} \in \hat{X}_h,$$

where $\tilde{U}_h^n$ denotes an approximate solution at time step $t^n$.

The final full Newton algorithm based on a contraction of the residuals reads:

**Algorithm 9.5** (Residual-based Newton's method with backtracking line search and simplified Newton steps)**.** *Given an initial Newton guess $\hat{U}_h^{n,0} \in \hat{X}_h$. For the iteration steps $j = 0, 1, 2, 3, \ldots$:*

1. *Find $\delta\hat{U}_h^n \in \hat{X}_h$ such that*

$$A'(\hat{U}_h^{n,j})(\delta\hat{U}_h^n, \hat{\Psi}) = -A(\hat{U}_h^{n,j})(\Psi) + \hat{F}(\hat{\Psi}) \quad \forall \hat{\Psi} \in \hat{X}_h \tag{179}$$
$$\hat{U}_h^{n,j+1} = \hat{U}_h^{n,j} + \lambda_j \delta\hat{U}_h^n, \tag{180}$$

*for $\lambda_j = 1$.*

2. *The criterion for convergence is the contraction of the residuals:*

$$\|R(\hat{U}_h^{n,j+1})\|_\infty < \|R(\hat{U}_h^{n,j})\|_\infty. \tag{181}$$

3. *If (181) is violated, re-compute in (179) $\hat{U}_{h,l}^{n,j+1}$ by choosing $\lambda_j^l = 0.5$, and compute for $l = 1, ..., l_M$ (e.g. $l_M = 5$) a new solution*

$$\hat{U}_h^{n,j+1} = \hat{U}_h^{n,j} + \lambda_j^l \delta\hat{U}_h^n,$$

*until (181) is fulfilled for a $l^* < l_M$ or $l_M$ is reached. In the latter case, no convergence is obtained and the program aborts.*

4. *In case of $l^* < l_M$ we check next the stopping criterion:*

$$\|R(\hat{U}_h^{n,j+1})\|_\infty \leq TOL_N, \quad \text{(absolute)}$$
$$\|R(\hat{U}_h^{n,j+1})\|_\infty \leq TOL_N \|R(\hat{U}_h^{n,0})\|_\infty, \quad \text{(relative)}$$

*If this is criterion is fulfilled, set $\hat{U}_h^n := \hat{U}_h^{n,j+1}$. Else, we increment $k \to k+1$ and goto Step 1.*

**Remark 9.6** (On using simplified-Newton steps). *Usually, when the Newton reduction rate*

$$\theta_k = \frac{\|R(\hat{U}_h^{n,j+1})\|}{\|R(\hat{U}_h^{n,j})\|},$$

*was sufficiently good, e.g., $\theta_k \leq \theta_{max} < 1$ (where e.g. $\theta_{max} \approx 0.1$), a common strategy is to work with the 'old' Jacobian matrix, but with a new right hand side.*

**Remark 9.7** (Initial Newton guess for time-dependent problems). *In time-dependent problems the 'best' initial Newton guess is the previous time step solution; namely*

$$\hat{U}_h^{n,0} := \hat{U}_h^{n-1}.$$

**Remark 9.8** (Dirichlet boundary conditions). *In Newton's method, non-homogeneous Dirichlet boundary conditions are only prescribed on the initial guess $\hat{U}_h^{n,0}$ and in all further updates non-homogeneous Dirichlet conditions are replaced by homoegeneous Dirichlet conditions. The reasons is that we only need to prescribe these conditions once per Newton iteration and not several times, which would lead to wrong solution.*

The directional derivative $\hat{A}'(\hat{U})(\delta\hat{U}, \hat{\Psi})$ that is utilized previously, is defined in the same fashion as Gâteaux derivative.

**Definition 9.9.** *The definition of the directional derivative in terms of a semi-linear form is based on the original definition of the Gâteaux derivative from Definition 3.35 and reads:*

$$\hat{A}'(\hat{U})(\delta\hat{U}, \hat{\Psi}) := \lim_{\varepsilon \to 0} \frac{1}{\varepsilon} \left\{ \hat{A}(\hat{U} + \varepsilon\delta\hat{U})(\hat{\Psi}) - \hat{A}(\hat{U})(\hat{\Psi}) \right\} = \frac{d}{d\varepsilon} \left. \hat{A}_h(\hat{U} + \varepsilon\delta\hat{U})(\hat{\Psi}) \right|_{\varepsilon=0}.$$

### 9.1.4 A sophisticated Newton method with line-search backtracking and intermediate quasi-Newton solves

For highly nonlinear problems such as FSI it is necessary to extend the basic Newton algorithm by two important features:

- If starting values are not close enough that the local Newton method will converge, we globalize by using a damped Newton strategy;

- Within the local, quadratic, convergence radius, Newton's method converges fastly and then quasi-Newton steps can be used to reduce computational cost.

### 9.1.5 An error-oriented Newton method

For ill-conditioned problems such as they often arise in PDEs, standard residual based Newton methods are more likely to fail [69]. For this reason, a slightly more complicated version can be implemented. We present both philosophies in the following.

**Algorithm 9.10** (Error-oriented Newton's method)**.** *The characteristic of this procedure is that it allows within one Newton iteration for an increase of the residual where necessary, i.e., this procedure allows for a violation of $\|res_{n+1}\| < \|res_n\|$. The main criterion is based on a decrease of the norm of update $\delta U^k$. Set $\lambda_{min}$. Choose an initial Newton guess $\mathbf{U}^0$: For $n = 1, 2, 3, \ldots$:*

1. *Solve*
$$\mathbf{B}'(\mathbf{U}^n)\mathbf{Z}^n = -\big(\mathbf{B}(\mathbf{U}^n) - \mathbf{f}\big)$$

2. *Check if $\|\mathbf{Z}^n\|_{l_2} \leq TOL$. If yes, solution found and set*
$$\mathbf{U}^* := \mathbf{U}^n + \mathbf{Z}^n.$$

   *If not and $k > 0$ compute a prediction value for the damping factor:*
$$\lambda_n := \min(1, \mu_n), \quad \mu_n := \frac{\|\mathbf{Z}^{n-1}\| \cdot \|\mathbf{Z}^n_{simp}\|}{\|\mathbf{Z}^n_{simp} - \mathbf{Z}^n\| \cdot \|\mathbf{Z}^n\|}.$$

   *Check if*
$$\lambda_n < \lambda_{min} \tag{182}$$

   *then stop. Convergence failure. Abort computation.*

3. *If $\lambda_n > \lambda_{min}$ continue and compute trial iterate*
$$\mathbf{U}^{n+1} := \mathbf{U}^n + \lambda_n \mathbf{Z}^n \tag{183}$$

   *and evaluate the new residual $\mathbf{B}(\mathbf{U}^{n+1})$. Solve the simplified linear system using the old Jacobian:*
$$\mathbf{B}'(\mathbf{U}^n)\mathbf{Z}^{n+1}_{simp} = -\big(\mathbf{B}(\mathbf{U}^{n+1}) - \mathbf{f}\big)$$

4. *Compute the monitoring functions:*
$$\theta_n := \frac{\|\mathbf{Z}^{n+1}_{simp}\|}{\|\mathbf{Z}^n\|}, \quad \mu'_n := \frac{0.5\|\mathbf{Z}^n\| \cdot \lambda_n^2}{\|\mathbf{Z}^{n+1}_{simp} - (1 - \lambda_n)\mathbf{Z}^n\|}.$$

5. *If $\theta_n \geq 1$ (no convergence of the updates), then set*
$$\lambda_n := \lambda'_n := \min(\mu'_n, \frac{1}{2}\lambda_n)$$

   *and go to (182) and continue from there.*

6. *If $\theta_n < 1$, we have convergence and continue with the next steps.*

   a) *If $\lambda'_n = \lambda_n = 1$, check if*
$$\|\mathbf{Z}^{n+1}_{simp}\| \leq TOL$$

   *then stop and the solution is found:*
$$\mathbf{U}^* := \mathbf{U}^{n+1} + \mathbf{Z}^{n+1}_{simp}.$$

   b) *Else accept $\mathbf{U}^{n+1}$ (computed in (183)) as new iterate. Then increment $n \to n+1$ and goto to the beginning to Step 1.*

**Remark 9.11** (Combination of stopping criteria)**.** *In practice it turned out that a combination of stopping criteria worked quite well:*
$$\min\{\|F(x^{k+1})\|, \|\delta x^k\|\} \leq \varepsilon.$$

## 9.2 Excurse to linearization methods for Navier-Stokes

Since the resulting fluid problem is nonlinear because of $N(v)$, important linearizations have been proposed in order to facilitate the solution of this time-stepping scheme.

**9.2.0.1 Stokes linearization**   Using the Stokes linearization (for small Reynolds numbers), the nonlinearity can be treated fully explicitly:

$$v + \delta t \nabla p = v^{n-1} - \delta t N(v^{n-1})\delta t\theta f + \delta t(1-\theta)f^{n-1}, \quad \nabla \cdot v = 0.$$

This simplifies the problem as it is now linear and in each step, the symmetric and positive Stokes-operator must be inverted.

**9.2.0.2 Oseen linearization**   For higher Reynold's numbers, the so-called Oseen linearization can be consulted:

$$v + \delta t\theta\tilde{N}(v) + \delta t\nabla p = v^{n-1} - \delta t(1-\theta)\tilde{N}(v^{n-1})\delta t\theta f + \delta t(1-\theta)f^{n-1}, \quad \nabla \cdot v = 0,$$

where

$$\tilde{N}(v) = \tilde{v} \cdot \nabla v,$$

where, for instance a constant extrapolation $\tilde{v} = v^{n-1}$ or linear extrapolation $\tilde{v} = 2v^{n-1} - v^{n-2}$ can be employed. Here, at each step, a (linear) nonsymmetric diffusion-transport operator must be inverted.

**9.2.0.3 Newton linearization - fully nonlinear treatment of convection**   This is the linearization scheme that is described afterwards for fully-coupled fluid-structure interaction.

$$v + \delta t\theta(v^n \cdot \nabla v^{n-1} + v^{n-1} \cdot \nabla v^n) + \delta t\nabla p = v^{n-1} - \delta t(1-\theta)\tilde{N}(v^{n-1})\delta t\theta f + \delta t(1-\theta)f^{n-1}, \quad \nabla \cdot v = 0,$$

## 9.3 Evaluation of directional derivatives

Due to the large size of the Jacobian matrix and the strongly nonlinear behavior of fluid-structure interaction problems in the monolithic ALE framework, the calculation of the Jacobian matrix can be cumbersome. Nevertheless, in this context, we use the exact Jacobian matrix to identify the optimal convergence and accuracy properties of the Newton method. The derivation of directional derivatives is also illustrated by means of several examples presented elsewhere [83, 196, 241]. For more details on the computation of the directional derivatives on the interface, we refer the reader to [73, 200]. Evaluation of the directional derivatives for fluid-structure interaction with help of *automatic differentiation* is demonstrated by Dunne [73].

### 9.3.1 First some simple examples

Recall that we need to differentiate in each direction by using Definition 9.9.

**Example 9.12.** *Let $u$ be the solution variable for*

$$A(u)(\varphi) = (\nabla u, \nabla \varphi)$$

*be the residual. Then, the directional derivative in direction $\delta u$ is given by:*

$$A'(u)(\delta u, \varphi) = (\nabla \delta u, \nabla \varphi).$$

**Example 9.13.** *Let $p$ and $u$ solution variables for*

$$A(p,u)(\varphi) = (-pI + \rho\nu(\nabla u + \nabla u^T), \nabla \varphi)$$

*be the residual. Then, the directional derivative in direction $\{\delta p, \delta u\}$ is given by:*

$$A'(p,u)(\{\delta p, \delta u\}, \varphi) = (-\delta p I + \rho\nu(\nabla \delta u + \nabla \delta u^T), \nabla \varphi).$$

**Remark 9.14.** *Hopefully you noticed that everything was linear so far.* ⋄

**Example 9.15.** *Let $v$ and $u$ solution variables for*

$$A(v, u)(\varphi) = (v\nabla u, \nabla \varphi)$$

*be the residual. Then, the directional derivative in direction $\{\delta v, \delta u\}$ is given by:*

$$A'(v, u)(\{\delta v, \delta u\}, \varphi) = (\delta v \nabla u + v \nabla \delta u, \nabla \varphi)$$

*using the chain rule.*

Despite the fact that we later account on block system, let us explain what we mean by *taking all directional derivatives in the context of finite elements*. Let $V_h := \{\varphi_1, \ldots, \varphi_N\}$ a finite element space. The relation between derivatives and linear equation system is as follows. Given $u \in V_h$, the residual reads:

$$A(u_h)(\varphi_h) = (\nabla u_h, \nabla \varphi_h) \quad \forall \varphi_h \in V_h.$$

Now we build the derivative in direction $\delta u_h$:

$$A'(u_h)(\delta u_h, \varphi_h) = (\nabla \delta u_h, \nabla \varphi_h) \quad \forall \varphi_h \in V_h.$$

Recall that $\delta u_h = \sum_{j=1}^{N} u_j \varphi_j$. Now, we replace $\delta u_h$ by all test functions using its property being a linear combination and for all test functions:

$$A'(u_h)(\varphi_i, \varphi_j) = \sum_j u_j (\nabla \varphi_j, \nabla \varphi_i)$$

Then, we obtain $Ax = b$ with

$$A = \begin{pmatrix} (\nabla \varphi_1, \nabla \varphi_1) & \ldots & (\nabla \varphi_N, \nabla \varphi_1) \\ & \vdots & \\ (\nabla \varphi_1, \nabla \varphi_N) & \ldots & (\nabla \varphi_N, \nabla \varphi_N) \end{pmatrix} \tag{184}$$

and $x = (u_1, \ldots, u_N)^T$.

**Remark 9.16.** *Do not forget: the test function dictates the row! In symmetric problems like for Poisson problems this does not matter, but in non-symmetric problems (transport, Navier-Stokes) this is important.* ⋄

### 9.3.2 Directional derivatives of fluid-structure

In this section, we apply the previous concepts to the evaluation of the directional derivatives for fluid-structure interaction. We examin term by term. As before, let the solution $\hat{U}_h^n = \{\hat{v}_{f,h}^n, \hat{v}_{s,h}^n, \hat{u}_{f,h}^n, \hat{u}_{s,h}^n, \hat{p}_{f,h}^n, \hat{p}_{s,h}^n\} \in \widehat{X}_h$ be given. Further, let $\delta \hat{U}_h^n = \{\delta \hat{v}_{f,h}^n, \delta \hat{v}_{s,h}^n, \delta \hat{u}_{f,h}^n, \delta \hat{u}_{s,h}^n, \delta \hat{p}_{f,h}^n, \delta \hat{p}_{s,h}^n\} \in \widehat{X}_h$. In the following, we omit explicit notation of 'h' and 'n'.

The Jacobian $\hat{A}'(\hat{U})(\delta \hat{U}, \hat{\Psi})$ is split up into fluid contributions and structure terms:

$$\hat{A}'(\hat{U})(\delta \hat{U}, \hat{\Psi}) := \hat{A}'_f(\hat{U}_f)(\delta \hat{U}_f, \hat{\Psi}_f) + \hat{A}'_s(\hat{U})(\delta \hat{U}_s, \hat{\Psi}_s).$$

Using the previous arrangement (107), we deal with

$$\hat{A}'_f(\hat{U}_f)(\delta \hat{U}_f, \hat{\Psi}_f) \tag{185}$$
$$= \hat{A}'_{f,T}(\hat{U}_f)(\delta \hat{U}_f, \hat{\Psi}_f) + \hat{A}'_{f,I}(\hat{U}_f)(\delta \hat{U}_f, \hat{\Psi}_f) + \hat{A}'_{f,E}(\hat{U}_f)(\delta \hat{U}_f, \hat{\Psi}_f) + \hat{A}'_{f,P}(\hat{U}_f)(\delta \hat{U}_f, \hat{\Psi}_f), \tag{186}$$

and

$$\hat{A}'_s(\hat{U}_s)(\delta \hat{U}_s, \hat{\Psi}_s) \tag{187}$$
$$= \hat{A}'_{s,T}(\hat{U}_s)(\delta \hat{U}_s, \hat{\Psi}_s) + \hat{A}'_{s,I}(\hat{U}_s)(\delta \hat{U}_s, \hat{\Psi}_s) + \hat{A}'_{s,E}(\hat{U}_s)(\delta \hat{U}_s, \hat{\Psi}_s) + \hat{A}'_{s,P}(\hat{U}_s)(\delta \hat{U}_s, \hat{\Psi}_s). \tag{188}$$

The concrete evaluation of each term on the fully discrete level is derived in the following.

**Basic relations**

In the sequel, we often use the short-hand-notation

$$\partial_b A(\delta z) := \frac{\partial A}{\partial b}(\delta z),$$

for the derivative of a tensor $A$ w.r.t. $b$ in direction $\delta z$. We begin with the basic relations that are required for each of the subproblems. For the deformation gradient $\widehat{F}$, it holds in a direction $\delta \hat{z} \in H^1(\widehat{\Omega})$:

$$\partial_z \widehat{F}(\delta \hat{z}) = \widehat{\nabla} \delta \hat{z}, \quad \partial_z \widehat{F}^T(\delta \hat{z}) = \widehat{\nabla} \delta \hat{z}^T. \tag{189}$$

In the following, we recall the evaluation of the inverse relations (see, e.g., [137])

$$\partial_z \widehat{F}^{-1}(\delta \hat{z}) = -\widehat{F}^{-1}\widehat{\nabla}\delta \hat{z}\widehat{F}^{-1}, \quad \partial_z \widehat{F}^{-T}(\delta \hat{z}) = -\widehat{F}^{-T}\widehat{\nabla}\delta \hat{z}^T \widehat{F}^{-T}.$$

Finally, the derivative of the determinant $\hat{J}$ can be expressed as

$$\partial_z \hat{J}(\delta z) = \hat{J}\mathrm{tr}(\widehat{F}^{-1}\widehat{\nabla}\delta z).$$

**Fluid's Cauchy stress tensor**

In the fluid part, we are concerned with the evaluation of directional derivatives in the three directions $\delta \hat{v}_f, \delta \hat{p}_f$ and $\delta \hat{u}_f$. We start with the Cauchy stress tensor $\widehat{\sigma}_f = \widehat{\sigma}_{f,vu} + \widehat{\sigma}_{f,p}$:

$$\partial_v \widehat{\sigma}_{f,vu}(\delta \hat{v}_f) = 2\hat{\rho}_f \nu_f (\widehat{\nabla}\delta \hat{v}_f \widehat{F}^{-1} + \widehat{F}^{-T}\widehat{\nabla}\delta \hat{v}_f^T),$$
$$\partial_p \widehat{\sigma}_{f,p}(\delta \hat{p}_f) = -\delta \hat{p}_f \hat{I},$$
$$\partial_u \widehat{\sigma}_{f,vu}(\delta \hat{u}_f) = 2\hat{\rho}_f \nu_f (\widehat{\nabla}\hat{v}_f(-\widehat{F}^{-1}\widehat{\nabla}\delta \hat{u}\widehat{F}^{-1}) + (-\widehat{F}^{-T}\widehat{\nabla}\delta \hat{u}^T \widehat{F}^{-T})\widehat{\nabla}\hat{v}_f^T).$$

Summarizing these contributions yields

$$\partial_U \widehat{\sigma}_{f,vu}(\delta \hat{U}_f) = \partial_v \widehat{\sigma}_{f,vu}(\delta \hat{v}_f) + \partial_u \widehat{\sigma}_{f,vu}(\delta \hat{u}_f), \qquad \partial_U \widehat{\sigma}_{f,p}(\delta \hat{U}_f) = \partial_p \widehat{\sigma}_{f,p}(\delta \hat{v}_p).$$

Thus, the derivative of the transformed Cauchy stress tensor in the reference domain reads:

$$\partial_U(\hat{J}\widehat{\sigma}_f \widehat{F}^{-T})(\delta \hat{U}_f) = \hat{J}\mathrm{tr}(\widehat{F}^{-1}\widehat{\nabla}\delta \hat{u}_f)\widehat{\sigma}_f \widehat{F}^{-T} + \hat{J}\partial_U \widehat{\sigma}_f(\delta \hat{U}_f)\widehat{F}^{-T} + \hat{J}\widehat{\sigma}_f(-\widehat{F}^{-T}\widehat{\nabla}\delta \hat{u}_f^T \widehat{F}^{-T}).$$

The Cauchy stress tensor is decomposed by reason motivated in Problem 8.14. It is obvious that this decomposition must be considered in the linearization process, too.

**Fluid's convection term**

For the treatment of the convection term (also including the ALE convection term), we use the relation $\hat{u}_f \cdot \widehat{\nabla}\hat{v}_f = \widehat{\nabla}\hat{v}_f\, \hat{u}_f$ and decompose the convection term as

$$\hat{\rho}_f \hat{J}(\widehat{F}^{-1}(\hat{v}_f - \hat{w}) \cdot \widehat{\nabla})\hat{v}_f = \hat{\rho}_f \hat{J}(\widehat{\nabla}\hat{v}_f \widehat{F}^{-1})\hat{v}_f - \hat{\rho}_f \hat{J}(\widehat{\nabla}\hat{w}\widehat{F}^{-1})\hat{v}_f.$$

With the help of the previously introduced basic relations, the derivative of the first part reads:

$$\partial_U(\hat{\rho}_f \hat{J}(\widehat{\nabla}\hat{v}_f \widehat{F}^{-1})\hat{v}_f)(\delta \hat{U}_f) = \hat{\rho}_f \hat{J}\mathrm{tr}(\widehat{F}^{-1}\widehat{\nabla}\delta \hat{u}_f)(\widehat{\nabla}\hat{v}_f \widehat{F}^{-1})\hat{v}_f \tag{190}$$

$$+ \hat{\rho}_f \hat{J}(\widehat{\nabla}\delta \hat{v}_f \widehat{F}^{-1})\hat{v}_f \tag{191}$$

$$+ \hat{\rho}_f \hat{J}(\widehat{\nabla}\hat{v}_f(-\widehat{F}^{-1}\widehat{\nabla}\delta \hat{u}_f \widehat{F}^{-1})\hat{v}_f \tag{192}$$

$$+ \hat{\rho}_f \hat{J}(\widehat{\nabla}\hat{v}_f \widehat{F}^{-1})\delta \hat{v}_f. \tag{193}$$

In the second part, we cannot directly differentiate the fluid domain velocity $\hat{w}$. As previously discussed this term is constructed (linear in time) with the help of the displacements $\hat{u}_f$. Thus, in Equation (190), we only must replace the second term. Using the construction of $\hat{w} = \frac{1}{k}(\hat{u}_f - \hat{u}_f^{n-1})$ in which $\hat{u}_f^{n-1}$ denotes the solution of the previous time step, we readily get

$$\partial_u \hat{w}(\delta \hat{u}_f) := \partial_u \frac{1}{k}(\hat{u}_f - \hat{u}_f^{n-1})(\delta \hat{u}_f) = \frac{1}{k}\delta \hat{u}_f. \tag{194}$$

With this, we obtain for the second equation on the right-hand-side in (190)

$$\frac{1}{k}\hat{\rho}_f\hat{J}(\widehat{\nabla}\delta\hat{u}_f\widehat{F}^{-1})\hat{v}_f.$$

In the remaining terms of (190), we replace $\widehat{\nabla}\hat{v}_f$ with $\widehat{\nabla}\hat{w}$.

**Fluid's time derivative**

We continue with the time derivative of the fluid term:

$$\hat{\rho}_f\hat{J}\partial_t\hat{v}_f \approx \hat{\rho}_f\hat{J}^{n,\theta}\frac{\hat{v}_f - \hat{v}_f^{n-1}}{k},$$

where we employ (110) for the temporal discretization. First, we obtain

$$\partial_u\hat{J}^{n,\theta}(\delta\hat{u}_f) = \partial_u(\theta\hat{J} + (1-\theta)\hat{J}^{n-1})(\delta\hat{u}_f) = \theta\hat{J}\mathrm{tr}(\widehat{F}^{-1}\widehat{\nabla}\delta\hat{u}_f). \tag{195}$$

Next, we get

$$\partial_v\frac{1}{k}(\hat{v}_f - \hat{v}_f^{n-1})(\delta\hat{v}_f) = \frac{1}{k}\delta\hat{v}_f.$$

With this equation, we compute for (195):

$$\partial_U\big(\hat{\rho}_f\frac{1}{k}\hat{J}^{n,\theta}(\hat{v}_f - \hat{v}_f^{n-1})\big)(\delta\hat{U}_f) = \hat{\rho}_f\frac{\theta}{k}\hat{J}\mathrm{tr}(\widehat{F}^{-1}\widehat{\nabla}\delta\hat{u}_f)(\hat{v}_f - \hat{v}_f^{n-1}) + \hat{\rho}_f\frac{1}{k}\hat{J}^{n,\theta}(\delta\hat{v}_f).$$

**Fluid's incompressibility**

We proceed with the incompressibility term of the fluid. To compute the derivative, we utilize a byproduct of the divergence relation of the Piola transformation:

$$\widehat{\mathrm{div}}(\hat{J}\widehat{F}^{-1}\hat{v}_f) = \hat{J}\mathrm{tr}(\widehat{\nabla}\hat{v}_f\widehat{F}^{-1}).$$

Then, we get

$$\partial_v\hat{J}\mathrm{tr}(\widehat{\nabla}\hat{v}_f\widehat{F}^{-1})(\delta\hat{v}_f) = \hat{J}\mathrm{tr}(\widehat{\nabla}\delta\hat{v}_f\widehat{F}^{-1}),$$
$$\partial_u\hat{J}\mathrm{tr}(\widehat{\nabla}\hat{v}_f\widehat{F}^{-1})(\delta\hat{u}_f) = \hat{J}\mathrm{tr}(\widehat{F}^{-1}\widehat{\nabla}\delta\hat{u}_f)\mathrm{tr}(\widehat{\nabla}\hat{v}_f\widehat{F}^{-1}) - \hat{J}\mathrm{tr}(\widehat{\nabla}\hat{v}_f\widehat{F}^{-1}\widehat{\nabla}\delta\hat{u}_f\widehat{F}^{-1}).$$

**Fluid's mesh motion**

It remains to consider the derivative of the mesh motion equation. Using the harmonic mesh motion model (see definition of $\hat{\sigma}_{\mathrm{mesh}}$ in (74)), we readily obtain

$$\partial_u(\alpha_u\widehat{\nabla}\hat{u}_f)(\delta\hat{u}_f) = \alpha_u\widehat{\nabla}\delta\hat{u}_f.$$

Using the linear-elastic mesh motion model (see definition of $\hat{\sigma}_{\mathrm{mesh}}$ in (61)), we get

$$\partial_u(\alpha_\lambda(\mathrm{tr}\,\hat{\epsilon})\hat{I} + 2\alpha_\mu\hat{\epsilon})(\delta\hat{u}_f) = \alpha_\lambda\frac{1}{2}(\mathrm{tr}\,(\widehat{\nabla}\delta\hat{u}_f + \widehat{\nabla}\delta\hat{u}_f^T)\hat{I} + \alpha_\mu(\widehat{\nabla}\delta\hat{u}_f + \widehat{\nabla}\delta\hat{u}_f^T).$$

**Fluid's do-nothing condition**

Next, we consider the derivative of the boundary term $\hat{g}_f := -\hat{\rho}_f\nu_f\widehat{F}^{-T}\widehat{\nabla}\hat{v}_f^T$ on $\widehat{\Gamma}_{f,N}$ (see (50)):

$$\partial_U(-\hat{\rho}_f\nu_f\widehat{F}^{-T}\widehat{\nabla}\hat{v}_f^T)(\delta\hat{U}_f) = \hat{\rho}_f\nu_f(\widehat{F}^{-T}\widehat{\nabla}\delta\hat{u}_f^T\widehat{F}^{-T})\widehat{\nabla}\hat{v}_f^T - \hat{\rho}_f\nu_f\widehat{F}^{-T}\widehat{\nabla}\delta\hat{v}_f^T.$$

**Fluid's stabilization**

Finally, we explain the differentiation of the stabilization term. In this expression, we only differentiate the first argument although the second argument also depends on the solution variable. Using the derivative of the convection term, we readily obtain

$$\hat{S}'_{\mathrm{stab}}(\hat{U}_f)(\delta\hat{U}_f, \hat{\Psi}_f) = (\partial_U(\hat{\rho}_f\hat{J}(\widehat{\nabla}\hat{v}_f\widehat{F}^{-1})\hat{v}_f)(\delta\hat{U}_f), \delta_{K,n}(\widehat{F}^{-1}\hat{v}_f \cdot \widehat{\nabla})\hat{\psi}_f^v)_{\widehat{K}_f}, \tag{196}$$

on each cell $\widehat{K}_f \in \mathcal{T}_h$.

**Structure's constitutive tensors**

We continue with the description for the derivatives of the structure subproblem. Using standard elasticity (i.e., the damping terms are omitted) with the STVK model, we only must compute the derivatives with respect to $\hat{u}_s$. In the presence of incompressible materials, we also account for the pressure $\hat{p}_s$. Finally, the consideration of strong damping makes it necessary to compute derivatives with respect to $\hat{v}_s$.

Let us begin with the Green-Lagrange tensor that is employed to formulate the STVK material:

$$\partial_u \widehat{E}(\delta \hat{u}_s) = \frac{1}{2}(\widehat{\nabla}\delta \hat{u}_s^T \widehat{F} + \widehat{F}^T \widehat{\nabla}\delta \hat{u}_s).$$

Then, the constitutive tensor $\widehat{\Sigma} := \widehat{\Sigma}(\hat{u}_s)$ reads

$$\partial_u \widehat{\Sigma}(\delta \hat{u}_s) = \lambda_s \frac{1}{2}\text{tr}(\widehat{\nabla}\delta \hat{u}_s^T \widehat{F} + \widehat{F}^T \widehat{\nabla}\delta \hat{u}_s)\hat{I} + \mu_s(\widehat{\nabla}\delta \hat{u}_s^T \widehat{F} + \widehat{F}^T \widehat{\nabla}\delta \hat{u}_s).$$

For the incompressible IMR material, we obtain

$$\partial_p \widehat{\sigma}_{\text{IMR}}(\delta \hat{p}_s) = -\delta \hat{p}_s \hat{I},$$
$$\partial_u \widehat{\sigma}_{\text{IMR}}(\delta \hat{u}_s) = \mu_1(\delta \hat{u}_s \widehat{F}^T + \widehat{F}\delta \hat{u}_s^T) - \mu_2(\widehat{F}^{-T}\widehat{\nabla}\delta \hat{u}_s^T \widehat{F}^{-T}\widehat{F}^{-1} + \widehat{F}^{-T}\widehat{F}^{-1}\widehat{\nabla}\delta \hat{u}_s \widehat{F}^{-1},$$

and from this, we readily deduce

$$\partial_p \widehat{\sigma}_{\text{INH}}(\delta \hat{p}_s) = -\delta \hat{p}_s \hat{I},$$
$$\partial_u \widehat{\sigma}_{\text{INH}}(\delta \hat{u}_s) = \mu_1(\delta \hat{u}_s \widehat{F}^T + \widehat{F}\delta \hat{u}_s^T).$$

**Structure's damping terms**

Finally, using strong damping, we compute the derivatives in the direction $\delta \hat{v}_s$ of $\hat{\epsilon}(\hat{v}_s)$. Then,

$$\partial_v \hat{\epsilon}(\hat{v}_s)(\delta \hat{v}_s) = \frac{1}{2}(\widehat{\nabla}\delta \hat{v}_s + \widehat{\nabla}\delta \hat{v}_s^T).$$

**Proposition 9.17.** *Let $k := t^n - t^{n-1}$ the time step size and $0 \leq \theta \leq 1$. At each Newton step (179), we solve a linear system with the residual $\hat{A}(\hat{U})(\hat{\Psi}) - \hat{F}(\hat{\Psi})$. The Jacobian of this problem is split into*

$$\hat{A}'(\hat{U})(\delta\hat{U}, \hat{\Psi}) := \hat{A}'_f(\hat{U}_f)(\delta\hat{U}_f, \hat{\Psi}_f) + \hat{A}'_s(\hat{U}_s)(\delta\hat{U}_s, \hat{\Psi}_s).$$

*Using the arrangements (185) and (187), we deal with the following expressions in the fluid domain (including SUPG stabilization):*

$$\begin{aligned}
\hat{A}'_{f,T}(\hat{U}_f)(\delta\hat{U}_f, \hat{\Psi}_f) &= \hat{\rho}_f \frac{\theta}{k}(\hat{J}tr(\widehat{F}^{-1}\widehat{\nabla}\delta\hat{u}_f)(\hat{v}_f - \hat{v}_f^{n-1}), \hat{\psi}_f^v)_{\widehat{\Omega}_f} + \hat{\rho}_f \frac{1}{k}(\hat{J}^{n,\theta}(\delta\hat{v}_f), \hat{\psi}_f^v)_{\widehat{\Omega}_f} \\
&\quad + \hat{\rho}_f(\hat{J}(\widehat{\nabla}\hat{v}_f\widehat{F}^{-1})(\delta\hat{v}_f - k^{-1}\delta\hat{u}_f), \hat{\psi}_f^v)_{\widehat{\Omega}_f}, \\
&\quad + \hat{\rho}_f(\hat{J}tr(\widehat{F}^{-1}\widehat{\nabla}\delta\hat{u}_f)(\widehat{\nabla}\hat{v}_f\widehat{F}^{-1})(\hat{v}_f - \hat{w}), \hat{\psi}_f^v)_{\widehat{\Omega}_f} \\
&\quad + \hat{\rho}_f(\hat{J}(\widehat{\nabla}\delta\hat{v}_f\widehat{F}^{-1})(\hat{v}_f - \hat{w}), \hat{\psi}_f^v)_{\widehat{\Omega}_f} \\
&\quad + \hat{\rho}_f(\hat{J}(\widehat{\nabla}\hat{v}_f(-\widehat{F}^{-1}\widehat{\nabla}\delta\hat{u}_f\widehat{F}^{-1})(\hat{v}_f - \hat{w}), \hat{\psi}_f^v)_{\widehat{\Omega}_f} \\
\hat{A}'_{f,E}(\hat{U}_f)(\delta\hat{U}_f, \hat{\Psi}_f) &= (\partial_U(\hat{J}\widehat{\sigma}_{f,vu}\widehat{F}^{-T})(\delta\hat{U}_f), \hat{\psi}_f^v)_{\widehat{\Omega}_f} + \langle\partial_U g_f(\delta\hat{U}), \hat{\psi}_f^v\rangle_{\widehat{\Gamma}_N} \\
&\quad - (\rho_f\hat{J}tr(\widehat{F}^{-1}\widehat{\nabla}\delta\hat{u}_f)\hat{f}_f, \hat{\psi}_f^v)_{\widehat{\Omega}_f}, \\
\hat{A}'_{f,I}(\hat{U}_f)(\delta\hat{U}_f, \hat{\Psi}_f) &= (\alpha_u\widehat{\nabla}\delta\hat{u}_f, \widehat{\nabla}\hat{\psi}_f^u)_{\widehat{\Omega}_f} \\
&\quad + (\hat{J}tr(\widehat{\nabla}\delta\hat{v}_f\widehat{F}^{-1}), \hat{\psi}_f^p)_{\widehat{\Omega}_f} + (\hat{J}tr(\widehat{F}^{-1}\widehat{\nabla}\delta\hat{u}_f)tr(\widehat{\nabla}\hat{v}_f\widehat{F}^{-1}), \hat{\psi}_f^p)_{\widehat{\Omega}_f} \\
&\quad - (\hat{J}tr(\widehat{\nabla}\hat{v}_f\widehat{F}^{-1}\widehat{\nabla}\delta\hat{u}_f\widehat{F}^{-1}), \hat{\psi}_f^p)_{\widehat{\Omega}_f}, \\
\hat{A}'_{f,P}(\hat{U}_f)(\delta\hat{U}_f, \hat{\Psi}_f) &= (\partial_U(\hat{J}\widehat{\sigma}_{f,p}\widehat{F}^{-T})(\delta\hat{U}_f), \widehat{\nabla}\hat{\psi}_f^v)_{\widehat{\Omega}_f}, \\
\hat{S}'_{stab}(\hat{U}_f)(\delta\hat{U}_f, \hat{\Psi}_f) &= (\partial_U(\hat{\rho}_f\hat{J}(\widehat{\nabla}\hat{v}_f\widehat{F}^{-1})\hat{v}_f)(\delta\hat{U}_f), \delta_{K,n}(\widehat{F}^{-1}\hat{v}_f \cdot \widehat{\nabla})\hat{\psi}_f^v)_{\widehat{K}_f},
\end{aligned}$$

*and in the solid domain (inlcuding solid damping terms), we have:*

$$\begin{aligned}
\hat{A}'_{s,T}(\hat{U}_s)(\delta\hat{U}_s, \hat{\Psi}_s) &= k^{-1}(\hat{\rho}_s\delta\hat{v}_s, \hat{\psi}_s^v)_{\widehat{\Omega}_s} + k^{-1}(\hat{\rho}_s\hat{u}_s, \hat{\psi}_s^u)_{\widehat{\Omega}_s} - (\hat{\rho}_s\delta\hat{v}_s, \hat{\psi}_s^u)_{\widehat{\Omega}_s} \\
&\quad + (\partial_U\hat{P}(\delta\hat{U}_s), \hat{\psi}_s^p)_{\widehat{\Omega}_s}, \\
\hat{A}'_{s,E}(\hat{U}_s)(\delta\hat{U}_s, \hat{\Psi}_s) &= (\partial_u(\widehat{F}\widehat{\Sigma})(\delta\hat{u}_s), \widehat{\nabla}\hat{\psi}_s^v)_{\widehat{\Omega}_s} \\
&\quad + \gamma_w(\delta\hat{v}_s, \hat{\psi}_s^v)_{\widehat{\Omega}_s} + \gamma_s(\partial_v\hat{\epsilon}(\hat{v}_s)(\delta\hat{v}_s), \hat{\psi}_s^v)_{\widehat{\Omega}_s}, \\
\hat{A}'_{s,I}(\hat{U}_s)(\delta\hat{U}_s, \hat{\Psi}_s) &= (\partial_U\hat{P}(\delta\hat{U}_s), \hat{\psi}_s^p)_{\widehat{\Omega}_s}, \\
\hat{A}'_{s,P}(\hat{U}_s)(\delta\hat{U}_s, \hat{\Psi}_s) &= (\partial_U(\hat{J}\widehat{\sigma}_{s,p}\widehat{F}^{-T})(\delta\hat{U}_s), \widehat{\nabla}\hat{\psi}_s^v)_{\widehat{\Omega}_f}.
\end{aligned}$$

### 9.3.3 Illustration of Newton performance: computational structure mechanics (CSM) tests

In this section, we illustrate the Newton performance, the relation between timestep size and Newton convergence, and the consequences of a linear solid model. The investigation is performed with the help of a structural mechanics test with the same configuration as the FSI benchmark. For this test, reference values are available.
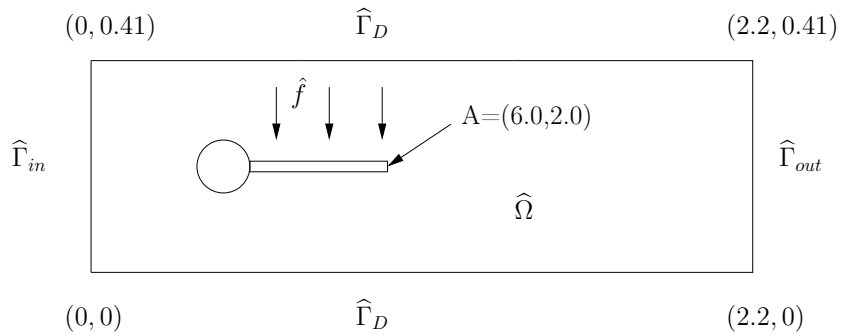


Figure 53: Computational structure mechanics (CSM) test with elastic beam with circle-center $C = (0.2, 0.2)$ and radius $r = 0.05$.
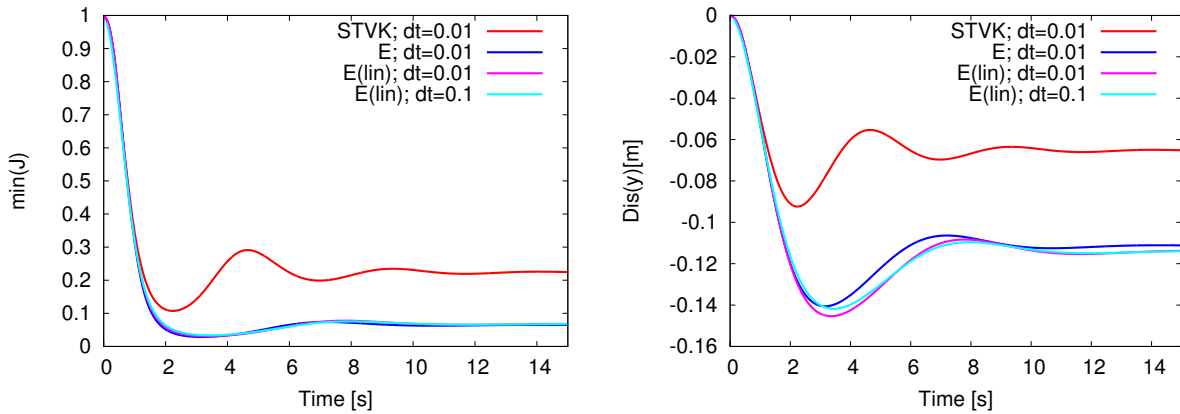
Figure 54: Computational structure mechanics (CSM) tests: CSM 1 [140]. Comparisons of different solid models: $\widehat{\Sigma}_{lin} = \mu(\nabla u + \nabla u^T)$, $\widehat{\Sigma} = \mu\widehat{E}$, and $\widehat{F}\Sigma = 2\mu\widehat{E} + \lambda tr(\widehat{E})I$ (STVK). Using linear or slightly nonlinear models yield a much larger (wrong!) deflection of the elastic beam than using the standard nonlinear STVK model. However, both nonlinear models show much worse Newton convergence than the linear model. In fact, using the larger time step $\delta t = 0.1s$ cause the Newton solver break down.

Newton convergence at time step 2 with $\delta t = 0.1s$ and using the slightly nonlinear model $\widehat{\Sigma} = \mu\widehat{E}$:

```
1        1.91506e-02        r        3
2        1.50366e-02        r        3
3        1.20513e-02        r        4
4        1.16064e-02        r        3
5        1.14506e-02        r        2
6        1.13437e-02        r        1
7        9.10672e-03        r        0
8        2.03220e-03        r        0
9        2.36171e-07                 0
10       3.24662e-08        r        0
         1.23206e-09
```

*The first column shows the number of Newton iterations, the second column displays the Newton residual, the third column shows if the Jacobian is re-build, and the fourth column displays the number of line search iterations.*

From this table, we are able to explain several things. First, the (absolute) stopping criterion for Newton's method in this test is $10^{-8}$. Second, up to iteration No. 8, the Newton solver converges very slowly while seeking for a good starting value in order to obtain super-linear or quadratic convergence. Fast convergence is then seen in the last two steps. While a good starting value needs to be found, the Newton method even needs line search iterations. Once, we are in the convergence radius, the matrix even does need to be re-build.

The corresponding table using a smaller time step $\delta = 0.01s$ reads:

```
1        2.19937e-03        r        0
2        1.34133e-05                 0
         4.16041e-09
```

*The same configuration with a smaller time step yields much fast convergence, without any line search steps and only one matrix build-up.*

## 9.4 Structure and solution of the discrete linear equation systems

In this final subsection of this chapter, we discuss the structure of the discrete linear equation systems and possible solution strategies. For linear problems such Poisson's problem, linearized elasticity or linear MM-PDEs, we solve immediately for the solution variable. In nonlinear problems such as Navier-Stokes, elasticity or fluid-structure interaction, linear equations must be solved within the nonlinear iteration (here Newton's method) (179). Therein, the linear equations are solved for Newton's update $\delta U_h^n$; more details are presented below.

### 9.4.1 Stationary linearized elasticity

As previsously discussed, the spatial discretization is based upon a space $V_h$ with basis $\{\varphi_1, \ldots, \varphi_N\}$ where $N$ is the dimension of this space. Here we solve the problem: Find $u_h \in V_h$ such that

$$A(u_h, \varphi_h) = F(\varphi_h) \quad \forall \varphi_h \in V_h.$$

This relation does in particular hold for each test function $\varphi_i, i = 1, \ldots, N$:

$$A(u_h, \varphi_h^i) = F(\varphi_h^i) \quad \forall \varphi_h^i, i = 1, \ldots, N$$

The solution $u_h$ we are seeking for is a linear combination of all test functions, i.e., $u_h = \sum_{j=1}^N u_j \varphi_h^j$. Inserting this relation into the bilinear form $A(\cdot, \cdot)$ yields

$$\sum_{j=1}^N a(\varphi_h^j, \varphi_h^i) u_j = f(\varphi_h^i), \quad i = 1, \ldots, N.$$

It follows for the ingredients of the linear equation system:

$$u = (u_j)_{j=1}^N \in \mathbb{R}^N, \quad b = (f_i)_{i=1}^N \in \mathbb{R}^N, \quad A = a_{ij} = a(\varphi_h^J, \varphi_h^i)$$

The resulting linear equation systems reads:
$$Au = b$$

**Remark 9.18.** *In the matrix $A$ the rule is always as follows: the test $\varphi_h^i$ function determines the row and the trial function $\varphi_h^j$ the column. This does not play a role for symmetric problems (e.g., Poisson's problem) but becomes important for nonsymmetric problems such as for example Navier-Stokes (because of the convection term).*

**Remark 9.19.** *In the matrix, the degrees of freedom that belong to Dirichlet conditions (here only displacements since we assume Neumann conditions for the phase-field) are strongly enforced by replacing the corresponding rows and columns as usual in a finite element code.*

**Example 9.20** (3D linearized elasticity). *In this vector-valued problem, we have $3N$ test functions since the solution vector is an element of $\mathbb{R}^3$: $u_h = (u_h^{(1)}, u_h^{(2)}, u_h^{(3)})$. Thus in the boundary value problem*

$$Find \ u_h \in V_h : \quad (\nabla u_h, \varphi_h) = (f, \varphi_h) \quad \forall \varphi_h \in V_h,$$

*the bilinear form is tensor-valued:*

$$a(\varphi_h^j, \varphi_h^i) = \int_\Omega \nabla \varphi_h^j : \nabla \varphi_h^i \, dx = \int_\Omega \begin{pmatrix} \partial_1 \varphi_h^{1,j} & \partial_2 \varphi_h^{1,j} & \partial_3 \varphi_h^{1,j} \\ \partial_1 \varphi_h^{2,j} & \partial_2 \varphi_h^{2,j} & \partial_3 \varphi_h^{2,j} \\ \partial_1 \varphi_h^{3,j} & \partial_2 \varphi_h^{3,j} & \partial_3 \varphi_h^{3,j} \end{pmatrix} : \begin{pmatrix} \partial_1 \varphi_h^{1,i} & \partial_2 \varphi_h^{1,i} & \partial_3 \varphi_h^{1,i} \\ \partial_1 \varphi_h^{2,i} & \partial_2 \varphi_h^{2,i} & \partial_3 \varphi_h^{2,i} \\ \partial_1 \varphi_h^{3,i} & \partial_2 \varphi_h^{3,i} & \partial_3 \varphi_h^{3,i} \end{pmatrix} dx$$

**Example 9.21** (Example in 1D). *Let us illustrate and specify how the entries of the system matrix can be computed in 1D.*

### 9.4.2 Stationary Stokes

Let $U_h = \{v_h, p_h\}$, $X_h := V_h \times L_h = H_0^1 \times L_0$ and $\Psi = \{\psi^v, \psi^p\}$. The problem reads:

$$\text{Find } U_h \in X_h \text{ such that: } A(U_h, \Psi_h) = F(\Psi_h) \quad \forall \Phi \in X_h,$$

where

$$A(U_h, \Psi_h) = (\nabla v_h, \nabla \psi_h^v) - (p_h, \nabla \cdot \psi_h^v) + (\nabla \cdot v_h, \psi_h^p),$$
$$F(\Psi_h) = (f_f, \psi_h^v).$$

Let us choose as basis:

$$V_h = \{\psi_h^{v,i}, i = 1, \ldots, N_V := dimV_h\},$$
$$L_h = \{\psi_h^{p,i}, i = 1, \ldots, N_P := dimL_h\}.$$

Please pay attention that $V_h := (V_h)^d$ is a vector-valued space with dimension $d$. If follows:

$$(\nabla v_h, \nabla \psi_h^{v,i}) - (p_h, \nabla \cdot \psi_h^{v,i}) \quad i = 1, \ldots, N_V,$$
$$(\nabla \cdot v_h, \psi_h^{p,i}) \quad i = 1, \ldots, N_P,$$

Setting:

$$v_h = \sum_{j=1}^{N_V} v_j \psi_h^{v,j}, \quad p_h = \sum_{j=1}^{N_P} p_j \psi_h^{p,j}$$

yield the discrete equations:

$$\sum_{j=1}^{N_V} (\nabla \psi_h^{v,j}, \nabla \psi_h^{v,i}) v_j - \sum_{j=1}^{N_P} (\psi_h^{p,j}, \nabla \cdot \psi_h^{v,i}) p_j, \quad i = 1, \ldots, N_V,$$
$$\sum_{j=1}^{N_v} (\nabla \cdot \psi_h^{v,j}, \psi_h^{p,i}), \quad i = 1, \ldots, N_P.$$

With this, we obtain the following matrices:

$$A := (\nabla \psi_h^{v,j}, \nabla \psi_h^{v,i})_{ij=1}^{N_V, N_V}, \quad B := -(\psi_h^{p,j}, \nabla \cdot \psi_h^{v,i})_{ij=1}^{N_V, N_P}, \quad -B^T = (\nabla \cdot \psi_h^{v,j}, \psi_h^{p,i})_{ij=1}^{N_P, N_V}.$$

These matrices form the block system:

$$\begin{pmatrix} A & B \\ -B^T & 0 \end{pmatrix} \begin{pmatrix} v \\ p \end{pmatrix} = \begin{pmatrix} f \\ 0 \end{pmatrix}, \tag{197}$$

where $v = (v_i)_{i=1}^{N_V}, p = (p_i)_{i=1}^{N_P}$.

### 9.4.3 Nonstationary Stokes

Let us extend the previous ideas to nonstationary problems. For the sake of simplicity, we set $\theta = 1$ (backward Euler). Let $U_h^n = \{v_h^n, p_h^n\}$ the solution at time $t^n$ and as before $X_h := V_h \times L_h = H_0^1 \times L_0$ and $\Psi = \{\psi^v, \psi^p\}$. Using the Rothe method (first time, then space), leads to a scheme in which at each time $t^n$ a quasi-stationary problem needs to be solved:

$$\text{At time } t^n, \text{ find } U_h^n \in X_h \text{ such that: } A(U_h^n, \Psi_h) = F(\Psi_h) \quad \forall \Phi \in X_h,$$

where

$$A(U_h^n, \Psi_h) = (v_h^n, \psi_h^v) + \delta t(\nabla v_h^n, \nabla \psi_h^v) - \delta t(p_h^n, \nabla \cdot \psi_h^v) + \delta t(\nabla \cdot v_h^n, \psi_h^p),$$
$$F(\Psi_h) = (v_h^{n-1}, \psi_h^v) + \delta t(f_f, \psi_h^v).$$

Setting things as in the previous section yields the discrete system:

$$\sum_{j=1}^{N_V}\Big[(\psi_h^{v,j},\psi_h^{v,i}) + (\nabla\psi_h^{v,j},\nabla\psi_h^{v,i})\Big]v_j - \sum_{j=1}^{N_P}(\psi_h^{p,j},\nabla\cdot\psi_h^{v,i})p_j, \quad i=1,\dots,N_V,$$

$$\sum_{j=1}^{N_v}(\nabla\cdot\psi_h^{v,j},\psi_h^{p,i}), \quad i=1,\dots,N_P,$$

where $(\psi_h^{v,j},\psi_h^{v,i})_{ij=1}^{N_V,N_V} =: M$ is a mass matrix. This leads to the block system:

$$\begin{pmatrix} \frac{1}{\delta t}M + A & B \\ -B^T & 0 \end{pmatrix}\begin{pmatrix} v^n \\ p^n \end{pmatrix} = \begin{pmatrix} f^n - M^{n-1} \\ 0 \end{pmatrix},$$

with (the vector) $M^{n-1} := (v_h^{n-1},\psi_h^{v,i})_{i=1}^{N_V}$.

### 9.4.4 Stationary Navier-Stokes (nonlinear)

In this part, we go back to stationary problems but make them nonlinear. The simplest example within these lecture notes is Navier-Stokes' convection term. Rather than solving directly for $v_h$ and $p_h$ we solve now for the (Newton) updates $\delta v_h$ and $\delta p_h$ - later more.

The problem reads:

$$\text{Find } U_h \in X_h \text{ such that: } A(U_h)(\Psi_h) = F(\Psi_h) \quad \forall\Phi \in X_h,$$

where

$$A(U_h)(\Psi_h) = (v_h\cdot\nabla v_h,\psi_h^v) + \frac{1}{Re}(\nabla v_h,\nabla\psi_h^v) - (p_h,\nabla\cdot\psi_h^v) + (\nabla\cdot v_h,\psi_h^p),$$

$$F(\Psi_h) = (f_f,\psi_h^v).$$

Here, we added the dimensionless Reynolds number $Re$ in order to be aware how the equations change their type if $Re$ is either small or large.

**Remark 9.22** (Notations for bilinear and semilinear forms). *If the PDE is linear, we use the notation for a bilinear form: $A(U_h,\Psi_h)$. If the PDE is nonlinear, this is indicated in the notation by using $A(U_h)(\Psi_h)$.*

We learned in Section 9.1, we prefer Newton's method to solve the nonlinear problem. Given an initial guess $U_h^0 := \{v_h^0,p_h^0\}$, we must solve the problem:

Find $\delta U_h := \{\delta v_h,\delta p_h\} \in X_h$ such that: $A'(U_h^l)(\delta U_h,\Psi_h) = -A(U_h^l)(\Psi_h) + F(\Psi_h), \quad U_h^{l+1} = U_h^l + \delta U_h$.

Here,

$$A'(U_h^l)(\delta U_h,\Psi_h) = (\delta v_h\cdot\nabla v_h^l + v_h^l\cdot\nabla\delta v_h,\psi_h^v) + \frac{1}{Re}(\nabla\delta v_h,\nabla\psi_h^v) - (\delta p_h,\nabla\cdot\psi_h^v) + (\nabla\cdot\delta v_h,\psi_h^p),$$

$$F(\Psi_h) = (f_f,\psi_h^v),$$

$$A(U_h^l)(\Psi_h) = (v_h^l\cdot\nabla v_h^l,\psi_h^v) + \frac{1}{Re}(\nabla v_h^l,\nabla\psi_h^v) - (p_h^l,\nabla\cdot\psi_h^v) + (\nabla\cdot v_h^l,\psi_h^p).$$

As explained, we solve now for the updates and their respresentation with the help of the shape functions:

$$\delta v_h = \sum_{j=1}^{N_V}\delta v_j\psi_h^{v,j}, \quad \delta p_h = \sum_{j=1}^{N_P}\delta p_j\psi_h^{p,j}$$

With that the discrete, linearized convection operator reads:

$$L := (\psi_h^{v,j}\cdot\nabla v_h^l + v_h^l\cdot\nabla\psi_h^{v,j},\psi_h^{v,i})_{ij=1}^{N_V,N_V}.$$

The block structure reads:

$$\begin{pmatrix} L + \frac{1}{Re}A & B \\ -B^T & 0 \end{pmatrix}\begin{pmatrix} \delta v \\ \delta p \end{pmatrix} = \begin{pmatrix} f - [L^l + \frac{1}{Re}A^l + B] \\ 0 - [-B^T]^l \end{pmatrix},$$

where we have added on the right hand side the vectors of Newton's residual.

### 9.4.5 Nonstationary problems 1: Navier-Stokes

In nonstationary Navier-Stokes, we combine the ideas from the previous two sections. The block structure reads:

$$\begin{pmatrix} \frac{1}{\delta t}M + L + \frac{1}{Re}A & B \\ -B^T & 0 \end{pmatrix} \begin{pmatrix} \delta v \\ \delta p \end{pmatrix} = \begin{pmatrix} f - [residual] \\ 0 - [residual] \end{pmatrix}.$$

For hight Reynolds numbers, the diffusion term $A$ vanishes and for small time steps the mass term $M$ remains.

### 9.4.6 Nonstationary problems 2: Nonlinear elasticity

Given an initial guess $U_h^0 := \{v_h^0, u_h^0\}$, we must solve at each time $t^n$ the problem:

Find $\delta U_h^n := \{\delta v_h^n, \delta u_h^n\} \in X_h$ such that: $A'(U_h^{n,l})(\delta U_h, \Psi_h) = -A(U_h^{n,l})(\Psi_h) + F(\Psi_h), \quad U_h^{n,l+1} = U_h^{n,l} + \delta U_h.$

Here,

$$A'(U_h^{n,l})(\delta U_h, \Psi_h) = (\frac{1}{\delta t}\delta v_h, \psi_h^v) + \theta(F'(\delta u_h)\Sigma(u_h^n) + F(u_h^n)\Sigma'(\delta u_h), \nabla\psi_h^v) + (\frac{1}{\delta t}\delta u_h, \psi_h^v) - \theta(\delta v_h, \psi_h^u)$$

$$F(\Psi_h) = (f_s, \psi_h^v) + (\frac{1}{\delta t}v_h^{n-1}, \psi_h^v) + (\frac{1}{\delta t}u_h^{n-1}, \psi_h^u) - (1-\theta)(F(u_h^{n-1})\Sigma(u_h^{n-1}), \nabla\psi_h^v) + (1-\theta)(v_h^{n-1}, \psi_h^u),$$

$$A(U_h^{n,l})(\Psi_h) = (\frac{1}{\delta t}v_h^n, \psi_h^v) + \theta(F(u_h^n)\Sigma(u_h^n), \nabla\psi_h^v) + (\frac{1}{\delta t}u_h^n, \psi_h^v) - \theta(v_h^n, \psi_h^u).$$

The block structure reads:

$$\begin{pmatrix} \frac{1}{\delta t}M_{vv} & A_{vu} \\ M_{uv} & \frac{1}{\delta t}M_{uu} \end{pmatrix} \begin{pmatrix} \delta v \\ \delta u \end{pmatrix} = \begin{pmatrix} f_s - [residual] \\ 0 - [residual] \end{pmatrix}.$$

### 9.4.7 Nonstationary problems 3: Fluid-structure interaction

The principal challenge in fluid-structure interaction is its multi-domain character, i.e., certain equations are only prescribed in parts of the computational domain $\widehat{\Omega}$. While deriving the linear equation systems, we account for this fact and derive seperately the systems for $\widehat{\Omega}_f$ and $\widehat{\Omega}_s$.

For spatial discretization, we use the previously introduced spaces $V_h \times W_h \times L_h$ with vector valued basis

$$\{\psi_i \,|\, i = 1, \ldots, N\},$$

where the basis functions are primitive (they are only non-zero in one component), so we can separate them into velocity, displacement, and pressure basis functions and sort them accordingly:

$$\psi_i = \begin{pmatrix} \chi_i^v \\ 0 \\ 0 \end{pmatrix}, \text{ for } i = 1, \ldots, N_v,$$

$$\psi_{(N_v+i)} = \begin{pmatrix} 0 \\ \chi_i^u \\ 0 \end{pmatrix}, \text{ for } i = 1, \ldots, N_u,$$

$$\psi_{(N_v+u+i)} = \begin{pmatrix} 0 \\ 0 \\ \chi_i^p \end{pmatrix}, \text{ for } i = 1, \ldots, N_p,$$

where $N_v + N_u + N_p = N$.

In FSI, the system reads in short notation

$$AU = b$$

where

$$A = \begin{pmatrix} A_F & 0 \\ 0 & A_S \end{pmatrix}, \quad U = \begin{pmatrix} U_F \\ U_S \end{pmatrix}, \quad b = \begin{pmatrix} b_F \\ b_S \end{pmatrix}.$$

Here,

$$A_F = \begin{pmatrix} \frac{1}{\delta t}M + L + \frac{1}{Re}A & B & C_1 \\ -B^T & 0 & C_2 \\ 0 & 0 & A_{MMPDE} \end{pmatrix}, \quad A_S = \begin{pmatrix} \frac{1}{\delta t}M_{vv} & A_{vu} \\ M_{uv} & \frac{1}{\delta t}M_{uu} \end{pmatrix}.$$

The matrices $M_{vv}, A_{vu}, M_{uv}, M_{uu}$ stem from the discretization of the nonlinear, nonstationary solid system. Here $M_{**}$ are mass matrices and $A_{vu}$ a matrix from a second order operator; namely $-\widehat{\nabla} \cdot (\widehat{F}\widehat{\Sigma})$. The full system to be solved at each Newton step reads:

$$\begin{pmatrix} \frac{1}{\delta t}M + L + \frac{1}{Re}A & B & C_1 & 0 & 0 \\ -B^T & 0 & C_2 & 0 & 0 \\ * & * & A_{MMPDE} & 0 & 0 \\ 0 & 0 & 0 & \frac{1}{\delta t}M_{vv} & A_{vu} \\ 0 & 0 & 0 & M_{uv} & \frac{1}{\delta t}M_{uu} \end{pmatrix} \begin{pmatrix} \delta v_f \\ \delta p_f \\ \delta u_f \\ \delta v_s \\ \delta u_s \end{pmatrix} = \begin{pmatrix} f_f - [residual] \\ 0 - [residual] \\ 0 - [residual] \\ f_s - [residual] \\ 0 - [residual] \end{pmatrix}. \tag{198}$$

Here, $C_1$ and $C_2$ are the coupling terms because the fluid domain deformation enters into the Navier-Stokes equations. The *-terms can arise in the coupling as explained by Heil [126]. The $[residual]$ terms indicate to substract the residual $A(U)(\Phi)$ using Newton's method (179). For careful numerical implementation and correct development of preconditioners, one might also need to distuingish interface contributations as discussed in detail in [253, 254]. In fact, in system (198) it is not immediately clear how the solid matrix $A_S$ couples to the fluid-MMPDE-matrix $A_F$. As done in [254], let us also distuingish between inner DoFs and DoFs that touch the FSI-inteface $\widehat{\Gamma}_i$. Then, we obtain the system:

$$\begin{pmatrix} \frac{1}{\delta t}M + L + \frac{1}{Re}A & \frac{1}{\delta t}M + L + \frac{1}{Re}A & B & C_1 & C_2 & 0 & 0 & 0 & 0 \\ \frac{1}{\delta t}M + L + \frac{1}{Re}A & \frac{1}{\delta t}M + L + \frac{1}{Re}A & B & C_3 & C_4 & 0 & 0 & D_1 & D_2 \\ -B^T & -B^T & 0 & C_5 & C_6 & 0 & 0 & 0 & 0 \\ 0 & 0 & 0 & A_{MMPDE} & A_{MMPDE} & 0 & 0 & 0 & 0 \\ 0 & 0 & 0 & A_{MMPDE} & I & 0 & 0 & 0 & -I \\ 0 & 0 & 0 & 0 & 0 & \frac{1}{\delta t}M_{vv} & \frac{1}{\delta t}M_{vv} & A_{vu} & A_{vu} \\ 0 & -I & 0 & 0 & 0 & M_{uv} & M_{uv} & \frac{1}{\delta t}M_{uu} & I \\ 0 & 0 & 0 & 0 & 0 & \frac{1}{\delta t}M_{vv} & \frac{1}{\delta t}M_{vv} & A_{vu} & A_{vu} \\ 0 & 0 & 0 & 0 & 0 & M_{uv} & M_{uv} & \frac{1}{\delta t}M_{uu} & \frac{1}{\delta t}M_{uu} \end{pmatrix} \begin{pmatrix} \delta v_f \\ \delta v_{f,\Gamma} \\ \delta p_f \\ \delta u_f \\ \delta u_{f,\Gamma} \\ \delta v_s \\ \delta v_{s,\Gamma} \\ \delta u_s \\ \delta u_{s,\Gamma} \end{pmatrix} = \begin{pmatrix} f_f - [residual] \\ 0 - [residual] \\ 0 - [residual] \\ 0 - [residual] \\ 0 - [residual] \\ f_s - [residual] \\ 0 - [residual] \\ 0 - [residual] \\ 0 - [residual] \end{pmatrix}. \tag{199}$$

In this matrix, for instance we have now the terms:

$$I\delta u_{f,\Gamma} - I\delta u_{s,\Gamma} = 0,$$
$$-I\delta v_{f,\Gamma} + I\delta v_{s,\Gamma} = 0.$$

These represent the Dirichlet coupling terms $u_f = u_s$ and $v_f = v_s$ on the interface $\Gamma_i$. The traction interface condition is realized in the terms $D_1$ and $D_2$.

**Remark 9.23.** *For similar matrix structure see for instance [151] our published work.*

## 9.5 Preconditioning

For problems in 3D or large systems in 2D, the usage of a direct solver (LU decomposition with Gaussian elimination) becomes prohibitive because of computational cost and memory requirements. Consequently, one aims for iterative solvers such as for example, Krylov-based iterative methods, i.e., GMRES method (non-symmetric problems), the CG method (symmetric problems) or even better multigrid (geometric or algebraic) methods. The key point is however that the condition number is bad for all kind of PDEs discretizations (a second order operator has $cond(A) \sim \frac{1}{h^2}$) but in particular for fluid-structure interaction since all physical parameters have a wide range of values ($\nu_f \sim 10^{-3}$ to $\mu_s \sim 10^6$). Thus, we need to precondition the system with a matrix $P^{-1}$ such that the condition number of the modified system $P^{-1}A$ is moderate:

$$Au = b \quad \Rightarrow P^{-1}Au = P^{-1}b.$$

It is obvious that the ideal choice would be $P^{-1} = A^{-1}$. Of course, finding $A^{-1}$ is in most cases impossible. Thus an approximation will do the job and here triangular $P^{-1}$ are already good. We illustrate this for a specific (and famous) example for the Stokes equations (namely the Schur complement) and derive additionally a preconditioner of our FSI system (this system has several similarities with the one derived by Heil [126]).

In FSI, various solution schemes have been employed over the last years:

- Monolithic solution [12, 16, 17, 66, 78, 106, 126, 127, 139, 150, 198, 199, 224, 230, 253, 254];

- Partitioned: [11, 68, 155, 156, 158, 162, 223].

**Remark 9.24** (Our FSI solver). *Our monolithic FSI solver in sequential form was published in [151]. Shortly later, our parallel version was designed in [150].*

### 9.5.1 Stokes

Taking the block system (197), the following preconditioner works:

$$P^{-1} = \begin{pmatrix} A^{-1} & 0 \\ B^{-1} & \Sigma^{-1} \end{pmatrix}$$

This idea is known as block Schur complement preconditioner. We can check this as follows:

$$P^{-1}A = \begin{pmatrix} A^{-1} & 0 \\ B^{-1} & \Sigma^{-1} \end{pmatrix} \begin{pmatrix} A & B \\ -B^T & 0 \end{pmatrix} = \begin{pmatrix} I & A^{-1}B \\ 0 & I \end{pmatrix},$$

which is a block-trianglur matrix that can be solved fast and efficiently. Inside, $P^{-1}$, the inverse of $A^{-1}$ can be obtained in the case of Stokes with a CG method or a multigrid solver. The inverse of the Schur complement

$$\Sigma = B^T A^{-1} B$$

is based on the following consideration:

$$\Sigma = B^T A^{-1} B \sim \nabla^T \Delta^{-1} \nabla \sim I \sim M_{pp},$$

where $M_{pp}$ is the mass matrix of the pressure space. Thus,

$$\Sigma^{-1} \sim M_{pp}^{-1}.$$

### 9.5.2 Fluid-Structure Interaction

In FSI it is worthy to split the subproblems on the solver level into a fluid part and a solid part. Thus the system matrix reads:

$$\begin{pmatrix} A_F & 0 \\ 0 & A_S \end{pmatrix}$$

where $A_F$ and $A_S$ have been explained in 9.4.7. Here, a block diagonal preconditioner reads:

$$P^{-1} = \begin{pmatrix} P_F^{-1} & 0 \\ 0 & P_S^{-1} \end{pmatrix},$$

which means that we need to find good preconditioners for the fluid and the solid system separetely. In the fluid system, a Schur complement idea works. A nice overview of different preconditioning techniques is provided in [254].

## 9.6 Loops

We briefly summarize in this section, how many loops are present in order to assemble the Jacobian matrix of a nonstationary nonlinear system of an initial/boundary value problem.

```
for n = 1,2,3, ... , N_T // timestepping
 for l = 1,2,3, ... , until ||res|| < TOL // Newton steps
  for K = 1,2,3, ... , N_K // all cell of the spatial mesh
   for i = 1,2,3, ... , N_V // Local degrees of freedom on a cell
    for j = 1,2,3, ... , N_V // Local degrees of freedom on a cell
     for q = 1,2,3, ... , N_Q // Quadrature points (in most cases Gaussian quadrature)
      A(U_h^{n,l})(\psi_h)
        -> A(\psi_h^j, \psi_h^i)_K
        -> \int_K A(\psi_h^j,\psi_h^i)
        -> \sum_{q=1}^{N_q} \omega_q A(\psi_h^j(\xi_q),\psi_h^i(\xi_q)).
```

Here, $N_T, N_K, N_V$ and $N_Q$ are a priori determined and denote the total number of time steps $N_T$, the total number of mesh cells $N_K$, the local total number of degrees of freedom on a cell $N_V$ (e.g., $Q_1^c$ has $N_V = 4$ for a scalar-valued problem in 2D and for example for Navier-Stokes: $3 * dim(Q_1^c) + dim P_1^{dc} = 4 + 4 + 4 + 3 = 15$ (local) degrees of freedom on a cell.) Finally, $N_Q$ denotes the number of quadrature points to be used for the integration. Here, $\omega_q$ denote the quadrature weights and $\xi_q$ the quadrature points.

## 9.7 An example of finite-difference-in-time, Galerkin-FEM-in-space-discretization and linearization in a Newton setting

I believe that the discretization of nonlinear time-dependent partial differential equations is finally very similar to solving Poisson's problem. Hopefully, I convince the reader in this section.

We are given the following example:

**Problem 9.25.** *Let the following PDE be given (we omit any 'hats'): Find $v$ and $u$, for allmost all times, such that*
$$\partial_t^2 u - J\nabla \cdot \sigma(v)F^{-T} = f, \quad in \ \Omega, \quad plus \ bc. \ and \ initial \ cond.,$$
*and where (as before) $J := J(u), F := F(u)$ and $\sigma(v) = (\nabla v + \nabla v^T)$.*

**9.7.0.1 Time discretization**   We aim to apply a One-Step-$\theta$ scheme applied to the mixed problem:

$$\partial_t v - J\nabla \cdot \sigma(v)F^{-T} = f,$$
$$\partial_t u - v = 0.$$

One-Step-$\theta$ discretization with time step size $k$, and $\theta \in [0,1]$, leads to

$$\frac{v - v^{n-1}}{k} - \theta J\nabla \cdot \sigma(v)F^{-T} - (1-\theta)J^{n-1}\nabla \cdot \sigma(v^{n-1})(F^{-T})^{n-1} = \theta f + (1-\theta)f^{n-1},$$

$$\frac{u - u^{n-1}}{k} - \theta v - (1-\theta)v^{n-1} = 0.$$

**9.7.0.2 Spatial pre-discretization: weak form on the continuous level**   We multiply by the time step $k$, apply with test functions from suitable spaces $V$ and $W$ and obtain the weak formulations

$$(v - v^{n-1}, \varphi) + k\theta(J\sigma(v)F^{-T}, \nabla\varphi) + k(1-\theta)(J^{n-1}\sigma(v^{n-1})(F^{-T})^{n-1}, \varphi)$$
$$= k\theta(f, \varphi) + k(1-\theta)(f^{n-1}, \varphi) \quad \forall\varphi \in V,$$
$$(u - u^{n-1}, \psi) + k\theta(v, \psi) + k(1-\theta)(v^{n-1}, \psi) = 0 \quad \forall\psi \in W.$$

Sorting terms on left and right hand sides:

$$(v, \varphi) + k\theta(J\sigma(v)F^{-T}, \nabla\varphi)$$
$$= (v^{n-1}, \varphi) - k(1-\theta)(J^{n-1}\sigma(v^{n-1})(F^{-T})^{n-1}, \varphi)$$
$$+ k\theta(f, \varphi) + k(1-\theta)(f^{n-1}, \varphi) \quad \forall \varphi \in V,$$
$$(u, \psi) + k\theta(v, \psi) = (u^{n-1}, \psi) - k(1-\theta)(v^{n-1}, \psi) \quad \forall \psi \in W.$$

**9.7.0.3 A single semi-linear form - first step towards Newton solver** Now, we build a single semi-linear form $A(\cdot)(\cdot)$ and right hand side $F(\cdot)$. Let[24] $U := \{v, u\} \in V \times W$ and $\Psi := \{\varphi, \psi\} \in V \times W$: Find $U \in V \times W$ such that:

$$A(U)(\Psi) = (v, \varphi) + k\theta(J\sigma(v)F^{-T}, \nabla\varphi) + (u, \psi) + k\theta(v, \psi)$$
$$F(\Psi) = (v^{n-1}, \varphi) - k(1-\theta)(J^{n-1}\sigma(v^{n-1})(F^{-T})^{n-1}, \varphi) + k\theta(f, \varphi)$$
$$+ k(1-\theta)(f^{n-1}, \varphi)(u^{n-1}, \psi) - k(1-\theta)(v^{n-1}, \psi)$$

for all $\Psi \in V \times W$.

**9.7.0.4 Evaluation of directional derivatives - second step for Newton solver** We follow Section 9.3.1. Let $\delta U := \{\delta v, \delta u\} \in V \times W$. Then the directional derivative of $A(U)(\Psi)$ is given by:

$$A'(U)(\delta U, \Psi) = (\delta v, \varphi) + k\theta\Big(J'(\delta u)\sigma(v)F^{-T} + J\sigma'(\delta v)F^{-T} + J\sigma(v)(F^{-T})'(\delta u), \nabla\varphi\Big)$$
$$+ (\delta u, \psi) + k\theta(\delta v, \psi),$$

where we applied the chain rule for the term $J\sigma(v)F^{-T}$. Here, in the 'non-prime' terms in the nonlinear part; namely $J, F^{-T}$ and $\sigma(v)$, the previous Newton solution is inserted. We have now all ingredients to perform the Newton step (179).

**9.7.0.5 Spatial discretization in finite-dimensional spaces and linear system** In the final step, we assume conforming finite-dimensional subspaces $V_h \subset V$ and $W_h \subset W$ with $V_h := \{\varphi_1, \ldots, \varphi_N\}$ and $W_h := \{\psi_1, \ldots, \psi_M\}$. Then, the update solution variables in each Newton step are given by:

$$\delta v_h := \sum_{j=1}^{N} v_j \varphi_j, \quad \text{and} \quad \delta u_h := \sum_{j=1}^{M} u_j \psi_j.$$

For the linearized semi-linear form $A'(U)(\delta U, \Psi)$, we have:

$$A'(U_h)(\delta U_h, \Psi_h)$$

and with this ($A_{ij}$ representing the entries of the Jacobian):

$$A_{ij} := A'(U_h)(\Psi_j, \Psi_i) = \sum_{j=1}^{N} v_j (\varphi_j, \varphi_i)$$
$$+ k\theta\Big(\sum_{j=1}^{M} u_j J(\psi_j)\sigma(v)F^{-T} + J(\sum_{j=1}^{N} v_j \sigma'(\varphi_j))F^{-T} + J\sigma(v)(\sum_{j=1}^{M} u_j (F^{-T})'(\psi_j)), \nabla\varphi_i\Big)$$
$$+ \sum_{j=1}^{M} u_j (\psi_j, \psi_i) + k\theta \sum_{j=1}^{N} v_j (\varphi_j, \psi_i)$$

for all test functions running through $i = 1, \ldots, N, N+1, \ldots, M$.

---

[24]Of course, the solution spaces for ansatz- and test functions might differ.

# 10 Error Estimation and Mesh Adaptivity

In this chapter, we leave forward modeling and concentrate on further aspects beyond:

- Sensitivity analysis;

- Error estimation and mesh adaptivity.

All these topics have in common that either implicitly or explicitly, a quantity of interest $J$ is subject of our investigation. Often, this quantity of interest is associated with calculating derivatives of solutions to FSI problems with respect to the given data. Such derivatives with respect to given data such as volume forces or boundary values have been used excessively in numerical papers concerned with sensitivity calculations or derivative based minimization problems, see, e.g., [5, 166, 183, 202, 213, 231]. In addition, sensitivity calculations are required for certain a posteriori error estimation techniques, such as the DWR-method [15, 29, 30]. Studies with a particular emphasize on FSI problems are carried out, for instance in [74, 119, 196, 234, 242]. Steps of optimization-related problems subject to FSI have been tackled in, e.g., [34, 51, 183, 202].

## 10.1 Preliminiaries and motivation of error estimation

Important aspects are error control and mesh adaptivity. The question is to address the error between a computed solution $u_h$ and the exact solution $u$ in a certain error norm. This leads to a posteriori error estimators.

Why is this important? Global refinement in three dimensions is still (despite nowadays high performance computing) a very effective approach to reduce the computational cost. The key is to refine only such regions that are of interest. The 'interest' depends on several factors ... Optimal mesh refinement is defined to refine as less elements as needed in order to reduce the error in as less steps as possible under a given tolarance. The elements that are chosen for refinement are chosen with the help of (local) error indicators.

Refinement indicators:

$$\eta_\omega(u_h) := \sum_{K \in \mathbb{T}_h} \rho_K \omega_K$$

where $\rho_K$ are local residuals and $\omega_K$ are local weights.
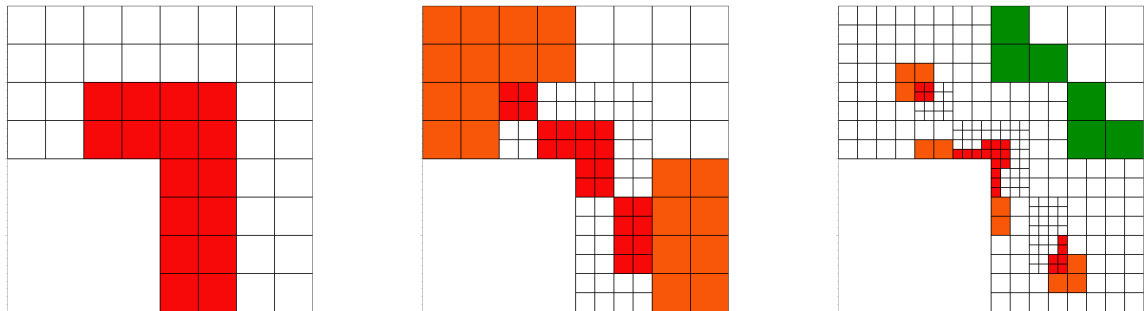


Figure 55: Meshes on level 0, level 0 and 1, level 0,1,2.

## 10.2 Goal-oriented error estimation with the dual-weighted residual method

The goal of this section is

- To introduce a novel variational localization technique [204][25] for the dual-weighted residual (DWR) method and highlighting why this formulation is preferrable (at least for coupled multiphysics problems such as fluid-structure interaction) compared to the classical method [29].

---

[25]Another variational technique based on filtering was introduced in [44].

The DWR method goes back to Becker & Rannacher [29, 30, 191] and is based on pioneering work by Eriksson, Estep, Hansbo and Johnson [76]. The key idea is based on duality principles well-known in optimization [4].

The DWR approach has been further developed in [2, 111, 182]. A summary is provided in [15]. Applications include fluid-dynamics [27, 149], structural dynamics [194, 195], and further to complex multiphysics problems like chemically reactive flows [43]. We are specifically interested in fluid-structure interaction references [88, 119, 196, 242, 256].

The DWR method allows for estimating the error $u - u_h$ between the exact solution $u \in V$ (for a function space $V$) to the PDE and the Galerkin solution $u_h \in V_h \subset V$ in general functionals $J : V \to \mathbb{R}$. These functionals can be norms but also more general expressions, like point-values, (local) averages or technical expressions like (in the case of fluid dynamics) lift- or drag-coefficients. Error estimators based on the DWR method always consist of residual evaluations, that are weighted by adjoint sensitivity measures. These sensitivities are the solution to adjoint problems that measure the influence of the error functional $J$. For adaptive mesh refinement, we need to localize the error estimator $\eta(u_h, z_h) \approx J(u) - J(u_h)$ (for its definition see Equation (208)). The quality of this approximation procedure can be measured by the *effectivity index* $\mathrm{eff}_h$, defined as

$$\mathrm{eff}_h := \frac{\eta(u_h, z_h)}{J(u) - J(u_h)}. \tag{200}$$

Similar to the effectivity index (200), we define the *indicator index* to measure the quality of the localization process:

$$\mathrm{ind}_h := \frac{\sum_i |\eta_i|}{|J(u) - J(u_h)|}. \tag{201}$$

It is not possible to reach strict effectivity with $\mathrm{ind}_h \to 1$ in the context of goal-oriented errors. The functional error $J(u) - J(u_h)$ has a sign, and hence the error can vanish, although the solution shows a very large approximation error, e.g. by symmetry reasons. The local estimator values $\eta_i$ may have changing sign, such that $\sum_i |\eta_i|$ may be a strong over-estimation. However, we will aim at strategies, where $\mathrm{ind}_h$ is uniformly bounded in $h$.

Following [191], we briefly explain why adaptive mesh refinement is not straightforward. In fact the mechanisms of error propagation highly depends on the differential operator:

- Diffusion terms cause slow isotropic error decay and global error pollution might occur from local irregularities;

- Transport terms propagate local errors in the transport direction but errors decay exponentially in the crosswind direction;

- Reaction terms cause isotropic exponential error decay, but stiff behavior may occur in the coupling of error components.

These requirements can not be estimated analytically and we aim for designing a computational feed-back process that combines error estimation and mesh adaptation in order to obtain economical discretizations for computing the quantity of interest $J$.

Let us again concentrate on stationary formulations in order to learn the techniques. The Galerkin approximation to Equation (102) (neglecting the time derivatives and stabilization terms), reads: Find $\hat{U}_h = \{\hat{v}_{f,h}, \hat{v}_{s,h}, \hat{u}_{f,h}, \hat{u}_{s,h}, \hat{p}_{f,h}\} \in \widehat{X}_{h,D}^0$, where $\widehat{X}_{h,D}^0 := \{\hat{v}_{f,h}^D + \hat{V}_{f,\hat{v},h}^0\} \times \hat{\mathcal{L}}_{s,h} \times \{\hat{u}_{f,h}^D + \hat{V}_{f,\hat{u},h}^0\} \times \{\hat{u}_{s,h}^D + \hat{V}_{s,h}^0\} \times \hat{L}_{f,h}^0$, such that

$$\hat{A}(\hat{U}_h)(\hat{\Psi}_h) = \hat{F}(\hat{\Psi}_h) \quad \forall \hat{\Psi}_h \in \widehat{X}_h. \tag{202}$$

The solution $\hat{U}_h$ is used to calculate an approximation $J(\hat{U}_h)$ of the goal-functional $J(\hat{U}) : \widehat{X} \to \mathbb{R}$. This functional is assumed to be sufficiently differentiable. Concretely, it is used for the evaluation of point values (the deflection of the valve), line integrals (the computation of the stresses), or domain integrals ($L^2$-norm of the velocity).

**Example 10.1.** *The error of a deflection $\hat{u}_s$ in y-direction at some point $\hat{p} \in \widehat{\Omega}$ can be estimated using the following (regularized) functional:*

$$J(\hat{u}_{s,y}) := |B_\varepsilon|^{-1} \int_\varepsilon \hat{u}_{y,s} \, d\hat{x} = \hat{u}_{y,s}(\hat{p}) + O(\varepsilon^2),$$

where $B_\varepsilon$ is the $\varepsilon$-ball around the point $\hat{p}$.

**Example 10.2.** *The error of mean normal fluxes over lower-dimensional manifolds. For example, we compute the error of wall stresses in y-direction along the interface between the fluid and the structure, which can be estimated with*

$$J(\hat{U}) := \int_{\hat{S}} \hat{J}\hat{\sigma}_f \widehat{F}^{-T} \hat{n}_f \, \hat{d} \, d\hat{s},$$

*where $\hat{d}$ is a unit vector perpendicular to the mean flow direction. Later, we compute the wall stresses along the interface of the aorta $\hat{S} := \widehat{\Gamma}_{aorta}$. In particular, accurate wall stress measurement is important for clinical applications.*

We use the (formal) Euler-Lagrange method, to derive a computable representation of the approximation error $J(\hat{U}) - J(\hat{U}_h)$. Concretely, the task is

$$\min\{J(\hat{U}) - J(\hat{U}_h)\} \quad \text{s.t. } \hat{A}(\hat{U})(\hat{\Psi}) = \hat{F}(\hat{\Psi}) \quad \forall \hat{\Psi} \in \widehat{X}.$$

As usual for optimization problems, we introduce a dual variable $\hat{Z}$ (usually referred to as *sensitivity*) to formulate the Lagrangian functional

$$\mathcal{L}(\hat{U}, \hat{Z}) = J(\hat{U}) + \hat{F}(\hat{Z}) - \hat{A}(\hat{U})(\hat{Z}).$$

We obtain the optimality system

$$\mathcal{L}'_{\hat{Z}}(\hat{U}, \hat{Z})(\delta\hat{Z}) = \widehat{F}(\delta\hat{Z}) - \hat{A}(\hat{U})(\delta\hat{Z}) = 0 \quad \delta\hat{Z} \in \widehat{X},$$
$$\mathcal{L}'_{\hat{U}}(\hat{U}, \hat{Z})(\delta\hat{U}) = J'(\hat{U})(\delta\hat{U}) - \hat{A}'_{\hat{U}}(\hat{U})(\delta\hat{U}, \hat{Z}) = 0 \quad \delta\hat{U} \in \widehat{X}.$$

In this context, we deal with a *primal* problem and a *dual* problem. The primal problem corresponds to the original equation. In an appropriate discrete space $\widehat{X}_h \subset \widehat{X}$, the discrete problem reads:

$$\mathcal{L}'_{\hat{Z}}(\hat{U}_h, \hat{Z}_h)(\delta\hat{Z}_h) = \widehat{F}(\hat{Z}_h) - \hat{A}(\hat{U}_h)(\delta\hat{Z}_h) = 0 \quad \delta\hat{Z}_h \in \widehat{X}_h, \tag{203}$$

$$\mathcal{L}'_{\hat{U}}(\hat{U}_h, \hat{Z}_h)(\delta\hat{U}_h) = J'(\hat{U}_h)(\delta\hat{U}_h) - \hat{A}'_{\hat{U}}(\hat{U}_h)(\delta\hat{U}_h, \hat{Z}_h) = 0 \quad \delta\hat{U}_h \in \widehat{X}_h. \tag{204}$$

For given solutions $\{\hat{U}, \hat{Z}\}$ and $\{\hat{U}_h, \hat{Z}_h\}$ we obtain the following identity for the approximation error:

$$J(\hat{U}) - J(\hat{U}_h) = \mathcal{L}(\hat{U}, \hat{Z}) - \mathcal{L}(\hat{U}_h, \hat{Z}_h).$$

To *compute* this relation, we use the results of [30] and we obtain:

**Theorem 10.3.** *For any solution of the Problem 202, we obtain the error representation*

$$J(\hat{U}) - J(\hat{U}_h) = \frac{1}{2}\rho(\hat{U}_h)(\hat{Z} - \hat{\Psi}_h) + \frac{1}{2}\rho^*(\hat{U}_h, \hat{Z}_h)(\hat{U} - \hat{\Phi}_h) + \mathcal{R}_h^{(3)}, \tag{205}$$

*for all $\{\hat{\Phi}_h, \hat{\Psi}_h\} \in \widehat{X}_h \times \widehat{X}_h$ and with the primal and dual residuals:*

$$\rho(\hat{U}_h)(\hat{Z} - \hat{\Psi}_h) := -A(\hat{U}_h)(\cdot), \tag{206}$$

$$\rho^*(\hat{U}_h, \hat{Z}_h)(\hat{U} - \hat{\Phi}_h) := J'(\hat{U}_h)(\cdot) - A'(\hat{U}_h)(\cdot, \hat{Z}_h). \tag{207}$$

*The remainder term is $\mathcal{R}_h^{(3)}$ is cubic in the primal and the dual errors. This error identity can be used to drive an automatic mesh refinement process and/or can be adopted to estimate the error.*

*Proof.* We refer to [30] for a proof of this theorem. □

Neglecting the remainder results in the error estimator

$$\eta(u_h, z_h) = \frac{1}{2}\rho(\hat{U}_h)(\hat{Z} - \hat{\Psi}_h) + \frac{1}{2}\rho^*(\hat{U}_h, \hat{Z}_h)(\hat{U} - \hat{\Phi}_h). \tag{208}$$

The dual variable $\hat{Z} = \{\hat{z}_f^v, \hat{z}_s^v, \hat{z}_f^u, \hat{z}_s^u, \hat{z}_f^p\}$ is computed with the corresponding (linearized) dual problem (obtained as first equation in (203))

$$A'(\hat{U}_h)(\hat{\Psi}_h, \hat{Z}_h) = J'(\hat{\Psi}_h), \quad \forall \hat{\Psi}_h \in \tilde{X}_h, \tag{209}$$

where not necessarily $\tilde{X}_h = \widehat{X}_h$. The matrix $\hat{A}'$ denotes the transposed matrix of the primal problem and it is assembled as one further Newton Jacobian in the nonlinear solution process; we refer to [15]. The dual Problem (209) can be solved with a global higher approximation or local higher interpolation. With these solutions, we obtain approximations of the differences $\hat{Z} - \hat{\Psi}_h$ in the error representation (205). The solvability of the primal problem and the dual problem is not for granted, we refer for a deeper discussion to [74].

### 10.2.1 The classical DWR localization for simplified fluid-structure interaction

In this section, we first present the classical localization in which we need to deal with integration by parts in the backward sense. Consequently we need then to evaluate second-order operators as well as several face terms. However, these computations are not only costly from the software point of view, but they are also subject to simple mistakes when writing down the error estimator.

**Proposition 10.4.** *With the previous assumptions, we have for stationary fluid-structure interaction the error representation*

$$J(\hat{U}) - J(\hat{U}_h) \approx \eta_h^f + \eta_h^s + \eta_h^i, \tag{210}$$

*where we split the local error indicators into fluid $\eta_h^f$, structure $\eta_h^s$, and interface contributions $\eta_h^i$. In detail, we have*

$$\eta_h^f := \sum_{\hat{K} \in \hat{\mathcal{T}}_h} \big\{ (-\hat{\rho}_f \hat{J}(\widehat{F}^{-1}\hat{v}_f \cdot \widehat{\nabla})\hat{v}_f + \widehat{\nabla} \cdot \widehat{\sigma}_{appr} - \widehat{\nabla}\hat{p}_f, \hat{z}_f^v - \hat{\psi}_h^v)_{\hat{K}_f} \tag{211}$$

$$+ \frac{1}{2}([\hat{J}\widehat{\sigma}_f \widehat{F}^{-T}\hat{n}_f], \hat{z}_f^v - \hat{\psi}_h^v)_{\partial \hat{K}_f \setminus \partial \widehat{\Omega} \cup \widehat{\Gamma}_i} + (\widehat{div}(\hat{J}\widehat{F}^{-1}\hat{v}_f), \hat{z}_f^p - \hat{\psi}_h^p)_{\hat{K}_f} \tag{212}$$

$$+ (\widehat{\nabla} \cdot \widehat{\sigma}_{mesh}, \hat{z}_f^u - \hat{\psi}_h^u)_{\hat{K}_f} + \frac{1}{2}([\widehat{\sigma}_{mesh}\hat{n}_f], \hat{z}_f^u - \hat{\psi}_h^u)_{\partial \hat{K}_f \setminus \partial \widehat{\Omega} \cup \widehat{\Gamma}_i} \big\} \tag{213}$$

$$\tag{214}$$

*and*

$$\eta_h^s := \sum_{\hat{K} \in \hat{\mathcal{T}}_h} \big\{ (\widehat{\nabla} \cdot \widehat{\Sigma}_{appr}, \hat{z}_s^v - \hat{\psi}_h^v)_{\hat{K}_s} + \frac{1}{2}([\widehat{F}\widehat{\Sigma}_{appr}\hat{n}_s], \hat{z}_s^v - \hat{\psi}_h^v)_{\partial \hat{K}_s \setminus \partial \widehat{\Omega} \cup \widehat{\Gamma}_i} \big\}, \tag{215}$$

*and*

$$\eta_h^i := \sum_{\hat{K} \in \hat{\mathcal{T}}_h} \big\{ \frac{1}{2}([\hat{J}\widehat{\sigma}_f \widehat{F}^{-T}\hat{n}_f], \hat{z}_f^v - \hat{\psi}_h^v)_{\widehat{\Gamma}_i} + \frac{1}{2}([\widehat{\sigma}_{mesh}\hat{n}_f], \hat{z}_f^u - \hat{\psi}_h^u)_{\widehat{\Gamma}_i} \tag{216}$$

$$+ \frac{1}{2}([\widehat{F}\widehat{\Sigma}_{appr}\hat{n}_s], \hat{z}_s^v - \hat{\psi}_h^v)_{\widehat{\Gamma}_i} \big\}, \tag{217}$$

*where $\widehat{\sigma}_{mesh}$ was defined in Section 7.3.5 and where $[\cdot]$ denotes the jump across inter-cell boundaries.*

The previous declared error representation consists of the *cell residuals* (measuring the consistency of the discrete solution $\hat{U}_h$) and the edge terms $[\cdot]$ (measuring the discrete smoothness). The latter one has similar properties to the smoothness-based refinement indicators as introduced before. The residuals terms are weighted with so-called *sensitivity factors*

$$\hat{z}_{f,s}^v - \hat{\psi}_h^v, \quad \hat{z}_{f,s}^u - \hat{\psi}_h^u, \quad \hat{z}_f^p - \hat{\psi}_h^p,$$

that are obtained by solving the dual Problem (209).

**Proposition 10.5.** *From the previous error representation, we derive the following approximate error estimate*

$$|J(\hat{U}) - J(\hat{U}_h)| \approx \sum_{\hat{K} \in \hat{\mathcal{T}}_h} \eta_{\hat{K}}, \quad \eta_{\hat{K}} := \sum_{i=1}^{8} \rho_K^{(i)} \omega_K^{(i)},$$

*with the residual terms and the weights*

$$\rho_K^{(1)} := || - \hat{\rho}_f \hat{J}(\widehat{F}^{-1}\hat{v}_f \cdot \widehat{\nabla})\hat{v}_f + \widehat{\nabla} \cdot \hat{\sigma}_{appr} - \widehat{\nabla}\hat{p}_f||_{\hat{K}}, \qquad \omega_K^{(1)} := ||\hat{z}_f^v - \hat{\psi}_h^v||_{\hat{K}},$$

$$\rho_K^{(2)} := ||\widehat{\nabla} \cdot \widehat{\Sigma}_{appr}||_{\hat{K}}, \qquad \omega_K^{(2)} := ||\hat{z}_s^v - \hat{\psi}_h^v||_{\hat{K}},$$

$$\rho_K^{(3)} := ||\widehat{\nabla} \cdot \hat{\sigma}_{mesh}||_{\hat{K}}, \qquad \omega_K^{(3)} := ||\hat{z}_f^u - \hat{\psi}_h^u||_{\hat{K}},$$

$$\rho_K^{(4)} := ||\widehat{div}(\hat{J}\widehat{F}^{-1}\hat{v}_f)||_{\hat{K}}, \qquad \omega_K^{(4)} := ||\hat{z}_f^p - \hat{\psi}_h^p||_{\hat{K}},$$

$$\rho_K^{(5)} := \frac{1}{2}\hat{h}_K^{-1/2}||[\hat{J}\hat{\sigma}_f\widehat{F}^{-T}\hat{n}_f]||_{\partial\hat{K}\cup\widehat{\Gamma}_i}, \qquad \omega_K^{(5)} := \frac{1}{2}\hat{h}_K^{1/2}||\hat{z}_f^v - \hat{\psi}_h^v||_{\partial\hat{K}\cup\widehat{\Gamma}_i},$$

$$\rho_K^{(6)} := \frac{1}{2}\hat{h}_K^{-1/2}||[\widehat{F}\widehat{\Sigma}_{appr}\hat{n}_s]||_{\partial\hat{K}\cup\widehat{\Gamma}_i}, \qquad \omega_K^{(6)} := \frac{1}{2}\hat{h}_K^{1/2}||\hat{z}_s^v - \hat{\psi}_h^v||_{\partial\hat{K}\cup\widehat{\Gamma}_i},$$

$$\rho_K^{(7)} := \frac{1}{2}\hat{h}_K^{-1/2}||[\hat{\sigma}_{mesh}\hat{n}_f]||_{\partial\hat{K}\cup\widehat{\Gamma}_i}, \qquad \omega_K^{(7)} := \frac{1}{2}\hat{h}_K^{1/2}||\hat{z}_f^u - \hat{\psi}_h^u||_{\partial\hat{K}\cup\widehat{\Gamma}_i}.$$

*The weights $\omega^{(i)}$ are approximated by post-processing of the discrete dual solution.*

### A mesh adaptation algorithm

Let an error tolerance TOL be given. Local error indicators from an a posteriori error estimate on the mesh $\hat{\mathcal{T}}_h$ are extracted to realize the mesh adaption:

$$|J(\hat{U}) - J(\hat{U}_h)| \leq \eta := \sum_{\hat{K} \in \mathbb{T}_h} \eta_{\hat{K}} \quad \text{for all cells } \hat{K} \in \hat{\mathcal{T}}_h.$$

This information is used to adapt the mesh using the following strategy:

1. Compute the primal solution $\hat{U}_h$ and the dual solution $\hat{Z}_h$ on the present mesh $\hat{\mathcal{T}}_h$.

2. Determine the cell indicator $\eta_{\hat{K}}$ at each cell $\hat{K}$.

3. Compute the sum of all indicators $\eta := \sum_{\hat{K} \in \hat{\mathcal{T}}_h} \eta_{\hat{K}}$.

4. Check, if the stopping criterion is satisfied: $|J(\hat{U}) - J(\hat{U}_h)| \leq \eta \leq TOL$, then accept $\hat{U}_h$ within the tolerance $TOL$. Otherwise, proceed to the following step.

5. Mark all cells $\hat{K}_i$ that have values $\eta_{\hat{K}_i}$ above the average $\frac{\alpha\eta}{N}$ (where $N$ denotes the total number of cells of the mesh $\mathbb{T}_h$ and $\alpha \approx 1$).

Other mesh adaption strategies are discussed in [15, 30].

**Remark 10.6** (Drawbacks of the classical approach)**.** *Partial integration (similar to [43]) is not required. Consequently, we neither need to evaluate a strong form nor face terms in the inner part of the domain. Consequently, lengthy terms and computational costly evaluations are avoided.* ⋄

### 10.2.2 A partition-of-unity based localization for fluid-structure interation

In order to overcome the previous difficulties with second-order operators and face evaluations, a novel estimator has been designed in [204]. The basic idea, to work with a weak form of the error estimator is the same as proposed several years earlier in [43].

What are now the key features?

- In addition to Remark 10.6, it is the ease of implementation and accuracy (in particular for situations as shown before: fluid-structure solid growth, reactive flow coupled to Navier-Stokes);

- this is achieved by keeping the weak form and introducing a partition-of-unity (PU), which can be of lowest order (e.g., $Q_1$ elements);

- Straightforward to employ;

- Does not require patched meshes.

**10.2.2.1 Formulation for Poisson's problem**    Let the PU be denoted by $V_h^{(1)}$ (without restrictions on Dirichlet boundaries) and with its usual nodal basis $\{\psi_h^i, \ i = 1, \ldots, N^{(1)}\}$. The local error indicator for Poisson's problem,

$$(\nabla u, \nabla \varphi) = (f, \varphi) \quad \forall \varphi \in V,$$

is then given by [204]

$$\eta_i^{\mathrm{PU}} = \sum_{j=1}^{N^{(r)}} \left\{ (f, (\phi_{2h}^{(2),j} - \phi_h^j)\psi_h^i)_\Omega - \left(\nabla u_h, \nabla((\phi_{2h}^{(2),j} - \phi_h^j)\psi_h^i)\right)_\Omega \right\} \vec{z}_j, \tag{218}$$

and it can be efficiently computed in an element-wise manner, as only few test-functions $\phi_h^j$, $\phi_{2h}^{(2),j}$ and $\psi_h^i$ overlap on every element $K \in \Omega_h$.

For the application, we only need evaluations of the right hand side and the residual with modified test-function. This localization technique can be readily applied to general meshes in two and three dimensions. In contrast to the filtering approach, we do not require special mesh structures, such as patches. In particular for three dimensional simulations, the use of patched meshes can substantially increases the problem size. However, the problem of obtaining good approximations to the weights $z - i_h z$ and $u - i_h u$ remains and here, using reconstruction of patches still is one of the most efficient strategies.

**10.2.2.2 Formulation for FSI**   Extending from Poisson's to FSI, the primal DWR estimator for stationary fluid-structure interaction reads:

**Proposition 10.7.**

$$\eta_i^{PU} = \sum_{j=1}^{N^{(r)}} -(\hat{\rho}_f \hat{J}(\widehat{F}^{-1}\hat{v}_f \cdot \widehat{\nabla})\hat{v}_f), \hat{\psi}^v)_{\widehat{\Omega}_f} - (\hat{J}\widehat{\sigma}_f \widehat{F}^{-T}, \widehat{\nabla}\hat{\psi}^v)_{\widehat{\Omega}_f} + \langle \hat{g}_f, \hat{\psi}^v \rangle_{\widehat{\Gamma}_N}$$

$$- (\widehat{F}\widehat{\Sigma}, \widehat{\nabla}\hat{\psi}^v)_{\widehat{\Omega}_s} - (\widehat{\sigma}_{mesh}, \widehat{\nabla}\hat{\psi}^u)_{\widehat{\Omega}_f} - (\widehat{div}(\hat{J}\widehat{F}^{-1}\hat{v}_f), \hat{\psi}^p)_{\widehat{\Omega}_f}$$

*where the weighting functions are defined as*

$$\hat{\psi}^v := (\phi_{2h,v}^{(2),j} - \phi_{h,v}^j)\psi_h^i,$$
$$\hat{\psi}^u := (\phi_{2h,u}^{(2),j} - \phi_{h,u}^j)\psi_h^i,$$
$$\hat{\psi}^p := (\phi_{2h,p}^{(2),j} - \phi_{h,p}^j)\psi_h^i$$
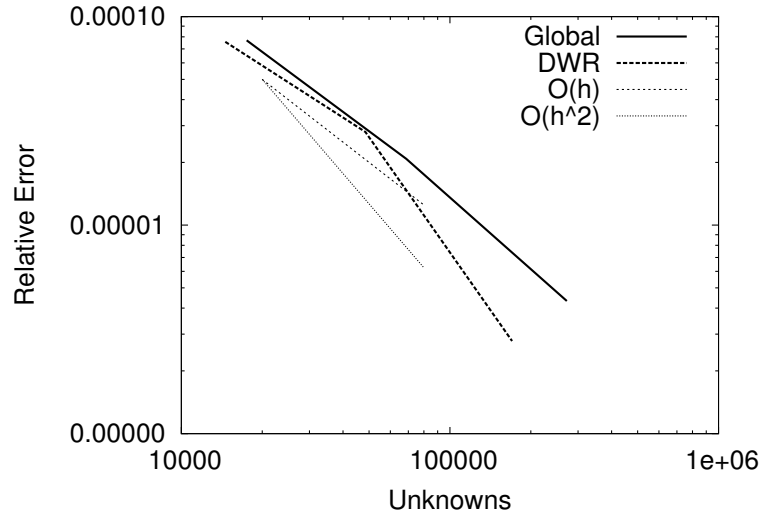


Figure 56: FSI 1-benchmark: Error plots for point value $u_y$ error estimation.
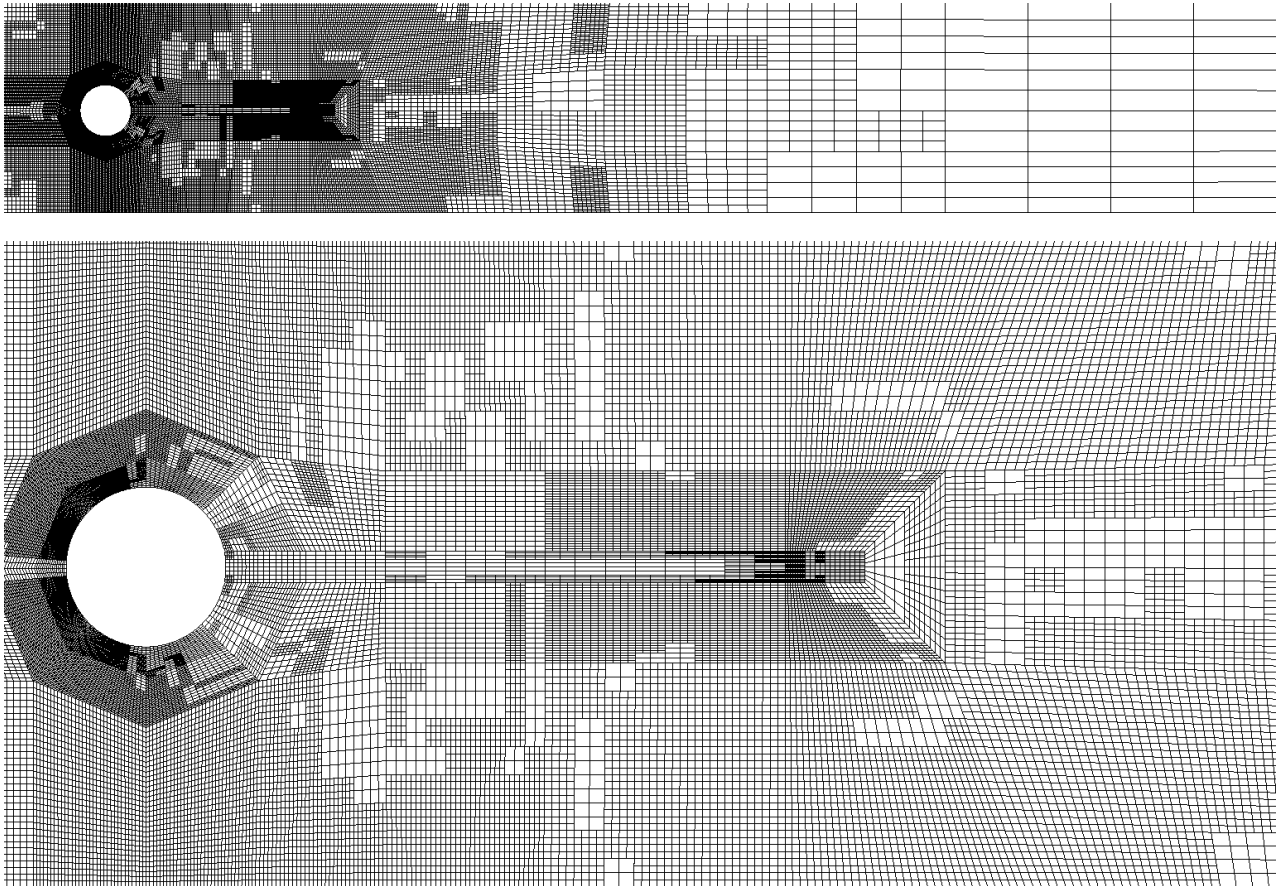
Figure 57: FSI 1-benchmark: locally-refined meshes. Whole mesh and zoom-in to the point estimation $u_y$.

Table 6: Effectivity indices: FSI 1-benchmark

| DoF | $u_y$ | Eff(global) | DoF | $u_y$ | Eff(dwr) |
|---|---|---|---|---|---|
| 17504 | $8.96e - 04$ | $2.92e - 1$ | 14572 | $8.95e - 4$ | $3.43e - 1$ |
| 68736 | $8.40e - 04$ | $3.70e - 1$ | 48420 | $8.47e - 4$ | $3.13e - 1$ |
| 272384 | $8.24e - 04$ | $6.06e - 1$ | 170416 | $8.22e - 4$ | $9.55e - 1$ |

# 11 Gradient-Based Optimization

In this section, we concentrate on stationary problems. Parts of the material presented here has been taken from [202]. We first describe general concepts and then proceed with optimal control and parameter estimation problems for Navier-Stokes and FSI. General and nicely-written introductions can be found e.g., in [134, 179, 228, 233].

## 11.1 The setting

- For optimization we consider the following setting: by $J : \mathcal{X} \to \mathbb{R}$ we denote a given functional of interest. We assume, that $J$ is two times continuously Fréchet differentiable.

**Example 11.1.** *Such a functional can be the measurement of wall-stresses, flow rates or a bending moment.*

Furthermore, by $Q_d$ we denote a finite dimensional set of control parameters that enter the state problem. We notice that the developed algorithms of this study could also be used for infinite control spaces; for optimization with parabolic equations we refer the reader to [168]. Among endless possibilities for the control $q \in Q_d$, common examples are material parameters, inflow rates or pressure-drops. For a given $q \in Q_d$, the controlled state-equation is split into the (nonlinear) state part and a control term which linearly depends on the control $q \in Q_d$:

$$U \in v_D + \mathcal{X} : \quad A(U)(\Phi) + B(U)(q, \Phi) = 0 \quad \forall \Phi \in \mathcal{X}, \tag{219}$$

where the exact definition of the control form $B(\cdot)(\cdot, \cdot)$ depends on the particular choice of the control type. To keep the notation easy in the present section, we combine the state operator and the control operator into one common semi-linear form:

$$A(q, U)(\Phi) := A(U)(\Phi) + B(U)(q, \Phi).$$

The goal of our optimization problem is to determine the optimal parameters $q \in Q_d$ such that the functional of interest $J(\cdot)$ gets minimal. This quantity of interest is completed by a regularization term of Tikhonov type, which involves a corresponding regularization parameter $\alpha$. Then, the cost functional reads:

$$J(q, U) := J(U) + \frac{\alpha}{2}||q - \bar{q}||_Q^2, \tag{220}$$

with a reference control $\bar{q} \in Q_d$ and a suitable norm $|| \cdot ||_Q$ in the control-space. We consider the following optimization problem:

**Problem 11.2** (Constrained optimization). *Minimize the cost functional $J(q, U)$ subject to the state equation $A(q, U)(\Phi) = 0$ (as defined in (219)) for $(q, U) \in Q \times \{v_D + \mathcal{X}\}$.*

The constrained optimization problem on the space $Q_d \times \mathcal{X}$ is reformulated into an unconstrained optimization problem on the space $Q_d$. Therefore, we assume the existence of the solution operator $S : Q_d \to v_D + \mathcal{X}$ with a unique solution $U = S(q)$. Herewith, we define the reduced cost functional $j : Q_d \to \mathbb{R}$ by

$$j(q) := J(q, S(q)). \tag{221}$$

Thus, the constrained optimization problem can be formulated by means of

**Problem 11.3** (Unconstrained optimization). *Minimize $j(q)$ for $q \in Q_d$.*

**Remark 11.4.** *Because of the nonlinear structure of the state equation (219), the reduced cost functional is in general not convex (even if the cost functional $J(q, U)$ would be so).* ⋄

Using the reduced formulation of Problem 11.3, the existence of the optimization problem could be shown with the help of calculus of variations (see, e.g., [164]). A detailed analysis of theoretical results discussing the well-posedness of this general optimality system as well as the existence and uniqueness of possible optimal solutions are found in the literature, see e.g. [134, 228].

Then:

**Problem 11.5.**
$$j(q) := J(q, S(q)) \rightarrow \min, \quad A(q, S(q))(\Psi) = 0 \quad \forall \Psi \in V. \tag{222}$$

*The local existence and sufficient regularity of $S$ is assumed.*

The solution to the unconstrained Problem 11.5 is characterized by the first-order necessary-optimality condition:
$$j'(q)(\delta q) = 0 \quad \forall \delta q \in Q_d. \tag{223}$$
The second-order necessary-optimality which guarantees a (local) minimum reads:
$$j''(q)(\delta q, \delta q) \geq 0 \quad \forall \delta q \in Q_d. \tag{224}$$

In the following, we concentrate on the (formal) computation of the optimality conditions that are employed for the implementation. The most easy way to express them is done by means of the Lagrangian $\mathcal{L} : Q_d \times \mathcal{X} \times \mathcal{X} \rightarrow \mathbb{R}$:
$$\mathcal{L}(q, U, Z) := J(q, U) - A(q, U)(Z). \tag{225}$$
With the help of the Lagrangian, we derive the optimality system (Karush-Kuhn-Tucker - KKT system) for a triple $(q, U, Z) \in Q_d \times \mathcal{X} \times \mathcal{X}$:

$$
\begin{aligned}
\mathcal{L}'_Z(q, U, Z)(\Phi) = 0 \quad &\forall \Phi \in \mathcal{X} \qquad &\text{(State Equation)}, \\
\mathcal{L}'_U(q, U, Z)(\Phi) = 0 \quad &\forall \Phi \in \mathcal{X} \qquad &\text{(Adjoint Equation)}, \\
\mathcal{L}'_q(q, U, Z)(\delta q) = 0 \quad &\forall \delta q \in Q_d \qquad &\text{(Gradient Equation)},
\end{aligned}
$$

or equivalently

$$
\begin{aligned}
A(q, U)(\Phi) &= 0 \qquad &\forall \Phi \in \mathcal{X}, \\
A'_U(q, U)(\Phi, Z) &= J'_U(q, U)(\Phi) \quad &\forall \Phi \in \mathcal{X}, \\
A'_q(q, U)(\delta q, Z) &= J'_q(q, U)(\delta q) \quad &\forall \delta q \in Q_d.
\end{aligned} \tag{226}
$$

**Remark 11.6.** *The KKT system is equivalent to the first-order necessary-optimality condition stated before, if the linearization of the semi-linear form is regular enough. We note that this system could be directly discretized with a Galerkin finite element method. Another approach (see [24, 28, 168]) that uses the reduced formulation is discussed in the following.* ⋄

## 11.2 Solution process of the reduced formulation

In the following, we discuss the solution process of the unconstrained optimization problem. The philosophy of this section follows [24, 28, 168]; their results have been built upon the earlier studies elsewhere [133, 227]. The algorithms are still general enough to be independent from fluid-structure interaction.

We use the standard Newton method to solve the optimization problem. On this level, because we need to work with the discretized control space $Q_d$, we introduce its basis

$$\{\tau q_i \,|\, i = 1, 2, 3, \ldots, \dim Q_d\}.$$

Specifically, the control space $Q_d$ in this work is always finite dimensional with one or two parameters:

$$\text{span}\{q_1, q_2\} =: Q_d = \mathbb{R}^2,$$

i.e., $\dim Q_d = 2$.

With these preliminaries, Newton's method to solve Problem 11.3 reads: For $l = 0, 1, \ldots$, solve

$$
\begin{aligned}
j''(q^l)(\delta q, \tau q) &= -j'(q^l)(\delta q) \quad \forall \tau q \in Q_d, \\
q^{l+1} &= q^l + \omega \delta q,
\end{aligned} \tag{227}
$$

with a line search parameter $\omega \in (0, 1]$ which will be specified in Algorithm 11.9. Specifically, the residual and the Hessian of Newton's method (227) can be computed with the help of the following two results:

**Proposition 11.7** (Residual of Newton's method)**.** *Let* $q \in Q_d, U = S(q) \in \mathcal{X}$ *and* $Z \in \mathcal{X}$ *the dual solution be obtained after solving the first and second equation of the KKT system* (226)*. Then the residual of Newton's method* (227) *is defined as*

$$j'(q)(\delta q) := \mathcal{L}'_q(q, U, Z)(\delta q),$$

*i.e., in explicit representation*

$$j'(q)(\delta q) := \alpha_T(q, \tau q)_Q - A'_q(q, U)(\tau q, Z).$$

*Proof.* The proof uses standard techniques. Details can be found in [28]. □

**Proposition 11.8** (Hessian of Newton's method)**.** *Let* $q \in Q_d, U = S(q) \in \mathcal{X}$ *and* $Z \in \mathcal{X}$ *and* $\delta q \in Q_d$ *be given. Further, let* $\delta U \in \mathcal{X}$ *be the solution of the tangent problem*

$$\delta U \in \mathcal{X}, \quad A'_U(q, U)(\delta U, \Phi) = -A'_q(q, U)(\delta q, \Phi) \quad \forall \Phi \in \mathcal{X},$$

*and* $\delta Z \in \mathcal{X}$ *the solution of the adjoint Hessian problem*

$$A'_U(q, U)(\Phi, \delta Z) = J''_{UU}(q, U)(\delta U, \Phi) - A''_{UU}(q, U)(\delta U, \Phi, Z) - A''_{qU}(q, U)(\delta q, \Phi, Z) \quad \forall \Phi \in \mathcal{X}.$$

*Then it holds for all* $\tau q \in Q_d$*:*

$$j''(q)(\delta q, \tau q) := \alpha_T(\delta q, \tau q)_Q - A''_{qq}(q, U)(\delta q, \tau q, Z) - A''_{Uq}(q, U)(\delta U, \tau q, Z) - A'_q(q, U)(\tau q, \delta Z).$$

*This is equivalent to*

$$
\begin{aligned}
j''(q)(\delta q, \tau q) = {}& \mathcal{L}''_{qq}(q, U, Z)(\delta q, \tau q) \\
& + \mathcal{L}''_{Uq}(q, U, Z)(\delta U, \tau q) \\
& + \mathcal{L}''_{Zq}(q, U, Z)(\delta Z, \tau q) \quad \text{for } \tau q \in Q.
\end{aligned}
$$

*Proof.* For the proof this statement (including its time-dependent version), we refer to Becker et al. [28]. The stationary version of this proposition is easily derived by neglecting all time derivatives, which concludes the assertion. □

Let us summarize the important equations.

**Lagrangian**

$$\mathcal{L}(q, u, z) = J(q, u) - A(q, u)(z)$$

**State Equation**

$$a(q, u)(\phi) = 0$$

**Dual Equation**

$$
\begin{aligned}
& \mathcal{L}'_u(q, u, z)(\phi) = 0 \\
\Leftrightarrow{}& a'_u(q, u)(\phi, z) = J'_u(q, u)(\phi)
\end{aligned}
$$

**Tangent Equation**

$$
\begin{aligned}
& \mathcal{L}''_{qz}(q, u, z)(\delta q, \phi) + \mathcal{L}''_{uz}(q, u, z)(\delta u, \phi) = 0 \\
\Leftrightarrow{}& a'_u(q, u)(\delta u, \phi) + a'_q(q, u)(\delta q, \phi) = 0
\end{aligned}
$$

**Dual Hessian Equation**

$$\mathcal{L}''_{qu}(q,u,z)(\delta q, \phi) + \mathcal{L}''_{uu}(q,u,z)(\delta u, \phi)$$
$$+ \mathcal{L}''_{zu}(q,u,z)(\delta z, \phi) = 0$$
$$\Leftrightarrow a'_u(q,u)(\phi, \delta z) + a'_{uu}(q,u)(\delta u, \phi, z)$$
$$+ a'_{qu}(q,u)(\delta q, \phi, z) = J''_{uu}(q,u)(\cdot, \cdot)$$

**Newton left hand side: first derivative**

$$j'(q)(\delta q) = \mathcal{L}'_q(q,u,z)(\delta q) \quad \text{(Gradient equation)}$$
$$\Leftrightarrow j'(q)(\delta q) = -a'_q(q,u)(\delta q, z) + J'_q(q,u)(\delta q)$$

**Newton right hand side: second derivative**

$$j''(q)(\delta q, \delta r) = \mathcal{L}''_{qq}(q,u,z)(\delta q, \delta r) + \mathcal{L}''_{uq}(q,u,z)(\delta u, \delta r)$$
$$+ \mathcal{L}''_{zq}(q,u,z)(\delta z, \delta r)$$
$$\Leftrightarrow j''(q)(\delta q, \delta r) = J''_{qq}(q,u)(\delta q, \delta r) - a''_{qq}(q,u)(\delta q, \delta r, z)$$
$$- a''_{uq}(q,u)(\delta u, \delta r, z) - a'_q(q,u)(\delta r, \delta z).$$

The two previously mentioned propositions form the basis of the following optimization algorithm:

**Algorithm 11.9** (Optimization loop). *Given an initial control $q^0 \in Q_d$ iterate for $l = 0, 1, \ldots$:*

1. *Compute the state solution $U^l = \{v^l, p^l, u^l\}$:*
$$U^l \in v_D + \mathcal{X}, \quad A(q^l, U^l)(\Phi) = 0 \quad \forall \Phi \in \mathcal{X}.$$

2. *Compute adjoint solution $Z^l = \{z_v^l, z_p^l, z_u^l\}$:*
$$Z^l \in \mathcal{X}, \quad A'_U(q^l, U^l)(\Phi, Z^l) = J'_U(q^l, U^l)(\Phi) \quad \forall \Phi \in \mathcal{X}.$$

3. *Evaluate Newton's right hand side (Proposition 11.7) for $Q_d \ni \tau q = \tau q_i$, $(i = 1, 2, \ldots \dim Q_d)$:*
$$j'(q^l)(\delta q_i) := \alpha_T(q^l, \tau q_i)_Q - A'_q(q^l, U^l)(\tau \hat{q}_i, Z^l), \quad i = 1, 2, \ldots \dim Q_d.$$

4. *Assemble the coefficient vector $f \in \mathbb{R}^{\dim Q_d}$ (as representation for the right hand side $\nabla j(q^l) \in Q_d$ of Newton's method):*
$$Gf = (j'(q^l)(\tau q_i))_{i=1}^{\dim(Q_d)}, \quad G_{ij} = (\tau q_j, \tau q_i)_Q,$$
*where $j'(q^l)(\tau q_i) = (\nabla j(q^l), \tau q_i) = \sum_{j=1}^{\dim Q_d} f_j(\tau q_j, \tau q_i)_Q$.*

5. *Compute the tangent solution $\delta U^l = \{\delta v^l, \delta p^l, \delta u^l\}$:*
$$\delta U^l \in \mathcal{X}, \quad A'_U(q^l, U^l)(\delta U^l, \Phi) = -A'_q(q^l, U^l)(\delta q, \Phi) \quad \forall \Phi \in \mathcal{X}.$$

6. *Compute the adjoint for Hessian solution $\delta Z^l = \{\delta z_v^l, \delta z_p^l, \delta z_u^l\}$:*
$$\delta Z^l \in \mathcal{X}, \quad A'_U(q^l, U^l)(\Phi, \delta Z^l) = J''_{UU}(q^l, U^l)(\delta U^l, \Phi)$$
$$- A''_{UU}(q^l, U^l)(\delta U^l, \Phi, Z^l) - A''_{qU}(q^l, U^l)(\delta q, \Phi, Z^l) \quad \forall \Phi \in \mathcal{X}.$$

7. *Evaluate Newton's left hand side (Proposition 11.8) for $Q_d \ni \tau q = \tau q_i$, $(i = 1, 2, \ldots \dim Q_d)$:*
$$j''(q^l)(\delta q, \tau q_i) := \alpha_T(\delta q, \tau q_i)_Q - A''_{qq}(q^l, U^l)(\delta q, \tau q_i, Z^l)$$
$$- A''_{Uq}(q^l, U^l)(\delta U^l, \tau q_i, Z^l) - A'_q(q^l, U^l)(\tau q_i, \delta Z^l) \quad \forall \delta q \in Q_d.$$

8. *Assemble the coefficient vector* $h \in \mathbb{R}^{\dim(Q_d)}$ *(as representation of the left hand side* $j''(q^l)(\delta q, \tau q_i)$ *of Newton's method):*

$$Gh = (j''(q^l)(\delta q, \tau q_i))_{i=1}^{\dim(Q_d)}$$

*where* $j''(q^l)(\delta q, \tau q_i) = (\nabla^2 j(q^l)(\delta q, \tau q_i)_Q)_{i=1}^{dimQ_d} = \sum_{j=1}^{dimQ_d} h_j(\tau q_j, \tau q_i)_Q.$

9. *Solve:* $j''(q^l)(\delta q, \tau q_i) = -j'(q^l)(\tau q_i)$ *with* $\tau q_i \in Q_d$ *via*

$$\text{Minimize} \quad j(q^l) + \langle f, d \rangle + \frac{1}{2}\langle Hd, d \rangle,$$

*with* $\langle a, b \rangle := a^T Gb$ *and* $H := G^{-1}K$. *Furthermore,* $K_{ij} = \nabla^2 j(q^l)(\delta q_j, \tau q_i)_Q)_Q$ *denotes the coefficient matrix of the Hessian* $\nabla^2 j(q^l)$ *and* $d \in \mathbb{R}^{dimQ_d}$ *represents the coefficient vector of* $\delta q$. *The solution is obtained by a CG-solver that requires matrix-vector products only.*

10. *Correction step:*

$$q^{l+1} = q^l + \omega \delta q,$$

*with* $\omega \in (0, 1]$ *as large as possible, such that*

$$j(q^l + \delta q) \leq j(q^l) + \omega \cdot \nabla j(q^l)\delta q.$$

*The parameter* $\omega$ *is determined via the Armijo-backtracking strategy. For details we refer the reader to [178, 179].*

11. *Increment* $l \to l + 1$.

12. *Repeat all steps until:* $|f| = \|\nabla j(q^l)\| < TOL$.

This section is devoted to the application of the presented scheme to fluid-structure interaction systems. First, we need to evaluate all derivatives necessary to assemble the systems required to carry out Algorithm 11.9. While an approximation of the derivatives would in principle be possible by using finite differences [119] or by automatic differentiation, see [73] in the context of fluid-structure interaction, we analytically calculate all these derivatives as shown in Section 9.3.

### 11.2.1 State and adjoint equations

In steps 1, 2, 5 and 6 of the algorithm, we need to solve problems given in a variational formulation using the test- and trial-space $\mathcal{X}$. These infinite dimensional problems will be discretized using the finite element method. All these variational problems are surface-coupled problems with different equations in the fluid and the structure domain. All four problems include balancing conditions on the common interface $\Gamma_i$, where in the case of the state-equation in Step 1 these balancing conditions are standard conditions of continuous velocity and the dynamic coupling conditions of the interface stresses:

$$
\begin{aligned}
v_f &= 0 \quad \text{on } \Gamma_i. \\
J\hat{\sigma}_f F^{-T} n_f + F\Sigma_s n_s &= 0 \quad \text{on } \Gamma_i.
\end{aligned}
\tag{228}
$$

In [202] we provide details on all derived variational formulations appearing in Algorithm 11.9. For solving the nonlinear state equation, we employ a Newton method that requires the Jacobian of the semilinear-form $A(\cdot)(\cdot)$. This linearized equation utilizes the same bilinear form as the tangent equation in Step 5 of the algorithm. The coupling condition given by variational manners are the linearization of (228). Let $W = \{w_v, w_p, w_u\} \in \mathcal{X}$ be the unknown solution. Then, it holds on $\Gamma_i$:

$$
J\left\{\frac{d\hat{\sigma}_f}{dv_f}(w_v) + \frac{d\hat{\sigma}_f}{dp_f}(w_p) + \frac{d\hat{\sigma}_f}{du}(w_u) + \text{tr}(F^{-1}\nabla w_u)\hat{\sigma}_f - \hat{\sigma}_f F^{-1}\nabla w_u\right\} n_f
$$
$$
+ \left\{\nabla w_u \Sigma_s + F\frac{d\Sigma_s}{du}(w_u)\right\} n_s = 0, \quad w_f = 0. \tag{229}
$$

Once the Jacobian is implemented, the adjoint form is given by transposing the system matrix. Hence, the effort for solving the adjoint equations is comparable to an additional step of the state equation's Newton scheme. The balancing condition inherent in the adjoint equation is given by variational principles and is of Robin-type coupling all three adjoint variables $z_v$, $z_p$ and $z_u$. The derivation of the strong formulation of this coupling condition is cumbersome. In Figure 58 we show the velocity, displacement and pressure of the optimal state solution and their corresponding adjoint solutions. These visualizations are taken from [202].
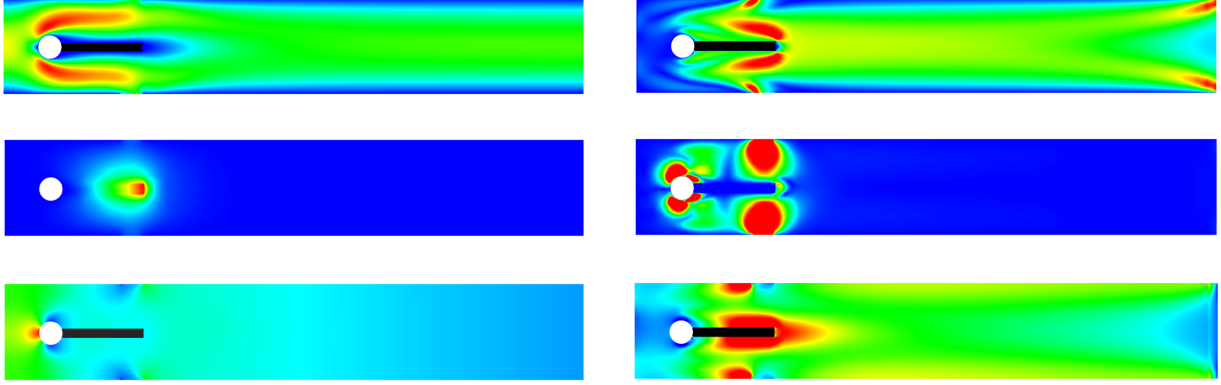


Figure 58: FSI-1 optimal control benchmark problem taken from [202]. Left: primal solutions of the optimal state for velocity, displacement, and pressure. Right: adjoint solutions for velocity, displacement and pressure at the right. Note, that velocity and pressure components are defined in the fluid domain only.

### 11.2.2 Implementation structure in DOpElib

The implementation is based on DOpElib and was initially inspired [26] by Gascoigne [26] and RoDoBo [209].

$$
\begin{array}{rcll}
\text{CellEquation (state)} & \Leftrightarrow & A(q,u)(\phi) & (230) \\
\text{CellEquationU (adjoint)} & \Leftrightarrow & A'_u(q,u)(\phi,z) & (231) \\
\text{CellEquationUT (tangent)} & \Leftrightarrow & A'_u(q,u)(\delta u,\phi) & (232) \\
\text{CellEquationUTT (adjoint hessian)} & \Leftrightarrow & A'_u(q,u)(\phi,\delta z) & (233) \\
\text{CellEquationQ (gradient)} & \Leftrightarrow & A'_q(q,u)(\delta q,z) & (234) \\
\text{CellEquationQT (tangent)} & \Leftrightarrow & A'_q(q,u)(\delta q,\phi) & (235) \\
\text{CellEquationQTT (hessian)} & \Leftrightarrow & A'_q(q,u)(\delta q,\delta z) & (236) \\
\text{CellEquationUU (adjoint hessian)} & \Leftrightarrow & A''_{uu}(q,u)(\delta u,\phi,z) & (237) \\
\text{CellEquationQU (adjoint hessian)} & \Leftrightarrow & A''_{qu}(q,u)(\delta q,\phi,z) & (238) \\
\text{CellEquationUQ (hessian)} & \Leftrightarrow & A''_{uq}(q,u)(\delta u,\delta r,z) & (239) \\
\text{CellEquationQQ (hessian)} & \Leftrightarrow & A''_{qq}(q,u)(\delta q,\delta r,z) & (240) \\
\text{CellRightHandSide (state)} & \Leftrightarrow & f(\phi) & (241) \\
\text{CellMatrix (all)} & \Leftrightarrow & A'(q,u)(\delta u) & (242) \\
\text{ControlCellEquation (gradient or hessian)} & \Leftrightarrow & \mathcal{L}'_q(q,u,z)(\delta q) & (243) \\
\text{ControlCellMatrix (all)} & \Leftrightarrow & A(q,u)(\phi) & (244)
\end{array}
$$

---

[26] Actually in the years 2009/2010 when the project started.

Functionals

$$\begin{array}{rcll}
\text{Value (all)} & \Leftrightarrow & J(q,u) & (245) \\
\text{ValueU (all)} & \Leftrightarrow & J'_u(q,u)(\phi) & (246) \\
\text{ValueQ (all)} & \Leftrightarrow & J'_q(q,u)(\phi) & (247) \\
\text{ValueUU (all)} & \Leftrightarrow & J''_{uu}(q,u)(\psi,\phi) & (248) \\
\text{ValueQU (all)} & \Leftrightarrow & J''_{qu}(q,u)(\psi,\phi) & (249) \\
\text{ValueUQ (all)} & \Leftrightarrow & J''_{uq}(q,u)(\psi,\phi) & (250) \\
\text{ValueQQ (all)} & \Leftrightarrow & J''_{qq}(q,u)(\psi,\phi) & (251) \\
 & & & (252)
\end{array}$$

## 11.3 Boundary control of stationary fluid flow

Let us see whether we understood the concepts and compute a numerical test. The following example has been proposed by Roland Becker [23, 24].
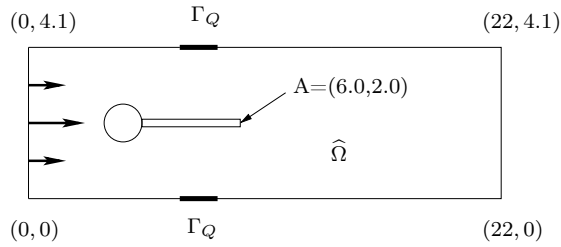


Figure 59: Flow around cylinder with elastic flag with circle-center $(2,2)$ and radius $r = 0.5$. Structure material: 'compressible St. Venant-Kirchhoff'.

**11.3.0.1 Configuration** Goal of optimization is drag minimization around the cylinder:

$$(J_{\text{Drag}}(U), 0) := (F_D, 0) = \int_S \sigma_f \cdot n_f \, e_1 \, ds. \tag{253}$$

As usually, the stress tensor is given by

$$\sigma_f = -pI + \rho\nu(\nabla v + \nabla v^T).$$

The Neumann control acts at the boundary $\Gamma_Q$ and is given by a piecewise constant control $q = \{q_1, q_2\} \in \mathbb{R}^2$. The initial values can be chosen as $q = 0.0$ or $q = 0.1$ for both components. The physical unknowns are a vector-velocity field $v$ and as scalar pressure field $p$. The semi-linear form of the problem reads:
Find $u = \{v, p\} \in \{v^{in} + V\} \times L^2$ and $q \in \mathbb{R}^2$ such that

$$A(q,u)(\phi) = \rho\nu(\nabla v + \nabla v^T, \nabla \phi^v)_{\Omega_f} + (\nabla v \, v, \phi^v)_{\Omega_f} - (p, \nabla \cdot \phi^v)_{\Omega_f} + (\nabla \cdot v, \phi^p)_{\Omega_f}$$
$$- (q, n \cdot \phi^v)_{\Gamma_Q} = 0.$$

for all test functions $\phi = \{\phi^v, \phi^p\} \in V$. Please note that the convection term differs from standard notation:

$$\nabla v \, v := (\nabla v)v = v \cdot \nabla v.$$

Further the pressure term can be rewritten as

$$-(p, \nabla \cdot \phi^v)_{\Omega_f} = -(pI, \nabla \phi^v)_{\Omega_f}$$

where $I$ denotes the identity matrix in 2D.

The target functional is considered as

$$j(v, p) = \int_{\Gamma_O} n \cdot \sigma(v, p) \cdot d\, ds,$$

where $\Gamma_O$ denotes the cylinder boundary, and $d$ is a vector in the direction of the mean flow. For theoretical and numerical reasons, this functional needs to be regularized, including the control variable $q$, such that

$$J(q, v, p) = j(v, p) + \frac{\alpha}{2}||q - q_0||,$$

where $\alpha$ is the Tikhonov parameter and $q_0$ some reference control.

The rest of the program is similar to the previous optimization problems where we formulate the state equation in a weak form $a(v, p)(\phi)$ such that the final problem reads

$$J(q, v, p) \to \min \quad \text{s.t.} \quad A(q, v, p)(\phi) = 0.$$

### 11.3.1 Equations for gradient-based optimization

The following terms are required for the optimization process:

**CellEquation (state):** Compute

$$A(q, u)(\phi) = \rho\nu(\nabla v + \nabla v^T, \nabla\phi^v)_{\Omega_f} + (\nabla v\, v, \phi^v)_{\Omega_f}$$
$$- (p, \nabla \cdot \phi^v)_{\Omega_f} + (\nabla \cdot v, \phi^p)_{\Omega_f}.$$

**CellMatrix (all):** Compute

$$A(q, u)(\phi_i, \phi_j) = \rho\nu(\nabla\phi_j^v + \nabla(\phi_j^v)^T, \nabla\phi_i^v)_{\Omega_f} + (\nabla\phi_j^v\, v + \nabla v\, \phi_j^v, \phi_i^v)_{\Omega_f}$$
$$- (\phi_j^p, \nabla \cdot \phi_i^v)_{\Omega_f} + (\nabla \cdot \phi_j^v, \phi_i^p)_{\Omega_f}$$

where the velocity $v$ of fluid's convection term depends the type of equation under investigation:

$$v = v^{n-1} \quad \text{(Previous Newton step for state matrix)}$$
$$v = v^{state} \quad \text{(Actual state solution for adjoint, gradient, etc.)}$$

**CellEquationU (adjoint):** Compute

$$a'_u(q, u)(\phi, z) = \rho\nu(\nabla\phi^v + \nabla(\phi^v)^T, \nabla z^v)_{\Omega_f} + (\nabla\phi^v\, v^{state} + \nabla v^{state}\phi^v, z^v)_{\Omega_f}$$
$$- (\phi^p I, \nabla z^v)_{\Omega_f} + (\nabla \cdot \phi^v, z^p)_{\Omega_f}$$

**CellEquationUT (tangent):** Compute

$$a'_u(q, u)(\delta u, \phi) = \rho\nu(\nabla\delta u^v + \nabla(\delta u^v)^T, \nabla\phi^v)_{\Omega_f} + (\nabla\delta u^v\, v^{state} + \nabla v^{state}\delta u^v, \phi^v)_{\Omega_f}$$
$$- (\delta u^p I, \nabla\phi^v)_{\Omega_f} + (\nabla \cdot \delta u^v, \phi^p)_{\Omega_f}$$

**CellEquationUTT (adjoint hessian):** Compute

$$a'_u(q, u)(\phi, \delta z) = \rho\nu(\nabla\phi^v + \nabla(\phi^v)^T, \nabla\delta z^v)_{\Omega_f} + (\nabla\phi^v\, v^{state} + \nabla v^{state}\phi^v, \delta z^v)_{\Omega_f}$$
$$- (\phi^p I, \nabla\delta z^v)_{\Omega_f} + (\nabla \cdot \phi^v, \delta z^p)_{\Omega_f}$$

**CellEquationUU (adjoint hessian):** Compute

$$a''_{uu}(q, u)(\delta u, \phi, z) = (\nabla\phi^v\, \delta u^{v,state} + \nabla\delta u^{v,state}\phi^v, z^v)_{\Omega_f}$$

Here: $z^v$ are the adjoint values as already shown before, and $\delta u^{v,state}$ are the tangent values which are already computed.

**BoundaryEquation (state):** Compute

$$A(q, u)(\phi) = -\rho\nu(\nabla v^T \cdot n, \phi^v)_{\Gamma_{out}} - (q_0, n \cdot \phi^v)_{\Gamma_{q0}} - (q_1, n \cdot \phi^v)_{\Gamma_{q1}}$$

**BoundaryMatrix (all):** Compute

$$A(q,u)(\phi_i, \phi_j) = -\rho\nu(\nabla(\phi_j^v)^T \cdot n, \phi_i^v)_{\Gamma_{out}}$$

**BoundaryEquationQ (gradient):** Compute

$$A_q'(q,u)(\delta q, z)[0] = -(1, n \cdot z^v)_{\Gamma_{q0}}$$
$$A_q'(q,u)(\delta q, z)[1] = -(1, n \cdot z^v)_{\Gamma_{q1}}$$

where $\delta q = 1$ since $q$ has been chosen constant.

**BoundaryEquationQT (tangent):** Compute

$$A_q'(q,u)(\delta q, \phi) = -(\delta q_0, \phi^v \cdot n)_{\Gamma_{q0}} - (\delta q_1, \phi^v \cdot n)_{\Gamma_{q1}}$$

**BoundaryEquationQTT (hessian):** Compute

$$A_q'(q,u)(\delta q, \delta z)[0] = -(1, n \cdot z^v)_{\Gamma_{q0}}$$
$$A_q'(q,u)(\delta q, \delta z)[1] = -(1, n \cdot z^v)_{\Gamma_{q1}}$$

where $\delta q = 1$ since $q$ has been chosen constant.

**BoundaryEquationU (adjoint):** Compute

$$A_u'(q,u)(\phi, z) = -\rho\nu(\nabla(\phi^v)^T \cdot n, z^v)_{\Gamma_{out}}$$

**BoundaryEquationUT (tangent):** Compute

$$A_u'(q,u)(\delta u, \phi) = -\rho\nu(\nabla(\delta u^v)^T \cdot n, \phi^v)_{\Gamma_{out}}$$

**BoundaryEquationUTT (adjoint hessian):** Compute

$$A_u'(q,u)(\phi, \delta z) = -\rho\nu(\nabla(\phi^v)^T \cdot n, \delta z^v)_{\Gamma_{out}}$$

**ControlCellEquation (gradient or hessian):**
**ControlCellMatrix (all):**
We turn now to the computation of the cost functional including the regularization term.
**BoundaryValue:**

$$J(q,u) = c_D \int_S \sigma_f(v,p) \cdot n\, e_1\, ds + \frac{\alpha}{2}\|q\|_{\Gamma_q}^2$$

where $c_D = 500$ and $\alpha > 0$

**BoundaryValueU:**

$$J_u'(q,u)(\phi) = c_D \int_S \sigma_f(\phi^v, \phi^p) \cdot ne_1\, ds$$

**BoundaryValueQ:**

$$J_q'(q,u)(\phi) = \alpha(q, \phi)_{\Gamma_q}$$

**BoundaryValueQQ:**

$$J_{qq}''(q,u)(\delta q, \phi) = \alpha(\delta q, \phi)_{\Gamma_q}$$

| DoF | $u_x(A)$ | $u_y(A)$ | $q$ |
|---|---|---|---|
| 5 032 | $2.38095e-05$ | 0.000920281 | 471742 |
| 19 488 | $2.37664e-05$ | 0.000844817 | 477626 |
| 76 672 | $2.35301e-05$ | 0.000837236 | 481284 |
| Uncontrolled | | | |
| 76 672 | $218.332e-05$ | 0.001999470 | 500 |
| FSI-1 benchmark results (without any control) | | | |
| 76 672 | $2.27036e-05$ | 0.000822894 | 500000 |

Table 7: FSI-1 parameter estimation problem. Initial control $q_{\text{initial}} = 500$, $\bar{q} = 5 \cdot 10^5$ and $\alpha = 10^{-5}$.

**11.3.1.1 Numerical results**  We consult our source code from [71] `Examples/OPT/StatPDE/Example3` (in version dopelib-2.0).

As starting values for $q$ we choose in a first run $q = 0$ and also $q = 0.1$ in order to see if we converge to the same optimal solution.

| DoF | $q_{\text{start}}$ | $q_{\text{top}}$ | $q_{\text{bottom}}$ | $J_{\text{opt}}$ | $\text{Drag}_{\text{opt}}$ | $J_{\text{start}}$ | $\text{Drag}_{\text{start}}$ |
|---|---|---|---|---|---|---|---|
| 6000 | 0.0 | 0.312 | 0.309 | 2.5595 | 2.46292 | 4.144 | 4.1443 |
| 6000 | 0.1 | 0.312 | 0.309 | 2.5595 | 2.46292 | 3.083 | 3.0731 |
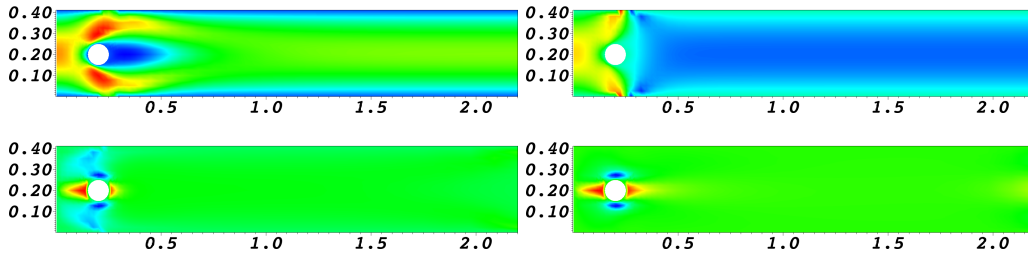


Figure 60: Stationary flow control: primal solution at the beginning and end of the optimization (top) and corresponding adjoint solution (bottom). For all solutions, we plot the $x$-velocity field.

## 11.4 FSI-1 parameter estimation benchmark

This second test is taken from [202] and we consider another extension of the FSI-1 benchmark problem and define a parameter identification test-case. We aim at identifying the Lamé coefficient $\mu_s$ in such a way, that the tip of the beam undergoes a given deformation $u_y(A) = 8.2 \cdot 10^{-4}$ (i.e., close to the solution of the uncontrolled configuration in the original FSI-1 benchmark problem). All material parameters as well as the boundary data is chosen as in the previous section. For identifying the parameter we choose the following regularized functional:

$$J(q, U) = \|u_y - \bar{u}_y\|^2 + \frac{\alpha}{2}\|q - \bar{q}\|^2,$$

with $q = \mu_s$ (the Lamé coefficient) and $\bar{u}_y = 8.2 \cdot 10^{-4}$. Furthermore, we choose $\bar{q} = 5 \cdot 10^{-5}$ and a small Tikhonov parameter $\alpha = 10^{-5}$.

The initial control value is given by $q_{\text{initial}} = \mu_{\text{initial}} = 500$, far away from the optimal state. In Table 7 we indicate the results of the optimization algorithm. In Figure 61 we show plots of the state and adjoint solution for this optimization problem.
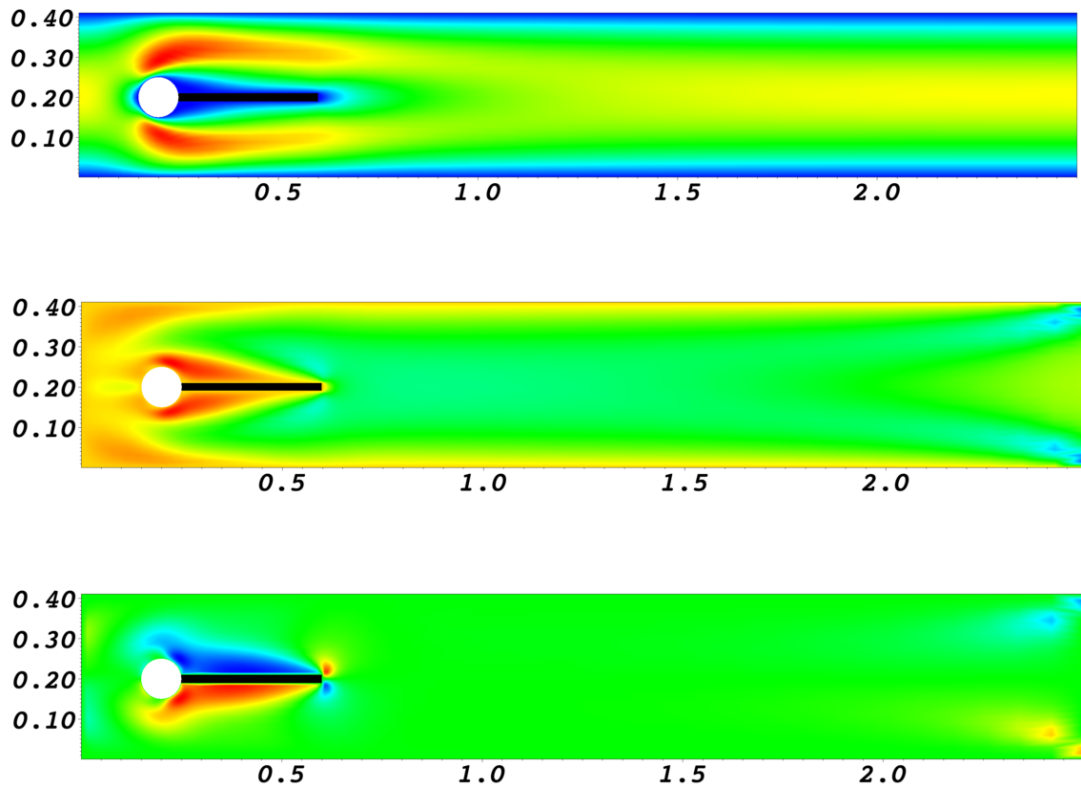
Figure 61: FSI parameter estimation: x-velocity profile (top) and corresponding adjoint solution in $v_x$ direction (middle) and adjoint solution in $v_y$ direction (bottom).

### 11.4.1 Monolithic versus partitioned coupling in Newton's optimization loop

We want to draw our attention to an interesting study in comparing monolithically-coupled fluid-structure interaction and partitioned coupling on the level of the outer optimization loop. This is achieved by neglecting the ALE-transformation in the adjoint, tangent and additional Hessian. Then, we clearly observe that monolithic coupling allows for higher accuracy as shown in Figure 11.4.1. This is in perfect agreement with partitioned (weak and strong) coupling and a monolithic approach for the forward problem. If you wish to satisfy a good tolerance for the coupling conditions, you either need to use a partitioned algorithm with strong coupling (i.e., possibly many subiterations in each time step) or you should use a monolithically-coupled scheme.
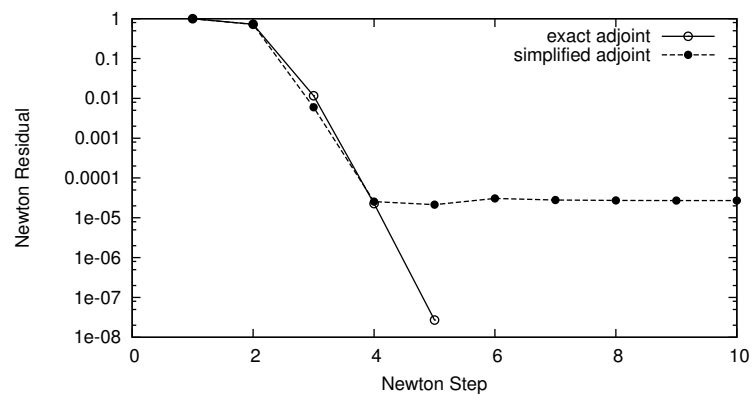
Figure 62: Convergence of the Newton iteration considering exact adjoint equations and a simplification neglecting the adjoint coupling conditions. Figure taken from [202].

# 12 Simulations

In this chapter, we discuss several numerical tests and benchmarks. The focus is to provide tools and methods how numerical results can be interpreted and verified:

- For a new code from scratch: start simple and neglect nonstationary behavior and nonlinear terms first;

- Compare with accepted benchmarks and manufactured solutions if possible;

- Extend then to nonstationary and/or nonlinear equations;

- Check always the boundary conditions: these are one of the most-faced error sources;

- Try to write a code in a friendly way by using comments and coding standards: this makes it much easier either for others to use your code or to work together on a code or to re-use your code after several years.

- If your code does not produce the correct findings there are several possibilities for debugging. For example:
  - Use a nonlinear solver but solve a linear equations: does the nonlinear solver converge in one step? Is there some kind of instability due to too large time steps?
  - Make your problem as linear as possible (neglect the convection term in Navier-Stokes and use linearized elasticity rather than STVK;
  - Check and compare different time-stepping schemes;
  - If your nonlinear solver does not converge: reduce inflow sources and/or right hand side forces, or reduce the time step in order to enhance the convergence radius.

Careful numerical testing might include:

- Systematic testing with different spatial meshes and different time step sizes: do goal functionals converge to a common limit?

- Comparing with manufactured solutions; if not available, compute a solution on a very fine mesh (and/or very small time step) and use this result as reference solution;

- Comparing with experimental findings.

## 12.1 The FSI benchmark FSI-2 [140]

### 12.1.1 Configuration

The computational domain has length $L = 2.5m$ and height $H = 0.41m$. The circle center is positioned at $C = (0.2m, 0.2m)$ with radius $r = 0.05m$. The elastic beam has length $l = 0.35m$ and height $h = 0.02m$. The right lower end is positioned at $(0.6m, 0.19m)$, and the left end is attached to the circle.
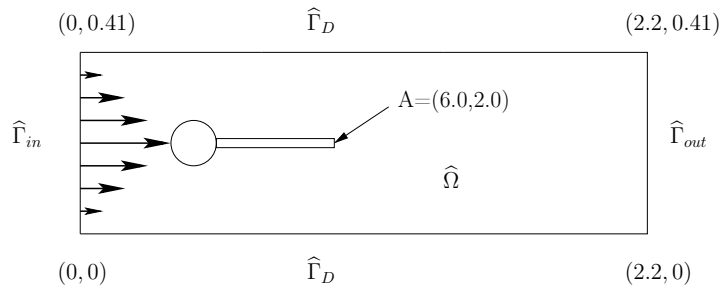


Figure 63: Flow around cylinder with elastic beam with circle-center $C = (0.2, 0.2)$ and radius $r = 0.05$.

Control points $A(t)$ (with $A(0) = (0.6, 0.2)$) are fixed at the trailing edge of the structure, measuring $x$- and $y$-deflections of the beam.

### 12.1.2 Equations

We use Formulation 7.26.

### 12.1.3 Boundary and intial conditions

For the upper, lower, and left boundaries, the 'no-slip' conditions for velocity and no zero displacement for structure are given. When using the second type of boundary conditions with the biharmonic mesh motion model, the displacement should be zero in normal direction and free in the tangential direction. This allows the fluid mesh the freedom to 'move' along the boundary and results in a better partition of the fluid mesh.

A parabolic inflow velocity profile is given on $\hat{\Gamma}_{in}$ by

$$v_f(0, y) = 1.5\bar{U}\frac{4y(H - y)}{H^2}, \quad \bar{U} = 1.0ms^{-1}.$$

At the outlet $\hat{\Gamma}_{out}$ the 'do-nothing' outflow condition is imposed which lead to zero mean value of the pressure at this part of the boundary.

For the non-steady tests one can start with a smooth increase of the velocity profile in time. We use

$$v_f(t; 0, y) = \begin{cases} v_f(0, y)\frac{1-\cos(\frac{\pi}{2}t)}{2} & \text{if } t<2.0\text{s} \\ v_f(0, y) & \text{otherwise.} \end{cases}$$

The term $v_f(0, y)$ is already explained above.

At the outlet $\hat{\Gamma}_{out}$, the 'do-nothing' [132] outflow condition is imposed leading to a zero mean value of the pressure at this part of the boundary.

### 12.1.4 Parameters

We choose for our computation the following parameters. For the fluid we use $\varrho_f = 10^3 kgm^{-3}$, $\nu_f = 10^{-3}m^2s^{-1}$. The elastic structure is characterized by $\varrho_s = 10^4 kgm^{-3}$, $\nu_s = 0.4$, $\mu_s = 5 * 10^5 kgm^{-1}s^{-2}$.

### 12.1.5 Quantities of interest / goal functionals

1) $x$- and $y$-deflection of the beam at $A(t)$.

2) The forces exerted by the fluid on the whole body, i.e., drag force $F_D$ and lift force $F_L$ on the rigid cylinder and the elastic beam. They form a closed path in which the forces can be computed with the help of line integration. The formula is evaluated on the fixed reference domain $\hat{\Omega}$ and reads:

$$(F_D, F_L) = \int_{\hat{S}} \hat{J}\hat{\sigma}_{all}\hat{F}^{-T} \cdot \hat{n} \, d\hat{s} \tag{254}$$

$$= \int_{\hat{S}(\text{circle})} \hat{J}\hat{\sigma}_f\hat{F}^{-T} \cdot \hat{n}_f \, d\hat{s} + \int_{\hat{S}(\text{beam})} \hat{J}\hat{\sigma}_f\hat{F}^{-T} \cdot \hat{n}_f \, d\hat{s}. \tag{255}$$

The quantities of interest for this time dependent test case are represented by the mean value, amplitudes, and frequency of $x$- and $y$-deflections of the beam in one time period $T$ of oscillations.

### 12.1.6 Results and discussions
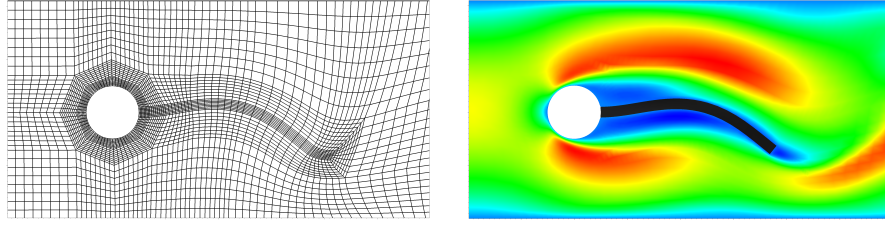


Figure 64: FSI 2 test case: mesh (left) and velocity profile in vertical direction (right) at time $t = 16.14s$.

Table 8: Results for the FSI 2 benchmark with the biharmonic mesh motion model and second type of boundary conditions. The mean value and amplitude are given for the four quantities of interest: $u_x, u_y[m], F_D, F_L[N]$. The frequencies $f_1[s^{-1}]$ and $f_2[s^{-1}]$ of $u_x$ and $u_y$ vary in a range of $3.83 - 3.88$ (ref. 3.86) and $1.92 - 1.94$ (ref. 1.93), respectively.

| DoF | $k[s]$ | $u_x(A)[\times 10^{-3}]$ | $u_y(A)[\times 10^{-3}]$ | $F_D$ | $F_L$ |
|---|---|---|---|---|---|
| 27744 | 3.0e-3 | $-13.63 \pm 11.80$ | $1.27 \pm 78.72$ | $207.22 \pm 71.13$ | $-0.57 \pm 230.6$ |
| 27744 | 2.0e-3 | $-13.72 \pm 11.84$ | $1.26 \pm 78.38$ | $208.12 \pm 71.18$ | $-0.30 \pm 232.6$ |
| 27744 | 1.0e-3 | $-13.74 \pm 11.85$ | $1.28 \pm 78.48$ | $209.46 \pm 71.43$ | $-0.06 \pm 231.7$ |
| 27744 | 0.5e-3 | $-13.66 \pm 11.81$ | $1.28 \pm 78.32$ | $208.96 \pm 71.60$ | $-0.06 \pm 238.2$ |
| 42024 | 3.0e-3 | $-13.34 \pm 11.57$ | $1.40 \pm 77.08$ | $204.81 \pm 68.54$ | $0.79 \pm 221.5$ |
| 42024 | 2.0e-3 | $-13.36 \pm 11.55$ | $1.28 \pm 77.18$ | $205.61 \pm 68.67$ | $0.51 \pm 223.0$ |
| 42024 | 1.0e-3 | $-13.38 \pm 11.58$ | $1.31 \pm 77.44$ | $206.11 \pm 68.26$ | $0.62 \pm 221.2$ |
| 42024 | 0.5e-3 | $-13.27 \pm 11.52$ | $1.23 \pm 77.25$ | $207.05 \pm 68.87$ | $0.30 \pm 230.6$ |
| 72696 | 3.0e-3 | $-14.43 \pm 12.46$ | $1.35 \pm 80.71$ | $212.50 \pm 76.40$ | $0.18 \pm 234.6$ |
| 72696 | 2.0e-3 | $-14.49 \pm 12.44$ | $1.19 \pm 80.66$ | $213.49 \pm 76.39$ | $0.13 \pm 235.7$ |
| 72696 | 1.0e-3 | $-14.49 \pm 12.46$ | $1.16 \pm 80.63$ | $213.39 \pm 75.25$ | $0.23 \pm 234.2$ |
| 72696 | 0.5e-3 | $-14.40 \pm 12.39$ | $1.25 \pm 80.55$ | $213.55 \pm 76.06$ | $0.30 \pm 240.2$ |
| (ref.) | 0.5e-3 | $-14.85 \pm 12.70$ | $1.30 \pm 81.70$ | $215.06 \pm 77.65$ | $0.61 \pm 237.8$ |

## 12.2 The FSI benchmark FSI-1 [140]

In this section, we provide the details for the stationary FSI-1 benchmark. The only change to the previous computations is that we now change $\bar{U}$ to

$$\bar{U} = 0.2ms^{-1}$$

The following results are taken from [200]. This test can be recomputed using [71, 117] with `dopelib/Examples/PDE/InstatPDE/Example2`. Therein Formulation 7.26 is used and 25 pseudo time steps using the backward Euler scheme are taken. Alternativly, a fully stationary code could have been developed.

Horizontal $\hat{u}^x$ and vertical $\hat{u}^y$ displacement in control point $\widehat{A} = (0.6, 0.2)$ in the *ALE formulation*. Left: global refinement, right: adaptive refinement.

| Dof's | $\hat{u}^x(A)$ | $\hat{u}^y(A)$ | Dof's | $\hat{u}^x(A)$ | $\hat{u}^y(A)$ |
|---|---|---|---|---|---|
| 5032 | 2.2635 | 8.7871 | 19,488 | 2.2635 | 8.7871 |
| 19,488 | 2.2821 | 8.1977 | 29,512 | 2.2793 | 8.2201 |
| 76,672 | 2.2736 | 8.1848 | 51,016 | 2.2733 | 8.1867 |
| 304,128 | 2.2691 | 8.1785 | 93,992 | 2.2710 | 8.1702 |
| 1,211,392 | 2.2676 | 8.1742 | 179,912 | 2.2700 | 8.1609 |
| | | | 351,720 | 2.2695 | 8.1556 |
| | $\cdot 10^{-5}$ | $\cdot 10^{-4}$ | | $\cdot 10^{-5}$ | $\cdot 10^{-4}$ |

Figure 65: FSI 1 test case. Table 7 taken from [200].

Table 9: Results taken from [244] for the FSI 1 benchmark with the biharmonic mesh motion model. The mean value and amplitude are given for the four quantities of interest: $u_x, u_y, F_D, F_L$.

| DoFs | $u_x(A)[\times 10^{-5}m]$ | $u_y(A)[\times 10^{-4}m]$ | $F_D[N]$ | $F_L[N]$ |
|---|---|---|---|---|
| 5445 | 2.3258 | 8.2397 | 14.6331 | 0.74577 |
| 20988 | 2.2808 | 8.1846 | 15.1434 | 0.74025 |
| 82368 | 2.2734 | 8.1751 | 15.3302 | 0.73982 |
| 326304 | 2.2703 | 8.1809 | 15.3776 | 0.74111 |

## 12.3 The FSI benchmark FSI-3 [140]

In the FSI-3 benchmark, we have now

$$\bar{U} = 2.0ms^{-1}$$

and also $\mu_s = 2.0 * 10^6 kgm^{-1}s^{-2}$. We take the results from [244][Section 4] and present them in Figure 66.
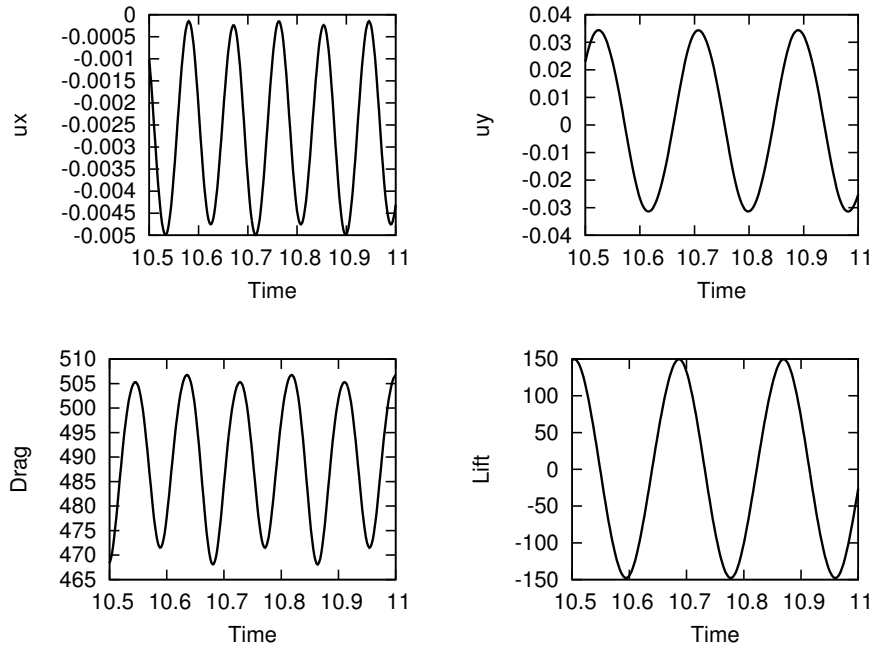


Figure 66: FSI 3. Top: the deflections of the beam, $u_x(A)$ and $u_y(A)$. Bottom: the drag and the lift computations over the path $S$ of the cylinder and the interface between the fluid and the structure. Taken from [244][Section 4].

| Unknowns | $\Delta t$ | $u_1(A)\ [\times 10^{-3}]$ | $u_2(A)\ [\times 10^{-3}]$ | $F_D$ | $F_L$ | $f_1$ | $f_2$ |
|---|---|---|---|---|---|---|---|
| 2b | 7176 | 5.0e-3 | $-2.44 \pm 2.32$ | $1.02 \pm 31.82$ | $473.5 \pm 56.97$ | $8.08 \pm 283.8$ | 11.07 | 5.29 |
|  | 7176 | 2.0e-3 | $-2.48 \pm 2.39$ | $0.92 \pm 32.81$ | $471.3 \pm 62.28$ | $6.11 \pm 298.6$ | 10.73 | 5.35 |
|  | 7176 | 1.0e-3 | $-2.58 \pm 2.49$ | $0.94 \pm 33.19$ | $470.4 \pm 64.02$ | $4.65 \pm 300.3$ | 10.69 | 5.36 |
|  | 27744 | 5.0e-3 | $-2.43 \pm 2.27$ | $1.41 \pm 31.73$ | $483.7 \pm 22.31$ | $2.21 \pm 149.0$ | 10.53 | 5.37 |
|  | 27744 | 2.0e-3 | $-2.63 \pm 2.61$ | $1.46 \pm 33.46$ | $483.3 \pm 24.48$ | $2.08 \pm 161.2$ | 10.66 | 5.43 |
|  | 27744 | 1.0e-3 | $-2.80 \pm 2.64$ | $1.45 \pm 34.12$ | $483.0 \pm 25.67$ | $2.21 \pm 165.3$ | 10.75 | 5.41 |
|  | 42024 | 2.5e-3 | $-2.40 \pm 2.26$ | $1.39 \pm 31.71$ | $448.7 \pm 21.16$ | $1.84 \pm 141.3$ | 10.72 | 5.42 |
|  | 42024 | 1.0e-3 | $-2.53 \pm 2.38$ | $1.40 \pm 32.49$ | $449.7 \pm 22.24$ | $1.61 \pm 142.8$ | 10.77 | 5.44 |
|  | 42024 | 5.0e-4 | $-2.57 \pm 2.42$ | $1.42 \pm 32.81$ | $450.1 \pm 22.49$ | $1.49 \pm 143.7$ | 10.79 | 5.42 |
|  | 72696 | 2.5e-3 | $-2.64 \pm 2.48$ | $1.38 \pm 33.25$ | $451.1 \pm 24.57$ | $2.04 \pm 150.6$ | 10.73 | 5.38 |
|  | 72696 | 1.0e-3 | $-2.79 \pm 2.62$ | $1.28 \pm 34.61$ | $452.0 \pm 25.78$ | $1.91 \pm 152.7$ | 10.78 | 5.42 |
|  | 72696 | 5.0e-4 | $-2.84 \pm 2.67$ | $1.28 \pm 34.61$ | $452.4 \pm 26.19$ | $2.36 \pm 152.7$ | 10.84 | 5.42 |

Figure 67: My FSI 3 results from [55][Method 2b in the last article of the book].

## 12.4 Implementation and software in ANS/deal.II and DOpElib; based on C++

To supplement our algorithmic discussion with some practical aspects, the reader is invited to test him/her-self some concepts presented so far.

### 12.4.1 Code versions

Implementations are present in two software packages deal.II [14] (source code [244] in ANS[27]) and DOpElib [71, 117]:

- ALE-FSI in deal.II (ANS) with biharmonic mesh motion
  http://www.archnumsoft.org/ [244] solving FSI benchmark problems [140]

- Nonstationary Navier-Stokes benchmark problems [214] at
  http://www.dopelib.uni-hamburg.de/ `Examples/PDE/InstatPDE/Example1`

- ALE-FSI benchmark problems [140] with biharmonic mesh motion at
  http://www.dopelib.uni-hamburg.de/ `Examples/PDE/InstatPDE/Example2`

- Biot-Lame-Navier system: augmented Mandel's benchmark at
  http://www.dopelib.uni-hamburg.de/ `Examples/PDE/InstatPDE/Example6`

- Stationary FSI optimization at
  http://www.dopelib.uni-hamburg.de/ `Examples/OPT/StatPDE/Example9`

We notice that the implementation is performed in a *practical* monolithic way that has two assumptions; namely, displacements and velocity are taken from globally-defined Sobolev spaces rather than restricting them to the sub-domains and one (major) limitation (the development of an iterative linear solver and preconditioners might be challanging since we do not distuingish the sub-problems in the system matrix). Putting these two limitations aside, the idea results in a fascinating easy way to implement multiphysics problems in non-overlapping domains.

**Remark 12.1.** *It has been appeared that the basic program structure could be easily generalized and extended to other complex multiphysics problems such as moving boundary problems with chemical reactions as well as pressure-elasticity-phase-field coupling.* ◇

---

[27]ANS = Archive of Numerical Software, http://www.archnumsoft.org/
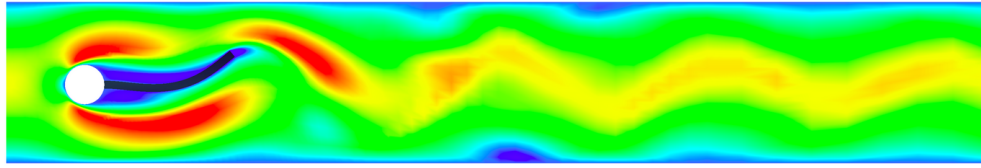
**Solving Monolithic Fluid-Structure Interaction Problems in Arbitrary Lagrangian Eulerian Coordinates with the deal.II Library**

**Thomas Wick**

We describe a setting of a nonlinear fluid-structure interaction problem and the corresponding solution process in the finite element software package deal.II. The fluid equations are transformed via the ALE mapping (Arbitrary Lagrangian Eulerian framework) to a reference configuration and these are coupled with the structure equations by a monolithic solution algorithm. To construct the ALE mapping, we use a biharmonic equation. Finite differences are used for temporal discretization. The derivation is realized in a general manner that serves for different time stepping schemes. Spatial discretization is based on a Galerkin finite element scheme. The nonlinear system is solved by a Newton method. Using this approach, the Jacobian matrix is constructed by exact computation of the directional derivatives. The implementation using the software library package deal.II serves for the computation of different fluid-structure configurations. Specifically, our geometry data are taken from the fluid-structure benchmark configuration that was proposed in 2006 in the DFG project Fluid-Structure Interaction I: Modelling, Simulation, Optimisation. Our results show that this implementation using deal.II is able to produce comparable findings.
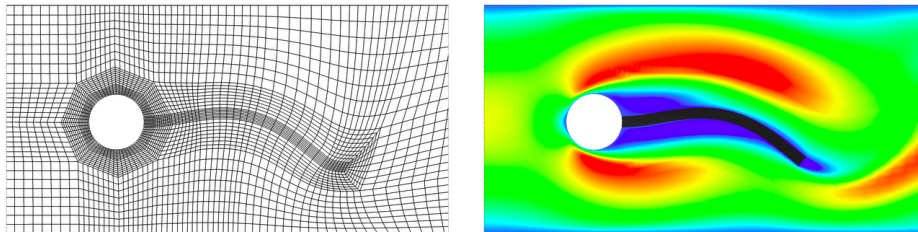


Figure 68: Reference [244] at http://www.archnumsoft.org/

## 12.4.2 Program structure

The structure of such a program for time-dependent nonlinear problems is as follows:

- Input of all data: geometry, material parameters, right hand side values

- Sorting and associating degrees of freedom

- Assembling the Jacobian

- Assembling the right hand side residual

- Newton's method

- Solution of linear equations

- Postprocessing (output, a posteriori error estimation, mesh refinement)

- Main routine including time step loop

### 12.4.3 Visualization with Visit or paraview

Our FSI formulations are computed in the fixed reference domain $\widehat{\Omega}$. Consequently, running the previous code will yield all results in $\widehat{\Omega}$. Here, no elastic beam will move! In order to see the 'moving' beam, we need to transform (recall $\hat{\mathcal{A}}$) from $\widehat{\Omega}$ to $\Omega$.

1. The first possiblity is to add to the solution vector `solution` in deal.II the displacements $\hat{u}$ such that

$$x = \hat{x} + \hat{u}(\hat{x}, t)$$

2. In Visit, we need:
    a) Open the file you want to display, e.g., `solution_fsi_2d_xxxxxx.vtk`
    b) Go to `OpAtts`
    c) `Transform`
    d) `Displace`
    e) Choose `Displacement variable`
    f) Choose the displacements in `Vectors`
    g) Type: `Vector mesh variable`
    h) In the definition, write
       `{x_dis,y_dis}`
    i) `Apply` , then `Dismiss`
    j) Now choose `Displacement variable` using the new expression in `Vectors` . Then `Apply`
    k) Now choose for instance in `Add`, for example `Pseudocolor` then `x_velo` and finally `Draw`

    Online information on the displacement operator can be found on [https://visit-sphinx-github-user-manual.readthedocs.io/en/develop/gui_manual/Operators/OperatorTypes/Displace_operator.html](https://visit-sphinx-github-user-manual.readthedocs.io/en/develop/gui_manual/Operators/OperatorTypes/Displace_operator.html)

3. In paraview, we need the `WarpByVector`. It is a filter (like in visit) that moves the coordinates along a vector (here the displacements).
    a) The user selects the data they wish to operate on from the Selection Window. It will be highlighted when this occurs.
    b) The user can then select `Filter->Alphabetical->Warp (Vector)` from the main menu or click on the Warp Warp Vector Button Button. This will open the Warp (Vector) Filter interface.
    c) The Vectors menu allows the user to select from various vectors (here the displacements) in the data set.
    d) The Scale factor box allows the user to specify the displacement (normal vector times scale factor)
    e) Finally `Apply` to activate the filter and the new output.

    Online information can be found on [https://kitware.github.io/paraview-docs/latest/python/paraview.simple.WarpByVector.html](https://kitware.github.io/paraview-docs/latest/python/paraview.simple.WarpByVector.html)

# 13 Wrap up

## 13.1 Quiz

1. How did we define FSI in this lecture? (Hint: which physical equations are coupled?)

2. What are the underlying physical principles and equations to study FSI?

3. Please write down the equations for conservation of mass and momentum.

4. What is the mathematical characterization of these underlying equations? (Hint: What type of PDEs are we dealing with?)

5. What is one of the typical difficulties of FSI? (Hint: Eulerian and Lagrangian coordinates)

6. Could you name a second challenge of FSI? (Hint: either as we had in the class or your own opinion)

7. What are the key quantities in continuum mechanics?

8. What is the physical interpretation of $\hat{J} > 0$?

9. What does mathematically happen if $\hat{J} \to 0$?

10. Why do we need the Piola transformation?

11. Write down the Green-Lagrange strain tensor $\hat{E}$.

12. Why do we need constitutive laws? Do you have an example for a fluid or a solid?

13. Which law from continuum mechanics yields the symmetry of Cauchy's stress tensor?

14. What is the difference between the 1st and 2nd Piola-Kirchhoff stress tensor?

15. How are incompressible fluids and solids characterized?

16. Write down the isothermal, incompressible Navier-Stokes equations in their natural framework.

17. What does the Reynolds number characterize?

18. How did we proof existence of linearized elasticity? Which assumptions need to be checked therein?

19. Write down the weak formulation of Navier-Stokes in natural coordinates.

20. What is the purpose of the inf-sup condition (on the continuous level) for Navier-Stokes?

21. What are the physical coupling conditions of fluid-structure interaction?

22. What is the difference between monolithic and partitioned coupling and their classification within strongly and loosely-coupled approaches?

23. What are the advantages of monolithic solution algorithms?

24. Define the ALE transformation and the ALE time derivative. (Hint: either in words or in terms of mathematical formulae).

25. Using the ALE approach, which equation needs to be transformed to the reference configuration?

26. Explain variational-monolithic coupling.

27. What is the difference between $\text{ALE}_{fx}$ and $\text{ALE}_{dm}$?

28. What is the 'third' condition using an ALE approach for FSI?

29. What is the purpose of MMPDEs?

30. How can we improve mesh regularity in an ALE approach? How is this realized in practice?

31. How many equations must be finally solved using an ALE-FSI approach?

32. What are the advantages and drawbacks of ALE-FSI?

33. How did we discretize FSI in this lecture?

34. Time-discretize the Navier-Stokes equations with a One-step-$\theta$ scheme.

35. Why do we use a mixed first-order-in-time system for the solid equations?

36. Which numerical stability concept should (must) be used for temporal discretization of fluid-structure interaction?

37. How can we stabilize the Crank-Nicolson scheme? Why is this (sometimes) important?

38. What is the idea of Galerkin FEM?

39. What is the discrete analogon of the inf-sup condition and why is this important?

40. What are the consequences of the discrete inf-sup condition (the BB-condition) for the choice of FEM spaces for spatial discretization of the Navier-Stokes equations?

41. Describe or just state the Taylor-Hood element.

42. What are numerical issues of the solution of Navier-Stokes for high Reynolds numbers?

43. Write down (without any hats) Newtons's defect correction for: Find $U_h \in X_h$ such that

$$A(U_h)(\Phi_h) = F(\Phi_h) \quad \forall \Phi \in X_h$$

44. Apply Newton's method to
$$A(u)(\phi) = F(\phi)$$
with $A(u)(\phi) = (u \cdot \nabla u, \phi)$ and $F(\phi) = (f, \phi)$.

45. How do we determine the block structure of a linear equation system of a coupled PDE system? What is the block structure of the incompressible Stokes equations?

## 13.2 The End

An African proverb says:

**"If you want to go fast, you go alone, but if you want to go far, you go together."**

And in fluid-structure interaction, it holds the same:

We have to go together!

**The reason being for 'the pleasure of finding things out' [28] together !**

---

[28]Richard P. Feynman (Nobel Prize 1965), Helix Books, 288 pages, 2005.

# References

[1] R. A. Adams. *Sobolev Spaces.* Academic Press, 1975.

[2] M. Ainsworth and J. T. Oden. A posteriori error estimation in finite element analysis. *Computer Methods in Applied Mechanics and Engineering*, 142(1-2):1–88, 1997.

[3] J. E. Akin, T. Tezduyar, and M. Ungor. Computation of flow problems with the mixed interface-tracking/interface-capturing technique (MITICT). *Comp. Fluids*, 36:2–11, 2007.

[4] G. Allaire. *Analyse numerique et optimisation.* Editions de l'Ecole Polytechnique, 2005.

[5] M. Allen and K. Maute. Reliability-based shape optimization of structures undergoing fluid-structure interaction phenomena. *Comput. Methods Appl. Mech. Engrg.*, 194(30-33):3472–3495, 2005.

[6] M. Asterino, F. Chouly, and F. Fernández. An added-mass free semi-implicit coupling scheme for fluid-structure interaction. *C. R. Acad. Sci. Paris, Sér. I.*, 347(1-2):99–104, 2009.

[7] M. Asterino and C. Grandmont. Convergence analysis of a projection semi-implicit coupling scheme for fluid-structure interaction problems. *Numer. Math.*, 116(4):721–767, 2008.

[8] G. Avalos, I. Lasiecka, and R. Triggiani. Beyond lack of compactness and lack of stability of a coupled parabolic-hyperbolic fluid-structure system. In K. Kunisch, J. Sprekels, G. Leugering, and F. Tröltzsch, editors, *Optimal Control of Coupled Systems of Partial Differential Equations*, volume 158 of *International Series of Numerical Mathematics*, pages 1–33. Birkhäuser Basel, 2009.

[9] F. Baaijens. A fictitious domain/mortar element method for fluid-structure interaction. *Int. J. Num. Methods Fluids*, 35(7):743–761, 2001.

[10] S. Badia, F. Nobile, and C. Vergara. Fluid-structure partitioned procedures based on Robin transmission conditions. *J. Comp. Phys.*, 227:7027–7051, 2008.

[11] S. Badia, F. Nobile, and C. Vergara. Robin-robin preconditioned krylov methods for fluid-structure interaction problems. *Computer Methods in Applied Mechanics and Engineering*, 198(33-36):2768 – 2784, 2009.

[12] S. Badia, Q. Quaini, and A. Quarteroni. Modular vs. non-modular preconditioners for fluid-structure interaction systems with large added-mass effect. *Comput. Methods. Appl. Mech. Engrg.*, 197:4216–4232, 2008.

[13] W. Bangerth, M. Geiger, and R. Rannacher. Adaptive Galerkin finite element methods for the wave equation. *Comput. Methods Appl. Math.*, 10:3–48, 2010.

[14] W. Bangerth, T. Heister, and G. Kanschat. *Differential Equations Analysis Library*, 2012.

[15] W. Bangerth and R. Rannacher. *Adaptive Finite Element Methods for Differential Equations.* Birkhäuser, Lectures in Mathematics, ETH Zürich, 2003.

[16] A. Barker and X. Cai. Two-level newton and hybrid schwarz preconditioners for fluid-structure interaction. *SIAM Journal on Scientific Computing*, 32(4):2395–2417, 2010.

[17] A. T. Barker and X.-C. Cai. Scalable parallel methods for monolithic coupling in fluid-structure interaction with application to blood flow modeling. *Journal of Computational Physics*, 229(3):642 – 659, 2010.

[18] S. Basting and M. Weissmann. A hybrid level set-front tracking finite element approach for fluid-structure interaction and two-phase flow applications. *J. Comp. Physics*, 255:228–244, 2013.

[19] Y. Bazilevs, V. M. Calo, T. Hughes, and Y. Zhang. Isogeometric fluid-structure interaction: theory, algorithms, and computations. *Comput. Mech.*, 43:3–37, 2008.

[20] Y. Bazilevs and K. Takizawa. *Advances in Computational Fluid-Structure Interaction and Flow Simulation*. Birkhäuser Basel, 2016.

[21] Y. Bazilevs, K. Takizawa, and T. Tezduyar. *Computational Fluid-Structure Interaction: Methods and Applications*. Wiley, 2013.

[22] Y. Bazilevs, K. Takizawa, and T. Tezduyar. *Computational Fluid-Structure Interaction: Methods and Applications*. Wiley, 2013.

[23] R. Becker. Mesh adaptation for stationary flow control. *J. Math. Fluid Mech.*, 3(4):317–341, 2001.

[24] R. Becker. Adaptive finite elements for optimal control problems. University of Heidelberg, 2004. Habilitationsschrift.

[25] R. Becker and M. Braack. A modification of the least-squares stabilization for the stokes equations. *Calcolo*, 38(4):173–199, 2001.

[26] R. Becker, M. Braack, D. Meidner, T. Richter, and B. Vexler. The finite element toolkit GASCOIGNE. HTTP://WWW.GASCOIGNE.UNI-HD.DE.

[27] R. Becker, V. Heuveline, and R. Rannacher. An optimal control approach to adaptivity in computational fluid mechanics. *IJNMF*, 40:105–120, 2002.

[28] R. Becker, D. Meidner, and B. Vexler. Efficient numerical solution of parabolic optimization problems by finite element methods. *Optim. Methods Softw.*, 22(5):813–833, 2007.

[29] R. Becker and R. Rannacher. A feed-back approach to error control in finite element methods: basic analysis and examples. *East-West J. Numer. Math.*, 4:237–264, 1996.

[30] R. Becker and R. Rannacher. An optimal control approach to a posteriori error estimation in finite element methods. *Acta Numerica, Cambridge University Press*, pages 1–102, 2001.

[31] T. Belytschko, J. Kennedy, and D. Schoeberle. Quasi-eulerian finite element formulation for fluid-structure interaction. Proceedings of Joint ASME/CSME Pressure Vessels and Piping Conference, page p.13. ASME paper 78-PVP-60, 1978.

[32] J. Berenger. A perfectly matched layer for the absorption of electromagnetic waves. *J. Comput. Phys.*, 114, 1994.

[33] C. Bernardi and E. Süli. Time and space adaptivity for the second-order wave equation. *Math. Models Methods Appl. Sci.*, 15(2):199–225, 2005.

[34] C. Bertoglio, P. Moireau, and J.-F. Gerbeau. Sequential parameter estimation for fluid-structure problems: Application to hemodynamics. *International Journal for Numerical Methods in Biomedical Engineering*, 28(4):434–455, 2012.

[35] M. Besier. *Adaptive Finite Element methods for computing nonstationary incompressible Flows*. PhD thesis, University of Heidelberg, 2009.

[36] M. Besier and R. Rannacher. Goal-oriented space-time adaptivity in the finite element galerkin method for the computation of nonstationary incompressible flow. *Int. J. Num. Meth. Fluids*, 70:1139–1166, 2012.

[37] M. Biot. Consolidation settlement under a rectangular load distribution. *J. Appl. Phys.*, 12(5):426–430, 1941.

[38] M. Biot. General theory of three-dimensional consolidation. *J. Appl. Phys.*, 12(2):155–164, 1941.

[39] M. Biot. Theory of elasticity and consolidation for a porous anisotropic solid. *J. Appl. Phys.*, 25:182–185, 1955.

[40] T. Bodnár, G. Galdi, and Š. Nečasová. *Fluid-Structure Interaction and Biomedical Applications*. Advances in Mathematical Fluid Mechanics. Springer Basel, 2014.

[41] J. Bonet and R. Wood. *Nonlinar Continuum Mechanics for Finite Element Analysis*. Cambridge University Press, Cambridge, 1997.

[42] M. Braack, E. Burman, V. John, and G. Lube. Stabilized finite element methods for the generalized Oseen equations. *Comput. Methods Appl. Mech. Engrg.*, 196(4-6):853–866, 2007.

[43] M. Braack and A. Ern. Adaptive computation of reactive flows with local mesh refinement and model adaptation. In e. a. M. Feistauer, editor, *Numerical Mathematics and Advanced Applications, ENUMATH 2003*, pages 159–168. Springer, 2004.

[44] M. Braack and A. Ern. Coupling multimodeling with local mesh refinement for the numerical solution of laminar flames. *CTM*, 8(4):771–788, 2004.

[45] M. Braack and P. Mucha. Directional do-nothing condition for the navier-stokes equations. *J. Comp. Math.*, 32:507–546, 2014.

[46] D. Braess. *Finite Elemente*. Springer-Verlag Berlin Heidelberg, Berlin, Heidelberg, vierte, überarbeitete und erweiterte edition, 2007.

[47] S. C. Brenner and L. R. Scott. *The mathematical theory of finite element methods*. Number 15 in Texts in applied mathematics ; 15 ; Texts in applied mathematics. Springer, New York, NY, 3. ed. edition, 2008.

[48] H. Brezis. *Analyse Fonctionnelle, Theorie et Applications*. Masson Paris, 1983.

[49] M. Bristeau, R. Glowinski, and J. Periaux. Numerical methods for the Navier-Stokes equations. *Comput. Phys. Rep.*, 6:73–187, 1987.

[50] A. Brooks and T. Hughes. Streamline upwind/Petrov-Galerkin formulations for convection dominated flows with particular emphasis on the incompressible Navier-Stokes equations. *Comput. Methods Appl. Mech. Engrg.*, 32(1-3):199–259, 1982.

[51] F. Bucci and I. Lasiecka. Optimal boundary control with critical penalization for a pde model of fluid-solid interactions. *Calc. Var. Partial Differential Equations*, 37(1-2):217–235, 2010.

[52] C. J. Budd, W. Huang, and R. D. Russell. Adaptivity with moving grids. *Acta Numerica*, 18:111–241, 5 2009.

[53] M. Bukac, S. Canic, R. Glowinski, B. Muha, and A. Quaini. A modular, operator-splitting scheme for fluid-structure interaction problems with thick structures. *International Journal for Numerical Methods in Fluids*, 74(8):577–604, 2014.

[54] M. Bukac, S. Canic, R. Glowinski, J. Tambaca, and A. Quaini. Fluid-structure interaction in blood flow capturing non-zero longitudinal structure displacement. *J. Comput. Phys.*, 2012. http://dx.doi.org/10.1016/j.jcp.2012.08.033.

[55] H.-J. Bungartz, M. Mehl, and M. Schäfer. *Fluid-Structure Interaction II: Modelling, Simulation, Optimization*. Lecture Notes in Computational Science and Engineering. Springer, 2010.

[56] H.-J. Bungartz and M. Schäfer. *Fluid-Structure Interaction: Modelling, Simulation, Optimization*, volume 53 of *Lecture Notes in Computational Science and Engineering*. Springer, 2006.

[57] E. Burman and M. Fernandez. Stabilization of explicit coupling in fluid-structure interaction involving fluid incompressibility. *Comput. Methods. Appl. Mech. Engrg.*, 198:766–784, 2009.

[58] G. F. Carey and J. T. Oden. *Finite Elements. Volume III. Compuational Aspects*. The Texas Finite Element Series, Prentice-Hall, Inc., Englewood Cliffs, 1984.

[59] P. Causin, J.-F. Gerbeau, and F. Nobile. Added-mass effect in the design of partitioned algorithms for fluid-structure problems. *Comput. Methods Appl. Mech. Engrg.*, 194:4506–4527, 2005.

[60] P. G. Ciarlet. *Lectures on Three Dimensional Elasticity.* Springer Berlin Heidelberg New York, 1983.

[61] P. G. Ciarlet. *Mathematical Elasticity. Volume 1: Three Dimensional Elasticity.* North-Holland, 1984.

[62] P. G. Ciarlet. *The finite element method for elliptic problems.* North-Holland, Amsterdam [u.a.], 2. pr. edition, 1987.

[63] R. Codina, G. Houzeaux, H. Coppola-Owen, and J. Baiges. The fixed-mesh {ALE} approach for the numerical approximation of flows in moving domains. *Journal of Computational Physics*, 228(5):1591 – 1611, 2009.

[64] D. Coutand and S. Shkoller. Motion of an elastic solid inside an incompressible viscous fluid. *Arch. Rational Mech. Anal.*, pages 25–102, 2005.

[65] D. Coutand and S. Shkoller. The interaction between quasilinear elastodynamics and the Navier-Stokes equations. *Arch. Rational Mech. Anal.*, 179:303–352, 2006.

[66] P. Crosetto, S. Deparis, G. Fourestey, and A. Quarteroni. Parallel algorithms for fluid-structure interaction problems in haemodynamics. *SIAM J. Sci. Comp.*, 33(4):1598–1622, 2011.

[67] R. Dautray and J.-L. Lions. *Mathematical Analysis and Numerical Methods for Science and Technology*, volume 5. Springer-Verlag, Berlin-Heidelberg, 2000.

[68] S. Deparis, M. Discacciati, G. Fourestey, and A. Quarteroni. Fluid-structure algorithms based on Steklov-Poincaré operators. *Comp. Methods Appl. Mech. Engrg*, 195(41-43):5797–5812, 2006.

[69] P. Deuflhard. *Newton Methods for Nonlinear Problems*, volume 35 of *Springer Series in Computational Mathematics*. Springer Berlin Heidelberg, 2011.

[70] J. Donea, S. Giuliani, and J. Halleux. An arbitrary lagrangian-eulerian finite element method for transient dynamic fluid-structure interactions. *Comput. Methods Appl. Mech. Engrg.*, 33:689–723, 1982.

[71] The Differential Equation and Optimization Environment: DOpELib. http://www.dopelib.net.

[72] T. Dunne. An Eulerian approach to fluid-structure interaction and goal-oriented mesh adaption. *Int. J. Numer. Methods in Fluids*, 51:1017–1039, 2006.

[73] T. Dunne. *Adaptive Finite Element Approximation of Fluid-Structure Interaction Based on Eulerian and Arbitrary Lagrangian-Eulerian Variational Formulations.* PhD thesis, University of Heidelberg, 2007.

[74] T. Dunne, T. Richter, and R. Rannacher. *Numerical simulation of fluid-structure interaction based on monolithic variational formulations*, pages 1–75. Comtemporary Challenges in Mathematical Fluid Mechanics. Springer, World Scientific, Singapore, 2010.

[75] A. S. Dvinsky. Adaptive grid generation from harmonic maps on riemannian manifolds. *Journal of Computational Physics*, 95(2):450 – 476, 1991.

[76] K. Eriksson, D. Estep, P. Hansbo, and C. Johnson. Introduction to adaptive methods for differential equations. In A. Iserles, editor, *Acta Numerica 1995*, pages 105–158. Cambridge University Press., 1995.

[77] L. C. Evans. *Partial differential equations.* American Mathematical Society, 2000.

[78] L. Failer and T. Richter. A parallel newton multigrid framework for monolithic fluid-structure interactions. accepted in Journal of Scientific Computing, 2019.

[79] C. Farhat, P. Geuzaine, and C. Grandmont. The discrete geometrical conservation law and the nonlinear stability of the ALE schemes for the solution of flow problems on moving grids. *J. Comp. Phys.*, 174:669–694, 2001.

[80] C. Fefferman. Existence and smoothness of the Navier-Stokes equations. Millenium Prize, -.

[81] M. Feistauer, J. Hasnedlová-Prokopová, J. Horacek, A. Kosik, and V. Kucera. {DGFEM} for dynamical systems describing interaction of compressible fluid and structures. *Journal of Computational and Applied Mathematics*, 254(0):17 – 30, 2013. Nonlinear Elliptic Differential Equations, Bifurcation, Local Dynamics of Parabolic Systems and Numerical Methods.

[82] Z. Feng and E. Michaelides. The immersed boundary-lattice Boltzmann method for solving fluid-particles interaction problems. *J. Comp. Phys.*, 195:602–628, 2004.

[83] F. Fernández and M. Moubachir. A Newton method using exact Jacobians for solving fluid-structure coupling. *Comput. Struct.*, 83:127–142, 2005.

[84] M. Fernández and J.-F. Gerbeau. *Algorithms for fluid-structure interaction problems*, pages 307–346. Volume 1 of Formaggia et al. [94], 2009.

[85] M. Fernandez, J.-F. Gerbeau, and C. Grandmont. A projection semi-implicit scheme for the coupling of an elastic structure with an incompressible fluid. *Int. J. Numer. Meth. Engng.*, 69:794–821, 2007.

[86] M. A. Fernandez and J. Mullaert. Displacement-velocity correction schemes for incompressible fluid-structure interaction. *Comptes Rendus Mathematique*, 349(17):1011 – 1015, 2011.

[87] M. FernÃ¡ndez. Coupling schemes for incompressible fluid-structure interaction: implicit, semi-implicit and explicit. *SeMA Journal*, 55(1):59–108, 2011.

[88] P. Fick, E. Brummelen, and K. Zee. On the adjoint-consistent formulation of interface conditions in goal-oriented error estimation and adaptivity for fluid-structure interaction. *Computer Methods in Applied Mechanics and Engineering*, 199:3369–3385, 2010.

[89] J. E. Flaherty. Course notes: Finite element analysis. Lecture notes, CSCI-6860 / MATH-6860.

[90] L. Formaggia, J.-F. Gerbeau, F. Nobile, and A. Quarteroni. On the coupling of 3d and 1d Navier-Stokes equations for flow problems in compliant vessels. *Comp. Methods Appl. Mech. Engig*, 191:561–582, 2001.

[91] L. Formaggia and F. Nobile. A stability analysis for the arbitrary Lagrangian Eulerian formulation with finite elements. *East-West Journal of Numerical Mathematics*, 7:105 – 132, 1999.

[92] L. Formaggia and F. Nobile. Stability analysis of second-order time accurate schemes for ALE-FEM. *Comp. Methods Appl. Mech. Engrg.*, 193(39-41):4097 – 4116, 2004.

[93] L. Formaggia, F. Nobile, A. Quarteroni, and A. Veneziani. Multiscale modelling of the circulatory system: a primilinary analysis. *Comp. Vis. Science*, 2:75–83, 75-83.

[94] L. Formaggia, A. Quarteroni, and A. Veneziani. *Cardiovascular Mathematics: Modeling and simulation of the circulatory system*. Springer-Verlag, Italia, Milano, 2009.

[95] L. Formaggia and A. Veneziani. Reduced and multiscale models for the human cardiovascular system. Technical Report 21, Lecture notes VKI Lectur Series, 2003.

[96] L. Formaggia, A. Veneziani, and C. Vergara. Flow rate boundary problems for an incompressible fluid in deformable domains: formulations and solution methods. *Comp. Methods Appl. Mech. Engrg.*, 199:677–688, 2010.

[97] R. Franck and R. Lazarus. *Mixed Eulerian-Lagrangian method*, volume In Methods in Computational Physics, pages 47–67. Academic Press: New York, 1964.

[98] S. Frei, B. Holm, T. Richter, T. Wick, and H. Yang. *Fluid-structure interactions: Fluid-Structure Interaction: Modeling, Adaptive Discretisations and Solvers*. de Gruyter, 2017.

[99] S. Frei and T. Richter. A locally modified parametric finite element method for interface problems. *SIAM Journal on Numerical Analysis*, 52(5):2315–2334, 2014.

[100] T.-P. Fries and T. Belytschko. The extended/generalized finite element method: An overview of the method and its applications. *Int. J. Numer. Meth. Engrg.*, 84:253–304, 2010.

[101] Y. Fung. *Biodynamics: Circulation.* Springer-Verlag, first ed. edition, 1984.

[102] C. FÃ¶rster, W. A. Wall, and E. Ramm. Artificial added mass instabilities in sequential staggered coupling of nonlinear structures and incompressible viscous flows. *Computer Methods in Applied Mechanics and Engineering*, 196(7):1278 – 1293, 2007.

[103] G. Galdi and R. Rannacher. *Fundamental Trends in Fluid-Structure Interaction.* World Scientific, 2010.

[104] E. S. Gawlik and A. J. Lew. High-order finite element methods for moving boundary problems with prescribed boundary evolution. *Computer Methods in Applied Mechanics and Engineering*, 278(0):314 – 346, 2014.

[105] F. Gazzola and M. Squassina. Global solutions and finite time blow up for damped semilinear wave equations. *Ann. I. H. Poincaré*, 23:185–207, 2006.

[106] M. Gee, U. Küttler, and W. Wall. Truly monolithic algebraic multigrid for fluid–structure interaction. *International Journal for Numerical Methods in Engineering*, 85(8):987–1016, 2011.

[107] T. Gerasimov, A. Stylianou, and G. Sweers. Corners give problems when decoupling fourth order equations into second order systems. *SIAM Journal on Numerical Analysis*, 50(3):1604–1623, 2012.

[108] J.-F. Gerbeau. Direct and inverse modeling in hemodynamics. Talk at the ENUMATH Conference in Leicester, 2011.

[109] A. Gerstenberger and W. A. Wall. An extended finite element method/lagrange multiplier based approach for fluid-structure interaction. *Computer Methods in Applied Mechanics and Engineering*, 197(19-20):1699–1714, 2008.

[110] A. J. Gil, A. A. Carreno, J. Bonet, and O. Hassan. The immersed structural potential method for haemodynamic applications. *J. Comp. Physics*, 229:8613–8641, 2010.

[111] M. Giles and E. Süli. Adjoint methods for pdes: a posteriori error analysis and postprocessing by duality. *Acta Numerica 2002*, pages 145–236, 2002. A. Iserles, ed.

[112] V. Girault and P.-A. Raviart. *Finite Element method for the Navier-Stokes equations.* Number 5 in Computer Series in Computational Mathematics. Springer-Verlag, 1986.

[113] R. Glowinski, T. Pan, T. Hesla, D. Joseph, and J. PÃ©riaux. A fictitious domain approach to the direct numerical simulation of incompressible viscous flow past moving rigid bodies: Application to particulate flow. *Journal of Computational Physics*, 169(2):363 – 426, 2001.

[114] R. Glowinski, T.-W. Pan, T. Hesla, and D. Joseph. A distributed lagrange multiplier/fictitious domain method for particulate flows. *International Journal of Multiphase Flow*, 25(5):755 – 794, 1999.

[115] R. Glowinski, T.-W. Pan, and J. Periaux. A fictitious domain method for dirichlet problem and applications. *Computer Methods in Applied Mechanics and Engineering*, 111(3-4):283 – 303, 1994.

[116] R. Glowinski and J. Periaux. Numerical methods for nonlinear problems in fluid dynamics. In *Proc. Intern. Seminar on Scientific Supercomputers.* North Holland, Feb. 2-6 1987.

[117] C. Goll, T. Wick, and W. Wollner. DOpElib: Differential equations and optimization environment; A goal oriented software library for solving pdes and optimization problems with pdes. *Archive of Numerical Software*, 5(2):1–14, 2017.

[118] C. Grandmont. Existence for a three-dimensional steady state fluid-structure interaction problem. *Journal of Mathematical Fluid Mechanics*, 4:76–94, 2002.

[119] T. Grätsch and K.-J. Bathe. Goal-oriented error estimation in the analysis of fluid flows with structural interactions. *Comp. Methods Appl. Mech. Engrg.*, 195:5673–5684, 2006.

[120] P. Grisvard. *Elliptic Problems in Nonsmooth Domains*, volume 24. Pitman Advanced Publishing Program, Boston, 1985.

[121] C. Groß mann and H.-G. Roos. *Numerische Behandlung partieller Differentialgleichungen*. Teubner-Studienbücher Mathematik ; Lehrbuch Mathematik. Teubner, Wiesbaden, 3., völlig überarb. und erw. aufl. edition, 2005.

[122] P. Hansbo and J. Hermansson. Nitsche's method for coupling non-matching meshes in fluid-structure vibration problems. *Comp. Mech.*, 32:134–139, 2003.

[123] P. Hansbo, J. Hermansson, and T. Svedberg. Nitsche's method combined with space-time finite elements for ALE fluid-structure interaction problems. *Comput. Meth. Appl. Mech. Engrg.*, 193:4195–4206, 2004.

[124] J. D. Hart, F. Baaijens, G. Peters, and P. Schreuers. A computational fluid-structure interaction analysis of a fiber-reinforced stentless aortic valve. *Journal of Biomechanics*, 36(5):699–712, 2003.

[125] J. Hasnedlová, M. Feistauer, J. Horacek, A. Kosik, and V. Kucera. Numerical simulation of fluid-structure interaction of compressible flow and elastic structure. *Computing*, 95(1):343–361, 2013.

[126] M. Heil. An efficient solver for the fully coupled solution of large-displacement fluid-structure interaction problems. *Comput. Methods Appl. Mech. Engrg.*, 193:1–23, 2004.

[127] M. Heil, A. L. Hazel, and J. Boyle. Solvers for large-displacement fluid-structure interaction problems: segregated versus monolithic approaches. *Comput. Mech.*, 43:91–101, 2008.

[128] B. Helenbrook. Mesh deformation using the biharmonic operator. *Int. J. Numer. Methods Engrg.*, pages 1–30, 2001.

[129] L. Heltai and F. Costanzo. Variational implementation of immersed finite element methods. *Computer Methods in Applied Mechanics and Engineering*, 229-232(0):110 – 127, 2012.

[130] C. Hesch, A. Gil, A. A. Carreno, J. Bonet, and P. Betsch. A mortar approach for fluid-structure interaction problems: Immersed strategies for deformable and rigid bodies. *Computer Methods in Applied Mechanics and Engineering*, 278(0):853 – 882, 2014.

[131] J. G. Heywood and R. Rannacher. Finite-element approximation of the nonstationary Navier-Stokes problem part iv: Error analysis for second-order time discretization. *SIAM Journal on Numerical Analysis*, 27(2):353–384, 1990.

[132] J. G. Heywood, R. Rannacher, and S. Turek. Artificial boundaries and flux and pressure conditions for the incompressible Navier-Stokes equations. *International Journal of Numerical Methods in Fluids*, 22:325–352, 1996.

[133] M. Hinze and K. Kunisch. Second order methods for optimal control of time-dependent fluid flows. *SIAM J. Control Optim.*, 40:925–946, 2001.

[134] M. Hinze, R. Pinnau, M. Ulbrich, and S. Ulbrich. *Optimization with PDE constraints*. Number 23 in Mathematical modelling: theory and applications. Springer, Dordrecht u.a., 2009.

[135] C. Hirt, A. Amsden, and J. Cook. An arbitrary Lagrangian-Eulerian computing method for all flow speeds. *J. Comput. Phys.*, 14:227–253, 1974.

[136] J. HOFFMAN, J. JANSSON, and M. STöCKLI. Unified continuum modeling of fluid-structure interaction. *Mathematical Models and Methods in Applied Sciences*, 21(03):491–513, 2011.

[137] G. Holzapfel. *Nonlinear Solid Mechanics: A continuum approach for engineering.* John Wiley and Sons, LTD, 2000.

[138] J. Hron. *Fluid structure interaction with applications in biomechanics*. PhD thesis, Charles University Prague, 2001.

[139] J. Hron and S. Turek. *A monolithic FEM/Multigrid solver for ALE formulation of fluid structure with application in biomechanics*, volume 53, pages 146–170. Springer-Verlag, 2006.

[140] J. Hron and S. Turek. *Proposal for numerical benchmarking of fluid-structure interaction between an elastic object and laminar incompressible flow*, volume 53, pages 146 – 170. Springer-Verlag, 2006.

[141] T. Hughes. *The finite element method*. Dover Publications, 2000.

[142] T. Hughes, J. Cottrell, and Y. Bazilevs. Isogeometric analysis: Cad, finite elements, nurbs, exact geometry and mesh refinement. *Computer Methods in Applied Mechanics and Engineering*, 194(39-41):4135 – 4195, 2005.

[143] T. Hughes, L. Franca, and M. Balestra. A new finite element formulation for computational fluid dynamics. v. circumventing the babuska-brezzi condition: a stable petrov-galerkin formulation of the stokes problem accommodating equal-order interpolation. *Comput. Methods Appl. Mech. Engrg.*, 59:85–99, 1986.

[144] T. Hughes, W. Liu, and T. Zimmermann. Lagrangian-Eulerian finite element formulation for incompressible viscous flows. *Comput. Methods Appl. Mech. Engrg.*, 29:329–349, 1981.

[145] J. Humphrey. *Cardiovascular Solid Mechanics: Cells, Tissues, and Organs*. Springer-Verlag New York, 2002.

[146] M. Ignatova, I. Kukavica, I. Lasiecka, and A. Tuffaha. On well-posedness and small data global existence for an interface damped free boundary fluid-structure model. *Nonlinearity*, 27(3):467, 2014.

[147] J. Janela, A. Moura, and A. Sequeira. Absorbing boundary conditions for a 3d non-Newtonian fluid-structure interaction model for blood flow in arteries. *Int. J. Engrg. Sci.*, 2010.

[148] B. Janssen. Vergleich verschiedener finite-elemente-approximationen zur numerischen lösung der plattengleichung. Master's thesis, Heidelberg University, April 2007.

[149] J. Jansson, J. Spuhler, C. Degirmenci, and J. Hoffman. Automated error control in finite element methods with applications in fluid flow. Technical Report at KTH, 2014.

[150] D. Jodlbauer, U. Langer, and T. Wick. Parallel block-preconditioned monolithic solvers for fluid-structure interaction problems. *International Journal for Numerical Methods in Engineering*, 117(6):623–643, 2019.

[151] D. Jodlbauer and T. Wick. A monolithic fsi solver applied to the fsi 1,2,3 benchmarks. In S. Frei, B. Holm, T. Richter, T. Wick, and H. Yang, editors, *Fluid-Structure Interaction: Modeling, Adaptive Discretization and Solvers*, Radon Series on Computational and Applied Mathematics. Walter de Gruyter, Berlin, 2017.

[152] C. Johnson. *Numerical solution of partial differential equations by the finite element method*. Cambridge University Press, Campridge, 1987.

[153] K. Koenigsberger. *Analysis 2*. Springer Lehrbuch. Springer, Berlin – Heidelberg – New York, 5. auflage edition, 2004.

[154] K. Königsberger. *Analysis 2*. Springer Lehrbuch. Springer, Berlin – Heidelberg – New York, 2., korrigierte und erw. auflage edition, 1997.

[155] P. Kuberry and H. Lee. A decoupling algorithm for fluid-structure interaction problems based on optimization. *Computer Methods in Applied Mechanics and Engineering*, 267(0):594 – 605, 2013.

[156] U. Küttler and W. A. Wall. *The dilemma of domain decomposition approaches in fluid-structure interactions with fully enclosed incompressible fluids*, volume 60 of *Domain decomposition methods in science and engineering XVII*, pages 575–582. Springer, Berlin, 2008.

[157] D. Kuzmin. Explicit and implicit fem-fct algorithms with flux linearization. *Journal of Computational Physics*, 228(7):2517 – 2534, 2009.

[158] U. Kättler and W. Wall. Fixed-point fluid-structure interaction solvers with dynamic relaxation. *Computational Mechanics*, 43(1):61–72, 2008.

[159] A. Ladd. Numerical simulations of particulate suspensions via a discretized Boltzmann equation. part i: theoretical foundations. *Journal of Fluid Mechanics*, 271, 1994.

[160] A. Ladd. Numerical simulations of particulate suspensions via a discretized Boltzmann equation. part ii: numerical results. *Journal of Fluid Mechanics*, 271, 1994.

[161] O. Ladyzhenskaya. *The mathematical theory of viscous incompressible flows.* Gordon and Breach, New York, 1969.

[162] U. Langer and H. Yang. Partitioned solution algorithms for fluid-structure interaction problems with hyperelastic models. *Journal of Computational and Applied Mathematics*, 276(0):47 – 61, 2015.

[163] A. Legay, J. Chessa, and T. Belytschko. An eulerian-lagrangian method for fluid-structure interaction based on level sets. *Computer Methods in Applied Mechanics and Engineering*, 195(17-18):2070 – 2087, 2006. Fluid-Structure Interaction.

[164] J.-L. Lions. *Optimal Control of Systems Governed by Partial Differential Equations*, volume 170 of *Grundlehren Math. Wiss.* Springer, Berlin, 1971.

[165] M. Lukacova-Medvidova, G. Rusnakova, and A. Hundertmark-Zauskova. Kinematic splitting algorithm for fluid-structure interaction in hemodynamics. *Computer Methods in Applied Mechanics and Engineering*, 265(0):83 – 106, 2013.

[166] E. Lund, H. Moller, and L. A. Jakobsen. Shape design optimization of stationary fluid-structure interaction problems with large displacements and turbulence. *Struct. Multidisc. Optim.*, 25:383–392, 2003.

[167] M. Luskin and R. Rannacher. On the soothing property of the Crank-Nicolson scheme. *Applicable Analysis*, 14(2):117 – 135, 1982.

[168] D. Meidner. *Adaptive Space-Time Finite Element Methods for Optimization Problems Governed by Nonlinear Parabolic Systems.* PhD thesis, University of Heidelberg, 2008.

[169] G. Mengalda, P. Tricerri, P. Crosetto, S. Deparis, F. Nobile, and L. Formaggia. A comparitive study of different nonlinear hyperelastic isotropic arterial wall models in patient-specific vascular flow simulations in the aortic arch. Technical Report 15, MOX Institute, Milano, 2012.

[170] A. Mikelić and M. F. Wheeler. Convergence of iterative coupling for coupled flow and geomechanics. *Comput Geosci*, 17(3):455–462, 2012.

[171] A. Mikelić and M. F. Wheeler. On the interface law between a deformable porous medium containing a viscous fluid and an elastic body. *M3AS*, 22(11):32, 2012.

[172] J. Mizerski. Modeling heart valve dynamics. Personal Correspondance, 2010.

[173] M. E. Moghadam, Y. Bazilevs, T.-Y. Hsia, I. E. Vignon-Clementel, and A. L. Marsden. A comparison of outlet boundary treatments for prevention of backflow divergence with relevance to blood flow simulations. *Comput. Mech.*, 48:277–291, 2011.

[174] M. Mooney. A theory of large elastic deformation. *Journal of applied Physics*, 11:582–592, 1940.

[175] A. Moura. *The Geometrical Multiscale Modelling of the Cardiovascular System: Coupling 3D FSI and 1D Models.* PhD thesis, Instituto Superior Técnico, Technical University of Lisbon, 2007.

[176] F. Nobile. *Numerical Approximation of Fluid-Structure Interaction Problems with Applications to Haemodynamics.* PhD thesis, École Polytechnique Fédérale de Lausanne, 2001.

[177] F. Nobile and C. Vergara. An effective fluid-structure interaction formulation for vascular dynamics by generalized Robin conditions. *SIAM J. Sci. Comput.*, 30(2):731–763, 2008.

[178] J. Nocedal and S. J. Wright. *Numerical Optimization.* Springer, New York, 1999.

[179] J. Nocedal and S. J. Wright. *Numerical optimization.* Springer Ser. Oper. Res. Financial Engrg., 2006.

[180] W. Noh. *A time-dependent two-space-dimensional coupled Eulerian-Lagrangian code*, volume 3 of *Methods Comput. Phys.*, pages 117–179. Academic Press, New York, 1964.

[181] E. Onate, S. Idelsohn, F. Delpin, and R. Aubry. The particle finite element method, an overview. *Int. J. Comput. Methods*, pages 1–43, 2004.

[182] J. Peraire and A. Patera. Bounds for linear-functional outputs of coercive partial differential equations: local indicators and adaptive refinement. In P. Ladeveze and J. Oden, editors, *Advances in Adaptive Computational Methods in Mechanics*, pages 199–215. Elsevier, Amsterdam, 1998.

[183] M. Perego, A. Veneziani, and C. Vergara. A variational approach for estimating the compliance of the cardiovascular tissue: An inverse fluid-structure interaction problem. *SIAM Journal on Scientific Computing*, 33(3):1181–1211, 2011.

[184] C. Peskin. *The immersed boundary method*, pages 1–39. Acta Numerica 2002, Cambridge University Press, 2002.

[185] S. Piperno and C. Farhat. Paritioned procedures for the transient solution of coupled aeroelastic problems - part ii: energy transfer analysis and three-dimensional applications. *Comput. Methods Appl. Mech. Engrg.*, 190:3147–3170, 2001.

[186] A. Quaini, S. Canic, R. Glowinski, S. Igo, C.J.Hartley, W. Zoghbi, and S. Little. Validation of a 3d comoputational fluid-structure interaction model simulating flow through elastic aperature. *Journal of Biomechanics*, 45:310–318, 2012.

[187] A. Quarteroni. What mathematics can do for the simulation of blood circulation. Technical report, MOX Institute, Milano, 2006.

[188] R. Rannacher. Finite element solution of diffusion problems with irregular data. *Numer. Math.*, 43:309–327, 1984.

[189] R. Rannacher. On the stabilization of the Crank-Nicolson scheme for long time calculations. Preprint, August 1986.

[190] R. Rannacher. Finite element methods for the incompressible Navier-Stokes equations. Lecture notes, August 1999.

[191] R. Rannacher. Adaptive Galerkin finite element methods for paritial differential equations. *J. Comput. Appl. Math.*, 128:205–233, 2001.

[192] R. Rannacher. Numerische methoden der Kontinuumsmechanik (Numerische Mathematik 3). Vorlesungsskriptum, 2001.

[193] R. Rannacher. *Probleme der Kontinuumsmechanik und ihre numerische Behandlung.* Heidelberg University Publishing, 2017.

[194] R. Rannacher and F.-T. Suttmeier. A posteriori error control in finite element methods via duality techniques: Application to perfect plasticity. *Computational Mechanics*, 21(2):123–133, 1998.

[195] R. Rannacher and F.-T. Suttmeier. A posteriori error estimation and mesh adaptation for finite element models in elasto-plasticity. *Computer Methods in Applied Mechanics and Engineering*, 176(1-4):333 – 361, 1999.

[196] T. Richter. Goal-oriented error estimation for fluid-structure interaction problems. *Comp. Methods Appl. Mech. Engrg.*, 223-224:38–42, 2012.

[197] T. Richter. FSI Book. in preparation, 2014.

[198] T. Richter. A monolithic geometric multigrid solver for fluid-structure interactions in ale formulation. *International Journal for Numerical Methods in Engineering*, pages n/a–n/a, 2015.

[199] T. Richter. *Fluid-structure interactions: models, analysis, and finite elements.* Springer, 2017.

[200] T. Richter and T. Wick. Finite elements for fluid-structure interaction in ALE and fully Eulerian coordinates. *Comp. Methods Appl. Mech. Engrg.*, 199:2633–2642, 2010.

[201] T. Richter and T. Wick. Fluid-structure interactions in ALE and Fully Eulerian coordinates. *PAMM*, 10(1):487–488, 2010.

[202] T. Richter and T. Wick. Optimal control and parameter estimation for stationary fluid-structure interaction. *SIAM J. Sci. Comput.*, 35(5):B1085–B1104, 2013.

[203] T. Richter and T. Wick. On time discretizations of fluid-structure interactions. In T. Carraro, M. Geiger, S. Körkel, and R. Rannacher, editors, *Multiple Shooting and Time Domain Decomposition Methods*, pages 377–400, Contributions in Mathematical and Computational Science, 2015.

[204] T. Richter and T. Wick. Variational localizations of the dual weighted residual estimator. *Journal of Computational and Applied Mathematics*, 279(0):192 – 208, 2015.

[205] T. Richter and T. Wick. *Einführung in die numerische Mathematik - Begriffe, Konzepte und zahlreiche Anwendungsbeispiele.* Springer, 2017.

[206] R. Rivlin. Large elastic deformations of isotropic materials. IV. further developments of the general theory. *Philosophical Transactions of the Royal Society of London*, A241:379–397, 1948.

[207] R. Rivlin. Large elastic deformations of isotropic materials. V. the problem of flexure. *Proceedings of the Royal Society of London*, A195:463–473, 1949.

[208] R. Rivlin. Large elastic deformations of isotropic materials. VI. further results in the theory of torsion, shear and flexure. *Philosophical Transactions of the Royal Society of London*, A242:173–195, 1949.

[209] RoDoBo: A C++ library for optimization with stationary and nonstationary PDEs. http://www.rodobo.uni-hd.de.

[210] P. A. Sackinger, P. R. Schunk, and R. R. Rao. A Newton-Raphson pseudo-solid domain mapping technique for free and moving boundary problems: a finite element implementation. *J. Comput. Phys.*, 125(1), 2005.

[211] P. Sagaut. *Large Eddy Simulation for incompressible flows.* Springer, 2006.

[212] N. D. D. Santos, J.-F. Gerbeau, and J. Bourgat. A partitioned fluid-structure algorithm for elastic thin valves with contact. *Comp. Methods Appl. Mech. Engrg.*, 197(19-20):1750–1761, 2008.

[213] M. Schäfer, D. Sternel, G. Becker, and P. Pironkov. *Efficient Numerical Simulation and Optimization of Fluid-Structure Interaction*, volume 53, pages 133–160. Springer-Verlag, 2010.

[214] M. Schäfer and S. Turek. *Flow Simulation with High-Performance Computer II*, volume 52 of *Notes on Numerical Fluid Mechanics*, chapter Benchmark Computations of laminar flow around a cylinder. Vieweg, Braunschweig Wiesbaden, 1996.

[215] M. Schmich and B. Vexler. Adaptivity with dynamic meshes for space-time finite element discretizations of parabolic equations. *SIAM J. Sci. Comput.*, 30(1):369 – 393, 2008.

[216] A. Settari and D. A. Walters. Advances in coupled geomechanical and reservoir modeling with applications to reservoir compaction. *SPE Journal*, 6(3):334–342, Sept. 2001.

[217] K. Stein, T. Tezduyar, and R. Benney. Mesh moving techniques for fluid-structure interactions with large displacements. *J. Appl. Mech.*, 70:58–63, 2003.

[218] K. Takizawa and T. Tezduyar. Computational methods for parachute fluid-structure interactions. *Archives of Computational Methods in Engineering*, 19:125–169, 2012.

[219] P. L. Tallec and S. Mani. Numerical analysis of a linearised fluid-structure interaction problem. *Numer. Math.*, 87:317–354, 2000.

[220] T. Tezduyar. Finite element methods for flow problems with moving boundaries and interfaces. *Archives of Computational Methods in Engineering*, 8(2):83–130, 2001.

[221] T. Tezduyar, M. Behr, and J. Liou. A new strategy for finite element computations involving moving boundaries and interfaces - the deforming-spatial-domain/space-time procedure: I. the concept and the preliminary numerical tests. *Comp. Methods Appl. Mech. Engrg.*, 94:339–351, 1992.

[222] T. Tezduyar, M. Behr, S. Mittal, and J. Liou. A new strategy for finite element computations involving moving boundaries and interfaces - the deforming-spatial-domain/space-time procedure: II. Computation of free-surface flows, two-liquid flows, and flows with drifting cylinders. *Comp. Methods Appl. Mech. Engrg.*, 94:353–371, 1992.

[223] T. Tezduyar and S. Sathe. Modeling of fluid-structure interactions with the space-time finite elements: solution techniques. *Int. J. Numer. Meth. Fluids*, 54:855–900, 2007.

[224] T. Tezduyar, S. Sathe, and K. Stein. Solution techniques for the fully discretized equations in computation of fluid-structure interaction with space-time formulations. *Comp. Methods Appl. Mech. Engrg.*, 195(41-43):5743–5753, 2006.

[225] T. Tezduyar, K. Takizawa, C. Moorman, S. Wright, and J. Christopher. Space-time finite element computation of complex fluid-structure interaction. *Int. J. Numer. Meth. Fluids*, 64:1201–1218, 2010.

[226] T. E. Tezduyar, M. Behr, S. Mittal, and A. A. Johnson. *Computation of Unsteady Incompressible Flows With the Finite Element Methods Space-Time Formulations, Iterative Strategies and Massively Parallel Implementations*, volume 143 of *New Methods in Transient Analysis, PVP-Vol. 246, AMD-Vol. 143*, pages 7–24. ASME, New York, 1992.

[227] F. Tröltzsch. On the Lagrange-Newton-SQP method for the optimal control of semilinear parabolic equations. *SIAM J. Control Optim.*, 38:294–312, 1999.

[228] F. Tröltzsch. *Optimale Steuerung partieller Differentialgleichungen - Theorie, Verfahren und Anwendungen*. Vieweg und Teubner, Wiesbaden, 2nd edition, 2009.

[229] S. Turek. *Efficient solvers for incompressible flow problems*. Springer-Verlag, 1999.

[230] S. Turek, J. Hron, M. Madlik, M. Razzaq, H. Wobker, and J. Acker. Numerical simulation and benchmarking of a monolithic multigrid solver for fluid–structure interaction problems with application to hemodynamics. Technical report, Fakultät für Mathematik, TU Dortmund, Feb. 2010. Ergebnisberichte des Instituts für Angewandte Mathematik, Nummer 403.

[231] S. Turek, J. Hron, M. Razzaq, H. Wobker, and M. Schäfer. *Numerical benchmarking of fluid-structure interaction: a comparison of different discretization and solution approaches*, pages 413–424. Fluid Structure Interaction II: modelling, simulation, optimization. Springer, Heidelberg, 2010.

[232] S. Turek, L. Rivkind, J. Hron, and R. Glowinski. Numerical analysis of a new time-stepping $\theta$-scheme for incompressible flow simulations. Technical report, TU Dortmund and University of Houston, 2005. Dedicated to David Gottlieb on the occasion of his 60th anniversary.

[233] M. Ulbrich and S. Ulbrich. *Nichtlineare Optimierung*. Birkhäuser Verlag, 2012.

[234] K. van der Zee, E. van Brummelen, and R. de Borst. Goal-oriented error estimation for Stokes flow interacting with a flexible channel. *International Journal of Numerical Methods in Fluids*, 56:1551–1557, 2008.

[235] W. A. Wall. *Fluid-Struktur-Interaktion mit stabilisierten Finiten Elementen.* PhD thesis, University of Stuttgart, 1999.

[236] W. A. Wall, A. Gerstenberger, U. Küttler, and U. Mayer. *An XFEM based fixed-grid approach for 3D fluid-structure interaction*, pages 327–349. Fluid Structure Interaction II: modelling, simulation, optimization. Springer, Heidelberg, 2010.

[237] H. Wang and T. Belytschko. Fluid-structure interaction by the discontinuous-Galerkin method for large deformations. *Int. J. Numer. Methods Engrg.*, 77:30–49, 2009.

[238] D. Werner. *Funktionalanalysis.* Springer, 2004.

[239] T. Wick. *Adaptive Finite Element Simulation of Fluid-Structure Interaction with Application to Heart-Valve Dynamics.* PhD thesis, University of Heidelberg, 2011.

[240] T. Wick. Adaptive finite elements for fluid-structure interactions on a prolongated domain: Applied to valve simulations. In *Comput. Methods Mech.*, Warsaw in Poland, May 9-12 2011.

[241] T. Wick. Fluid-structure interactions using different mesh motion techniques. *Computers and Structures*, 89(13-14):1456–1467, 2011.

[242] T. Wick. Goal-oriented mesh adaptivity for fluid-structure interaction with application to heart-valve settings. *Arch. Mech. Engrg.*, 59(6):73–99, 2012.

[243] T. Wick. Coupling of fully Eulerian and arbitrary Lagrangian-Eulerian methods for fluid-structure interaction computations. *Computational Mechanics*, 52(5):1113–1124, 2013.

[244] T. Wick. Solving monolithic fluid-structure interaction problems in arbitrary Lagrangian Eulerian coordinates with the deal.II library. *Archive of Numerical Software*, 1:1–19, 2013.

[245] T. Wick. Flapping and contact FSI computations with the fluid-solid interface-tracking/interface-capturing technique and mesh adaptivity. *Computational Mechanics*, 53(1):29–43, 2014.

[246] T. Wick. *Variational-Monolithic ALE Fluid-Structure Interaction: Comparison of Computational Cost and Mesh Regularity Using Different Mesh Motion Techniques*, pages 261–275. Springer International Publishing, Cham, 2017.

[247] T. Wick. Numerical methods for partial differential equations. Institute for Applied Mathematics, Leibniz Universitaet Hannover, Germany, 2018.

[248] T. Wick and W. Wollner. On the differentiability of fluid-structure interaction problems with respect to the problem data. RICAM report 2014-16 available on http://www.ricam.oeaw.ac.at/publications/reports/, Oct 2014.

[249] A. M. Winslow. Numerical solution of the quasilinear poisson equation in a nonuniform triangle mesh. *Journal of Computational Physics*, 1(2):149 – 172, 1966.

[250] J. Wloka. *Partielle Differentialgleichungen.* B. G. Teubner Verlag, Stuttgart, 1982.

[251] W. Wood. A unified set of single step algorithms. *Int. J. Numer. Meth. Eng.*, 20:2303–2309, 1984.

[252] W. Wood. *Practical time-stepping schemes.* Clarendon Press, 1990.

[253] H. Yang and U. Langer. A note on robust preconditioners for monolithic fluid-structure interaction systems of finite element equations. Technical report, 2014. RICAM preprint 2014-37, http://www.ricam.oeaw.ac.at/publications/reports/.

[254] H. Yang and U. Langer. Numerical simulation of fluid-structure interaction problems with hyperelastic models: A monolithic approach. Technical report, 2014. RICAM preprint 2014-09, http://www.ricam.oeaw.ac.at/publications/reports/.

[255] S. Yigit and M. H. M. Schäfer. Grid movement techniques and their influence on laminar fluid-structure interaction problems. *J. Fluids and Struct.*, 24(6):819–832, 2008.

[256] K. Zee, E. Brummelen, I. Akkerman, and R. Borst. Goal-oriented error estimation and adaptivity for fluid-structure interaction using exact linearized adjoints. *CMAME*, 200:2738–2757, 2011.

[257] L. Zhang, A. Gerstenberger, X. Wang, and W. K. Liu. Immersed finite element method. *Computer Methods in Applied Mechanics and Engineering*, 193(21-22):2051 – 2067, 2004. Flow Simulation and Modeling.

[258] S. Zhang and Z. Zhang. Invalidity of decoupling a biharmonic equation to two Poisson equations on non-convex polygons. *Int. J. Numer. Anal. Modeling*, 5(1):73–76, 2008.

# Index